Unclassified

SECURITY CLASSIFICATION OF THIS PAGE

REPORT DOCUMENTATION PAGE

Form Approved
OMB No. 0704-0188

1a. REPORT SECURITY CLASSIFICATION unclassified	1b. RESTRICTIVE MARKINGS n/a
2a. SECURITY CLASSIFICATION AUTHORITY n/a	3. DISTRIBUTION / AVAILABILITY OF REPORT Approved for public release Distribution unlimited
2b. DECLASSIFICATION / DOWNGRADING SCHEDULE n/a	
4. PERFORMING ORGANIZATION REPORT NUMBER(S) AFOSR-84-0012	5. MONITORING ORGANIZATION REPORT NUMBER(S)
6a. NAME OF PERFORMING ORGANIZATION Optical Society of America 6b. OFFICE SYMBOL (*If applicable*)	7a. NAME OF MONITORING ORGANIZATION Department of the Navy Office of Naval Research
6c. ADDRESS (*City, State, and ZIP Code*) 1816 Jefferson Place, NW Washington, DC 20036	7b. ADDRESS (*City, State, and ZIP Code*) 800 N Quincy Street Arlington, VA 22217-5000
8a. NAME OF FUNDING / SPONSORING ORGANIZATION 8b. OFFICE SYMBOL (*If applicable*)	9. PROCUREMENT INSTRUMENT IDENTIFICATION NUMBER N-00014-88-J-1207
8c. ADDRESS (*City, State, and ZIP Code*) Arlington, VA 22217-5000	10. SOURCE OF FUNDING NUMBERS PROGRAM ELEMENT NO. / PROJECT NO. / TASK NO / WORK UNIT ACCESSION NO

11. TITLE (*Include Security Classification*)
Organization of the Topical Meeting on Tunable Solid State Lasers - unclassified

12. PERSONAL AUTHOR(S)

13a. TYPE OF REPORT	13b. TIME COVERED	14. DATE OF REPORT (*Year, Month, Day*)	15. PAGE COUNT
final	FROM 8/30/88 TO 8/30/89	August 30, 1989	0

16. SUPPLEMENTARY NOTATION

17. COSATI CODES			18. SUBJECT TERMS (*Continue on reverse if necessary and identify by block number*)
FIELD	GROUP	SUB-GROUP	

19. ABSTRACT (*Continue on reverse if necessary and identify by block number*)

Progress and interest in solid state lasers generally, and in tunable solid state lasers specifically, continues to expand. Applications of these lasers include spectroscopy, remote sensing, ranging and imaging, and medicine. New solid state materials are providing lasers with higher output power, broader tunability, and more efficient pumping schemes. The quantum electronics and crystal chemistry properties of these new materials are leading to enhanced laser performance. At the meeting, sessions on sapphire, novel laser schemes, Cr lasers, forsterite and excited state absorption, solid state lasers for specialized applications, alexandrite lasers, Cr related issues, diode pumped lasers, nonlinear frequency conversion, 1.3 micron Nd lasers, infrared lasers and energy transfer, 2-micron lasers, rare earth laser materials, and Er lasers.

20. DISTRIBUTION / AVAILABILITY OF ABSTRACT ☒ UNCLASSIFIED/UNLIMITED ☐ SAME AS RPT. ☐ DTIC USERS	21. ABSTRACT SECURITY CLASSIFICATION unclassified
22a. NAME OF RESPONSIBLE INDIVIDUAL Jarus W. Quinn	22b. TELEPHONE (*Include Area Code*) 202/223-8130 / 22c. OFFICE SYMBOL

DD Form 1473, JUN 86 *Previous editions are obsolete.* SECURITY CLASSIFICATION OF THIS PAGE

TUNABLE SOLID STATE LASERS

CONFERENCE EDITION

Summaries of papers presented at the
Tunable Solid State Lasers
Topical Meeting

May 1-3, 1989

North Falmouth, Cape Cod
Massachusetts

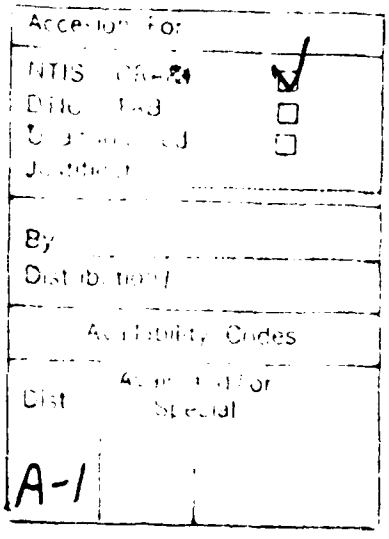

Cosponsored by

Optical Society of America

Lasers and Electro-Optics Society of IEEE

SDIO/Innovative Science and Technology Office

Optical Society of America
1816 Jefferson Place, N.W.
Washington, D.C. 20036
(202) 223-8130

Articles in this digest may be cited in other publications. In order to facilitate access to the original publication source, the following form for the citation is suggested:

> Name of Author(s), Title of Paper, Tunable Solid State Lasers, Technical Digest, (Optical Society of America, Washington, D.C. 1989) pp. xx-xx.

ISBN Number
Conference Edition 1-55752-090-9 (softcover)

Library of Congress Catalog Card Number
Conference Edition 88-62706

This material is based upon work supported by the SDIO/Innovative Science and Technology Office and the Office of Naval Research grant number N00014-88-J-1207 and the ONR Grant Authority identification number s400026srv02. The U.S. Government has a royalty license through the world in all copyrightable material contained herein.

TABLE OF CONTENTS

SUNDAY, APRIL 30, 1989

NAUSET LOBBY

6:00 PM-9:00 PM REGISTRATION/INFORMAL WELCOME RECEPTION

MONDAY, MAY 1, 1989

NAUSET LOBBY

7:00 AM-5:30 PM REGISTRATION/SPEAKER CHECKIN

NAUSET IV

8:00 AM-8:15 AM
OPENING REMARKS
Michael L. Shand, *Allied-Signal, Inc.*

8:15 AM-9:30 AM
MA Ti: SAPPHIRE I
Hans P. Jenssen, *Massachusetts Institute of Technology, Presider*

8:15 AM (Invited Paper)
MA1 Narrowband, High Energy Ti:Al_2O_3 Lidar Transmitter for Spacecraft Remote Sensing, Glen A. Rines, Peter F. Moulton, James Harrison, *Schwartz Electro-Optics, Inc.* Progress on the design and development of a Ti:Al_2O_3 laser for lidar applications is reported. Experiments with injection-seeded unstable resonators are presented. (p. 2)

8:45 AM
MA2 Recent Developments in SLM Pulsed Ti:Sapphire Oscillators, D. D. Lowenthal, C. H. Muller, K. W. Kangas. *Spectra Technology, Inc.* Experimental measurements and modeling results are presented on the scaling of grazing incidence SLM, pulsed Ti:sapphire oscillators. The use of diode and flashlamp pumping is discussed. (p. 4)

9:00 AM
MA3 Amplified Spontaneous Emission Measurement of a Line Narrowed, Tunable Ti:Al_2O_3 Amplifier Using Rubidium Absorption, James C. Barnes, Norman P. Barnes, George E. Lockard, Patricia L. Cross, *NASA Langley Research Center.* ASE generated by a Ti:Al_2O_3 laser amplifier has been measured using the atomic absorption of Rb gas at 0.780 μm. The transmission of the amplifier pulse by Rb is compared to model predictions. (p. 7)

9:15 AM
MA4 Mode-Locked Titanium Sapphire Laser with a Nonlinear Coupled External Cavity, J. Goodberlet, J. Wang, J. G. Fujimoto, P. A. Schulz, S. R. Henion, *Massachusetts Institute of Technology.* Output pulse shortening is demonstrated in a mode-locked titanium sapphire laser with a nonlinear coupled external cavity. Pulse durations were reduced from ~50 to ~1.6 ps. (p. 12)

MONDAY, MAY 1, 1989 — *Continued*

NAUSET III

9:30 AM-10:30 AM
MB Ti:SAPPHIRE II
Posters with Refreshments
Peter F. Moulton, *Schwartz Electro-Optics, Presider*

MB1 Highly Efficient, Widely Tunable Kilohertz Repetition Rate Ti:Sapphire Laser Pumped by a Nd:YLF Laser, Rama Rao, Gary Vaillancourt, *Excel Technology, Inc.;* H. S. Kwok, *SUNY at Buffalo;* C. P. Khattak, *Crystal Systems, Inc.* We report the successful development of an all-solid state kilohertz repetition rate Ti:sapphire laser pumped by a long pulse Nd:YLF laser. The Ti:sapphire laser has an average power exceeding 400 mW, a pulse duration of 10-12 ns, peak power in excess of 30 kW, and is tunable in the spectral region of 670-1070 nm for an input pump power of 1.7 W at 527 nm at 1 kHz. (p. 16)

MB2 Passive Mode-Locking of Flashlamp Pumped Titanium-Doped Sapphire, S. Oda, Y. Segawa, P. H. Kim, S. Namba, *Institute of Physical & Chemical Research, Japan;* N. Kodama, *Tosoh Corp., Japan.* Passive mode-locking with a saturable absorber (IR-125) is observed in a flashlamp pumped Ti:sapphire laser. (p. 19)

MB3 Dense-Plasma Light Source Pumped Ti:Sapphire Laser, In H. Hwang, *Hampton U.;* Kyo D. Song, Sang H. Choi, *Source Tek, Inc.* High energy (up to 0.5 J/2 μs) laser pulses were obtained from a Ti:sapphire crystal when it was pumped with a plasma light source, a hypocycloidal-pinch array. (p. 20)

MB4 Amplification of 25-ps AlGaAs Laser Diode Pulses at 1 kHz in Ti-Doped Sapphire, Santanu Basu, Paul May, Jean-Marc Halbout, *IBM T. J. Watson Research Center.* Amplification of 25-ps diode laser pulses at a 1-kHz repetition rate in Ti:Al_2O_3 is reported. A method of injection seeding is suggested to construct subpicosecond laser sources near 850 nm. (p. 23)

MB5 Efficient, High Average Power, Liquid Nitrogen Cooled Ti:Al_2O_3 Laser, S. R. Henion, P. A. Schulz, *MIT Lincoln Laboratory.* In a Ti:Al_2O_3 laser designed with a large gain region to avoid damage, the output power increased by a factor of four or more on cooling from 300 to 77 K. This result is important for mode-locking and for long pulsed pumping of high average power Ti:Al_2O_3 lasers. (p. 26)

NAUSET IV

10:30 AM-12:00 M
MC NOVEL LASER SCHEMES
William F. Krupke, *Lawrence Livermore National Laboratory, Presider*

10:30 AM (Invited Paper)
MC1 Flashlamp Pumped Titanium Sapphire Laser, Edward G. Erickson, *GTE Government Systems Corp.* A flashlamp pumped Ti:Al_2O_3 laser has been operated at GTE emitting >3.0 J/pulse at 2% efficiency at the center wavelength of 800 nm. We present the latest results achieved with flashlamp pumping of high titanium concentration, high optical quality Ti:S including energy vs wavelength. (p. 30)

11:00 AM (Invited Paper)
MC2 Efficient Tunable Solid State Laser Using Rhodamine Doped Silica, F. Salin, G. Le Saux, P. George, A. Brun, *Institut d'Optique Theorique et Appliquee, France;* J. Zarzycki, *U. Sciences & Techniques du Languedoc, France.* Laser properties of sulforhodamine doped silica gels are presented. Wide tunability (50 nm) and high efficiency (20%) were obtained. (p. 34)

11:30 AM (Invited Paper)
MC3 Diffraction Limited Solid State Lasers with Supergaussian Mirrors, G. Cerullo, V. Magni, R. Riva, O. Svelto, *Polytechnic U. Milan, Italy;* P. Laporta, *U. Rome, Italy.* Unstable resonators using mirrors of supergaussian reflectivity profile are proposed and their advantages are discussed. For the case of a flashlamp pumped Nd:YAG laser, diffraction limited output beams with energy up to 400 mJ have, in this way, been obtained. (p. 36)

12:00 M-1:30 PM LUNCH BREAK

NAUSET IV

1:30 PM-3:00 PM
MD MOSTLY Cr LASERS
Robert C. Morris, *Allied-Signal, Inc., Presider*

1:30 PM (Invited Paper)
MD1 Broadband Tunability of Gain-Flattened Quantum Well Semiconductor Lasers with an External Grating, Michael Mittelstein, David Mehuys, Amnon Yariv, *California Institute of Technology;* Rona Sarfaty, Jeffrey E. Ungar, *Ortel Corp.* Gain calculations utilizing second quantized state transitions predict flattened, broadband gain spectra. Uncoated lasers were grating-tuned over 105 nm and single-longitudinal-mode output exceeded 300 mW. (p. 40)

2:00 PM (Invited Paper)
MD2 Laser Performance and Spectroscopy of Cr^{3+} in $LiCaAlF_6$ and $LiSrAlF_6$, L. L. Chase, S. A. Payne, L. K. Smith, Wayne L. Kway, H. W. Newkirk, *Lawrence Livermore National Laboratory.* We report on the laser performance of Cr^{3+} doped $LiCaAlF_6$ and $LiSrAlF_6$ using laser- and flashlamp pumping. Spectroscopic properties relating to the laser performance are discussed. (p. 43)

2:30 PM
MD3 Growth and Characterization of $LiCaAlF_6Cr^{3+}$ for Solid State Laser Applications, Wayne L. Kway, H. W. Newkirk, and L. L. Chase, *Lawrence Livermore National Laboratory.* Large single crystals of $LiCaAlF_6Cr^{3+}$ were grown by the Czochralski technique. Materials preparation, growth control criteria, and crystal characterization are discussed. (p. 45)

2:45 PM
MD4 Chromium-Activated Forsterite Laser, V. Petricevic, R. R. Alfano, *CUNY-City College;* S. K. Gayen, *Stevens Institute of Technology.* Spectroscopic and quantum electronic properties, as well as the characteristics of laser action in chromium doped forsterite ($Cr:Mg_2SiO_4$), are presented. (p. 48)

MONDAY, MAY 1, 1989 — *Continued*

NAUSET III

3:00 PM-4:00 PM
ME FORSTERITE AND EXCITED STATE ABSORPTION
Posters with Refreshments
Gunter Huber, *University of Hamburg, Presider*

ME1 Laser Performance of Chromium-Aluminum Doped Forsterite, Horacio R. Verdun, Leonard M. Thomas, Donna M. Andrauskas, *Fibertek, Inc.;* Albert Pinto, *U.S. Army Night Vision & Electro-Optics Laboratory.* Chromium-aluminum doped forsterite, prepared by laser-heated pedestal growth, has been studied and found to lase in the 1220-1260-nm range. (p. 52)

ME2 Spectroscopic Properties and Fluoresence Dynamics in Cr^{3+} Doped Forsterite, R. Moncorge, *U. Lyon I, France;* G. Cormier, D. J. Simkin, *McGill U., Canada;* J. A. Capobianco, *Concordia U., Canada.* We report on measurements of polarized absorption, excitation, and time-resolved fluorescence lifetimes and quantum efficiencies in the Cr^{3+} doped forsterite ($Mg_2SiO_4:Cr^{3+}$) vibronic laser material. (p. 55)

ME3 Excited State Absorption in $Ti:YAlO_3$, K. F. Wall, R. L. Aggarwal, *MIT Lincoln Laboratory;* C. P. Khattak, *Crystals Systems, Inc.* Excited state absorption has been observed at 632.8 nm in $Ti:YAlO_3$ pumped with 532-nm radiation from a frequency doubled Q-switched (10-ns pulses) Nd:YAG laser. (p. 58)

ME4 Excited State Absorption of $Ti:YAlO_3$, T. Wegner, Gunter Huber, K. Petermann, *University of Hamburg, F. R. Germany.* Ti^{3+} doped $YAlO_3$ was supposed to be a suitable laser material for the yellow spectral range. However, in our experiments laser action is prevented due to excited state absorption. (p. 61)

ME5 Excited State Absorption Measurements in Cr^{3+} Doped $LaMgAl_{11}O_{19}$, R. Moncorge, H. Manaa, *U. Lyon I, France.* We report on excited state absorption and gain measurements in Cr^{3+} doped $LaMgAl_{11}O_{19}$ (LMA). (p. 64)

ME6 Time Resolved Excited State Absorption of $Mn^{2+}:MgAl_2O_4$, K. Petermann, R. Clausen, *University of Hamburg, F. R. Germany;* E. Heumann, M. Ledig, *University of Jena, D.R. Germany.* Time resolved excited state absorbtion of Mn^{2+} doped spinel has been investigated we believe for the first time. The measured spectra are attributed to intraionic transitions within the Mn^{2+} configurational model. (p. 67)

NAUSET IV

4:00 PM-5:30 PM
MF SOLID STATE LASERS FOR SPECIALIZED APPLICATIONS
Norman P. Barnes, *NASA Langley Research Center, Presider*

4:00 PM (Invited Paper)
MF1 Recent Advances in Tunable Solid State Lasers, A. P. Shcadarevich, *Institute of Physics, Academy of Sciences of Belorussiac, U.S.S.R.* (p. 72)

4:30 PM
MF2 Neodymium Ground State Depleted Laser Characterization and Demonstration, R. Beach, R. Solarz, S. Mitchell, William F. Krupke, L. Brewer, S. Weinzapfel, *Lawrence Livermore National Laboratory.* The recently proposed ground state depleted laser is described. This new class of rare earth doped solid state laser is characterized by a low ion doping density and a large fractional inversion density, permitting four level operation at high efficiency at room temperature. The theoretical description and experimental results from a specific system based on $Nd^{3+}:Y_2SiO_5$ lasing at 912 nm are presented. (p. 73)

4:45 PM
MF3 Continuous-Wave Tunable Oscillation and Superfluorescent Operation of a Monomode Yb^{3+} Doped Fiber Laser, D. C. Hanna, R. M. Percival, I. R. Perry, R. G. Smart, P. J. Suni, A. C. Tropper, *U. Southampton, U. K.* A monomode Yb^{3+} doped fiber laser has been tuned from 1010 to 1160 nm. Efficient Yb^{3+} doped superfluorescent emission has also been demonstrated at 974 and 1038 nm. (p. 75)

5:00 PM
MF4 Efficient 980-nm Operation of a Yb^{3+} Doped Silica Fiber Laser, J. R. Armitage, R. Wyatt, B. J. Ainslie, S. P. Craig-Ryan, *British Telecom Research Laboratories, U.K.* Spectroscopic measurements on Yb^{3+} doped silica fibers are presented. 980-nm operation of a Yb^{3+} laser with a slope efficiency of nearly 40% has been achieved. (p. 78)

5:15 PM
MF5 $^4I_{13/2} - {}^4I_{15/2}$ Emission and Absorption Cross Sections for Er^{3+} Doped Glasses, W. J. Miniscalco, L. J. Andrews, B. A. Thompson, T. Wei, B. T. Hall, *GTE Laboratories, Inc.* Emission and absorption cross sections at 1.5 μm have been measured for Er^{3+} doped glasses. Significant variations were found in peak and integrated cross sections. (p. 81)

OCEANFRONT DINING ROOM

6:30 PM CONFERENCE CLAMBAKE

NAUSET LOBBY

7:00 AM-12:30 PM REGISTRATION/SPEAKER CHECKIN

NAUSET IV

8:00 AM-9:15 AM
TuA ALEXANDRITE LASERS
Ivan A. Shcherbakov, *USSR Academy of Sciences, Presider*

8:00 AM
TuA1 Amplification of 100-fs Millijoule Pulses in Alexandrite Using Chirped Pulse Techniques, Maurice Pessot, Jeff Squier, Gerard Mourou, *U. Rochester;* Donald J. Harter, *Allied-Signal, Inc.* Chirped pulse amplification is used to generate 2-mJ pulses of 106-fs duration in an alexandrite amplifier. Compression of the pulse is achieved by using a sequence of intracavity prisms in conjunction with gratings to compensate both linear and quadratic dispersion in the amplifier. (p. 86)

8:15 AM
TuA2 Unstable Alexandrite Regenerative Amplifiers for Short Pulse Amplification, Jeff Squier, *U. Rochester;* Gerard Mourou, Phillippe Bado, *U. Michigan;* Donald J. Harter, *Allied-Signal, Inc.* Unstable alexandrite regenerative amplifiers which can amplify nanosecond, picosecond, and femtosecond pulses to energies in excess of 200 mJ are described. (p. 90)

8:30 AM
TuA3 Birefringence of Solid State Laser Media: Broadband Tuning Discontinuities and Their Application to Laser Line Narrowing, J. S. Krasinski, Y. B. Band, T. Chin, D. F. Heller, R. C. Morris, P. A. Papanestor, *Allied-Signal, Inc.* The birefringence of broadband solid state laser media can be exploited to provide spectral narrowing and continuous tunability of the laser output. (p. 94)

8:45 AM
TuA4 Frequency Downconversion of a Low Peak Power Alexandrite Laser Through Multiple Intracavity Stimulated Raman Scattering, F. de Rougemont, J. Frey, R. Frey, *Palaiseau Polytechnic, France.* Millijoule energy pulses tunable in the infrared have been obtained through intracavity vibrational and rotational stimulated Raman scattering of a 20-mJ alexandrite laser. (p. 97)

9:00 AM
TuA5 Enhancement of cw Alexandrite Laser Performance, R. E. Fonanno, *Lawrence Livermore National Laboratory;* Donald J. Harter, O. Montoya, *Allied-Signal, Inc.* We report on recent improvements in lamp pumped, cw alexandrite laser performance in pump reflector design, rod quality characterization, and resonators. (p. 100)

NAUSET III

9:15 AM-10:15 AM
TuB Cr RELATED ISSUES
Posters with Refreshments
William A. Sibley, *National Science Foundation, Presider*

TuB1 Laser Pump Chamber Optimization: Modeling and Experimental Verification of Absorption in Biaxial, Trichroic Media, Richard E. Boyd, Jerry W. Kuper, Donald J. Harter, *Allied-Signal, Inc.* Absorption modeling in solid state laser materials, including biaxial, pleochroic crystals, is described. Spatially resolved gain measurements verifying this model are discussed. (p. 104)

TuB2 Laser Pump Chamber Optimization: Raytrace Modeling and Optimization Algorithm, David Benfey, Richard E. Boyd, *Laser Technology Associates, Inc.;* David Brown, Donald J. Harter, *Allied-Signal, Inc.* Pump energy deposition in laser materials is optimized using 3-D raytracing and an algorithmic variation of pump chamber parameters. Analytical and experimental results are compared. (p. 106)

TuB3 Passively Q-Switched Narrow Line Alexandrite Laser, S. G.Post, *U.S. Air Force Weapons Laboratory;* N. Mukherjee, J. McIver, Y. S. Kuo, R. Pastel, *U. New Mexico.* Passive Q-switching with saturable dyes and line narrowing of an alexandrite laser is reported. A lasing linewidth < 0.005 Å has been achieved. (p. 109)

TuB4 Energy Levels of Cr^{3+} Ions in C_{3i} Sites of $Y_3Al_5O_{12}$, Clyde A. Morrison, *Harry Diamond Laboratories;* John B. Gruber, *San Jose State U.;* Marian E. Hills, *U.S. Naval Weapons Center.* The absorption spectra of Cr^{3+} in $Y_3Al_5O_{12}$ has been measured at low temperatures on low doped samples. Analysis of the results using a crystal field Hamiltonian of C_3, symmetry is presented. (p. 112)

TuB5 Iron-Group Lumophores: Broken Paradigms and Low Symmetry Thexi States, Christian K. Jorgensen, *U. Geneva, Switzerland.* Excited titanium(III), chromium(III), manganese(II), iron(III) . . . states have perplexing multidimensional potential surfaces and unpredictable nonradiative probabilities related to electron transfer bands and differing internuclear distances. (p. 115)

TuB6 Transparent Glass Ceramics Doped by Cr(III) and Codoped by Cr(III) and Nd(III) as Potential Materials for Tunable Lasers, Renata Reisfeld, *Hebrew U., Israel* The x-ray, EPR, and optical spectra including time resolved spectroscopy were studied for a variety of transparent glass ceramics doped by Cr(III) alone and by Cr(III) and Nd(III) for tunable lasers. (p. 118)

NAUSET IV

10:15 AM–12:15 PM
TuC DIODE PUMPED LASERS
Rudolf G. Buser, *U.S. Army Night Vision and Electro-Optics Laboratory, Presider*

10:15 AM (Invited Paper)
TuC1 Diode Pumped Solid State Lasers, I. I. Kuratev, Yu V. Tsvetkov, *Moscow Physical Technical Institute, U.S.S.R.* We have investigated the performance of diode laser pumped neodymium lasers operating in a cw mode, a Q-switched mode, and an intracavity frequency doubling mode. (p. 122)

10:45 AM (Invited Paper)
TuC2 Scalable Laser Configuration for Laser Diode Pumped Nd:YAG, J. Frauchiger, P. Albers, H. P. Weber, *U. Berne, Switzerland.* We describe a resonator design that combines the potential to reach high power level, beam quality, and efficiency in a laser diode pumped Nd:YAG system. The active medium is divided into several elements to increase the longitudinally pumped length in the crystals. (p. 124)

11:15 AM
TuC3 Spectroscopic and Laser Studies of Nd Doped Materials for Diode Pumped Lasers, T. Y. Fan, D. S. Knowles, A. Cassanho, *Massachusetts Institute of Technology;* Milan R. Kokta, *Union Carbide Corp.* Spectroscopic and laser properties of Nd:LaF_3, Nd:$LaMgAl_{11}O_{19}$ and Nd:BaY_2F_8 are reported. These materials are of interest for diode pumped lasers because of their long upper state lifetimes compared with Nd:YAG. (p. 126)

11:30 AM
TuC4 Continuously Tunable Single Frequency Nd:YAG Microchip Lasers, J. J. Zayhowski, A. Mooradian, *MIT Lincoln Laboratory.* Single frequency Nd:YAG microchip lasers have been constructed and characterized. They can be tuned continuously over several gigahertz, at rates from dc to tens of megahertz. (p. 128)

11:45 AM
TuC5 Measurements of Heating and Energy Storage in Diode-Pumped Nd:YAG, T. S. Chen, V. L. Anderson, O. Kahan, *Hughes Aircraft Co.* The heat parameter, defined as the heat deposited per unit of stored energy, in diode pumped Nd:YAG has been experimentally measured. The value is found to be 1.1 in a 200-μs pump pulse. (p. 131)

12:00 M
TuC6 Diode Laser End Pumped Neodymium Lasers: the Road to Higher Powers, R. A. Fields, T. S. Rose, M. E. Innocenzi, H. T. Yura, C. L. Fincher, *Aerospace Corp.* We have demonstrated what we believe to be the highest electrical efficiency (19%), optical efficiency (61%), and output power (1.22 W) from a diode pumped Nd:YVO_4 laser. The effects of mode size, thermal loading, and laser material on high power end pumping are discussed. (p. 134)

WEDNESDAY, MAY 3, 1989

NAUSET LOBBY

7:30 AM–5:30 PM REGISTRATION/SPEAKER CHECKIN

NAUSET IV

8:00 AM–9:15 AM
WA NONLINEAR FREQUENCY CONVERSION
Klaus Petermann, *University of Hamburg, Presider*

8:00 AM (Invited Paper)
WA1 Efficient, Broadly Tunable, Beta-Barium Borate Optical Parametric Oscillator Pumped by a Xenon-Chloride Laser, Kiroshi Komine, *Northrop Research & Technology Center.* Pump energy conversion efficiencies of up to 50% have been obtained with output between 420 and 1160 nm using an ultraviolet excimer pump laser. (p. 138)

8:30 AM
WA2 High Gain Nonlinear Optical Interactions with a 1.73-μm Pump, Norman P. Barnes, Keith E. Murray, *NASA Langley Research Center.* Two novel high gain optical interactions using an Er:YLF laser operating at 1.73 μm have been demonstrated, mixing with 3.39 μm in $AgGaSe_2$ and second harmonic generation in $LiNbO_3$. While mixing corresponded closely to theory, second harmonic generation did not, primarily because of poor crystal quality. A method of assessing crystal quality is vividly demonstrated. (p. 141)

8:45 AM
WA3 Optical Parametric Oscillation in KTP for Tunable Mid Infrared Lasers, J. T. Lin, J. L. Montgomery, *U. Central Florida.* We report tunable mid IR lasers using OPO in KTP crystals. Efficiencies are measured for various pump powers and cavity lengths. (p. 144)

9:00 AM

WA4 Temporal Pulse Synchronization for Optical Mixing, H. H. Zenzie, P. E. Perkins, *Sanders Associates, Inc.* We describe a novel method of temporally overlapping pulses originating from separate laser oscillators. Sum frequency mixing of $Ti:Al_2O_3$ and Nd:YAG in KD*P was used to demonstrate the technique experimentally. (p. 147)

NAUSET III

9:15 AM–10:30 AM

WB MOSTLY 1.3-MICRON Nd LASERS

Posters with Refreshments

Antonio Sanchez, *MIT Lincoln Laboratory, Presider*

WB1 Laser Techniques and Frequency Conversion for a Neodymium Based Blue Communication Transmitter, S. R. Bowman, B. J. Feldman, J. M. McMahon, *U.S. Naval Research Laboratory;* A. P. Bowman, *Pacific Sierra Research Corp.;* Donald Scarl, *Polytechnic U.* Recent work on a frequency converted Nd:YAlO$_3$ laser system which matches the atomic cesium resonance at 455 or 459 nm is described. (p. 152)

WB2 Absolute Wavelength Standard for a Tunable 1341-nm Crystal Laser, Donald Scarl, *Polytechnic U.* An optogalvanic signal from the 1341.1686-nm $5s—3p$ He transition has allowed the wavelength of a diode pumped temperature tunable Nd^{3+}:YAlO$_3$ laser to be set with a long term accuracy of 0.1 pm. (p. 155)

WB3 Tunable Single Frequency 1.3 μm Nd:YAlO Microlaser, L. S. Lingvay, G. J. Dixon, N. Djeu, *U. South Florida.* A single frequency Nd:YAlO microlaser at 1.3 μm using a metal film mode selector has been demonstrated. Continuous tuning over 15 GHz was obtained with good efficiency. (p. 158)

WB4 Nd:BeL Laser at 1365 nm, J. Richards, K. Fueloep, R. Seymour, D. Cashmore, P. Picone, M. Horsburgh, *Surveillance Research Laboratory, Australia.* A Nd:BeL laser is being developed to operate at 1365 nm with frequency tripling to the blue at 455 nm for compatibility with the cesium OLORD filter. Gain competition from other transitions and absorption by intracavity water vapor are the main problems encountered in the laser design. (p. 161)

WB5 Growth and Characterization of Ni Doped Garnets, Horacio R. Verdun, Leonard M. Thomas, Donna M. Andrauskas, *Fibertek, Inc.* The growth and spectroscopic characterization of the Ni-activated oxide garnets $Gd_3Ga_5O_{12}$ and $Gd_3Sc_2Al_3O_{12}$ are presented. (p. 163)

WB6 Growth and Characterization of Nd Doped Aluminates and Gallates with the Melilite Structure, Horacio R. Verdun, Linda R. Black, German F. de la Fuente, Donna M. Andrauskas, *Fibertek, Inc.* New crystals of the melilite structure with broad absorption at the $Al_xGa_{1-x}As$ diode pumping wavelength and with long fluorescence lifetimes are presented. (p. 166)

NAUSET IV

10:30 AM–11:45 AM

WC INFRARED LASERS AND ENERGY TRANSFER

Larry G. DeShazer, *Solidlite Corporation, Presider*

10:30 AM (Invited Paper)

WC1 New Materials for Infrared Lasers, A. A. Kaminski, *A. V. Shubnikow Institute of Crystallography, U.S.S.R.* (p. 170)

11:00 AM

WC2 Nonradiative Multiphonon Relaxation and Nonradiative Energy Transfer from the Strongly Quenched High Lying Levels of Nd^{3+} Ions in Laser Crystals, T. T. Basiev, A. Yu. Dergachev, Yu. V. Orlovskii, *Academy of Sciences of the U.S.S.R.;* S. Georgescu, A. Lupei, *Central Institute of Physics, Romania.* The probabilities of nonradiative multiphonon relaxation (NMR) and nonradiative energy transfer (NET) were calculated for the high lying levels $^4P_{3/2}$, $^4D_{3/2}$, $^4G_{7/2}$, $^4G_{5/2} + {}^2G_{7/2}$, and $^4F_{3/2}$ of Nd^{3+} ions in LaF_3, SrF_2, CaF_2, and $YLiF_4$ laser crystals from the measured kinetics of luminescence decay. The correlation between these NMR and NET probabilities was established. (p. 171)

11:15 AM

WC3 Enhanced Energy Transfer Processes in Codoped Solid State Laser Materials, F. X. Hartmann, *Institute for Defense Analyses;* S. R. Rotman, *Ben-Gurion U., Israel.* Enhanced energy transfer between donors and acceptors can be achieved in materials in which donor-acceptor pairing occurs. Theoretical analysis and experimental examples are presented. (p. 174)

11:30 AM

WC4 Gd^{3+} - Cr^{3+} Energy Transfer and Cr^{3+} Decay Dynamics in Cr^{3+} Doped GSGG, GSAG, and GGG, D. S. Hamilton, Li-Ji Lyu, *U. Connecticut;* G. J. Pogatshnik, *Southern Illinois U.* Time-resolved Cr^{3+} fluorescence measurements at 300 K and 77 K indicate a rapid Gd^{3+} - Cr^{3+} energy transfer in Cr^{3+} doped GSGG, GSAG, and GGG. (p. 177)

11:45 AM–1:30 PM LUNCH BREAK

NAUSET IV

1:30 PM–3:00 PM

WD 2-MICRON LASERS

Frank Allario, *NASA Langley Research Center, Presider*

1:30 PM (Invited Paper)

WD1 Cross Relaxation Solid State Lasers, B. M. Antipenko, *Leningrad State University, U.S.S.R.* (p. 182)

2:00 PM

WD2 Spectroscopic and Laser Properties of Tm Doped YAG at 2 μm, T. Becker, R. Clausen, Gunter Huber, *University of Hamburg, F. R. Germany;* E. W. Duczynski, P. Mitscherlich, *Lasertec Hamburg GmbH.* We have investigated the concentration dependence of Cr-Tm energy transfer, Tm-Tm cross relaxation, and laser action in Cr, Tm:YAG and Tm:YAG under 647 and 780-nm pumping. (p. 183)

2:15 PM

WD3 High Efficiency 2.09-μm Laser, Gregory J. Quarles, Charles L. Marquardt, Leon Esterowitz, *U.S. Naval Research Laboratory;* Annette Rosenbaum, *Sachs/Freeman Associates.* Studies of Cr to Tm transfer efficiencies have led to the optimization of dopant concentrations for a flashlamp pumped 2.09-μm Cr:Tm:Ho:YAG laser. We report slope efficiencies of >5.0% and overall efficiencies of 3.8%. (p. 186)

2:30 PM

WD4 Ho:Tm:Cr:YAG and Ho:Tm:Er:YAG Laser Performance at Intermediate Temperatures, Donald J. Gettemy, Norman P. Barnes, Patrica L. Cross, *NASA Langley Research Center;* Milan R. Kokta, *Union Carbide Corp.* Ho:Tm:Cr:YAG and Ho:Tm:Er:YAG lasers are two attractive prospects for eyesafe lasers. Performances of two different Ho:Tm:Cr:YAG and one Ho:Tm:Er:YAG lasers are measured and compared as a function of temperature, and performance is correlated with temperature dependent parameters. (p. 189)

2:45 PM
WD5 Tunable 2.3-μm Tm^{3+}:$LiYF_4$ Laser, R. C. Stoneman, Leon Esterowitz, *U.S. Naval Research Laboratory;* G. H. Rosenblatt, *Sachs/Freeman Associates.* Tunable laser emission is observed for the $^3H_4 \rightarrow {}^3H_5$ transition in Tm^{3+}:$LiYF_4$. Emission on eleven laser lines in the range 2.27 to 2.34 μm is observed. (p. 191)

NAUSET III

3:00 PM–4:00 PM
WE RARE EARTH LASER MATERIALS
Posters with Refreshments
Kenneth L. Schepler, *U.S. Air Force Wright Aeronautical Laboratory, Presider*

WE1 Fluorescence Dynamics in $LiYF_4$:Tm, Ho After 800 nm Laser Excitation, A. Brenier, R. Moncorge, C. Pedrini, *U. Lyon I, France.* The $Tm^{3+} \rightarrow Tm^{3+}$ and $Tm^{3+} \rightleftarrows Ho^{3+}$ energy transfer processes in $LiYF_4$ are investigated and some fluorescence quantum efficiencies are measured after 800-nm laser excitation. (p. 196)

WE2 Laser Emission at 1.47 μm from Fluorozirconate Glass Doped with Tm^{3+} and Tb^{3+}, G. H. Rosenblatt, R. J. Ginther, *Sachs/Freeman Associates;* R. C. Stoneman, Leon Esterowitz, *U.S. Naval Research Laboratory.* The Tm^{3+} $^3H_4 \rightarrow {}^3F_4$ laser transition is observed, we believe for the first time. The fluorozirconate glass host is codoped with Tb^{3+} to quench the lower laser level. (p. 200)

WE3 Continuous-Wave Oscillation of a Momomode Thulium Doped Silica Fiber Laser, D. C. Hanna, K. M. Percival, I. R. Perry, R. G. Smart, P. J. Suni, A. C. Tropper, *U. Southampton, U.K.* A thulium-doped fiber has been lased between 1.88 and 1.96 μm. Results suggest that thulium would be a good candidate for diode pumping at around 800 nm. (p. 203)

WE4 Energy Transfer Processes Among Cr, Tm, and Ho Ions in Yttrium Aluminum Garnet Crystals, G. Armagan, A. M. Buoncristiani, *Christopher Newport College;* B. DiBartolo, *Boston College;* A. T. Inge, *NASA Langley Research Center.* A systematic study of the spectroscopic properties of YAG crystals doped with Cr, Tm, and Ho determined the microscopic interaction parameters and energy transfer rates. (p. 206)

WE5 Er,Tm,Ho:YLF Laser for Spectroscopy Applications, A. Di Lieto, P. Minguzzi, F. Pozzi, M. Tonelli, *U. Pisa, Italy;* Hans P. Jenssen, *Massachusetts Institute of Technology.* A cw Er,Tm,Ho:YLF laser, optically pumped by an ion laser, is described. Tunability range, efficiency, and noise properties are studied in view of possible use in high resolution spectroscopy. (p. 209)

WE6 Optical Properties of Nd:$NaYF_4$ and Ho:$NaYF_4$, D. Knowles, A. Cassanho, Hans P. Jenssen, *Massachusetts Institute of Technology.* Spectroscopy on the new crystals Nd:$NaYF_4$ and Ho:$NaYF_4$ indicate that the integrated cross section of Nd is twice that of Nd:YAG, while Ho is similar to Ho:$LiYF_4$. (p. 211)

NAUSET IV

4:00 PM–5:30 PM
WF Er LASERS
Michael L. Shand, *Allied-Signal, Inc., Presider*

4:00 PM (Invited Paper)
WF1 Nonlinear Interactions in Scandium Garnets Doped by Chromium and Erbium Ions, V. A. Smirnov, Ivan A. Shcherbakov, *Academy of Sciences of the U.S.S.R.* In garnets doped with chromium and rare earth ions, the processes of energy transformation, including upconversion, are investigated. Their influence on laser properties is established. (p. 216)

4:30 PM
WF2 Er:YLF Laser Operation at 0.85 and 1.73 μm and the Possibility of Self-Cascade Lasing, Norman P. Barnes, Keith E. Murray, *NASA Langley Research Center.* Er:YLF has the potential for self-cascade or simultaneous lasing between the $^4S_{3/2}$ manifolds and $^4I_{9/2}$ manifolds, and the $^4I_{9/2}$ and $^4I_{13/2}$ manifolds. Self-cascade lasing is investigated by comparing the laser performance of Er:YLF operating at 1.73 μm on the $^4S_{3/2}$ to $^4I_{9/2}$ transition and at 0.85 μm on the $^4S_{3/2}$ to $^4I_{13/2}$ transition. Spectroscopic and laser evidence is presented to investigate the self-cascade lasing process. (p. 219)

4:45 PM
WF3 Upconversion Processes in Er-Activated Solid State Laser Materials, Harry Chou, Hans P. Jenssen, *Massachusetts Institute of Technology.* Quantitative models for Er activated solid state laser materials have been developed to predict the population dynamics of the Er multiplets. The upconversion rate constants have been deduced by fitting the model to spectroscopic data. (p. 221)

5:00 PM
WF4 Multiple Wavelength Lasing of (Erbium, Holmium): Yttrium Aluminum Garnet, Russell Kurtz, Laurie Fathe, Jason Machan, Michael Bass, Milton Birnbaum, *U. Southern California.* (Erbium, holmium):yttrium aluminum garnet lased at three wavelengths within a single pump pulse. Laser level lifetimes indicated moderate interaction between erbium and holmium ions. (p. 224)

5:15 PM
WF5 Visible and Infrared Laser Operation by Upconversion Pumping of Erbium Doped Fluorides, R. A. McFarlane, M. Robinson, *Hughes Research Laboratories;* S. A. Pollack, D. B. Chang, *Hughes Aircraft Co.;* Hans P. Jenssen, *Massachussets Institute of Technology.* Cooperative multi-ion energy transfer and two step excitation processes have been employed to achieve population inversion and laser action in erbium-doped $YLiF_4$ and BaY_2F_8. (p. 227)

5:30 PM–5:45 PM
CLOSING REMARKS
Hans P. Jenssen, *Massachusetts Institute of Technology*

MONDAY, MAY 1, 1989

NAUSET IV

8:15 AM–9:30 AM

MA1–MA4

Ti:SAPPHIRE I

Hans P. Jenssen, Massachusetts Institute of Technology, *Presider*

Narrowband, High Energy Ti:Al_2O_3 Lidar Transmitter for Spacecraft Remote Sensing

Glen A. Rines, Peter F. Moulton and James Harrison

Schwartz Electro-Optics, Inc.

45 Winthrop Street

Concord, MA 01742

One of the system applications which can be addressed by the unique properties of Ti:Al_2O_3 is remote-sensing of oxygen and water-vapor in the 725-950 nm wavelength region. NASA is interested, in particular, in the development of a space-based, differential-absorption lidar (DIAL) system which provides a spectrally-narrow (0.3-1.0 pm), high energy (0.5-1.0 J) output at 727, 760 and 940 nm. Ti:Al_2O_3 is particularly well-suited for this application because it provides the required tunability and high gain in a solid state medium that can, potentially, be operated with an all-solid-state optical pump (diode-laser-pumped, frequency-doubled Nd lasers). In this paper we report on the status of a NASA-funded, multi-year development effort to demonstrate, in the laboratory, a laser system capable of addressing these lidar system requirements.

The basic laser design is an injection-seeded oscillator/amplifier system. The design philosophy is that the best laser performance and system reliability will be obtained by addressing the line-narrowing issues in a master oscillator and the high energy requirement in a fundamental mode oscillator/amplifier arrangement. With this approach, the master oscillator design can be optimiz for single-axial-mode operation without concern for the limitations imposed by short-pulse high peak-power oscillators. Similarly the slave resonator can be designed to be an efficient, high energy oscillator without the limitations imposed when intracavity line-narrowing elements must be accommodated. Via injection-seeding the single-frequency property of the master oscillator can be created in the high energy slave oscillator. Within this general design concept there are different possible designs for both the master and slave oscillators which are amenable to the injection-seeding mechanism and which address the laser performance requirements. The selection of specific oscillator designs and the status of their development and integration into system configurations is presented in this paper.

In regard to the master oscillator development, we will report on both cw and pulsed design options which are being investigated. The cw oscillator development work to date has been done with Ar-ion laser pumping. The emphasis of this work has been to develop very low

threshold oscillators that could ultimately be pumped by a diode-laser-pumped, frequency-doubled, Nd laser. The results of cw experiments performed to date are as follows. In a standing-wave cavity with a 1.0-%-transmission output coupler we obtained a threshold of less than 250 mW input and an output power of 150 mW for 1.7 W of pump input. In experiments with a unidirectional, ring resonator we have demonstrated continuously tunable, single-frequency operation from 765 to 890 nm with a single mirror set. With 3.3 W of input power the ring laser produces >150 mW over the tuning range.

The option of a pulsed (quasi-cw) master oscillator is also being investigated. We have developed a long-pulse (200-400 μs) intracavity-frequency-doubled, Nd laser for optically pumping a quasi-cw Ti:Al_2O_3 oscillator. In long-pulse-green laser experiments we have obtained up to 70 mJ of green at 10 Hz. A ring resonator similar to the one used in the cw experiments will be tested with the long-pulse-green laser in the near future. The spatial and spectral properties of the quasi-cw Ti:Al_2O_3 master oscillator will be presented.

The gain-switched, Ti:Al_2O_3 slave oscillator and amplifiers in this system are optically pumped by a frequency-doubled, Nd:YLF laser which is being constructed at SEO under a subcontract arrangement with Sanders Associates of Nashua, NH. The operation of the Nd:YLF laser will be presented briefly as it relates to the performance of the gain-switched Ti:Al_2O_3 system.

The baseline design for the slave oscillator is a high energy, fundamental mode, unstable resonator. We are investigating both standing-wave and traveling-wave (ring) unstable resonators and the relative merits of each particularly in regard to injection-seeding properties. In experiments performed to date we have demonstrated 90 mJ of output at 10 Hz from a standing-wave, positive-branch, unstable resonator. The output in this experiment was pump-limited; no damage to optical components was incurred by either the pump beam or the intracavity Ti:Al_2O_3 beam. Experimental results with higher pump energies will be reported along with the results of injection-seeding experiments.

Recent Developments in SLM Pulsed Ti:Sapphire Oscillators

D.D. Lowenthal, C.H. Muller, K.W. Kangas
Spectra Technology, Inc.
2755 Northup Way
Bellevue, Washington 98004
(206) 827-0460

During the past year a single longitudinal mode (SLM), pulsed, Ti:Sapphire oscillator has been demonstrated [1] at Spectra Technology, Inc. This paper presents recent experimental results that characterize the behavior of this SLM oscillator over the wide tuning range of Ti:Sapphire, compares these measurements with analytical and numerical models, presents results on tuning ranges achieved while maintaining SLM operation, describes operation at 911 nm with efficient doubling to 459 nm, and describes ongoing efforts to achieve direct diode or flashlamp pumping as a replacement for pumping with doubled Nd:YAG.

Figure 1 presents the SLM output energy characteristics as a function of wavelength. In Figure 1a the multimode output energy is plotted versus wavelength for a 532 nm pump energy of 69 mJ. The pump beam diameter was ~1 mm resulting in a pump fluence of ~8 J/cm^2 (limited below this value by damage). Also, the threshold pump energy is shown versus wavelength. Note, under these pumping conditions the peak output energy per pulse is ~9 mJ at 800 nm and ~3 mJ at 900 nm. Larger output energies are possible with higher pump energies and larger pump beam diameters; however, the number of longitudinal modes will also increase. In Figure 1b the SLM output energy is plotted versus wavelength. Also included is a plot of the upper limit on pump energy that must not be exceeded if SLM operation is to be maintained. When SLM conditions are achieved both the output energy and ratio of gain to threshold gain remain constant over the tunable bandwidth. This property is easily understood in terms of the SLM startup properties of the grazing incidence oscillator and will be described.

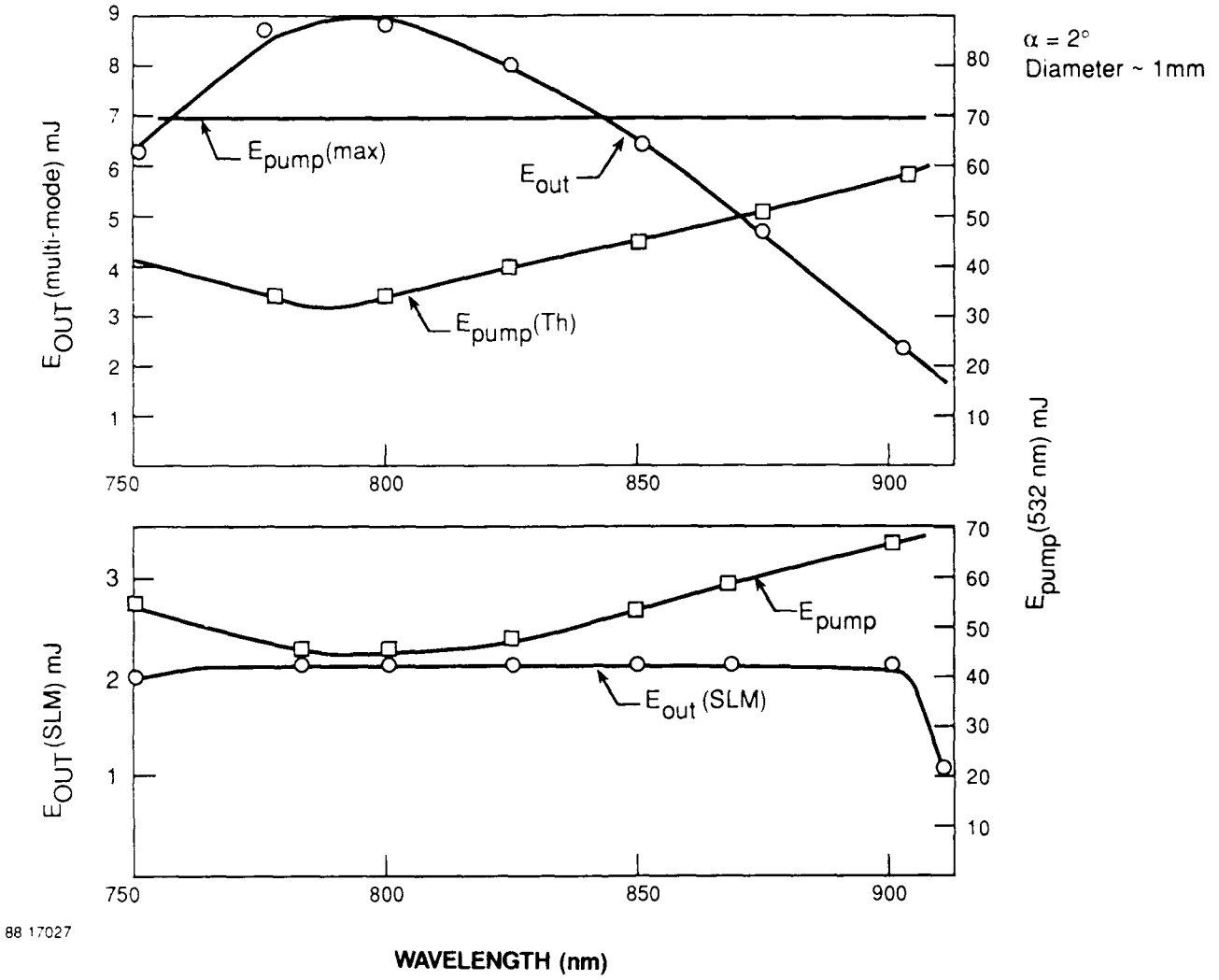

Figure 1. SLM, Ti:Sapphire, grazing incidence tuning characteristics. (a) Multimode operation and threshold conditions for lasing. (b) Single longitudinal mode operation and upper limit on pump fluence.

Figure 2 illustrates the current SLM oscillator configuration that allows tuning over many wave numbers while maintaining SLM operation. This configuration was first proposed for dye lasers by Littman[2]; it maintains an integral number of waves in the oscillator cavity during tuning. This feature has been used to sweep the oscillator through the Cs resonance lines at 455 nm. For these experiments the SLM oscillator was tuned to 911 nm and generated ~1 mJ per pulse. This output energy was then frequency doubled efficiently (25%) in KD*P to provide the narrow-band, 455 nm photons. The ability to frequency double efficiently implies good beam quality; and this is supported by near field measurements of smooth Gaussian like profiles.

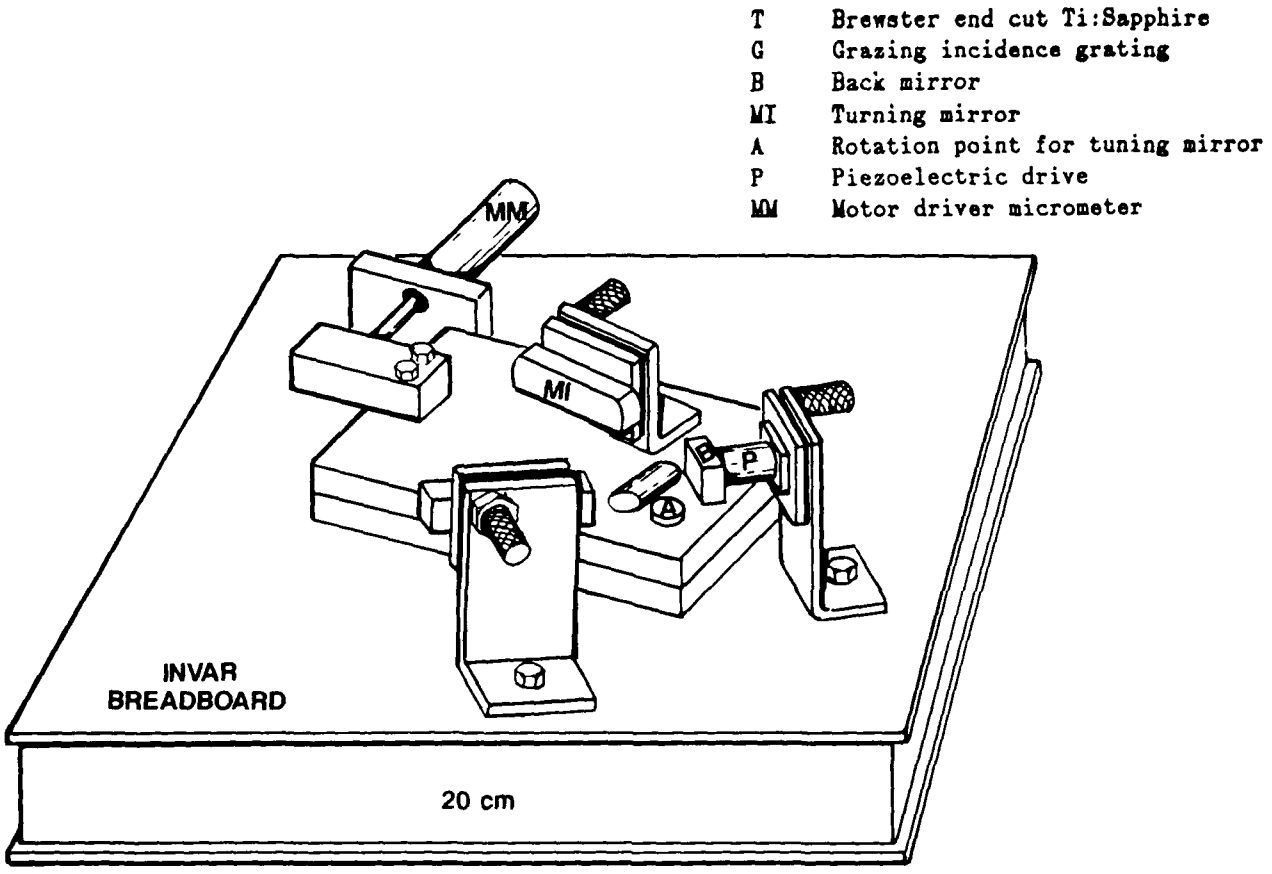

Figure 2. Current Ti:Sapphire grazing incidence configuration showing pivot point, A, location for SLM tuning. A piezoelectric driver, P, is used to tune the cavity length to an even number of wavelengths. The motor driven micrometer, MM, is used for coarse tuning.

All of our current experiments have been carried out using a doubled Nd:YAG as the laser pump source. A very useful variation would be diode or flashlamp pumping of the Ti:Sapphire gain medium. This approach would lead to a very compact, and nearly self-contained, tunable, SLM, oscillator.

Work supported under IRAD funding at Spectra Technology, Inc.

1. K.W. Kangas, D.D. Lowenthal and C.H. Muller, III, "Single Longitudinal Mode, Tunable, Pulsed, Ti:Sapphire Laser Oscillator," Opt. Lett. (Jan.'89); Laser Focus (Nov. 1988).

2. M.G. Littman, "Single-mode pulsed tunable dye laser," Appl. Opt. 23, 4465 (15 Dec.'84).

MA3-1

AMPLIFIED SPONTANEOUS EMISSION MEASUREMENT OF A LINE NARROWED, TUNABLE Ti:Al_2O_3 AMPLIFIER USING RUBIDIUM ABSORPTION

James C. Barnes, Norman P. Barnes, George E. Lockard, Patricia L. Cross
NASA Langley Research Center, Hampton, VA 23665-5225

Titanium-doped Sapphire, Ti^{3+}: Al_2O_3 , lasers are being considered for use as transmitters for NASA spaceborne LIDAR systems. These systems will require energies up to two joules per pulse at a ten hertz repetition rate . [1] In addition, the integrity of the LIDAR measurements require that 99.9% of the total transmitter pulse energy reside within a spectral interval equal to or less than 5 pm as viewed through a spectral window of 200 pm. [2] Given these requirements and the high gain nature of Ti^{3+}: Al_2O_3 , the possible generation of unacceptable levels of amplified spontaneous emission, ASE, becomes a concern, particularly for the amplifier stages of a high power transmitter. By developing modeling techniques to accurately predict ASE in amplifiers laser engineers will be better equipped to design Ti^{3+}: Al_2O_3 laser amplifiers to meet NASA energy and spectral purity requirements.

In this work transmission by rubidium (Rb) vapor as a function of wavelength and as a function of temperature was used to spectrally characterize a line-narrowed, tunable, Ti^{3+}: Al_2O_3 laser amplifier operating at ten hertz with a wavelength of ~0.780 μm. The transition between the ground state, $5^2S_{1/2}$ and the $5^2P_{3/2}$ electronic level of Rb provides the atomic absorption at 0.780 μm to characterize the amplifier output. [3], [4] The energy level diagram depicting the hyperfine splitting of the two isotopes present in the Rb used is shown in Figure 11, reproduced from [4]. The Rb absorption lines are used as narrowband interference filters. When the narrowband amplifier is tuned to an absorption peak all of the on line energy of the laser pulse is absorbed. The energy that is transmittted thru the cell is then considered to be ASE.

The experimental laser system consist of an oscillator, a regenerative amplifier, and amplifier. Each of which is longitudinally pumped by one of two frequency doubled Nd:YAG lasers operating at ten hertz. A line narrowed oscillator provides an injection pulse to the Q-switched regenerative amplifier and the output of the regenerative amplifier serves as the amplifier probe. The output of the amplifier mirrors the injection pulse wavelength and linewidth which are monitored by a 1m monochromator and 2cm spaced Fabry-Pebot interferometer respectively. The oscillator is line narrowed by etalons with air spacings of 10, 2, and 0.1mm. Gross tuning of the oscillator is by horizontal rotation of the optical axis through a SF-10 prism, medium tuning by rotation of a 10mm birefringent quartz plate about the axis perpendicular to its face, and fine tuning is accomplished by rotation of a tilted 1mm thick solid etalon about its vertical axis. All of the etalons were maintained at temperatures approximately 4°C above ambient to alleviate

wavelength drift and jitter due to room temperature changes. The laser linewidth was varied between 2 and 4pm.

The experimental arrangement is shown in Figure 2. The output of the amplifier is first split by a 70/30 beam splitter. The reflected beam is directed to a 2cm air spaced Burleigh interferometer generating a ring pattern which is imaged onto a 1024 element detector array with oscilloscope display for calculation of laser line-widths and into a one meter monochromator for wavelength measurements. The transmitted beam is attenuated by a Glan polarizer with the reflected beam serving as a reference incident on detector B. The beam transmitted by the Glan prism polarizer is expanded to a minimal 2cm diameter and attenuated further by neutral density filters before being introduced into the 30.5cm long Rb cell. The pulse incident on the cell is maintained between 40 and 50 nJ. At this energy the beam fluence is a factor of 3-4 below the fluence level necessary to produce saturation effects on the atomic absorption spectrum of the Rb vapor at 24°C, the minimum temperature, hence, the minimum vapor pressure for the data runs of this work. [5],[6] Spectral interference filters with bandpasses of 3 and 10nm centered at 780nm were also inserted into the incident beam path to ascertain the spectral distribution of the ASE within these two window limits.

A model was developed to correlate the measured transmission with the predicted transmission. Rb absorption around 0.78 μm results from the summation of the hyperfine lines of ^{85}Rb and ^{87}Rb. Each of the hyperfine lines has a Voight profile, calculated by convolving the natural Lorentzian linewidth with the Doppler broadened linewidth. As the laser operates only in the TEM_{oo} modes, the laser spectral bandwidth is modelled as a distribution of narrow lines. The distribution is modelled as the sum of two binomial distributions, the spectral bandwidth of which is equal to the measured spectral bandwidth of the laser. Transmission of the Rb cell is taken to be weighted sum of the transmission of the individual laser lines. Comparison of the calculated and measured transmission will be presented.

REFERENCES

[1] L. Holcomb, M. Sokoloski, F. Allario, and R. Nelms, "Technology For Active Remote Sensing From Space," in Proc. IAF Congr., Innsbruck, Austria, Oct. 1986.

[2] NASA LaRC FED-ESB, SOW for "Narrowband, High Energy Titanium-doped Sapphire LIDAR Transmitter for Spacecraft Remote Sensing," p.2, April 1987.

[3] H. Kopferman and H. Kruger, "Zur Hyperfine der Reasonanzlinien des Rubidiums," Z. Phys., Vol. 83, pp. 485-490, 1933.

[4] J. R. Beacham and K. L. Andrew, "Optical Study of the Hyperfine Structure of the Rubidium Resonance Lines," J. Opt. Soc., Vol. 61, pp. 231-235, 1971.

[5] A. V. Nowak and B. J. Krohn, "Spectral Characterization of a Tunable Alexandrite Laser by Rubidium Absorption at 780nm," IEEE J. Quantum Electron, Vol. QE-21, pp. 1607-1613, Oct. 1985.

[6] A. N. Nesmeyanov, Vapor-Pressure of the Elements. New York: Academic, p. 443, 1963.

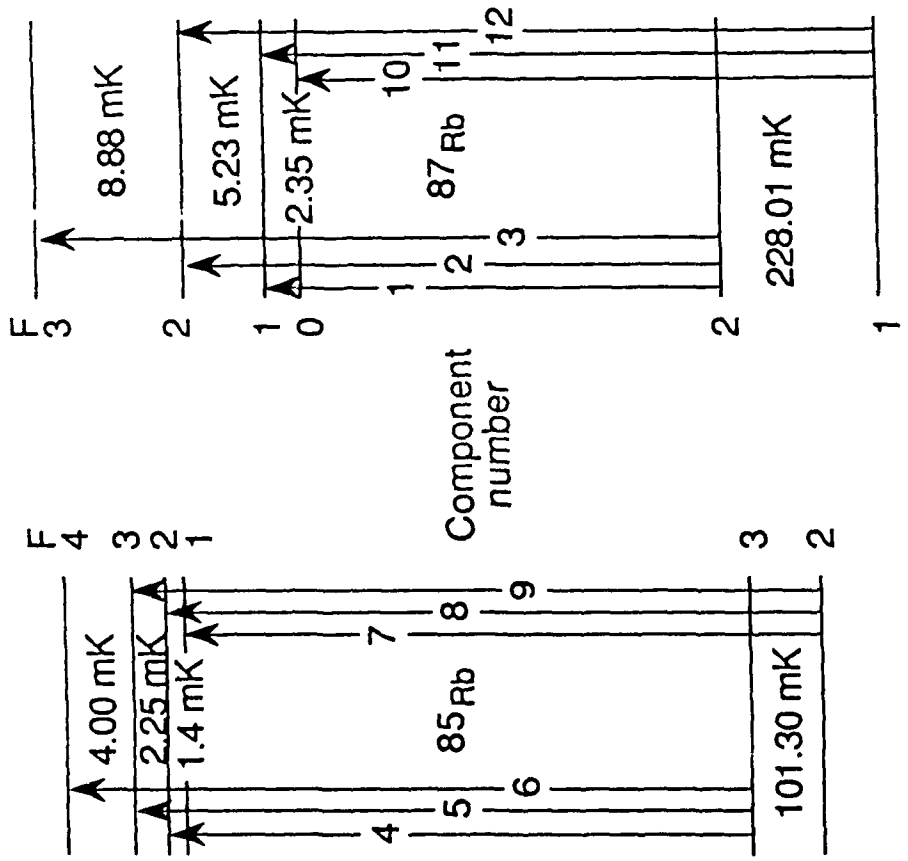

Fig. 1. Energy level diagram of the $5^2P_{3/2} \rightarrow 5^2S_{1/2}$ transition in atomic rubidium at 780 nm. The values and number of the transitions correspond to Fig. 2,[4].

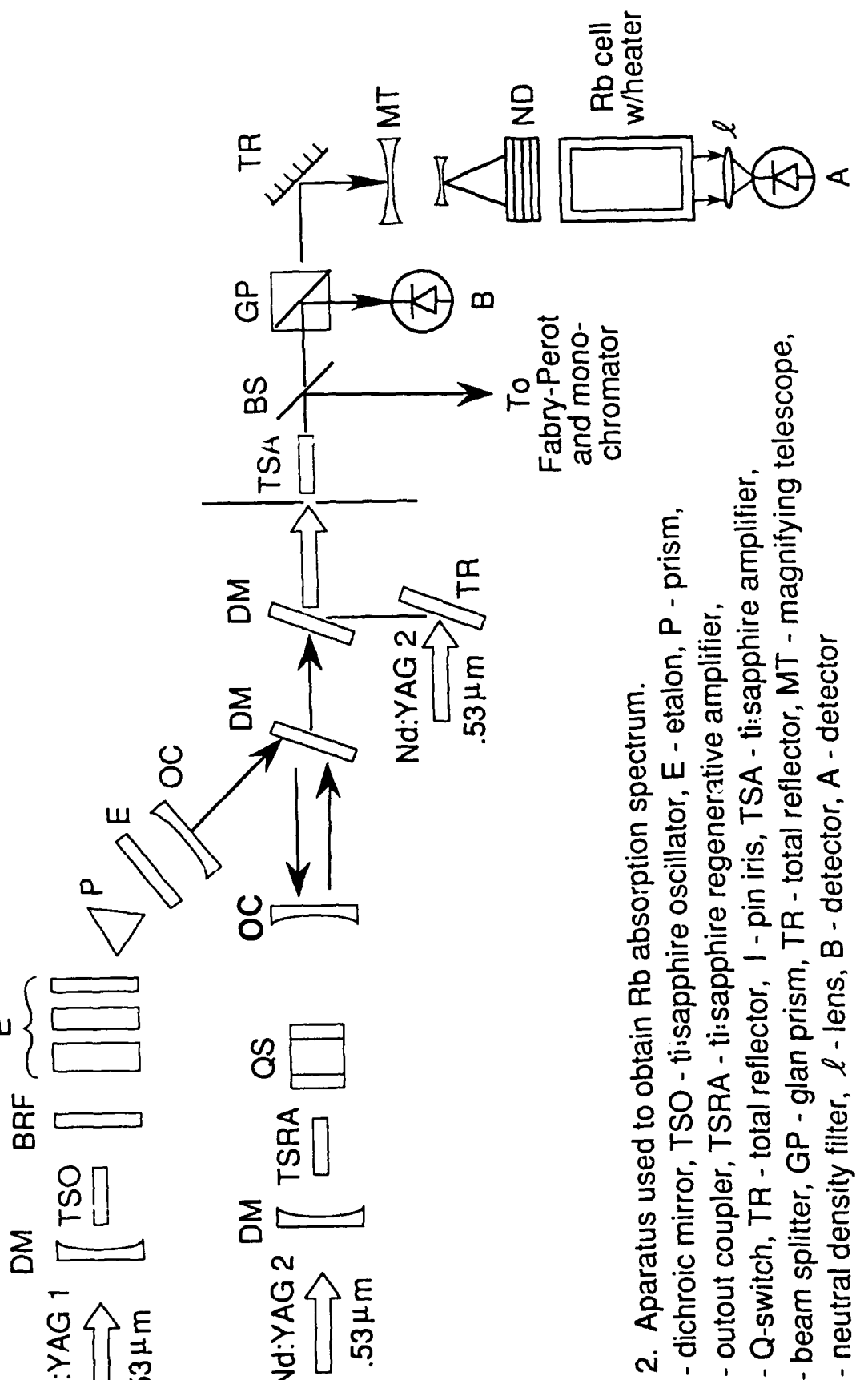

Fig. 2. Aparatus used to obtain Rb absorption spectrum.
DM - dichroic mirror, TSO - ti:sapphire oscillator, E - etalon, P - prism,
OC - outout coupler, TSRA - ti:sapphire regenerative amplifier,
QS - Q-switch, TR - total reflector, I - pin iris, TSA - ti:sapphire amplifier,
BS - beam splitter, GP - glan prism, TR - total reflector, MT - magnifying telescope,
ND - neutral density filter, ℓ - lens, B - detector, A - detector

Modelocked Titanium Sapphire Laser with a Nonlinear Coupled External Cavity

J. Goodberlet, J. Wang, and J. G. Fujimoto
Department of Electrical Engineering and
Computer Science and Research Laboratory
of Electronics
Massachusetts Institute of Technology
Cambridge, Massachusetts 02139
(617) 253-8528

and

P. A. Schulz and S. Henion
Lincoln Laboratory
Massachusetts Institute of Technology
Lexington, MA 02173

Summary

We describe the application of a nonlinear coupled cavity to enhance short pulse generation from a modelocked Ti:Al_2O_3 laser. Pulses from the modelocked laser are coupled into an optical fiber, self phase modulated, and reinjected into the main laser cavity. Pulse durations have been reduced from $\sim$ 50 ps to $\sim$ 1.6 ps.

Titanium sapphire (Ti:Al_2O_3) is an attractive laser material which has high energy storage, high damage threshold, a large gain bandwidth and broad tuning range[1]. High power pulsed and cw laser action has been demonstrated at room temperature in the wavelength range from 670 nm to 1 μm. While the large bandwith of Ti:Al_2O_3 makes it potentially attractive as a tunable source for ultrashort laser pulses, passive modelocking is difficult because of the relatively small gain cross section.

The use of feedback from an external cavity is a powerful technique for generating ultrashort pulses. This concept was first demonstrated in a soliton laser where pulse shaping was acomplished using an optical fiber in the anomalous dispersion regime[2]. However, recent experimental and theoretical investigations suggest a new mechanism for modelocking which utilizes self phase modulation and interferometric pulse shaping[3-6].

Self phase modulation in an optical fiber of an external cavity produces a frequency chirp on the pulse with frequency shifts on the leading and trailing edges of the pulse. This chirped pulse from the external cavity interferometrically combines with the unchirped pulse from the laser. If the phase of the pulse is controlled appropriately, the leading and trailing edges of the pulse can destructively interfere with respect to the peak of the pulse, thereby producing pulse shortening[6].

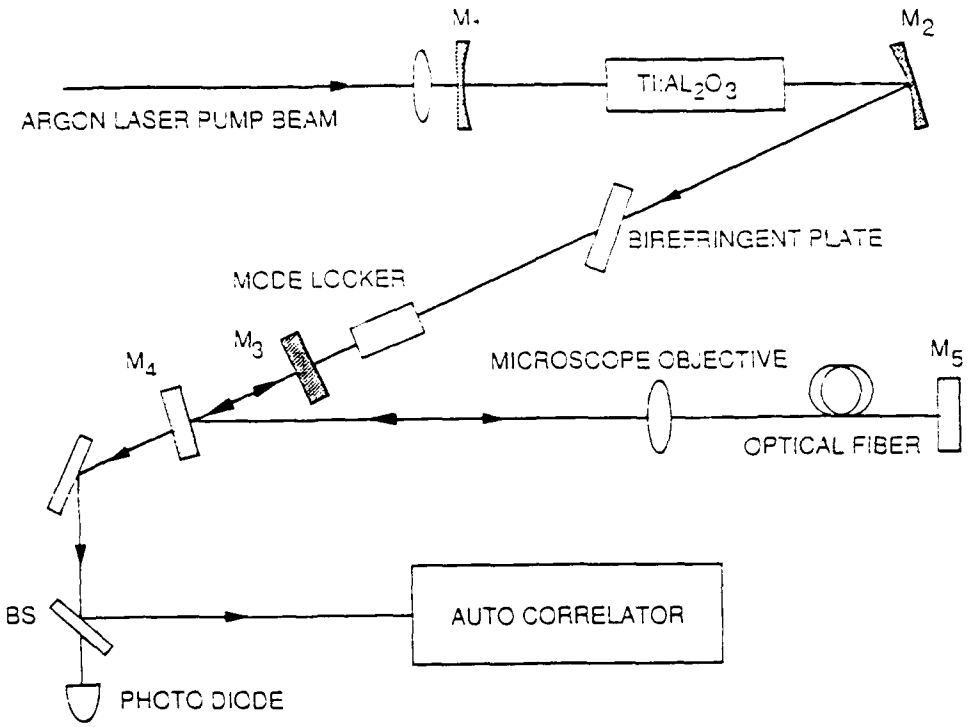

Fig. 1. Experimental setup.

Figure 1 shows a schematic of the modelocked Ti:Al_2O_3 laser. The main laser cavity consisted of a three mirror astigmatically compensated cavity formed by mirrors M1, M2, and M3. The pump source was a cw argon laser. A two centimeter long, Brewster cut, Ti:Al_2O_3 crystal was used as the gain medium The crystal was cooled to 0°C. The laser was modelocked with a resonant acousto-optic modulator operating at 60 MHz. Average powers of 750 mW could be obtained in modelocked operation.

The external cavity consisted of a beam splitter which coupled a portion of the laser output power into a single mode optical fiber. The end of the fiber was butt coupled to mirror M5 which retro-reflected the pulses, reinjecting them into the main laser cavity. The fiber and mirror M5 assembly was mounted on a micrometer stepping motor stage to match the length of the external resonator to the main laser cavity. In addition, since pulses from the external resonator must interferometrically combine with pulses in the main laser at the output mirror M3, the length of the external cavity was also controlled by a piezoelectric translator which could vary the phase of the pulses.

Figure 2 shows an autocorrelation of the modelocked Ti:Al_2O_3 laser output. Modelocking without the external resonator produced pulse durations of $\sim$ 50 ps (assuming Gaussian pulse shape). For these measurements the laser was operated with an output power of 500 mW at 770 nm. A double plate birefringent filter was used for wavelength tuning.

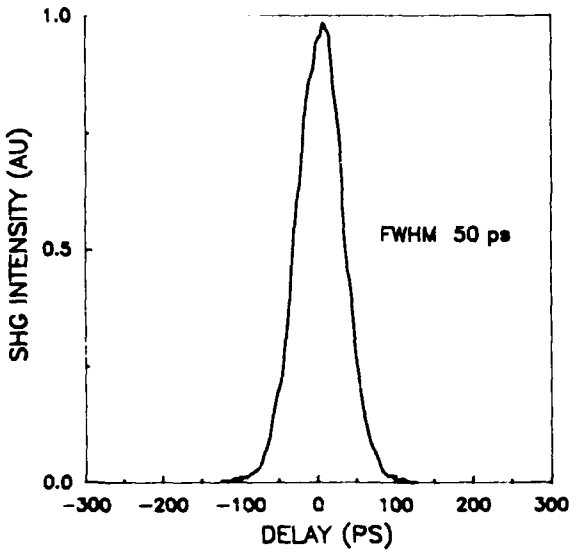

Fig. 2. Without external cavity.

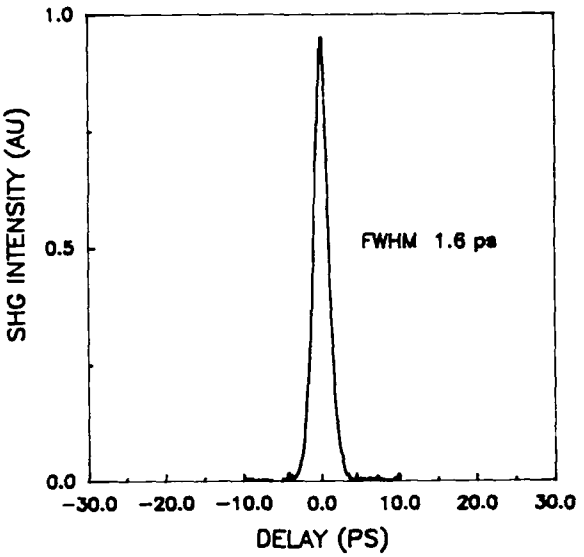

Fig. 3. With external cavity.

Figure 3 shows an autocorrelation of the output pulse from the laser including the nonlinear external cavity. The external cavity was operated with 100 mW of average power coupled into a 33 cm length of fiber. Under these conditions, the pulse duration was shortened to 1.6 ps. This pulse duration is commensurate with the bandwidth limit imposed by the two plate filter in the laser. Also, dispersive broadening in the optical fiber was recognized as a significant limiting factor for achieving femtosecond pulse durations. Previous investigations of external cavity modelocking have been performed near the dispersion minimum in optical fibers. However, since Ti:Al_2O_3 can produce extremely high output powers, dispersion may be reduced by using shorter fiber lengths. Results at this time are only preliminary and we believe that optimization of the operating parameters should produce shorter pulses.

We gratefully acknowledge helpful scientific suggestions from B. Zysset, L. Y. Liu, K. Hall, and H. Haus. This work was supported in part by the Joint Services Electronics Program Contract DAAL03-86-K-0002, the Air Force Office of Scientific Research Grant F49620-88C-0089, and the National Science Foundation 85-52701-ECS. The work at Lincoln Laboratory was supported by the U.S. Navy for the Strategic Defense Initiative Organization.

References

[1] P. F. Moulton, *J. Opt. Soc. Am. B* **3**, 125-133, Jan. 1986.
[2] L. F. Mollenauer and R. H. Stolen, *Opt. Lett.* **9**, 13 (1984).
[3] K. J. Blow and D. Wood, *J. Opt. Soc. Am. B* **5**, 629 (1988).
[4] K. J. Blow and B. P. Nelson, *Opt. Lett.* **13**, 1026 (1988).
[5] P. N. Kean, X. Zhu, D. W. Crust, R. S. Grant, N. Langford, and W. Sibbert, *Opt. Lett.* **14**, 39 (1989).
[6] J. Mark, L. Y. Liu, K. L. Hall, H. A. Haus, and E. P. Ippen, *Opt. Lett.* **14**, 48

MONDAY, MAY 1, 1989

NAUSET III

9:30 AM–10:30 AM

MB1–MB5

Ti:SAPPHIRE II / POSTER SESSION

Peter F. Moulton, Schwartz Electro-Optics, *Presider*

HIGHLY EFFICIENT, WIDELY TUNABLE KHz REP. RATE Ti:SAPPHIRE LASER PUMPED BY Nd:YLF LASER*

Rama Rao and Gary Vaillancourt
Excel Technology, Inc., 140–20 Keyland Court, Bohemia, N.Y. 11716
and
H.S. Kwok
State University of New York at Buffalo, Bonner Hall, Buffalo, N.Y. 14260
and
C.P. Khattak
Crystal Systems, Inc., 27 Congress Street, Salem, MA 01970

Abstract

Here we report, successful development of "all" solid state KHz repetition rate Ti:Sapphire laser pumped by a long pulse Nd:YLF laser. Ti:Sapphire laser delivers an average power exceeding 400 mW, pulse duration 10–12 nsec, peak power in excess of 30 KW and tunable in the spectral region of 670 nm –1070 nm for an input pump power of 1.7 Watts at 527 nm at 1 KHz.

Summary

In this we present, highly efficient and high repetition rate Ti:Sapphire laser tunable in a wide spectral region. In order to develop "all" solid state tunable laser and optimize the performance of Ti:Sapphire, first a long pulse (0.2–0.3 μsec) frequency–doubled Nd:YLF laser was designed and constructed. This laser was used to pump Ti:Sapphire crystal in a longitudinal pumping configuration. For an input power of 1.7 W at 527 nm and at 1 KHz, an output power of exceeding 400 mW and threshold pump power of 200 mW was observed at the peak of the gain curve of Ti:Sapphire at 800 nm. This is in contrast to Spectra Technology's recently reported (Laser Focus World, Jan. 1989, p. 25) results of an output power of 300 mW and threshold pump power of 3 W with an input power of 11.6 W in the Copper vapor laser pumped KHz Ti:Sapphire system. This highly efficient (23%) and low threshold performance of this new Ti:Sapphire laser is beleived to be due to the long pulse width of the Nd:YLF pump laser and as well as careful mode–matching of the pump beam to the cavity modes. A systematic study of pump pulse width versus Ti:Sapphire laser output is performed and the results will be discussed.

Tuning was carried out throughout the expected gain bandwidth of the laser by the insertion of Brewester's angled prism in the cavity. Observed tuning curves of the laser with different sets of optics is shown in Fig.1. This is the first time tuning was achieved in a wide spectral region from 670 nm to 1070 nm, in compared to the tuning range of 700–1000 nm reported for both cw Argon–ion pumped (Laser Focus, Dec. 1988, p. 12) and as well as dye laser pumped (Laser Focus World, Jan. 1989, p.9) Ti:Sapphire laser. In the present long pulse Nd:YLF pumped system, the output in the extended tail regions of the gain distribution of Ti:Sapphire was not dropping off as sharply as previously observed by many with 10–20 nsec pump pulse. The output at 690 nm, 800 nm, and 1.0 μ were observed to be approximately 350 mW, 400 mW, and 200 mW respectively for an input power of 1.7 W.

The temporal output of the Ti laser was observed to be considerably shorter than the pump pulse width; characteristic of gain switched operation. The gain switched operation of the Ti:Sapphire laser yielded an output pulse duration of 10–12 nsec with peak power exceeding 30 KW. With efficient frequency–doubling possible with the available high peak power of the system, a tunable radiation almost in the entire spectrum from UV to IR (335–1070 nm) becomes accessible at KHz repetition rates.

The output versus input energy (not absorbed energy) for various output coupler transmission at both ends of the gain curve (690 nm and 1.0 μ), are presented in Fig. 2 and 3 respectively. A detailed characterization of Ti:Sapphire performance including gain cross–section and cavity losses inferred from the laser threshold and slope efficiency will be presented.

* This work is supported by SDIO SBIR grant No. 88–C–0716 and NSF SBIR grant No. 8700034 and New York State Science & Technology Foundation grant No. SBIR (87)–139.

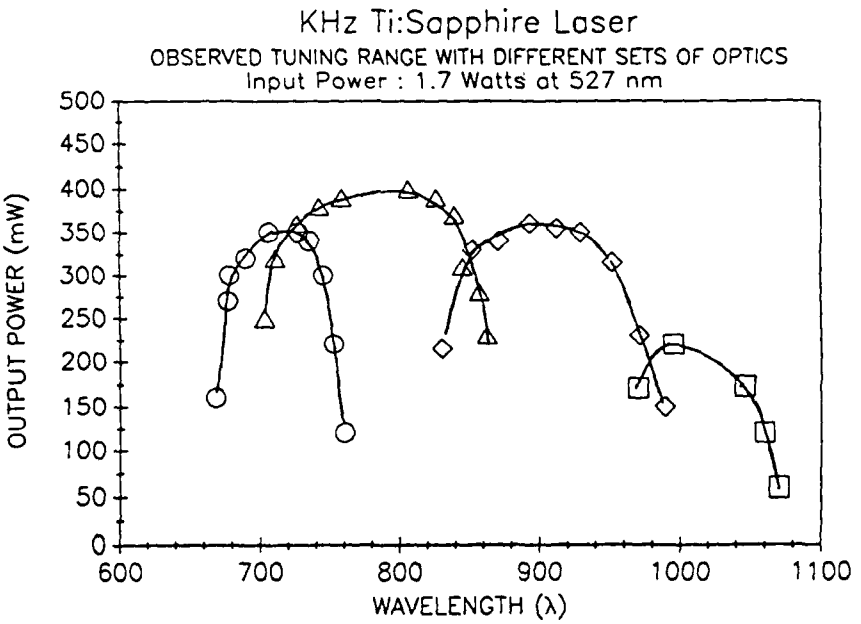

Fig.1. Observed tuning range of KHz Ti:Sapphire laser with different sets of optics.

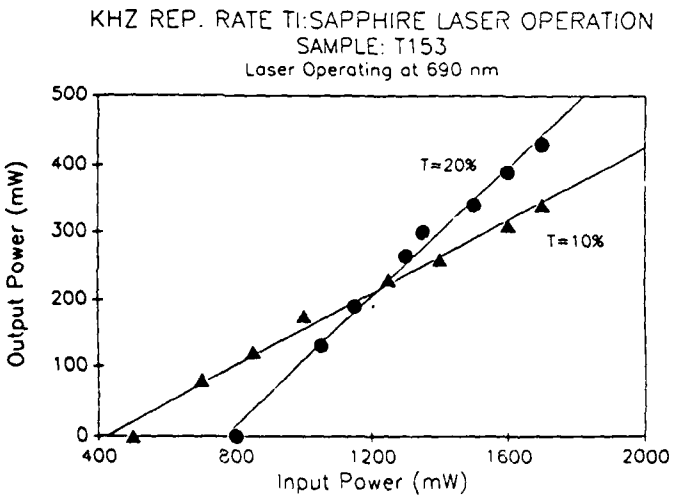

Fig.2. Input versus output energy of Ti:Sapphire laser operating at 690 nm for T = 10% and 20%

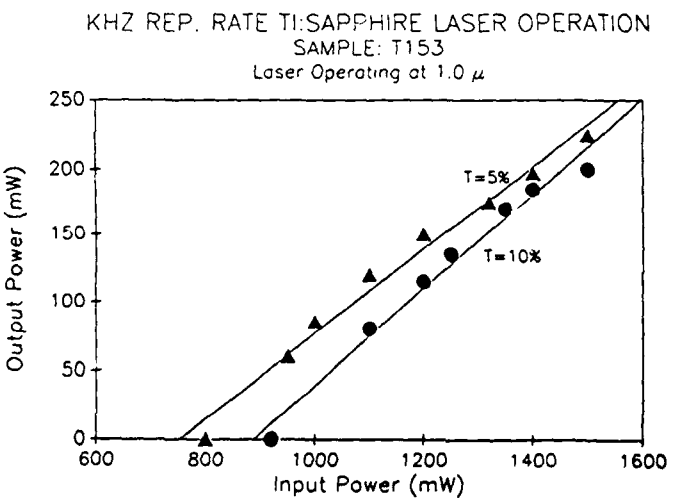

Fig.3. Input versus output energy of Ti:Sapphire laser operating at 1.0 μ for T =5% and 10%.

MB2-1

Paper Withdrawn

Dense-Plasma Light Source Pumped Ti Sapphire Laser

In H. Hwang+, Kyo D. Song, and Sang H. Choi
Source Tek Inc., 24 Carriage Hill Dr. Poquoson, VA 23662

The Ti sapphire is an attractive laser crystal for the development of a tunable solid state laser. This laser crystal has a wide absorption band(~200 nm) centered at near 490 nm and a wide tunning range(~350 nm) in the near infrared spectral range. Since the first laser operation of Ti sapphire crystal by P. Moulton[1], this laser material was pumped mostly by laser sources such as frequency-doubled Nd YAG, or dye lasers.

The first incoherent light source pumped Ti sapphire laser was reported by L. Esterowitz et al[2] by using a coaxial flashlamp. In the following research, P. Lacovara et al[3] reported a 300 mJ output energy from a linear flashlamp pumped Ti sapphire laser. However, due to the short lifetime(3~4μs) of the excited state of Ti^{+3} in the crystal host, the flashlamp must be discharged in a very short time for the efficient pumping and consequently the flashlamp life time is seriously shortened. Thus, the development of a powerful and long-life light source is a key issue for the reliable operation of an incoherent light source pumped Ti sapphire laser.

We report here a preliminary results of a Ti sapphire laser experiment in which a hypocycloidal-pinch(HCP) plasma light source was employed as the pumping source. The HCP device was proven to generate strong UV spectral power for the pumping of an iodine laser[4] and was successfully employed for the pumping of short wavelength dye laser[5,6]. The HCP is structually very strong and the electrical energy handling capability(>1kJ/inch) is much higher than any of conventional flashlamps. Also, the source inductance is very small(~20 nH) due to its coaxial structure therefore is suitable for obtaining fast rise time.

The experimental setup is depicted in Fig.1. The HCP light source is composed of a set of brass electrode disks and a set of Macor insulator disks alternately stacked. The operating gas used in this experiment was argon and the optimum pressure in the HCP device was found to be about 25 torr. The optical resonator is composed of a flat full reflector for the spectral range from 740 nm to 860 nm and a curved partial reflector. The size of Ti sapphire crystal used in this experiment was 6.4 mm dia. x 76.2 mm length and its figure of merit(FOM) was measured to be about 250. The end surfaces were not antireflection coated.

The output laser energies for different charging voltages of the energy storage capacitor(8μF) were measured with a surface absorbing disc calorimeter (Scientech 360001 with 362 indicator) as shown in Fig.2. An output energy of 0.5 J

was obtained with a 40% R output coupler when the charging voltage was 33 kV or the energy storered was 4.4 kJ. The laser pulse width measured with a Si photodiode had a FWHM of 2μs. The 0.5 J laser output energy obtained is among the highest of an incoherent light source pumped Ti sapphire lasers[7]. A redesign of the HCP light source is under way to improve the overall efficiency of the system because the present HCP light source was designed for the pumping of blue-green dye laser which requires a strong generation of near UV. Further effort will be stressed on the single longitudinal and transverse mode operation and the pulse shortening by employing Q-switch technique required for Lidar applications.

The authors would like to thank M. Kokta of the Union Carbide Corporation for the loan of the Ti sapphire laser rod. We also acknowledge the valuable advices of Ja H. Lee and Norman P. Barnes of NASA Langley Research Center. This research was supported in part by NASA Contract No. L-33522C monitored by A. Jaylink.

+ Research associate professor, Dept. of Physics, Hampton University, Hampton VA 23668

References

[1]. P. F. Moulton, Solid State Research Quarterly Technical Summary Report, MIT Lincoln Laboratory, (May 1~July 31,1982) pp. 15~21.

[2]. L. Esterowitz, R. Allen and C. P. Khattak, Tunable Solid State Lasers ed. P. Hammerling, A. B. Budgor and A. Pinto, Springer-Verlag, New York, N.Y. (1985) pp. 73~75.

[3]. P. Lacovara, L. Esterowtz and R. Allen, Optics Lett. 10, 273 (1985).

[4]. J. H. Lee, D. R. McFarland and F. Hohl, Appl. Optics 19, 3343 (1980).

[5]. K. S. Han, S. H. Nam and J. H. Lee, J. Appl. Phys. 55, 4113 (1984).

[6]. K. S. Han, C. H. Oh and J. H. Lee, J. Appl. Phys. 60, 3414 (1986).

[7]. E. G. Erickson, LEOS '88, Santa Clara, CA Oct. 30~Nov. 4, 1988, paper EL2-1.

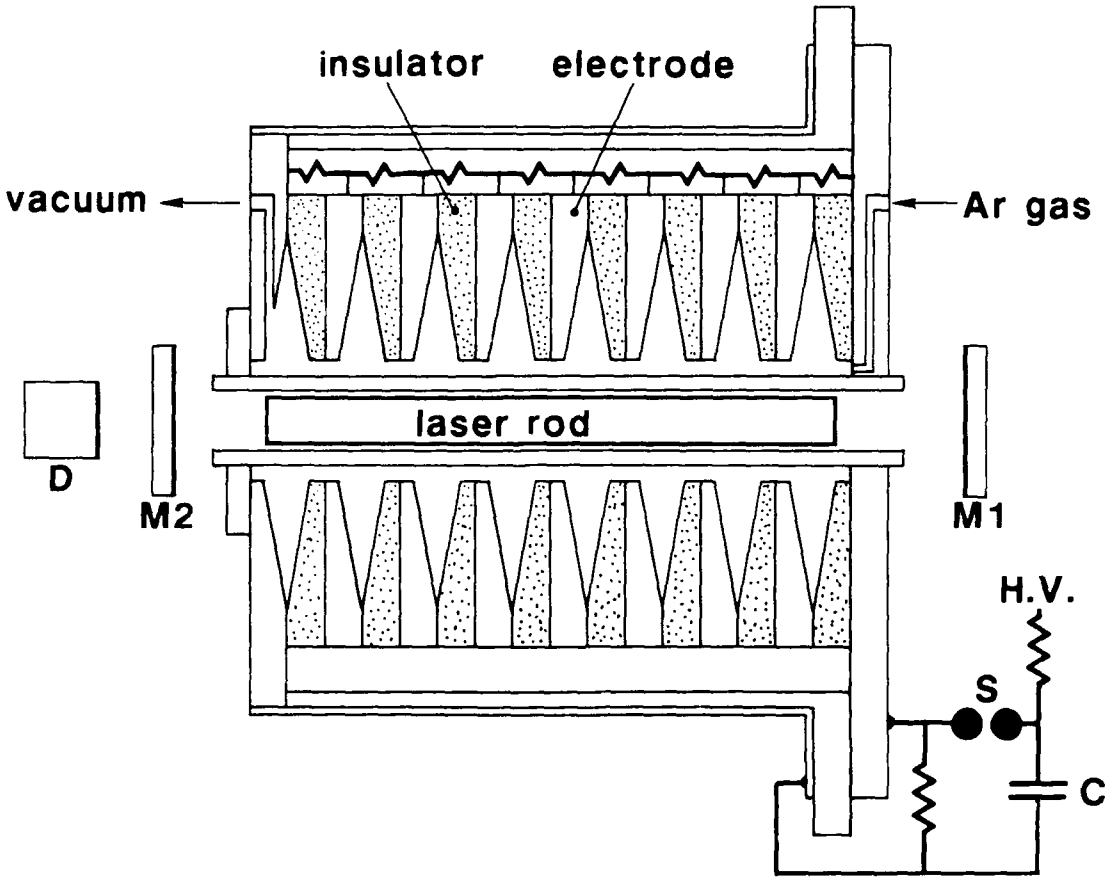

Fig. 1. Schematic diagram of the HCP light source pumped Ti sapphire laser.

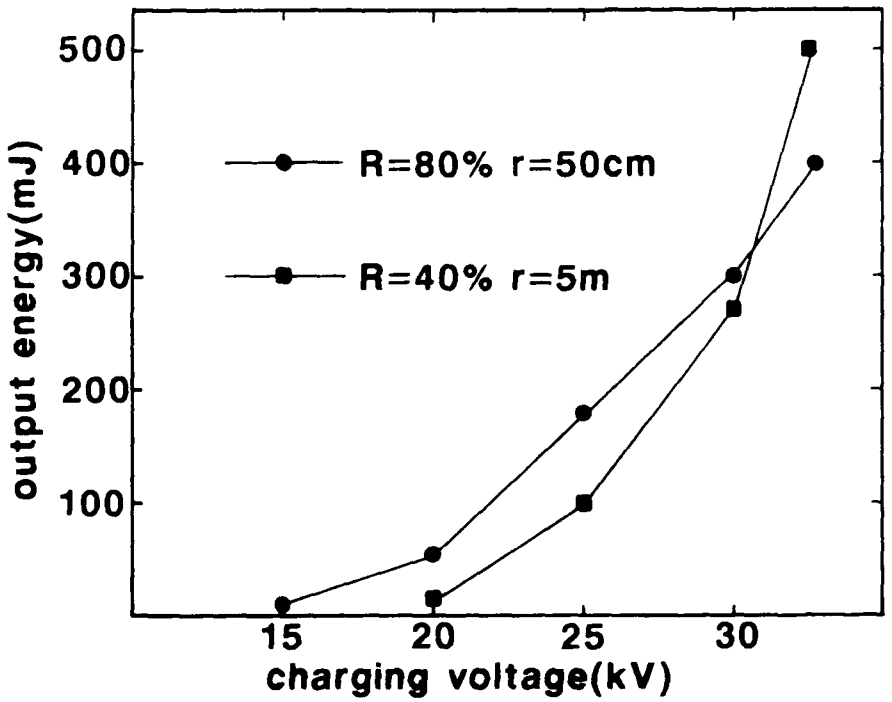

Fig. 2. Output energy dependence on the charging voltage to the energy storage capacitor for different output mirror parameters.

Amplification of 25-ps AlGaAs laser diode pulses at 1kHz in Ti-doped Sapphire

Santanu Basu, Paul May and Jean-Marc Halbout
IBM Research Division
Thomas J. Watson Research Center
P.O. - 218, Yorktown Heights, NY 10598

Introduction

The time-resolved spectroscopy of GaAs-AlGaAs multiple quantum wells requires a high-peak-power subpicosecond light source which is tunable near 850 nm. The laser source should operate at greater than 1 kHz repetition rate to facilitate lock-in detection techniques for improved signal to noise ratio. In the past, short pulses in this wavelength range has been produced by continuum generation in ethylene glycol by focused beams of ultrashort pulses from a 805 nm dye laser[1]. The Ti-doped sapphire has an emission spectrum extending from 600 nm to 1100 nm[2], and is an excellent candidate for generating tunable radiation near 850 nm. To obtain short pulses in this wavelength region, we propose to injection seed a gain-switched Ti-doped sapphire oscillator by 25-ps pulses from a laser diode. Upon injection seeding, the stored energy in the gain switched Ti-doped sapphire oscillator can be efficiently extracted in a series of 25-ps pulses separated by the cavity round trip time[3]. The resulting high peak output power would enable subpicosecond pulse generation by standard pulse compression techniques in a fiber-grating pair. Recently, an injection-seeded Ti-doped sapphire oscillator has generated 70 dB gain of 400 fs pulses from a synchronously pumped dye laser at 790 nm[4].

Experiment

In our experiment, an AlGaAs laser diode (Mitsubishi ML5101A) at 830 nm was gain-switched by the application of 90-ps-duration voltage pulses from a step recovery diode at 100 MHz to generate optical pulses with rise times of 24 ps. It was shown that the shortest pulses which can be obtained from this laser by spectrally filtering out the relaxation oscillations is 19 ps[5]. The laser diode has a rated wavelength tuning rate of 0.25 nm/°K. The experimental arrangement for gain measurement is shown in figure 1. A 15 mm long Ti-doped sapphire rod with ends cut at 60 degrees to the rod axis was used for the gain measurement. The diode laser beam was incident at Brewster angle and both the pump and the probe beams were π-polarized. The pump beam was obtained from a cw pumped and Q-switched Nd:YAG laser (Quantronix model 416). The

Nd:YAG laser is rated to produce 150-ns-long Q-switched pulses at 1.064 μm at up to 25 kHz repetition rate. The Q-switched laser output was frequency doubled to obtain 122 microjoule per pulse at 532 nm for pumping. The absorption of the pump beam in the 15 mm long crystal was measured to be 87.5%.

An anamorphic prism pair was used to generate a circular beam from the laser diode. The collimated pump and the probe beams were focused by means of a 75-mm focal length lens on the input face of the Ti-doped sapphire crystal. A synchroscan streak camera(Hamamatsu), a spectrometer and a power meter were used for gain measurement. The unamplified pulse shape as recorded on the streak camera is shown in figure 2(a). The pulse rise time is 24 ps and the long trailing edge is due to the relaxation oscillations in the gain switched laser diode. For this experiment, the input to the diode laser was 11.75-V pulses from a step-recovery diode at 100 MHz repetition rate in combination with a bias current pulse of 0.85 microsecond duration. The laser was biased below threshold. The bias current was optimized in the experiment to obtain the shortest pulse on the streak camera. The bias pulse was also optimally delayed with respect to the pump pulse for maximum gain. The amplified pulse is shown in figure 2(b). The amplification is 4.7 dB for an input pump energy of 122 μJ.

Discussion

The wavelength of GaAlAs laser diodes range from 800 nm to 860 nm, and the emission wavelength may be temperature tuned at a rate of 0.25 nm/^{0}K. Thus it is possible to construct widely tunable and high-peak-power subpicosecond laser sources in Ti-doped sapphire oscillators by injection seeding with short pulses from commercially available GaAlAs laser diodes.

A three mirror cavity oscillator comprising of two 12.5 cm radius of curvature high reflecting mirrors and a 10% T flat output coupler will be used for our injection seeding experiment. For a resonator length of 60 cm, the resonator beam waist is calculated to be 38 micron. With 122 μJ of input pump energy at 532 nm, and with a measured single pass exponential gain coefficient of 1.1, the output energy per pulse envelope is estimated to be 25 μJ. Upon injection seeding by 25-ps pulses from the diode laser, the energy will be extracted in a series of 25-ps pulses under a gain-switched pulse envelope. The high peak power of the injection seeded laser output will enable subpicosecond pulse generation by standard pulse compression technique. It should also be noted that the passively mode-locked diode lasers, which have generated 0.83 ps pulses, may also be used for injection seeding a Ti-doped sapphire oscillator[6]. We will report the gain switched laser operation in this paper.

1. W.H. Knox, J. Opt. Soc. Am. B, vol. 4(11), p. 1771, 1987.
2. P.F. Moulton, J. Opt. Soc. Am. B, vol. 3(1), p. 125, 1986.

3. S. Basu and R.L. Byer, paper THV1, Conference on Lasers and Electro-Optics, Anaheim, CA, 1988.
4. P. Schultz, M.J. Lagasse et. al., paper MEE2, OSA annual meeting, Santa Clara, CA, 1988.
5. S. Basu, P. May and J.M. Halbout, Picosecond Electronics and Optoelectronics Conference, Salt Lake City, Utah, 1989.
6. Y. Silberberg and P.W. Smith, IEEE J. Quantum Electron., vol. QE-22(6), p. 759, 1986.

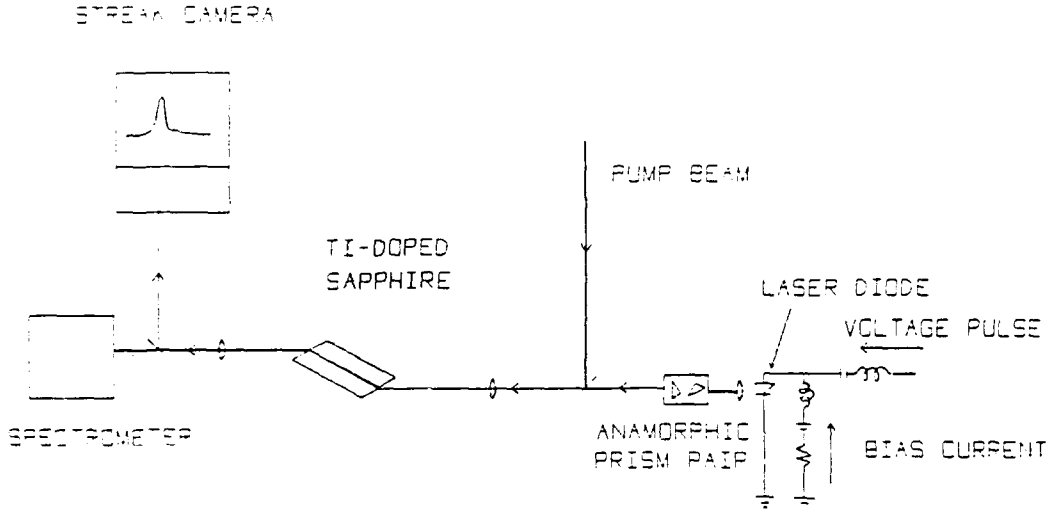

Figure 1. A schematic of the experimental arrangement for amplification of laser diode pulses at 1-kHz repetition rate in Ti-doped Sapphire.

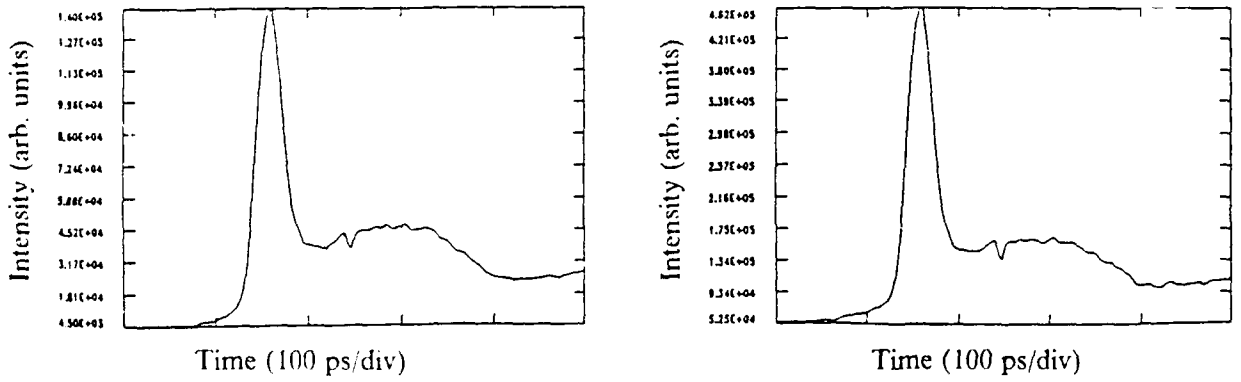

Figure 2. Streak Camera display of the laser diode output. (a) The 830-nm laser diode pulse in absence of the pump pulse, (b) The pulse amplified in Ti-doped Sapphire. The measured amplification is 4.7 dB at 122 μJ of pump energy. The baseline increase in (b) is due to the background fluorescence signal.

Efficient, High-Average-Power, Liquid-Nitrogen-Cooled Ti:Al_2O_3 Laser

S. R. Henion and P. A. Schulz

Lincoln Laboratory, Massachusetts Institute of Technology
Lexington, Massachusetts 02173

A high-average-power, efficient, single-transverse-mode Ti:Al_2O_3 laser suitable both for mode-locked operation and for long-pulsed, high-power pumping without damage to the laser crystal has been built using a large focal spot and liquid nitrogen cooling. A Ti:Al_2O_3 laser pumped by a 20-W argon-ion laser demonstrates a seven fold increase in power on cooling from 300 K to 77 K and has been mode-locked. This laser was also pumped by a 0.4-J, 150-μs long pulse in which liquid nitrogen cooling increased output power by a factor of four.

The achievement of efficient, high-average-power, single-transverse-mode solid state lasers is inhibited by pump-induced thermo-optical distortions.[1-3] These distortions are minimized by using small gain regions,[4] but high-power radiation focused onto small areas damages crystals. For example, a mode-locked laser with average power of 1 W and mode-locking frequency of 100 MHz generating 0.1-ps pulses has a peak intensity at a 20-μm beam waist radius of nearly 10^{10} W/cm^2, which is close to the damage threshold of Al_2O_3. Damage to the laser crystal can be avoided by designing the laser with a large spot size. The thermo-optical distortions inherent in high-power Ti:Al_2O_3 lasers with large spot sizes can be reduced by increasing the thermal conductivity.[5]

For Al_2O_3 the thermal conductivity[6] increases from 0.33 W/cm-K at 300 K to 10 W/cm-K at 77K, a factor of 30. Although the temperature dependence has not been measured in Ti:Al_2O_3, a substantial increase in thermal conductivity can be expected as the temperature is decreased.

The effects of cooling were observed for cw operation of a Ti:Al_2O_3 laser pumped by a 20-W argon ion laser. A folded, three-mirror, (R_1, R_2=25 cm; R_3=∞) astigmatically compensated cavity with a total length of 100 cm was used, similar to the cavity of Sanchez, *et al.*[7] The pump beam radius at the crystal was approximately 65 μm. With 15 W of green light absorbed by the 42-cm long crystal, the thermal heat load was 2×10^4 W/cm^3. The Ti:Al_2O_3 crystal was located in an evacuated, liquid nitrogen Dewar inside the laser cavity. Indium foil was used to obtain good thermal contact between the crystal and copper heat sink. Since the laser mirrors were outside the Dewar, low loss Brewster-angled windows formed the 10^{-7}-Torr vacuum seal. A view port was used to aid in alignment.

The Ti:Al_2O_3 laser was adjusted at room temperature to a maximum output of 0.4 W. Upon cooling, the output rose to 1.9 W. With the crystal at 77 K the mirrors were readjusted to obtain

an output power of 2.8 W. A 20% increase in output power is expected because the non-radiative rate decreases at lower temperatures. [8] However, the very large increase in output power with cooling is only consistent with a decrease in thermo-optical distortions upon cooling.

In our cavity the slope efficiency of 20% observed at 77 K is much larger than the slope efficiency observed at room temperature, but is no greater than has been obtained at room temperature in other cavities.[9] Our cavity is particularly susceptible to thermo-optic distortions due to the large spot size in the Ti:Al_2O_3 crystal and the three-mirror cavity configuration. The liquid nitrogen cooling alleviates thermal effects in the present cavity, but is unlikely to substantially improve operation of a cavity that is optimized for room temperature operation.

Assuming the dn/dT term in the equation for the focal length of the thermal lens[3] is the major contribution, the focal length for the operating conditions described above is 2.1 cm at 300 K and 65 cm at 77 K. Although the assumption that the focal length of the lens is much longer than the crystal length is not valid, these focal lengths are a qualitative indication of the strength of the thermo-optic effects. A simple thermal lens in the cavity can be easily compensated by changing the mirror separation to improve the laser performance. However, other thermo-optic effects such as astigmatism and spherical aberration cannot be compensated in this way. Hence, cooling or cavity parameter changes are necessary to obtain efficient high-power, single-transverse-mode operation.

Mode-locked output of the liquid-nitrogen-cooled Ti:Al_2O_3 laser has also been obtained using second harmonic mode locking.[10] With 15 W pump, 36-ps pulses at a repetition rate of 125 MHz with 0.8 W average power were generated. The mode locking was accomplished with a 125-MHz standing-wave acousto-optic modulator and a cavity length of 120 cm.

In addition, the same laser was used in pulsed operation with minor modifications. An amplified, mode-locked Nd:YAG was frequency doubled in $LiIO_3$ to pump the Ti:Al_2O_3 laser. The output of the pump at 532 nm consisted of 150-μs train of 100-ps pulses every 10ns, repeated at a 10 Hz rate and had an average power of 4 W. The crystal was moved away from the pump focus to avoid damage, resulting in a 200 μm beam radius.

Figure 1 shows the output power versus input power for cooled and uncooled operation of the pulsed laser. As in the cw case, the laser was adjusted for maximum output under uncooled conditions and then cooled. The cooling increased the output a factor of four. Based on a simple model,[7] the slope efficiency shown in Fig. 1 should be independent of non-radiative relaxation rates. Once again, the cooling reduces thermo-optic distortion and thereby increases efficiency.

We thank T.Y. Fan and W. E. DeFeo for collaboration in the pulsed laser work and J. Goodberlet and Professor J. G. Fujimoto for help in measuring the pulse width of the mode-locked laser.

References

1. P.A. Schulz, IEEE J. Quantum Electron., **QE-24**, 1039 (1988).
2. S. DeSilvestri, P. Laporta, and V. Magni, IEEE J. Quantum Electron., **QE-23**, 1999 (1987).
3. W. Koechner, *Solid State Laser Engineering* (New York: Springer-Verlag, 1978) p. 359.
4. A. Sanchez, R.L. Aggarwal, A.J. Strauss, and R.E. Fahey, IEEE J. Quantum Electron., **QE-24**, 995 (1988).
5. P.F. Moulton, J. Opt. Soc. Amer. B, **3**, 125 (1986).
6. C. Kittel, *Introduction to Solid State Physics*, 3rd ed (New York, J. Wiley and Sons, 1968) p. 192.
7. A. Sanchez, R.E. Fahey, A.J. Strauss, and R.L. Aggarwal, Opt. Lett., **11**, 363 (1986).
8. P. Albers, E. Stark, and G. Huber, J. Opt. Soc. Amer. B, **3**, 134 (1986).
9. A. Alfrey and T. Baer, Spectra-Physics (private communication) and Spectra-Physics Ti:Al_2O_3 laser product literature.
10. U. Keller, J.A. Valdmanis. M.C. Nuss, and A.M. Johnson, IEEE J. Quantum Electron., **QE-24**, 427 (1988).

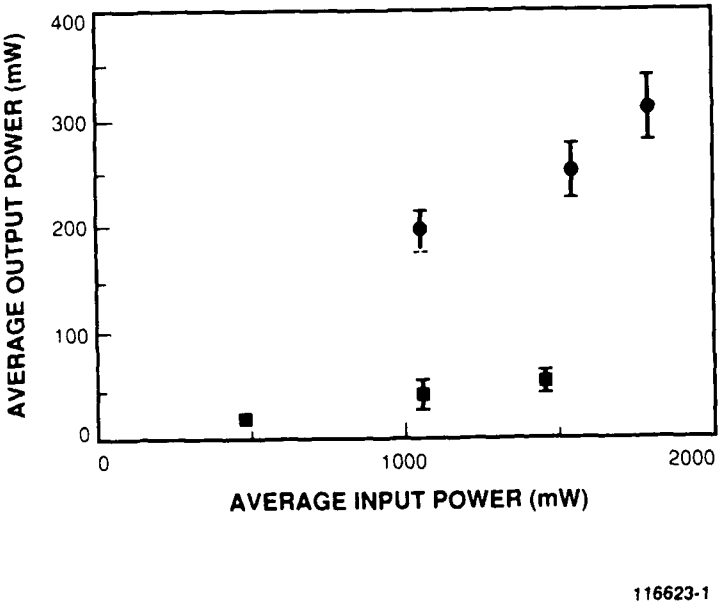

Figure 1. Laser output power improvement with cooling. When operated with liquid nitrogen cooling (circles), the average output power versus input power characteristics are improved by a factor of four compared with room temperature operation (squares). The Ti:Al_2O_3 laser was operating at 809 nm.

MONDAY, MAY 1, 1989

NAUSET IV

10:30 AM–12:00 M

MC1–MC3

NOVEL LASER SCHEMES

William F. Krupke, Lawrence Livermore National Laboratory, *Presider*

MC1-1

The Flashlamp Pumped Titanium Sapphire (Ti:S) Laser

Edward G. (Bud) Erickson
GTE Government Systems Corporation
P.O. Box 7188
Mountain View, CA 94039
(415) 966-2988

In late 1987, Union Carbide, while under subcontract tc GTE on a DARPA-sponsored program, solved the in-band (700-1000 nm) optical loss problem which has been plaguing the Ti:Sapphire laser material for six years. This breakthrough has allowed Ti^{3+} concentrations up to ~0.2% while maintaining 800 nm optical losses to as low as 0.4%/cm. With such high concentrations, high energy flashlamp pumping of Ti:Sapphire has become a reality. As of early January '89, output energies in excess of 3.0J/pulse at 800 nm in 12 micro-seconds with 2% efficiency and at 1PPS, and tuning between 670 nm and 1060 nm has been demonstrated. Over 1.4J/pulse at ~900nm has also been demonstrated. This paper will present the latest results achieved by May '89 in high energy, high average power flashlamp pumping of Ti:Sapphire, including energy per pulse at various wavelengths,
techniques for tuning and flashlamp considerations including short current pulse flashlamp lifetimes in excess of 10^8 shots. In addition, results of enhanced pump efficiency through fluorescent conversion of the lamp UV emissions to the visible pump band utilizing a flowing dye/solvent as a cooling fluid, will be presented.

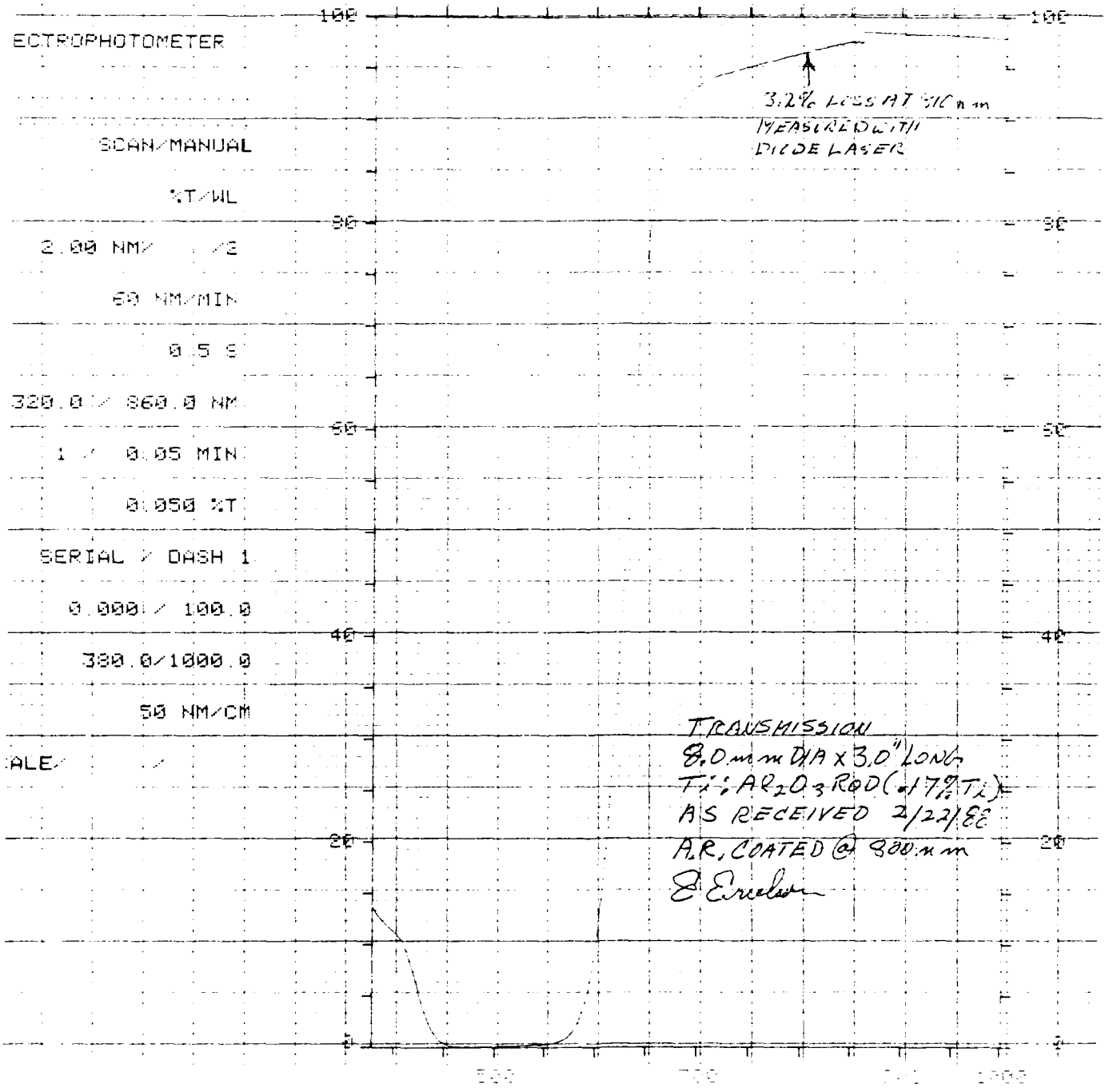
ECTROPHOTOMETER
SCAN/MANUAL
%T/WL
2.00 NM/ /3
60 NM/MIN
0.5 S
320.0 / 860.0 NM
1 / 0.05 MIN
0.050 %T
SERIAL / DASH 1
0.000 / 100.0
380.0/1000.0
50 NM/CM
ALE/ /
100
90
80
70
60
50
40
30
20
10
3.2% LOSS AT 810 nm
MEASURED WITH
DIODE LASER
TRANSMISSION
8.0 mm DIA x 3.0" LONG
Ti:AR2O3 ROD (.17% Ti)
AS RECEIVED 2/22/88
A.R. COATED @ 800 nm
E Ercelan

FIG 1

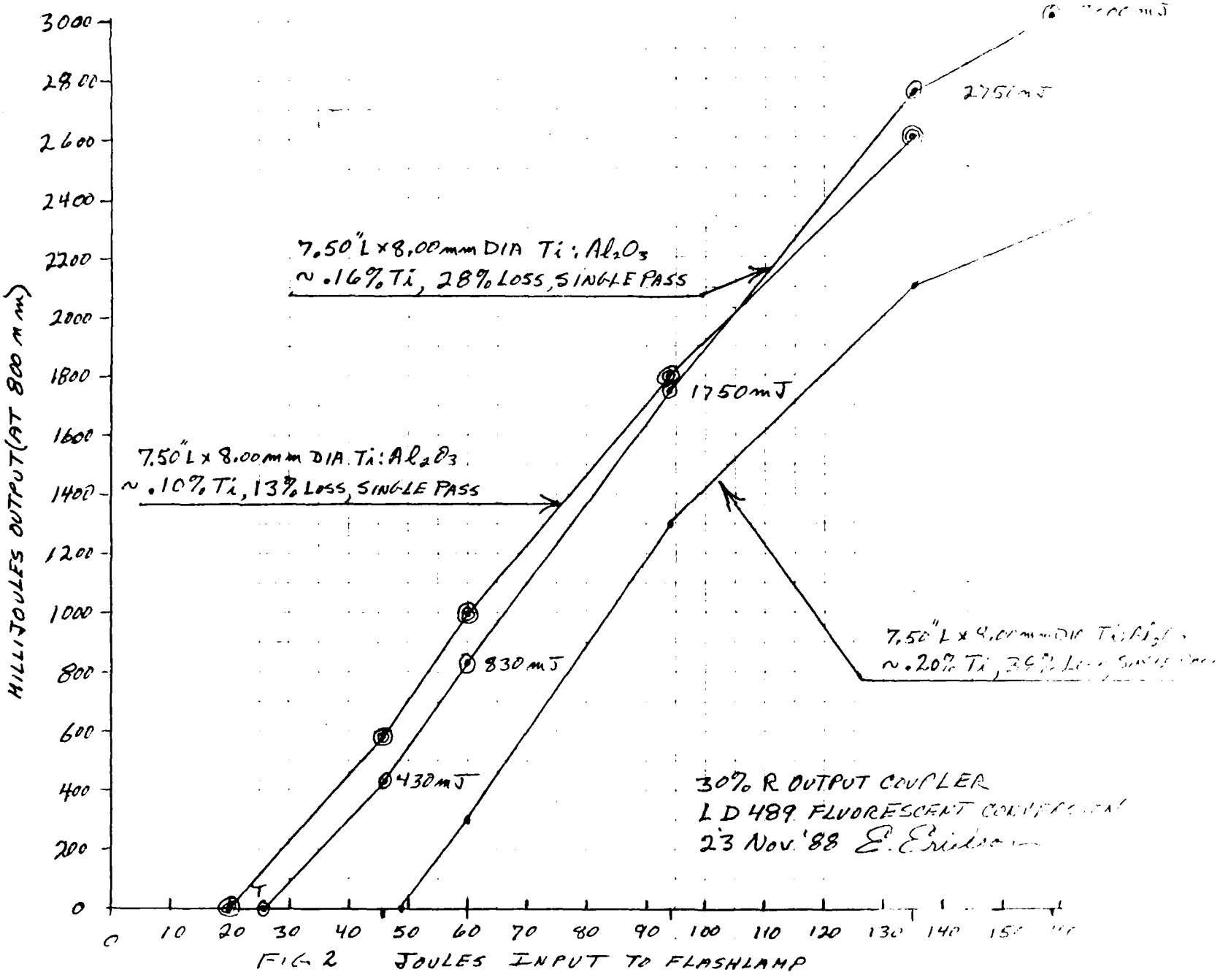
HILLIJOULES OUTPUT (AT 800 nm)
3000
2800
2600
2400
2200
2000
1800
1600
1400
1200
1000
800
600
400
200
0
0 10 20 30 40 50 60 70 80 90 100 110 120 130 140
JOULES INPUT TO FLASHLAMP
7.50"L x 8.00mm DIA Ti:Al2O3
~.16% Ti, 28% LOSS, SINGLE PASS
7.50"L x 8.00mm DIA Ti:Al2O3
~.10% Ti, 13% LOSS, SINGLE PASS
2751mJ
1750mJ
830mJ
430mJ
30% R OUTPUT COUPLER
LD 489 FLUORESCENT COUPLER
23 Nov '88 E. Erickson

FIG 2

11/11/83 9J/J in , 3J/J out

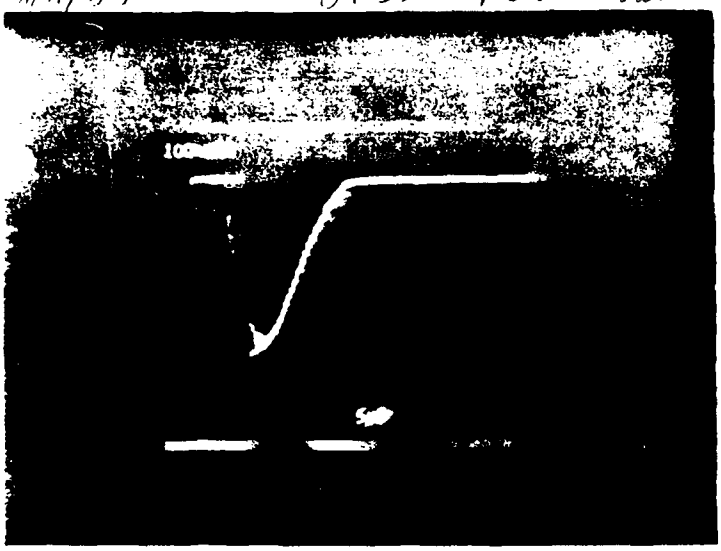

5μS/DIV

16KV LASER OUT I Pulse Trig

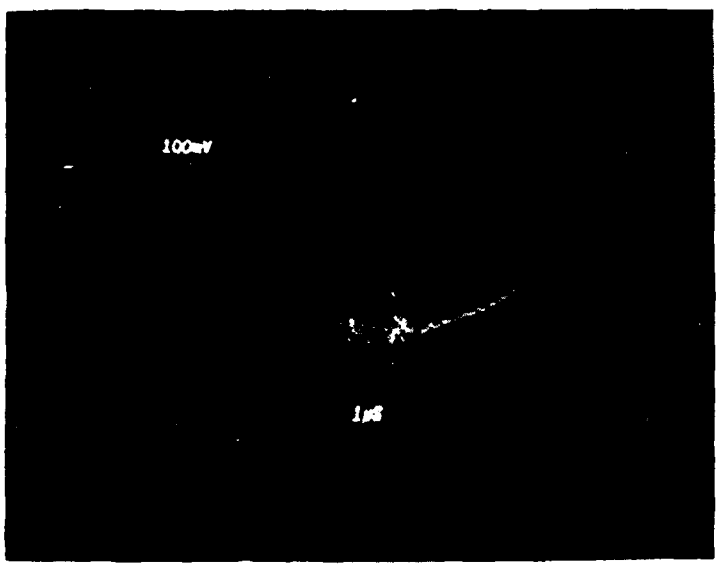

1μS/DIV

LASER O.T ~~480~~ mJ/P

(NEGATIVE GOING SIGNAL)

TEMPORAL PULSE SHAPE
800 mJ/P AT 800 nm
FLASHLAMP PUMPED $Ti:Al_2O_3$

FIG 3

EFFICIENT TUNABLE SOLID STATE LASER USING RHODAMINE DOPED SILICA

F. SALIN, G. LE SAUX, P. GEORGES, A. BRUN
and J. ZARZYCKI*

Institut d'Optique Théorique et Appliquée
B.P. 43, 91406 ORSAY Cédex, FRANCE

(*) Laboratoire des Matériaux Vitreux
Université des Sciences et Techniques du Languedoc
34060 MONTPELLIER, FRANCE

=====

Considerable effort has been directed in recent years to obtain new laser media for tunable solid state lasers. However, crystal growth reeds specialize equipement and production costs remain relatively high. Recent developments in the sol-gel techniques offer promising prospects in introducing dyes into inorganic matrices. Sol-gel methods enable single or multi-component glasses to be prepared at low temperature without having to reach the fusion temperature. It is possible to incorporate an organic dye into the starting mixture before the gelling process. The resulting doped gel can be dried at low temperature (60°C). This leads to an amorphous material (xerogel) with extremely fine pores (nanometer size) wich do not impair the optical properties of the material. The incorporated dye is uniformly embedded in the resulting inorganic host matrix. Recently laser ac-

tion has been reported in a transparent alumina-gel film doped with a laser dye (1) but with low efficiency. In the present work, tunable laser action is demonstrated in a silica gel doped with sulforhodamine 640.

Experiment were conducted with a heavily doped sample. The absorption band extend from 400 nm to 600 nm. The absorption of the sample is too important to be accurately measured. The fluorescence spectrum extend from 600 to 670 nm with a peak value at 620 nm. The fluorescence decay was recorded with a fast photodiode and gives an excited state lifetime of about 10 ns. The sample was pumped by a 6 ns pulse at 532 nm.

Laser action was achived with a two mirror cavity. Pumping with 532 nm, 6 ns pulses from a doubled Nd:YAG laser leads to laser emission at 621 nm. Using a simple uncoated glass plate as output coupler gives slope efficiency of about 20 %.

we have also investigated tunable properties of this laser.In this experiment one of the mirrors was replaced by a 600 g/mm grating used at Littrow incidence.By rotating the grating we were able to tune the laser wavelength over 50 nm.in this case the efficiency felt to 12 % .Results obtained with new samples

will be presented at the conference.

[1] Y.Kobayashi, Y. Kurokawa, Y. Imai and S. Muto

J. Non Cryst. Solids 105,198 (1988)

DIFFRATION LIMITED SOLID-STATE LASERS WITH SUPERGAUSSIAN MIRRORS

G.Cerullo, V.Magni, R.Riva, and O. Svelto

Centro Elettronica Quantistica e Strumentazione Elettronica, C.N.R.
Istituto di Fisica del Politecnico
P.za L. da Vinci 32, 20133 Milano, Italy

P.Laporta

Dipartimento di Ingegneria Elettronica,
II Università degli Studi di Roma,
Via O. Raimondo, 00173 Roma, Italy

SUMMARY

Unstable resonators with mirrors of radially variable reflectivity are very attractive for the generation of diffraction limited laser beams of high energy or power. This solution offers two main advantages: (i) Smooth profile and good propagation characteristics of the output beam. (ii) Reasonably large mode volume and high discrimination among transsverse modes. So far, a few laser cavities using mirrors of nearly gaussian reflectivity profile have been proposed and experimentally tested [1,2]. In this work we propose the use of mirrors with supergaussian reflectivity profile [3,4] and we point out the advantages of these mirrors compared to mirrors with gaussian profile. Furthermore, we consider two implementations of this type of output coupler, based on a radially variable interferometer or on radially variable evaporated thin films. The reasons for the choice and the advantages of the supergaussian reflectivity profile will be shown to be as follows: (i) The cavity modes turn out to be bell-shaped and considerably flatter than those obtainable from mirrors of gaussian profile. This substantially increases the mode volume within the active material yet preserving good diffraction properties. (ii) The mode equation is amenable

to a simple analytical solution within the framework of geometrical optics. This allows simple equations for the resonator design to be obtained.

Following this discussion on the advantages of supergaussian mirrors, some design procedure to determine the resonator configuration and the mirrors parameters will be presented. The aim here is to find the most suitable compromise between the filling of the active material by the transverse mode profile, the misalignment sensitivity, and the discrimination against the higher order modes.

For the experimental viewpoint, the techniques which have been used to obtain the supergaussian mirrors will be discussed. The application of these mirrors to a flashlamp--pumped Nd:YAG laser with unstable resonators of different magnifications will also be discussed. Diffraction limited output beams with nearly flat-top profile and output energies as high as 400 mJ (at 22.5 J input energy) have been obtained.

As a conclusion we can say that mirrors with supergaussian reflectivity profile will play a very important role both for cw and pulsed lasers when a diffraction limited beam of high power or energy is required.

REFERENCES

1. G.Giuliani, Y.K.Park and R.L.Byer
   Opt. Letters 5, 491 (1980)

2. N.McCarthy and P.Lavigne
   Opt. Letters 10, 553 (1985)

3. S.De Silvestri, P.Laporta, V.Magni, O.Svelto and V.Majocchi, Opt. Letters 13, 201 (1988)

4. S.De Silvestri, P.Laporta, V.Magni and O.Svelto
   IEEE J. Quantum Electron. QE-24, 1172 (1988)

NOTES

MONDAY, MAY 1, 1989

NAUSET IV

1:30 PM–3:00 PM

MD1–MD4

MOSTLY Cr LASERS

Robert C. Morris, Allied-Signal, Inc., *Presider*

BROADBAND TUNABILITY OF GAIN-FLATTENED QUANTUM WELL SEMICONDUCTOR LASERS WITH AN EXTERNAL GRATING

Michael Mittelstein, David Mehuys, and Amnon Yariv
Department of Applied Physics, 128-95
California Institute of Technology, Pasadena CA 91125

Rona Sarfaty and Jeffery E. Ungar
Ortel Corporation
2015 West Chestnut Street, Alhambra, CA 91803-1542

SUMMARY

Spectral tuning ranges reported for semiconductor injection lasers have been limited to below 10% of the central photon energy of operation until recently [1,2]. An improved understanding of the properties of quantum well lasers has allowed us to design optimized devices and implement simple external cavity configurations to achieve broadband tuning ranges exceeding 10% [3-6].

The gain bandwidth, and hence tuning range, of any semiconductor laser can be increased by increasing the population of the high energy states in the conduction and valence bands ("band-filling"). However, the tuning range of conventional double heterostructure semiconductor lasers is limited to approximately 100 meV by the current density at which these devices can be operated successfully. Quantum well lasers differ from double heterostructure lasers in that they possess a much reduced active volume; this reduces the current density required for operation and thereby opens opportunities for greater band-filling. Furthermore, they exhibit quantum-size effects due to their very small active layer thickness: the most striking consequences are quantized electron and hole states confined by the quantum-well structure. Band to band transitions involving the first quantized state only are invoked in low operating current density applications, while at moderate operating current densities second quantized state transitions contribute to increase the gain at the high photon energy side of the spectrum. Gain spectra calculations for quantum well injection lasers predict, for a particular pumping condition, a wide spectral range of nearly flat gain [3-6], as seen in Figure 1 trace (b). This nearly flat, wide gain spectrum is achieved by balancing the peak gain near the first and the second state transitions (see Figure 1 at 1.49 eV and 1.60 eV respectively) [3-6].

The separation in photon energy between the first and the second quantized state transitions is the prime parameter which determines the total width of the tuning range.

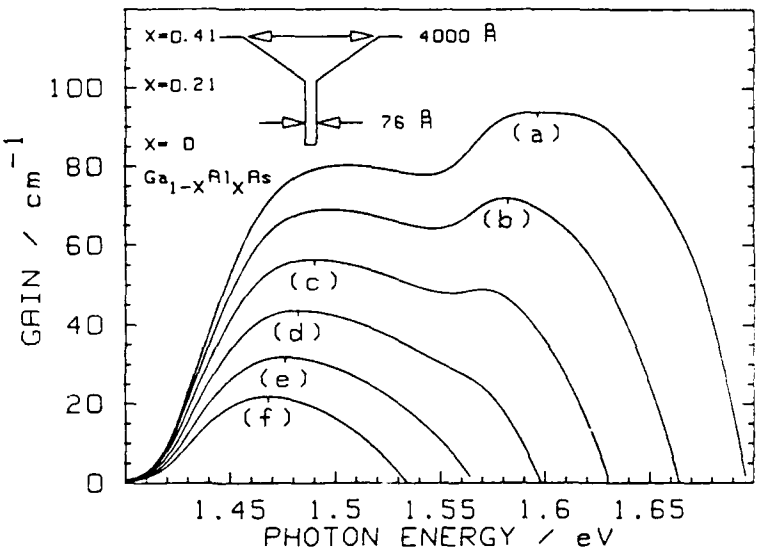

Figure 1: Computed gain spectra of the single-quantum-well structure shown in the inset. The pump current density is: (a) 1830, (b) 1350, (c) 950, (d) 630, (e) 405, and (f) 255 A cm^{-2} respectively.

This separation is controlled by the thickness of the quantum well and the laser structure. Properly designed quantum well lasers can have an effective tuning range, at moderate current densities, some 5 times larger than conventional semiconductor lasers at the same current density [6].

For the experiments, a Hansch type tunable laser oscillator is used, as shown in Figure 2. The waveguide at the rear facet of the laser emits a diffraction-limited expanding beam outside the crystal, which is collimated with a high numerical aperture lens system. This expanded beam illuminates a blazed diffraction grating in Littrow orientation. The orientation of the grating is such that the small transverse width of the waveguide forms the selective element for the dispersed light. The spectral resolution is estimated to be a quarter of a nm, which is sufficient to enforce single longitudinal mode operation of the short Fabry-Perot lasers used here. The lasers used in the experiments are uncoated for simplicity. The improvements due to anti-reflection coating are of second order at the operational conditions used.

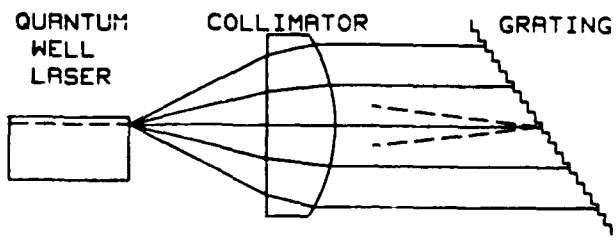

Figure 2: Schematic of the external resonator configuration.

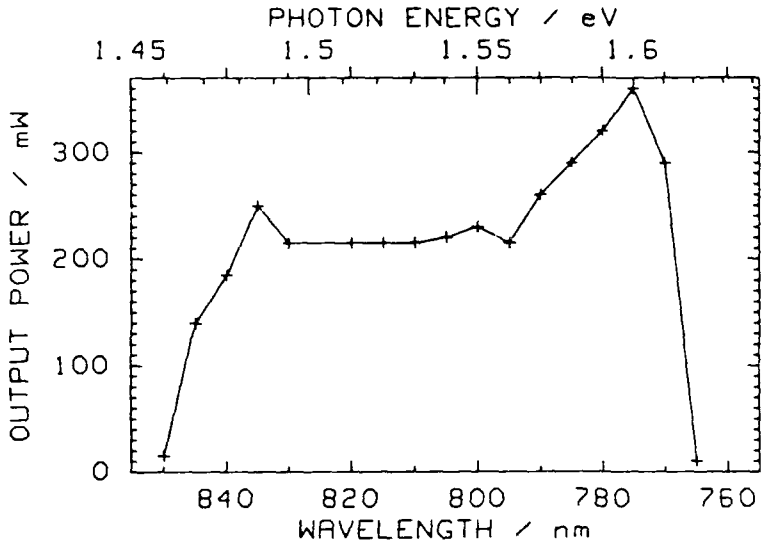

Figure 3: Resulting single mode output power of an external cavity grating-tuned single-quantum-well semiconductor laser.

Figure 3 indicates the maximum power output from the front facet (under pulsed current operation) for grating-tuned modes up to which single-longitudinal mode operation was maintained. Beyond that current, additional lasing was generally observed in a group of longitudinal modes near the free-running wavelength of 770 nm . Approximately 200 mW was measured over most of the width of the tuning range, while the maximum recorded output power exceeds 300 mW . Transverse electric polarization was maintained throughout. The wafers for the single-quantum-well lasers were grown by metalorganic chemical vapor deposition (MOCVD) at Ortel Corporation and by molecular beam epitaxy (MBE) at Caltech. This work was supported in part by the National Science Foundation and the Office of Naval Research, and M. Mittelstein acknowledges support from a Newport Research Award for this project.

[1] Wyatt R., K. H. Cameron, and M. R. Matthews,
Br. Telecom. Technol. J. **3**, 5 (1985).

[2] Epler, J. E., G. S. Jackson, N. Holonyak, Jr., R. L. Thornton, R. L. Paoli,
Appl. Phys. Lett. **47**, 779 (1985).

[3] Mittelstein, M., D. Mehuys, A. Yariv, R. Sarfaty, and J. E. Ungar,
OSA Annual Meeting Oct.31-Nov.4, 1988, Santa Clara, CA, paper PD6.

[4] Mehuys, D., M. Mittelstein, A. Yariv, R. Sarfaty, and J. E. Ungar,
Electron. Lett. **25**, 143 (1989).

[5] Mittelstein, M., D. Mehuys, A. Yariv, J. E. Ungar, and R. Sarfaty,
Appl. Phys. Lett. **54**, to be published in No.: 12 (1989).

[6] Mittelstein, M.,
Ph.D. Thesis, California Institute of Technology, Appl. Phys., March 1989.

Laser Performance and Spectroscopy of Cr^{3+} in $LiCaAlF_6$ and $LiSrAlF_6$

L. L. Chase, S. A. Payne, L. K. Smith, W. L. Kway, and H. W. Newkirk

University of California
Lawrence Livermore National Laboratory
P. O. Box 5508
Livermore, California 94550

We previously reported Kr-laser-pumped slope efficiencies of Cr^{3+} in $LiCaAlF_6$ (Cr:LiCAF) that were in the range of 50%, when utilizing 4.3% output coupling.[1] We now report that we have successfully lased Cr^{3+} in $LiSrAlF_6$ (Cr:LiSAF) as well; the experimental slope efficiencies obtained for Cr:LiSAF are displayed in Fig. 1 for two values of output coupling (O.C.). We can use the data in Fig. 1 to calculate an extrapolated slope efficiency η_o (known as the "intrinsic" slope efficiency[2]), that would be obtained from the laser if the material is completely devoid of passive loss. The results of this process yield η_o = 67% and 53% for Cr:LiCAF and Cr:LiSAF, respectively, to be compared with the quantum defect limited value of about 80%.

We flashlamp-pumped a Cr:LiCAF laser rod of dimension .5 x 2 cm. The temporal output of the laser emission is illustrated in Fig. 2. The laser rod had uncoated end faces and was pumped with a helical Xe flashlamp. As is clear from the figure, the threshold is near 63 J of stored electrical energy, and the output consists of many spikes. We attribute this high threshold to the fact that our cavity has not been optimized and the material used in these measurements is not of good optical quality.

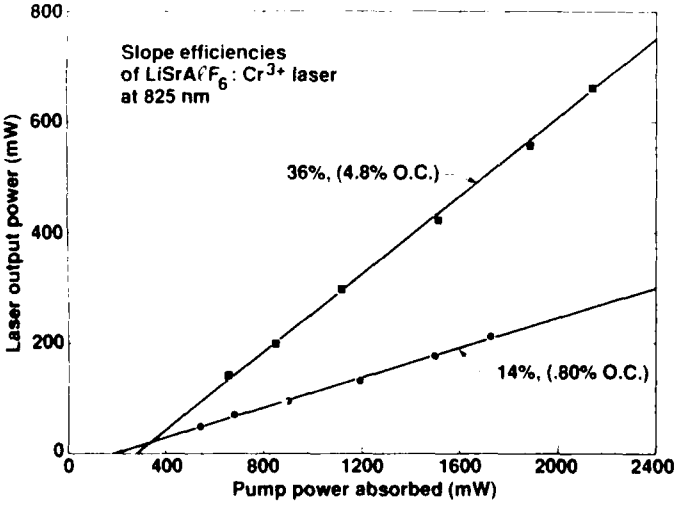

Fig 1.

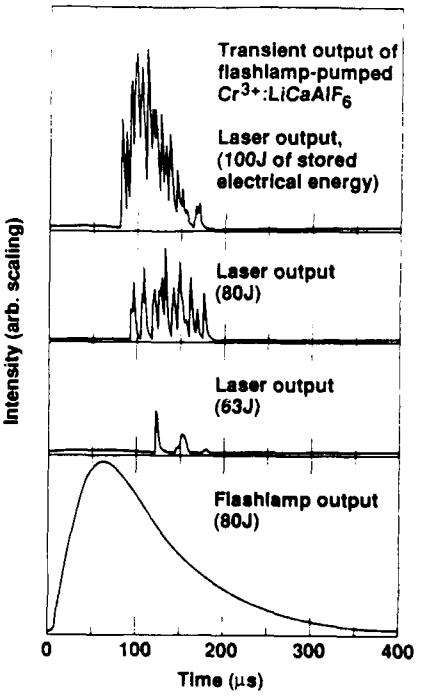

Fig. 2

The absorption and emission spectra of Cr:LiCAF and LiSAF are shown in Figs. 3 and 4. Note that the emission spectra tend to be significantly polarized along the c-axis of both crystals; the absorption bands show polarized behavior as well. On the basis of the crystal structure of LiCAF,[3] it is apparent that the Al-site, at which the Cr ion is known to substitute, imposes an odd-parity field of t_{2u} character on the metal ion. It is possible to show that the polarized spectra can be fully explained on the basis of this t_{2u} field.

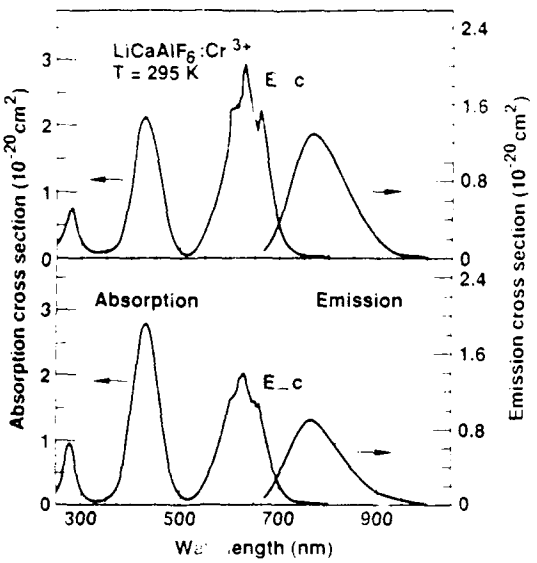

Fig. 3

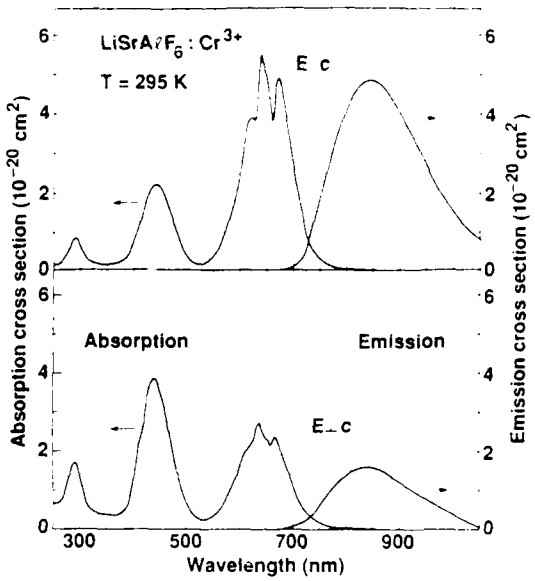

Fig. 4

For the case of the $Na_3Ga_2Li_3F_{12}:Cr^{3+}$ laser, we found that the intrinsic efficiency was only 28%, and that the low efficiency was predominantly the result of excited state absorption (ESA) losses.[3] Cr:LiCAF and LiSAF have exhibited much higher efficiencies of 67% and 53% due to low ESA loss. In fact, it can be shown that the t_{2u} static field, which is responsible for the oscillator strength and the polarized behavior of the spectra in Figs. 3 and 4, does not contribute oscillator strength to the ESA band near the emission peak. For this reason, the emission cross section is much larger than that of the ESA, and the laser efficiency is high.

1. S. A. Payne, L. L. Chase, H. W. Newkirk, L. K. Smith, and W. F. Krupke, IEEE J. Quant. Electron. 24, 2243 (1988).
2. J. A. Caird, S. A. Payne P. R. Staver, A. J. Ramponi, L. L. Chase, and W. F. Krupke, IEEE J. Quant. Electron. 24, 1077 (1988).
3. V. W. Viebahn, Z. Anorg. Allg. Chem. 386, 335 (1971).

This work was performed under the auspices of the Division of Materials Sciences of the Office of Basic Energy Sciences, U.S. Department of Energy, and by the Lawrence Livermore National Laboratory under Contract No.W-7405-ENG-48.

MD3-1

Growth and Characterization of $LiCaAlF_6:Cr^{3+}$ for Solid State Laser Applications

Wayne L. Kway, H. W. Newkirk, and L. L. Chase

University of California
Lawrence Livermore National Laboratory
P. O. Box 5508, Livermore, CA 94550

$LiCaAlF_6:Cr^{3+}$ single crystals doped with 3% CrF_3 (Cr:LiCAF) have been grown by the Czochralski (CZ) technique in dimensions up to 1" diameter and 3" in length (Fig. 1). In this paper, we will address several important criteria related to the growth and characterization of this material. Cr:LiCAF has recently been demonstrated to lase efficiently when using laser pumping of small crystals.[1] In this work we report on our efforts to grow large single crystals to be used for the flashlamp-pumped configuration.

Cr:LiCAF has been found to be congruently melting, as it is shown by the differential thermal analysis (DTA) plot in Fig. 2. However, since the congruency region appears to be very narrow (about 2 to 3 mole % for each of the components), it is of utmost importance to use high purity starting materials that are free of H_2O, OH^-, oxyfluoride, and oxide. Both LiF and CaF_2 may be obtained commercially as zone-refined optical grade single crystals. But in order to obtain high purity AlF_3 and CrF_3, we must sublime the material in an HF atmosphere. The charge is then formulated, blended, and hydro-fluorinated. We have found that it is beneficial to zone-refine the material for additional purification prior to CZ growth.

CZ growth is accomplished by stringent controls in atmosphere, temperature gradients, growth parameters, growth rate, and interface shape. The atmosphere is either pure argon or argon with HF. The furnace is powered by RF induction heating. With properly chosen crucible and insulating material, the temperature gradients obtained are relatively high and stable. By utilizing a slow pull rate of 2 mm/hr and a rotation rate of 20 rpm or higher, a convex interface shape is achieved. We chose the [100] as the growth direction to assure radial growth isotropy, since we found that growing in the [210] direction results in a highly anisotropic growth morphology and, therefore, very poor and non-uniform boule quality. Under these growth conditions, control of diameter and growth rate can be accomplished by weight control.

Characterization of the optical quality of the CZ grown crystals, as related to growth parameters and morphology, will be presented.

Reference

1. S. A. Payne, L. L. Chase, H. W. Newkirk, L. K. Smith, and W. F. Krupke, IEEE J. Quantum Electron. 24, 2243 (1988).

This work was performed under the auspices of the Division of Materials Sciences of the Office of Basic Energy Sciences, U.S. Department of Energy, and by the Lawrence Livermore National Laboratory under Contract No. W-7405-ENG-48.

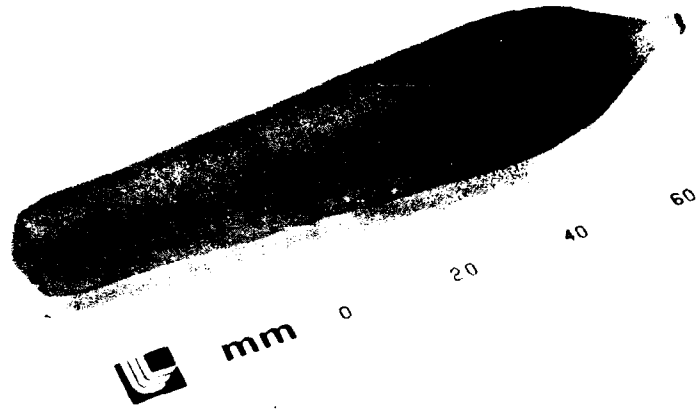

Fig. 1. Czochralski grown $LiCaAlF_6:Cr^{3+}$ crystal

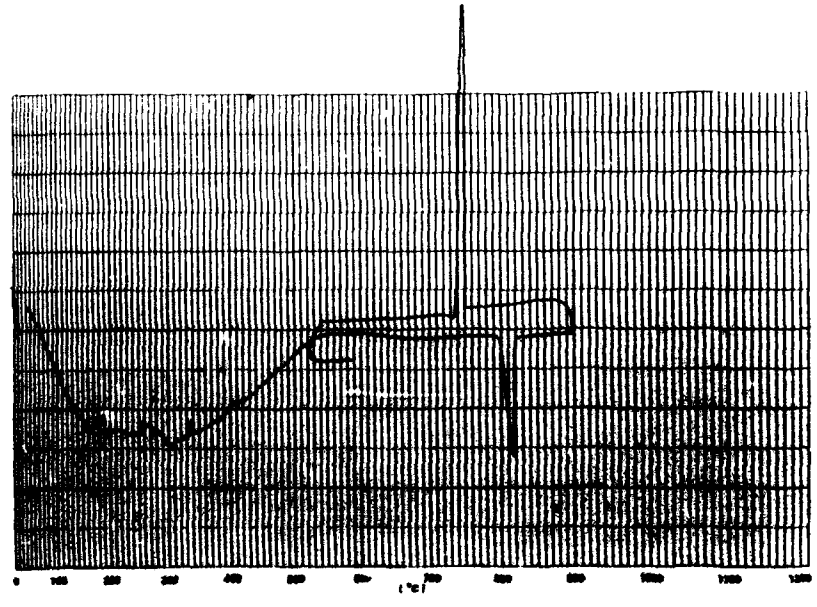

Fig. 2. DTA trace of $LiCaAlF_6:Cr^{3+}$
Czochralski grown single crystal

A Chromium-Activated Forsterite Laser

V. Petričević, S. K. Gayen,* and R. R. Alfano

Institute for Ultrafast Spectroscopy and Lasers, Departments of Physics and Electrical Engineering, City College of New York, New York, NY 10031.

* Department of Physics and Engineering Physics, Stevens Institute of Technology, Hoboken, New Jersey 07030.

Summary

The chromium-doped forsterite ($Cr:Mg_2SiO_4$) laser, a new member in the family of chromium-based, room-temperature, near-infrared vibronic lasers,[1] is emerging as a practical and useful source of coherent radiation in the near-infrared spectral region.[2,3] The Cr:forsterite system is unique both for its desirable laser properties, as well as for its interesting and intriguing spectroscopic properties. While successfully operated Cr-based tunable solid-state lasers like alexandrite, emerald, Cr:GSGG, together with $Ti:Al_2O_3$ span quite a different spectral range of 660-1090 nm, Cr:forsterite emits in the 1167-1345 nm range, centered on 1268 nm, the so-called "wavelength of zero material dispersion". The material dispersion will be minimal in this spectral range, making Cr:forsterite an extremely valuable source for optical communications. The most interesting spectroscopic feature of the Cr:forsterite crystal is that it is the first Cr-based system known to date where the 'lasing center' is other than the Cr^{3+} ion, presumably the tetravalent chromium (Cr^{4+}). In this paper, the unique spectroscopic, and laser properties of Cr:forsterite will be described.

The room-temperature absorption and emission spectra of Cr:forsterite are shown in Fig. 1(a). The absorption spectrum is characterized by three broad absorption bands centered at 1050 nm, 750 nm, and 480 nm, respectively. The emission spectrum spans the 680-1400 nm spectral range with peak at 1100 nm. The 750-nm and 480-nm absorption bands are attributed to transitions within the states of Cr^{3+} ion. A careful study reveals that the near-infrared absorption band centered at 1050 nm, and its Stokes-shifted fluorescence, presented in Fig. 1(b), are responsible for laser action in Cr:forsterite. These absorption and emission originate in transitions between the states of a center other than Cr^{3+}. The spectroscopic and theoretical evidences leading to this conclusion and the identification of this new lasing center will be presented.

Various laser-pumped laser experiments on Cr:forsterite system have been completed and will be reviewed:

* Pulsed laser action has been obtained for longitudinal pumping in a stable cavity by both the 1064-nm and 532-nm radiation.
* Continuous-wave operation has been demonstrated for longitudinal pumping by cw 1064-nm radiation in a nearly concentric cavity.
* Continuous tuning over the 1167-1345 nm spectral range, displayed in Fig. 2, has been obtained by using three different output couplers, and a birefringent, single-crystal quartz plate at Brewster's angle as the intra-cavity dispersive element.

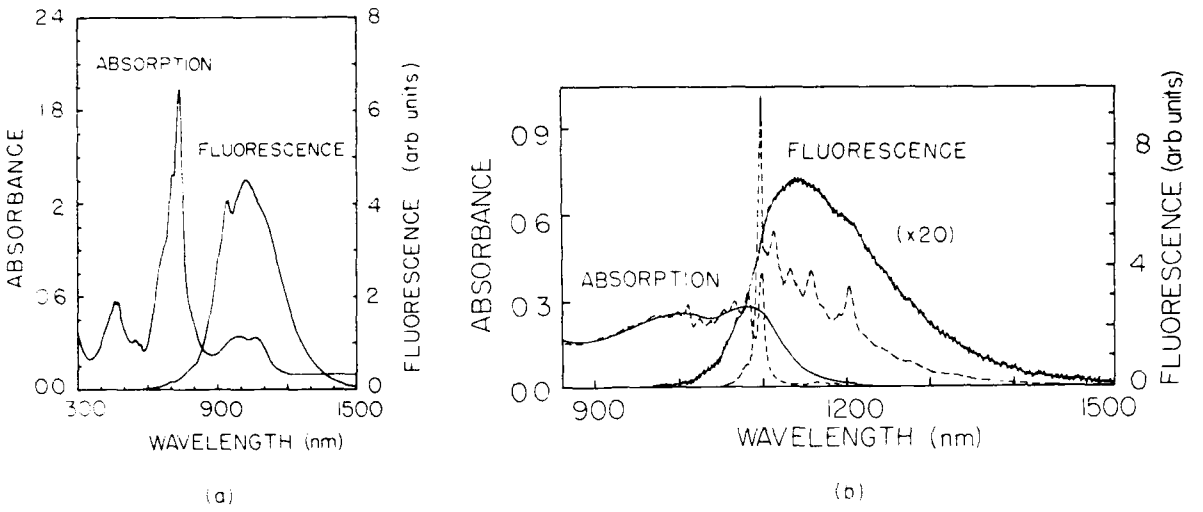

Fig. 1 Absorption and fluorescence spectra of Cr:forsterite: (a) room-temperature composite spectra showing contributions from both the optically-active centers present in the crystal (fluorescence excited by 488-nm radiation); (b) near-infrared spectra (fluorescence excited by 1064-nm radiation) attributed to transitions within the states of the 'lasing center' alone, presumed to be tetravalent chromium. All the spectra were taken for Ellb axis of the crystal, and for excitation along the a axis. The dotted curves in (b) are taken at 77 K, while the solid curves are taken at 300 K.

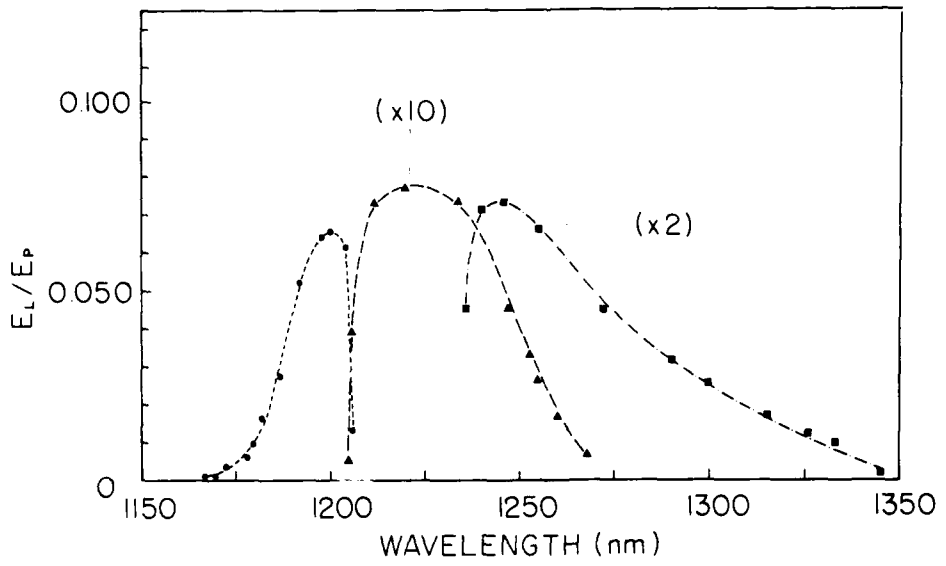

Fig. 2 The ratio of Cr:forsterite laser output (E_L) to the absorbed pump energy (E_P) as a function of wavelength. The three curves correspond to the three output couplers used in tuning measurement.

The successful cw operation and large fluorescence bandwidth of this system promise ultrashort pulse generation through mode-locked operation. Since large crystals may be readily grown, the system has the potential to be an amplifier medium in the infrared spectral region. Key spectroscopic and laser properties of Cr:forsterite are summarized in Table 1.

TABLE 1. Spectroscopic and laser properties of Cr-doped forsterite

Property	Value
Major pump bands	850-1200 nm, 600-850 nm, and 350-550 nm.
Fluorescence band	680-1400 nm
Room-temperature fluorescence lifetime	15 us
Cr-ion concentration	~ 7×10^{18} ions/cm^3
Lasing wavelength (center)	1235 nm (pulsed) 1244 nm (cw)
Spectral bandwidth	~ 30 nm (pulsed) ~ 12 nm (cw)
Slope efficiency	22% (pulsed) 6.8% (cw)
Tuning range	1167-1345 nm
Effective emission cross section	1.1×10^{-19} cm^2

We would like to acknowledge K. Yamagishi, H. Anzai, and Y. Yamaguchi of Mitsui Mining and Smelting Co., Japan for providing the crystals used in this study, and NASA and ARO for financial support.

References

1. J. A. Caird, S. A. Payne, P. R. Staver, A. J. Ramponi, L. L. Chase, and W. F. Krupke, IEEE J. Quantum Electron. **24**, 1077 (1988), and references therein.
2. V. Petričević, S. K. Gayen, R. R. Alfano, K. Yamagishi, H. Anzai, and Y. Yamaguchi, Appl. Phys. Lett. **52**, 1040 (1988).
3. V. Petričević, S. K. Gayen, and R. R. Alfano, Appl. Opt. **27**, 4162 (1988); and Appl. Phys. Lett. **53**, 2590 (1988).

MONDAY, MAY 1, 1989

NAUSET III

3:00 PM–4:00 PM

ME1–ME6

FORSTERITE AND EXCITED STATE ABSORPTION / POSTER SESSION

Gunter Huber, University of Hamburg, *Presider*

LASER PERFORMANCE OF CHROMIUM-ALUMINUM-DOPED FORSTERITE*

Horacio R. Verdún, Leonard M. Thomas and Donna M. Andrauskas
Fibertek, Inc.
510-A Herndon Parkway, Herndon, VA 22070

and

Albert Pinto
U.S. Army Night Vision and Electro-Optics Center
Fort Belvoir, VA 22060

1. Introduction

Chromium-doped forsterite (Mg_2SiO_4) has been found to lase in the 1.167-1.345 μm range of the spectrum when pumped with a pulsed[1,2] or CW[2] 1.064 μm Nd-YAG laser or with doubled 1.064 μm. The active center in this material is still uncertain, but there are reasons to believe that it is due to tetravalent chromium in the distorted tetrahedral site or a related defect. Fourfold-coordinated Cr^{IV} has been reported as present in crystals or glasses in only a few cases, and its existence has been well stablished in even fewer cases.[4] Its existence in forsterite could be explained by covalency effects, which are expected to be important for the high oxidation states of chromium, and as a result of a chemical equilibrium with Cr^{III} in the octahedral site. A similar claim has been made recently in connection with the absorption spectrum of chromium-doped $Gd_3Sc_2Ga_3O_{12}$ (GSGG) crystals grown under oxygen containing atmospheres or codoped with divalent cations.[5]

To our knowledge, forsterite and YAG are the only host crystals for which laser action beyond 1 μm has been reported when doped with chromium, and when grown or annealed in an oxidizing atmosphere. Oxygen annealed chromium-doped YAG has been found to lase in the 1.35-1.45 μm range when pumped with a 1.064 μm Nd-YAG laser.[6] Both systems have room temperature fluorescence lifetimes of a few microseconds (2.8 μs for forsterite and 4.3 μs for YAG). Many other chromium-doped garnets grown at Fibertek, Inc. have shown similar spectral features and fluorescence lifetimes[7].

The 1.1-1.6 μm spectral range was without an efficient and convenient tunable solid state laser medium until the discovery of these new materials. The demonstrated efficiencies in these initial developments of the chromium-activated forsterite and YAG lasers are already high but optimization steps are needed for both the material and system aspects of these new lasers.

In forsterite, Cr^{3+} substitutes for magnesium in the lattice at both the M1 and M2 sites (C_i and C_s point group symmetry respectively) with about 40% of the Cr^{3+} ions going into the M2 site. The nature of the compensation of the local electrical charge imbalance produced by this substitution is not very well

*Work supported by the U.S. Army Center for Night Vision and Electro-Optics, Fort Belvoir, VA.

established, but it is probable that for crystals grown in oxidizing atmospheres the compensation is obtained with doubly-charged Mg vacancies (Mg substituting for Si in the tetrahedral site is unlikely because of the large size of Mg^{2+} compared to the Si-O distance). The absence of a purposely added compensator makes the doping of forsterite with Cr^{3+} a rather difficult and uncontrollable process, and the concentration attained without a compensator is usually small.

Starting from the belief that the active center concentration in chromium-doped forsterite depends on the concentration of Cr^{3+}, it was decided to study the effect of the addition of Li and Al on Cr. Li^{1+} has about the same size as Mg^{2+} and could be substitutionally incorporated into the forsterite lattice. Al^{3+} could enter the forsterite lattice substituting for Mg^{2+} in either one of the two octahedral sites or substituting for Si in the tetrahedral site. Evidence from electron paramagnetic resonance[8] and electron-nuclear double resonance[9] experiments indicate that the latter possibility actually occurs. Several considerations required to explain the observed electrical properties of forsterite favor the latter substitution.[10]

2. Experimental

Chromium-doped forsterite crystals, codoped with lithium or aluminum, were grown at Fibertek, Inc. by the laser-heated pedestal growth method.[11] The growth atmosphere was typically 8% O_2 + 92% Ar. The crystal fibers prepared for this study were typically 2-3 mm in diameter, 30-40 mm in length and oriented along the c-axis.

The laser experiments were performed using the experimental set-up described in ref. 1.

3. Results

After a few attempts to grow chromium-lithium doped crystals it was obvious that the large evaporation from the molten zone, presumably due to loss of Li_2O, was preventing the growth of good quality crystals and because of this the effort was stopped. In contrast, the growth of chromium-aluminum doped crystals was very successful and good optical quality fibers with strong coloration were obtained. In particular, fiber LMT123, which was used in the as-grown condition for the laser experiment results presented here, had an absorption coefficient of 2 cm^{-1} at 1.06 μm as compared with 0.3 cm^{-1} of the chromium-only doped crystals grown under similar conditions. Because of significant evaporation losses, the final aluminum and chromium concentration in the crystal is unknown. The concentration of chromium and aluminum in the feed rod was 3at% and 1at% respectively. The as-grown fiber showed fairly high scattering. In a separate study a portion of this crystal was annealed in 20% O_2 atmosphere. The resultant material showed considerably less scattering.

The rod used for the laser performance measurements had a length of 1.41 cm and uncoated end faces that were polished flat and perpendicular to the rod axis. The room temperature fluorescence lifetime measured for this rod was 2.6 μs, which is

essentially the same as for the weakly absorbing chromium-only doped forsterite rod used for the study reported in ref. 1. The spectrum of the free running laser output spans the 1220-1260 nm range (10% base line). With the laser set-up used for these measurements, the maximum efficiency obtained was about 0.8% compared with the 8% obtained under similar conditions with a chromium-only doped crystal.[1]

4. Conclusions

We believe that the high scattering observed in the rod is limiting the efficiency of the laser. The reduction of the scattering losses with annealing will clearly result in much higher efficiency values. Apart from this effect, which is probably due to the growth method used in this study, codoping with aluminum clearly increases the incorporation of chromium by forsterite without affecting fluorescence lifetime. The almost total absorption of the 1.064 μm pump beam in about 2 cm length of active medium is now a possible fact which will facilitate the design of very compact laser systems in the 1 μm spectral region.

5. References

1. H. R. Verdún, L. M. Thomas, D. M. Andrauskas, T. McCollum, and A. Pinto, Appl. Phys. Lett. **53**, 2593 (1988).
2. V. Petricević, S. K. Gayen, and R. R. Alfano, Appl. Phys. Lett. **53**, 2590 (1988).
3. V. Petricević, S. K. Gayen, R. R. Alfano, K. Yamagishi, H. Anzai, and Y. Yamaguchi, Appl. Phys. Lett. **52**, 1040 (1988).
4. A. B. P. Lever, Inorganic Electronic Spectroscopy (2nd ed.) (Elsevier, Amsterdan, Oxford, New York, Tokyo, 1984). Also, C. Rosenblum and S. L. Holt, in Transition Metal Chemistry, edited by R. L. Carlin (Marcel Decker, New York, 1972).
5. S. E. Stokowski, M. H. Randles, and R. C. Morris, IEEE J. Quantum Electron. **QE-24**, 934 (1988).
6. N. B. Angert, N. I. Borodin, V. M. Garmash, V. A. Zhitnyuk, A. G. Okhrimchuk, O. G. Siyuchenko, and A. V. Shestakov, Sov. J. Quantum Electron. **18**, 73 (1988).
7. H. R. Verdún, L. Black, L. Thomas, and D. M. Andrauskas, to be published.
8. H. Rager, Phys. Chem. Minerals **1**, 371 (1977). Also S. Nagel and H Rager. ibid **12**, 291 (1985).
9. L. V. Bershov, J. M. Gaite, S. S. Hafner, and H. Rager, Phys. Chem. Minerals **9**, 95 (1983).
10. F. J. Morin, J. R. Oliver, and R. M. Housley, Phys. Rev. B **19**, 2886 (1979).
11. H. R. Verdún, Patent application in process.
12. R. S. Feigelson, in Tunable Solid State Lasers, Proceedings of the First International Conference, La Jolla, Calif., June 13-15, 1984, edited by P. Hammerling, A. B. Budgor and A. Pinto (Springer-Verlag, Berlin, Heidelberg, New York, 1985) p 129.

ME2-1

SPECTROSCOPIC PROPERTIES AND FLUORESCENCE DYNAMICS IN Cr^{3+} - DOPED FORSTERITE

R.Moncorge and G.Cormier*
Universite de Lyon I , UA 442 CNRS
69622 Villeurbanne , France
J.A.Capobianco** and D.J.Simkin*
* Mc Gill University , Department of Chemistry
Montreal H36-2K6 (Quebec) , Canada
** Concordia University ,Department of Chemistry
Montreal H36-1M8 (Quebec) , Canada

SUMMARY

Room temperature vibronic laser action has been found recently in a number of Cr^{3+} doped silicates [1, 2, 3] and more particularly in the case of chromium-doped forsterite $Mg_2SiO_4:Cr^{3+}$. Though the spectral range for laser emission is expected to extend from ~ 850 to 1300 nm , it is reported an effective wavelength tunability between ~ 1210 and 1260 nm . The authors [3] attribute this reduced tunability to the mirror transmissions and to parasitic impurity absorptions . They also invoke an overall fluorescence lifetime of ~ 15 μs .

We report here on detailed measurements of polarized absorption , excitation and time-resolved fluorescence spectra as well as of fluorescence lifetimes and quantum efficiencies .

From this study we obtain evidences for three very distinct fluorescence origins - and not only one as it is implicitly suggested in Ref.3 - which are not yet completely understood .

Very briefly , we observe a long-lived fluorescence extending from ~ 650 to 1100 nm with lifetimes ranging between 320 and 40 μs with a slight component of ~ 2.7 us when going from the short to the longer wavelengths .This fluorescence is weak and is obtained by using a dye laser excitation at 575 nm along the b axis of the crystal and for E // a , and by resolving the signal at long times after the laser pulse , i.e. with a 6μs gatewidth and a 80 μs delay . This long-lived fluorescence is typical of Cr^{3+} ions in an intermediate octahedral crystal field for which the ^2E and the $^4T_2$ excited states compete for emission. This is confirmed by our low temperature data .

The other fluorescences are obtained by resolving the signal at short times after the excitation laser pulse . They have been observed for example by using a dye laser excitation at 640 nm along the b axis of the crystal and E // c , and by resolving the signal with a 1 μs gatewidth and 2 and 10 μs delays . In this case we distinguish two broad band fluorescences . The one ,corresponding to a fluorescence lifetime of ~ 2.7 μs is very strong and extends from about 1000 to 1500 nm and the other , much weaker than the former and corresponding to a fluorescence lifetime of ~ 20 μs , extends (after deconvolution) from about 800 to 1100 nm . These long-wavelength emissions migth be characteristics of Cr^{3+} ions in low crystal fields of octahedral symmetry . Indeed there are similarities in the positions and the shapes of both the absorption and the emission bands with the ones found for example in Cr^{3+} doped fluoride hosts such as MgF_2 and CaF_2 [4] .

Subsequently a discussion concerning the occurrence of Cr^{2+} and Cr^{4+} ions is developped . We also consider dynamical processes such as energy transfers and non-radiative relaxations .

This work was supported by a Quebec-France cooperation program on the new laser materials .

REFERENCES

1. A.A. Kaminskii and S.E. Sarkisov (to be published)
2. S.L. Lai , B.H.T. Chai , M. Long and M.D. Shinn . IEEE J. of Q.E. 24 , 1922 (1988)
3. V. Petricevic , S.K. Gayen and R.R. Alfano . Appl.Phys. Lett. 52 , 1040 (1988)
4. S.A. Payne , L.L. Chase and W.F. Krupke . J. Chem.Phys. 86 , 3455 (1986)

Excited-State Absorption in Ti:$YAlO_3$

K. F. Wall and R. L. Aggarwal

Lincoln Laboratory, Massachusetts Institute of Technology

Lexington, Massachusetts 02173

and

C. P. Khattak

Crystals Systems, Inc.

27 Congress Street, Salem, Massachusetts 01970

In an attempt to measure small-signal gain at 632.8 nm in Ti:$YAlO_3$ pumped with 532 nm radiation from a frequency-doubled Q-switched (10 ns pulses) Nd:YAG laser, we observed pump-induced loss. The induced absorption was found to decay on a time scale characteristic of the fluorescence lifetime[1] (11.4 $\pm$ 0.5 μs) and is therefore identified as an excited-state absorption. The excited-state absorption loss was measured as a function of the incident pump fluence up to 1.7 J/cm^2. Excited-state absorption was not observed at 800 nm.

The measurements were made on a 6.5-mm-long, unoriented, single-crystal specimen taken from a polycrystalline ingot grown with 0.3 wt.% Ti_2O_3 in $YAlO_3$ by using the unseeded heat exchanger method.[2] The Ti^{3+} concentration in this sample was estimated[1] to be 3.6 x 10^{19} cm^{-3}, corresponding to a value of 0.08 wt.% of Ti_2O_3. A nearly collinear configuration for the He-Ne signal beam (632.8 nm) and 532 nm pump beam was used. The polarizations of the pump and signal beams were parallel to each other.

Figure 1(a) shows the temporal behavior of the pump-induced absorption coefficient α_p for an incident fluence of 0.6 J/cm^2; t = 0 denotes the time at which the pump beam was incident on the sample. A plot of the natural logarithm of α_p versus time is shown in Fig. 1(b). Note that the pump-induced absorption decays with a time constant of 12.7 $\pm$ 1.0 μs. The similarity of this time

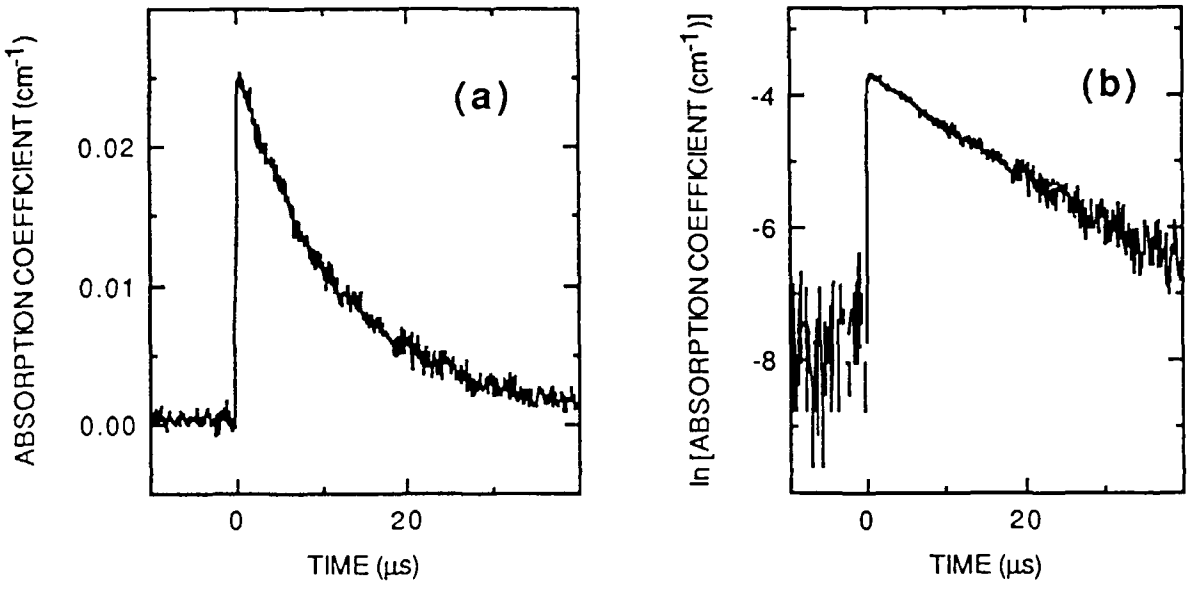

Fig. 1. Temporal decay of the pump-induced absorption coefficient α_p at 632.8 nm: (a) α_p versus time t, and (b) the natural logarithm of α_p versus t. The pump fluence was 0.6 J/cm^2.

constant and the fluorescence lifetime of Ti^{3+} in $YAlO_3$ has led us to conclude that the pump-induced absorption is due to transitions originating from the excited-state of Ti^{3+}.

It should be pointed out that the term "excited-state absorption" is normally used to denote transitions from a given excited-state to still higher excited states belonging to the same species. Transitions from the 3d excited state of Ti^{3+} to higher excited states within the Ti^{3+} manifold are unlikely because the 4p and 4f levels (for the free ion) are 16 and 29 eV above the 3d ground state, respectively. Recently, lasing has been reported[3] for a 3.5-mm-long Ti:$YAlO_3$ crystal. This suggests that the observed excited-state absorption is not intrinsic to Ti:$YAlO_3$. Thus, we conclude that the excited-state absorption in our crystal is due to charge transfer transitions to energy levels of unidentified defects.

The value of α_p at $t = 0$ versus incident pump fluence is shown in Fig. 2. We note that α_p does not increase linearly with pump fluence. The saturation behavior of α_p at high pump fluence

may arise from the saturation of the available defects.

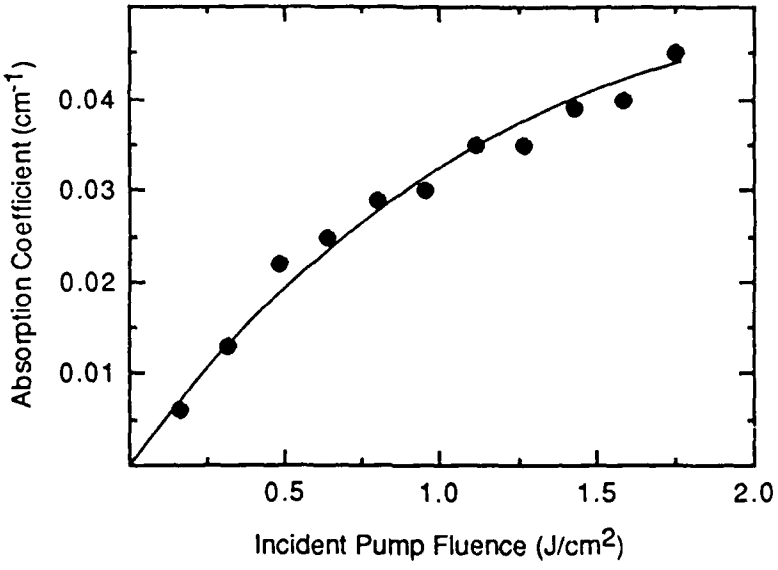

Fig. 2. The variation of the pump-induced absorption coefficient α_p at t = 0 with incident pump fluence.The data are shown by filled circles and the solid line is a simply a guide to the eye.

This work was supported in part by the Department of the Navy for SDIO. The crystal used in this work was grown at Crystal Systems, Inc. under the sponsorship of the U.S. Army, Contract No. DAAB07-87-F065 administered by CNVEO, Fort Belvoir, VA.

1. C. P. Khattak, F. Schmid, K. F. Wall, and R. L. Aggarwal, to be presented at the SPIE 1989 Technical Symposia on Aerospace Sensing, Orlando, Florida.
2. C. P. Khattak and F. Schmid, in *Advances in Optical Materials,* edited by S. Musikant, Proc. SPIE, Vol. 505, 4 (1984).
3. J. Kvapil, M. Koselja, J. Kvapil, B. Perner, V. Skoda, J. Kubelka, K. Hamal, and V. Kubacek, Czech. J. Phys. **B38**, 237 (1988).

ME4-1

Excited -state absorption measurements in Cr^{3+} -doped $LaMgAl_{11}O_{19}$.

R. Moncorgé and H. Manaa.
Laboratoire de physico-chimie des materiaux luminescents
U.A 442 CNRS, Université de Lyon I.
69622 Villeurbanne, France.

Many works have been devoted in the last years to the excited -state absorption (E.S.A) processes in the Cr^{3+} doped compounds, and to the models which can be used to interpret and possibly to predict the experimental data. We know for example that these systems can be divided into different categories depending on the strength of the crystal field at the Cr^{3+} site. The ones called "high field" systems, for they correspond to crystal field and Racah parameters such as $Dq/B > 2.3$, have a ^2E lowest excited state and they are characterized by $^2E \longrightarrow {}^4A_2$ sharp line emissions -the R line of the famous ruby Laser for example- as well as $^2E \longrightarrow$ higher doublet states E.S.A. transitions (ref.1.); in this case, the single configuration coordinate (S.C.C.) model, based on crystal field calculations and the assumption of linear electron -phonon coupling to a_{1g} symmetry modes, gives about the right positions and the right shapes for the observed optical bands. The systems which correspond to Dq and B parameters such as $Dq/B < 2.3$ are called "low field" systems. They have a $^4T_2$ lowest excited state and they are characterized by $^4T_2 \longrightarrow {}^4A_2$ broad band emmissions -as in GSGG : Cr^{3+} - and $^4T_2 \longrightarrow$ higher quartet states E.S.A. transitions (ref.2.); now the observed E.S.A. bands lie at higher energies and they are much broader than those predicted by the S.C.C. model, thus alternative solutions including linear as well as quadratic coupling to e_g and/or t_{2g} low symmetry phonons have to be considered (ref.3 & 4). Of course there are intermediate

cases: (i) systems such as alexandrite, for which the ^2E level is the lowest metastable level, and the ^2E to upper doublets E.S.A. transitions predominate, with evidences, however, for thermally activated transitions from the above $^4T_2$ to the upper quartets (ref.3.); (ii) systems such as the one concerned in this paper, i.e. LMA: Cr^{3+} (ref.5.), for which different kinds of Cr^{3+} sites corresponding to "high field" to "low field" situations coexist.

More precisely, we report first on measurements of excited state absorption spectra and cross sections at low and high temperatures in the U.V.-visible as well as in the near infrared domains.

Then the results are compared with the predictions of the crystal field calculations and the SCC model. Two kinds of Cr^{3+} sites seem to predominate: "high field" Cr^{3+} sites with about the same Dq/B value as in ruby and "medium field" Cr^{3+} sites with a Dq/B value closer to the one of emerald. Both situations give comparable excited state absorption cross-sections, the ones in the infrared being more important than in the visible domain.

In the end we report on fluorescence quantum efficiencies, gain measurements and laser tests.

This work was partially supported by DRET (French Army Division) under contract 84/071 . The crystals were grown at LETI (Grenoble, France) by Mrs C. Wyon and J.J Aubert and were kindly supplimed to us by Prof. D. Vivien of ENSCP (Paris, France).

References:

1. W.M. Fairbank Jr, G.K. Klauminzer and A.L Shallow Phys. Rev. B 11 ,60(1975).
2. L.J. Andrews in Tunable Solide State Lasers II, A.B. Budgor, L. Esterowitz and L.G. Deshazer, Eds (Springer Verlag, Berlin, 1986) p 44.

3. L. L. Chase and S. A. Payne . Topical Meeting on Tunable Solid State Lasers Technical Digest Series, 1987, Vol. 20, (Optical society of America, Washingtong DC, 1987), p 43.

4. R. M. Bartram, J. C. Charpie, L. J. Andrews and A. Lempicki. Phys. Rev. B 34, 2741 (1986).

5. F. Michel -Calendini, K. Bellafrouh, V. Ponçon and G. Boulon Proceed. 1st Int. Laser M2P Conf. Lyon (France), R. Bacis, R. Lambert, A. B. Vannes eds (J. de Physique colloque C7 -1987) p 497.

ME5-1

Excited State Absorption of $Ti:YAlO_3$

T. Wegner, G. Huber, K. Petermann

Institut für Angewandte Physik, Universität Hamburg

Jungiusstr. 11, D-2000 Hamburg 36, FRG

In comparison to Ti^{3+} doped sapphire the absorption and emission spectra of $Ti^{3+}:YAlO_3$ are shifted to shorter wavelengths. The fluorescence lifetime at roomtemperature has been measured to be 11.4 µs. This value is a factor of three longer than in sapphire and may be advantageous in case of flashlamp pumping. But so far no laser action has been achieved in our laboratory, although Kvapil et al. have published some hints at stimulated emission. However, the maximum efficiency of $3.5 \cdot 10^{-4}$ under laser pumping is extremly small [1].

Our laser experiments were carried out with Czochralski grown crystals doped with $1.7 \cdot 10^{19}$ cm^{-3} Ti (0,085 mol %) in a nearly concentric cavity. An Ar ion laser at 488/515 nm wavelength as well as a doubled Nd:YAG-laser at 532 nm wavelength was used as pumping source. Despite the good optical quality and the high pump power (≈ 4 W absorbed power in the quasi-cw experiment and more than 100 mJ pump energy in the pulsed case) lasing could not be achieved.

To find out, why $Ti:YAlO_3$ is not lasing, excited state absorption (ESA) was measured between 370 nm and 690 nm with a conventional setup (cw pump beam, chopped test beam). The resulting spectrum yielded a very strong ESA effect for wavelengths shorter than 550 nm. After adding the Ti^{3+} zero phonon energy (18500 cm^{-1}) to the measured ESA spectrum the dashed curve in the figure below is obtained. The ground state absorption spectrum (GSA) of a 78 µm platelet is also shown in this figure. The absorption at 280 nm is identified as a charge transfer band of Fe impuries [2], whereas the broad band around 230 nm is attributed to a Ti^{3+} -> Ti^{4+} charge transfer in analogy to $Ti:Al_2O_3$. In undoped $YAlO_3$ this band is not observed.

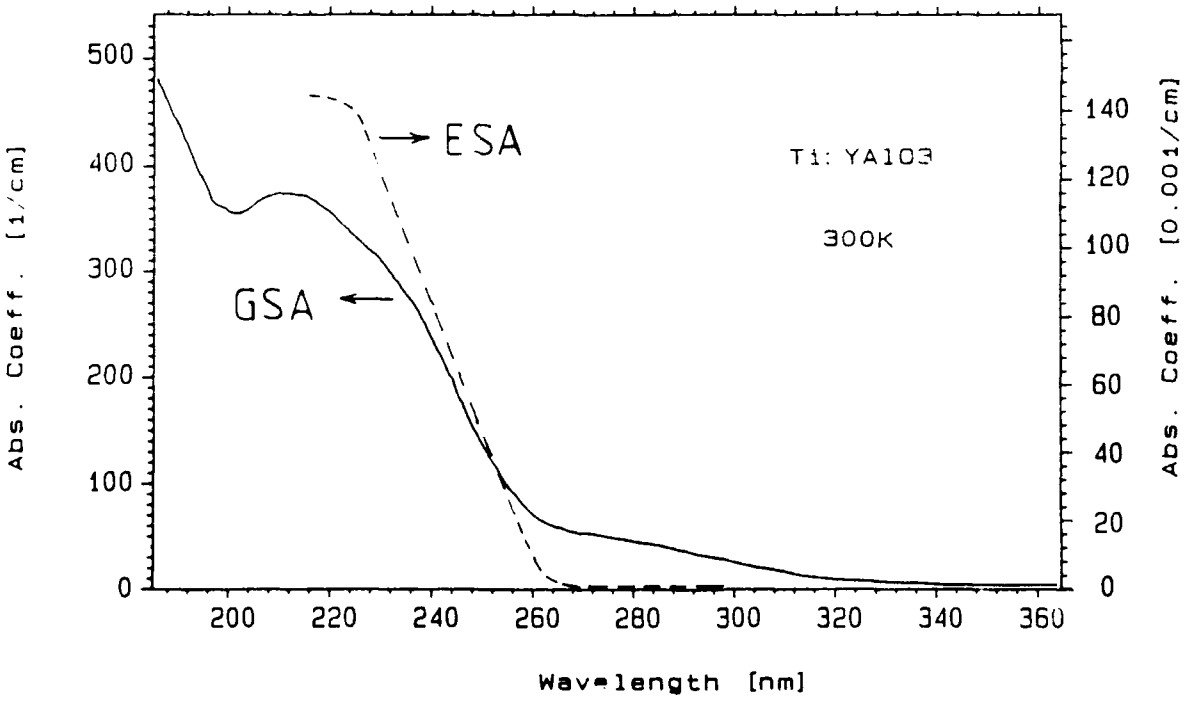

ESA and GSA spectra of $Ti:YAlO_3$

By comparing both, the ESA and GSA spectrum, it can be concluded, that the Ti charge transfer band is giving rise to the strong excited state absorption. From the pumping conditions an ESA cross section of about $1 \cdot 10^{-18}$ cm^2 is calculated for the 488 nm Ar wavelength. The peak cross section is estimated to be 10^{-17} cm^2, which matches well the expected value of a charge transfer band. Note, that this cross section is two orders of magnitude higher than the GSA value. In $Ti:Al_2O_3$ no ESA effect is measured in the whole spectral range.

The results clearly inticate, that in contrast to $Ti:Al_2O_3$ the pump efficiency of $Ti:YAlO_3$ is drastically decreased by ESA at high pump intensities. Therefore it is very unlikely to get this material lasing and if so, the efficiency will be extremely small.

References

[1] J.Kvapil, M.Koselja, J.Kvapil, B.Perner, V.Skoda, J.Kubelka, K.Hamel, V.Kubecek, Czech. J. Phys. B38 (1988) 237

[2] H.H.Tippins, Phys. Rev. B2, No. 1 (1970) 126

Time Resolved Excited State Absorption of $Mn^{2+}:MgAl_2O_4$

K.Petermann, R.Clausen
Institut für Angewandte Physik, Universität Hamburg
Jungiusstr.11, D-2000 Hamburg 36, FRG
E.Heumann, M.Ledig
Sektion Physik, Universität Jena
Max-Wien-Platz 1, DDR-6900 Jena, GDR

At first sight, Mn^{2+} in a low crystal field seems to be a suitable candidate for short wav ıth solid state lasers [1]. In spinel ($MgAl_2O_4$) Mn^{2+} occupies the tetrahedrally coordinated Mg sites providing a low crystal field environment. Under 456 nm Ar-laser excitation very bright green fluorescence is observed. However, no laser action could be obtained due to excited state absorption (ESA). In this paper we present time resolved ESA-measurements of $Mn:MgAl_2O_4$.

A 3 ps pump pulse of a tripled Nd glass laser (351 nm) was used for excitation of the Mn^{2+} ions and a 3 ps probe continuum for measuring the ESA. The delaytime between pump pulse and probe pulse was adjusted between zero and 2700 ps. Both, the probe beam and a reference beam were recorded by an optical multichannel analyzer OMA2.

The figure below shows the measured ESA spectra for 0, 900 and 2700 ps delaytime between pump and probe pulse. The steady state spectrum is taken from ref.[1]. Immediately after the pump pulse a broad absoprtion band is measured with the maximum at about 790 nm. 900 ps after the laser pulse this broad band disappears and four new absorptions at 830 nm, 715 nm, 655 nm and 550 nm are observed. With 2700 ps delaytime these bands

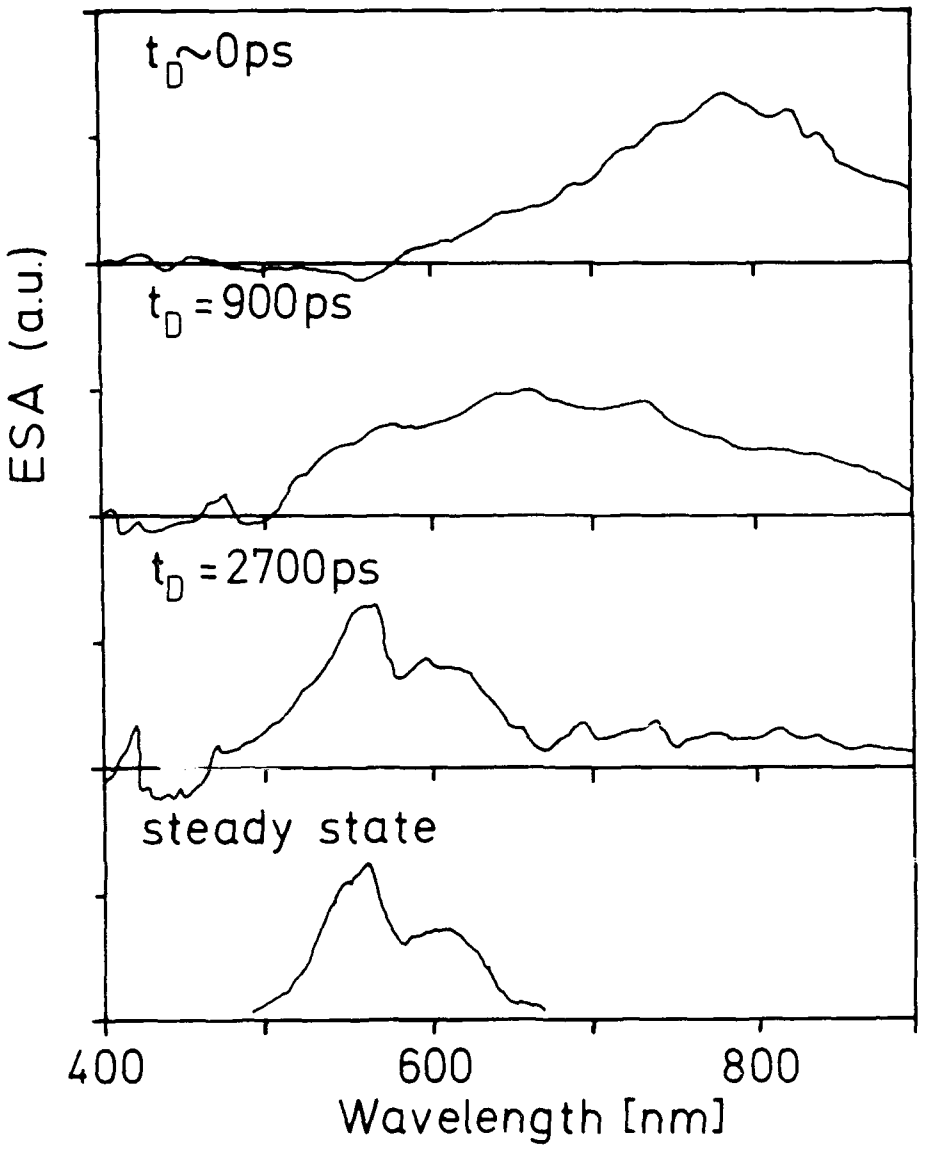

Mn^{2+} ESA spectra for various delaytimes

vanish again and two quite sharp peaks at 560 nm and at 600 nm develop. These peaks are also observed in the steady state experiment.

All spectra can be interpreted by intraionic transitions in the Mn^{2+} configurational coordinate model. At first electrons are created in the excited ^4E (^4D) level by absorption of the 351 nm pump pulse. At the same time the $^2T_1(^2I)$ and $^2A_2(^2I)$

levels are thermally populated giving rise to the 790 nm ESA. The lifetime of these coupled levels is 1050 ps as deduced from the time dependence of the ESA.

Subsequently the electrons relax down to the lowest excited $^4T_1(^4G)$ level via the intermediate $^4T_2(^4G)$ level. From this short living level ($\tau \approx 250$ ps) ESA is observed too with transitions $^4T_2(^4G) \rightarrow {}^4A_2(^4F)$ at 715 nm and $^4T_2(^4G) \rightarrow {}^4T_1(^4F)$ at 655 nm (900 ps curve). The remaining bands can be attributed to doublet-doublet transitions. Finally the electrons reach the lowest excited state ($\tau = 6.2$ ms). ESA is measured again terminating at the same quartet states as in the previous case (2700 ps curve).

These experiments clearly show, that the expected laser wavelength near 520 nm is strongly absorbed by two excited states, i.e. no gain and no laser action can occur.

[1] R. Clausen, K. Petermann, IEEE J. Quantum Electr. 24, No. 6, (1988), 1114

NOTES

MONDAY, MAY 1, 1989

NAUSET IV

4:00 PM–5:30 PM

MF1–MF5

SOLID STATE LASERS FOR SPECIALIZED APPLICATIONS

Norman P. Barnes, NASA Langley Research Center,
Presider

RECENT ADVANCES IN TUNABLE SOLID STATE LASERS

A.P. Shcadarevich
Institute of Physics
Leninski Aven. 70
Minsk, USSR 220072

Review of recent progress and current activity in tunable transition ion lasers in the Institute of Physics in Minsk (USSR) is presented.

NEODYMIUM GROUND STATE DEPLETED LASER CHARACTERIZATION AND DEMONSTRATION

R. Beach, R. Solarz, S. Mitchell, W. Krupke, L. Brewer, and S. Weinzapfel

Lawrence Livermore National Laboratory

P. O. Box 5508, L-487

Livermore, CA 94550

(415) 423-8986

SUMMARY

A recently proposed class of rare earth doped solid state lasers is described. These Ground State Depleted (GSD) lasers are characterized by a low laser ion doping density (5-10x10^{18} ions/cc) and a large fractional excited population inversion density (4-8x10^{18} ions/cc). For efficiency, these lasers must be pumped by narrowband (<few nm), intense (>10-50 kW/cm^2) sources. Four level operation at room temperature is obtained and efficient lasing to the ground electronic state manifold is achieved. The design domain of GSD lasers is dominated by the pump transition cross section (2-10x10^{-20} cm^2) and the associated saturation fluence/flux (2-10 J/cm^2 and 10-50 kW/cm^2). The GSD laser gain element is typically optically thick (Lambert Law) at the pump wavelength, but is substantially bleached at the working pump intensity.

Spectroscopic measurements have been performed in various Nd doped glass and crystalline materials to extract parameters (stark resolved emission spectra, branching ratios, fluorescence lifetimes, and stimulated emission cross sections) important to the design of a GSD laser. This study has allowed us to identify several systems amenable to experimental demonstration. The results of a demonstration in one of these systems consisting of a sample of Nd doped Y_2SiO_5 which is pumped by a flash lamp excited dye laser will be presented. Measurements are made to document the degree to which the ground state of the laser has been depleted, as well as measurements of extraction efficiency. An important problem present in GSD lasers, illustrated by the results of our demonstration, is holding off the gain of the Nd $^4F_{3/2} - {}^4I_{11/2}$ transition which typically has an emission cross section 5 to 10 times larger than the desired $^4F_{3/2} - {}^4I_{9/2}$ transition cross section. Several possible techniques for holding off the $^4F_{3/2} - {}^4I_{11/2}$ transition are discussed. These techniques include segmented laser designs, and the co-doping of laser samples with elements having a large absorption cross section in the 1.06 micron region while being relatively free of absorption in the 0.92 micron region of the spectrum. A system based on Yttrium Orthosilicate and co-doped with Nd and Sm will be presented as an example of the latter type GSD design along with available experimental results.

Continuous-wave tunable oscillation and superfluorescent operation of a monomode Yb^{3+}-doped fibre laser.

D.C. Hanna, R.M. Percival, I.R. Perry, R.G. Smart, P.J. Suni and A.C. Tropper, Department of Physics, University of Southampton, Southampton SO9 5NH, United Kingdom

1. INTRODUCTION

We have recently reported the results of a preliminary study of an Yb^{3+}-doped monomode silica fibre laser [1]. These results showed that Yb^{3+}-doped fibre lasers offer low thresholds, the possibility of pumping with AlGaAs diode lasers and a wide tuning range (from 1015nm to 1140nm).

The work described here is the result of a more detailed investigation of the Yb^{3+} system. An extended tuning range has been realised and oscillation on the 3-level transition at 974nm has been demonstrated. In addition, efficient superfluorescent emission at 974nm and 1038nm has been achieved.

The Yb^{3+}-doped fibre used in this experiment was characterised by an Yb^{3+} concentration of 575 ppm, numerical aperture of 0.16, cut-off wavelength 800nm and core diameter of 3.7μm. The pump source used was a Styryl 9M dye laser tunable over the range 800-920nm.

Figure 1 shows the energy level diagram of Yb^{3+}. The absorption band corresponding to the transition labeled 'PUMP' is centered at 910nm, but we have earlier shown that wavelengths as short as 800nm can efficiently excite the system. Level e has a lifetime of 700μs. Figure 2 shows the emission spectrum of the fibre, observed in sidelight to avoid self-absorption of the generated light. The peak centered at 974nm results from emission on the (3-level) e to a transition. The broad peak centered at 1035nm is a result of emission from e to the other Stark levels in the ground state. Only one Stark component is resolved in this room temperature emission spectrum. Unresolved Stark components, whose positions are not known, are indicated by dashed lines in Figure 1. This broad feature makes Yb^{3+} ideal candidate for a widely tunable laser system. We also note that Yb^{3+} has no further energy levels in the near infra-red or visible regions. Thus excited state absorption will not degrade the performance at high powers.

2. TUNABLE OPERATION

The resonator configuration shown in figure 3 was initially chosen to investigate tunable operation. The pump wavelength was 840nm in order to simulate pumping with a laser diode. Tuning was achieved by tilting the mirror M1 to selectively feed back a particular wavelength into the fibre. As can be seen from figure 4 (curve A) a tuning range from 1020nm to 1150nm was obtained. The fluctuations in the tuning curve were due to the a lack of control of the polarisation state of the light in the cavity. This problem

was overcome by using fibre loop polarisation controllers as described by Lefevre [2]. We also found that a single high dispersion prism provided insufficient discrimination to prevent simultaneous lasing at more than one wavelength. This problem was solved by the use of an additional prism. These two improvements allowed the tuning range to be extended from 1010nm to 1160nm (figure 4, curve B) and resulted in a smoother tuning curve.

Typically the threshold incident power of this laser was 60mW. Output powers were limited to 100μW owing to the >99.5% reflectivity of M1. Higher output coupling would result in higher output powers.

3. 3-LEVEL AND SUPERFLUORESCENT EMISSION

In addition to observing laser emission on the broad feature in figure 1, we have also observed lasing on the transition from e to a. Since this transition is 3-level in nature it requires higher pump intensities to reach threshold. To minimise the threshold we pumped the fibre at 900nm, close to the absorption peak at 910nm. With a butted high reflector on the input end and 20% output coupling at the other end, laser threshold was reached with 10mW of pump power absorbed. The slope efficiency was found to be 6%. With the available pump laser up to 300μW of output could be generated. Higher slope efficiencies are expected with optimised output coupling.

In addition to the laser behaviour described above, we have also observed efficient superfluorescent emission (amplified spontaneous emission) from this fibre at 974nm and at 1038nm. For this experiment a length of fibre was pumped through a butted high reflector as described above. The other end was terminated in index matching liquid to avoid oscillation off the fibre-air interface.

Optimum output power at 1038nm was achieved by pumping the fibre at 850nm. With 70mW of absorbed pump power, 31mW of output power was measured in a 19nm (FWHM) band. Optimised performance at 974nm resulted from pumping at 900nm. At this wavelength 10mW of output in a 2nm wide band was obtained with 30mW of absorbed pump power. In both cases the slope efficiencies were approximately 15%.

The 974nm superfluorescent emission is of great interest since this wavelength has recently been shown to be near the optimum for pumping Er^{3+}-doped fibre amplifiers [3].

4. REFERENCES

1. Hanna D.C., Percival R.M., Perry I.R., Smart R.G., Suni P.J., Townsend J.E. and Tropper A.C., Electron. Lett., 24, 1111-1113 (1988)
2. Lefevre, H.C., Electr. Lett., 16, 778-80 (1980)
3. Laming, R.I., Poole, S.B. and Tarbox, E.J., Opt.Lett. 13, 1084-6 (1988)

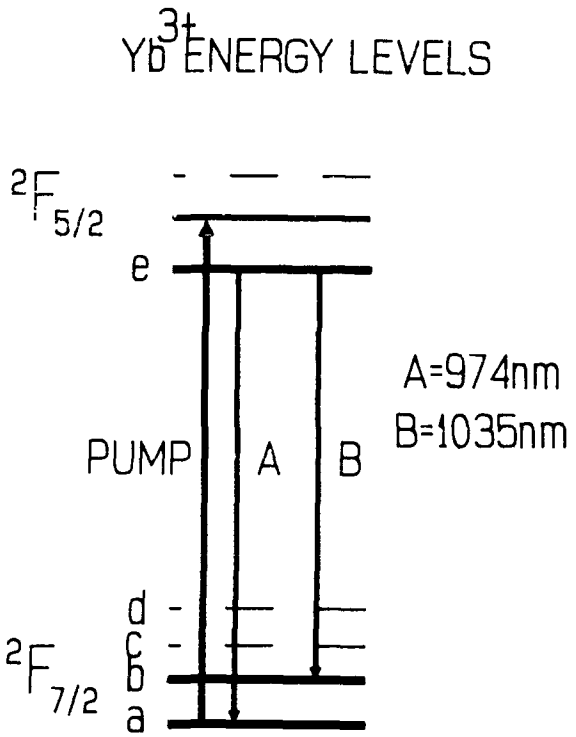

fig.1

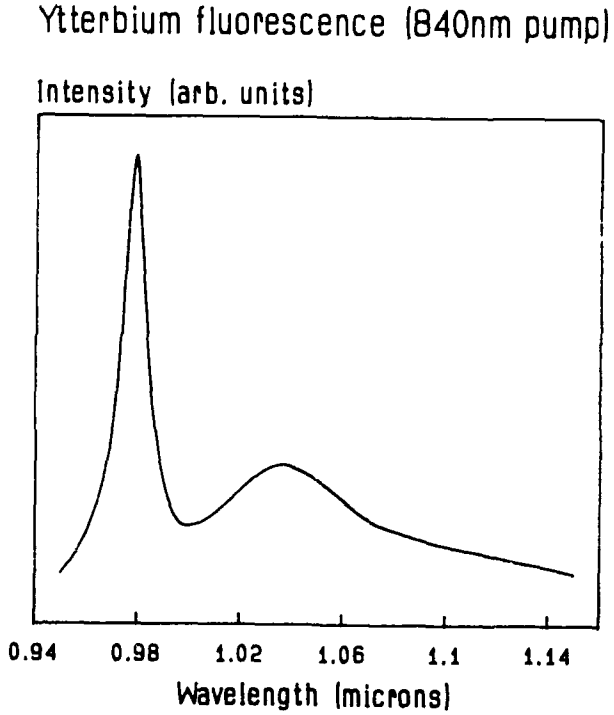

fig.2

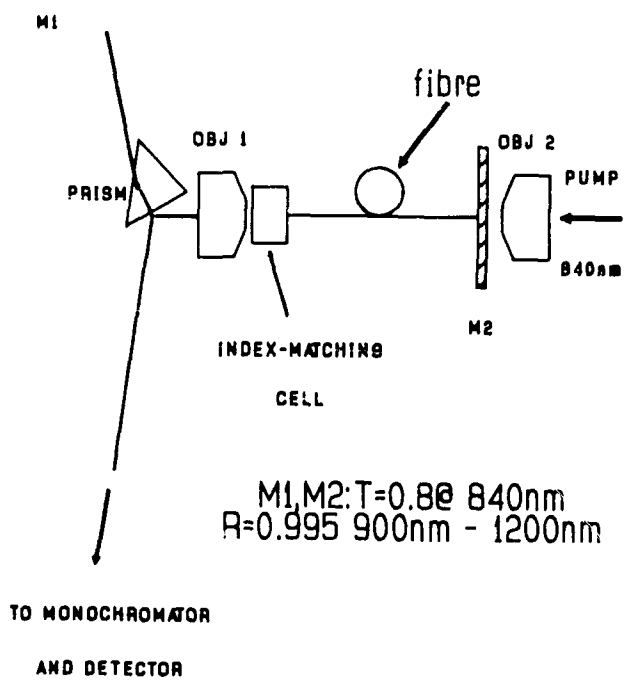

fig. 3

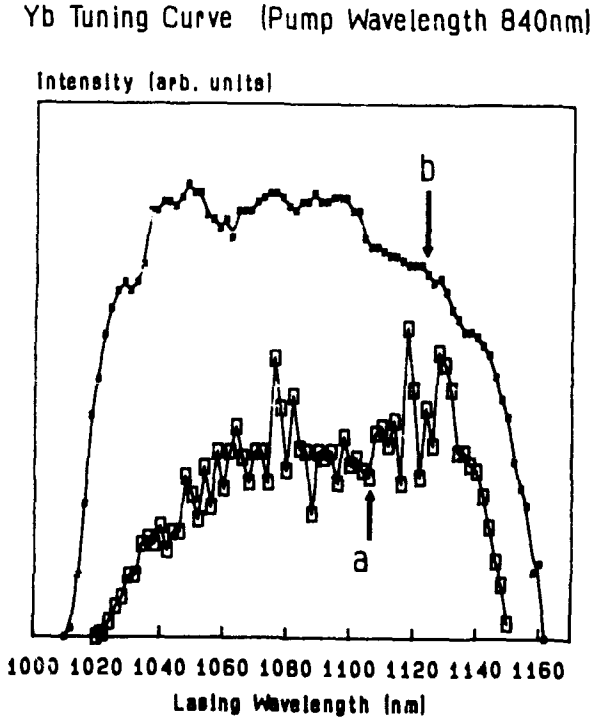

fig. 4

EFFICIENT 980nm OPERATION OF AN Yb^{3+} DOPED SILICA FIBRE LASER

J R Armitage, R Wyatt, B J Ainslie & S P Craig-Ryan
British Telecom Research Laboratories
Martlesham Heath
Ipswich
Suffolk IP5 7RE
ENGLAND

One of the major advantages of fibre lasers over their bulk counterparts is the possibility of achieving extremely high pump intensities by using a small core fibre and yet maintaining this small pump spot size over distances large compared to its Rayleigh length. Although this particular feature of fibre lasers is of some advantage in the case of four-level systems, it is of major significance for the operation of three-level lasers where the pump intensity requirements are frequently so high as to preclude CW operation in bulk samples. In this paper, results of spectroscopic measurements and of lasing experiments on Yb^{3+} doped fibres will be presented, and for the first time three-level operation of an Yb^{3+} doped laser at 980nm is reported. Since the slope efficiency is so high, this laser may well prove to be a useful source for pumping 1.5μm Er^{3+} doped fibre amplifiers as there is no excited state absorption of pump photons by Er^{3+} ions at this wavelength. [1]

The Yb^{3+} doped fibre used in the initial experiments consisted of a SiO_2-Al_2O_3-P_2O_5 core of diameter 2.1μm (Δn = 0.03) which was doped with around 2×10^{20} Yb^{3+} ions per cm^3. The fluorescence and absorption spectra of this fibre were measured, from which the spectral variation of the absorption and emission cross-sections could be calculated. These results are shown in Figure 1.

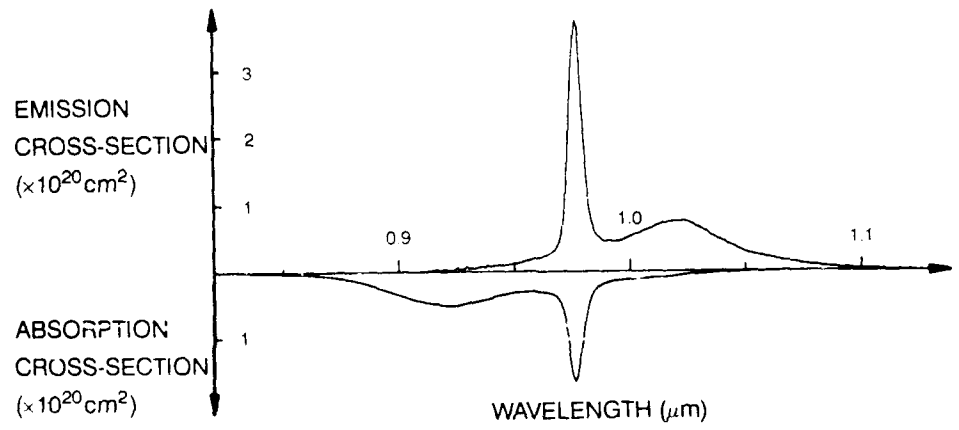

Figure 1 - Variation of absorption and emission cross-sections for Yb^{3+} ions in silica

For wavelengths greater than 1.04μm there is negligible ground-state absorption and so lasers operating at such wavelengths are essentially four-level systems. [2] In contrast, for an Yb^{3+} laser to operate at 980nm, the peak of the fluorescence spectrum, significant depopulation of the ground-state manifold *must* occur.

To assess the efficiency of different pumping wavelengths, the Yb^{3+} fluorescence, transverse to the fibre, was measured as a function of pump power in the fibre .

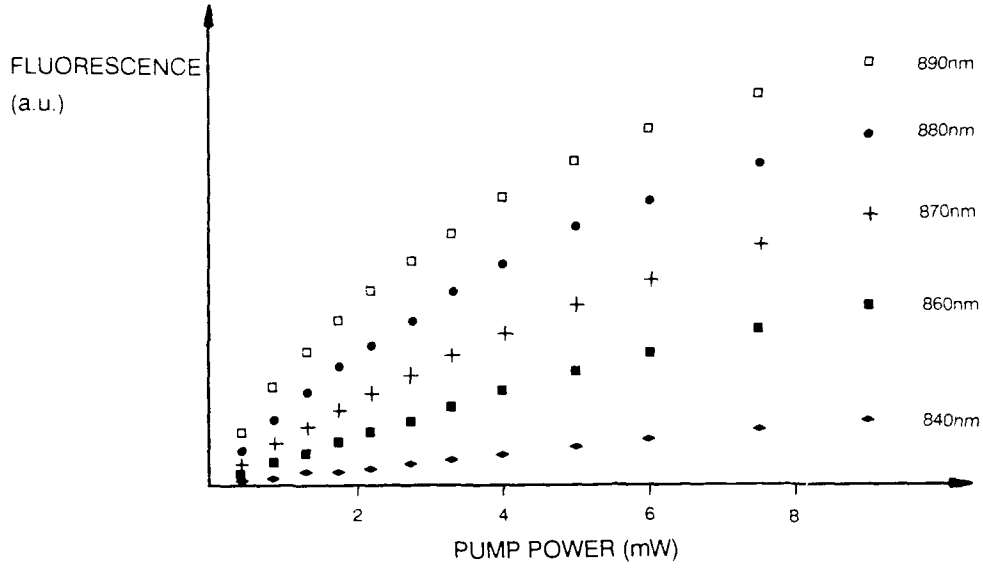

Figure 2 - Variation of Yb^{3+} fluorescence with pump power for various pump wavelengths

Since the fluorescence is proportional to the upper laser level population, these graphs show how the upper laser level population evolves with increasing pump power. Although the short wavelength tail of the absorption spectrum extends down to 840nm, the absorption cross-section at this wavelength is very low. Direct pumping of the Yb^{3+} ions at 840nm by GaAlAs lasers to produce gain at 980nm, is therefore going to be very inefficient, as extremely high pump intensities will be required. Nevertheless, it may be possible to produce a Nd^{3+}-Yb^{3+} fibre [3] and to utilise energy transfer from the Nd^{3+} ions to achieve laser action in the Yb^{3+} system. The efficiency of such a pumping scheme is under investigation. In the pure Yb^{3+} system however, pumping at wavelengths nearer 920nm will be very much more favourable. Although in Figure 2 the fluorescence signal corresponding to a fully inverted Yb^{3+} population remains unknown, the fact that the curves depart significantly from their low power linear behaviour indicates that depopulation of the ground-state manifold is occurring.

Since the single-pass gain at 980nm for this laser is so high and there are no problems with excited state absorption of either lasing or pump photons, initial laser experiments were attempted pumping at 890nm with a very simple configuration, using the 4% Fresnel reflections from the cleaved fibre ends to form the cavity. In order to achieve laser action at 980nm in a cavity with 'broad-band' reflectors, careful consideration must be given to the choice of fibre length, for if the fibre is too long the 1.03μm transition will reach threshold first. Experimentally, it was found necessary to use fibre lengths less than 12cm. The lasing

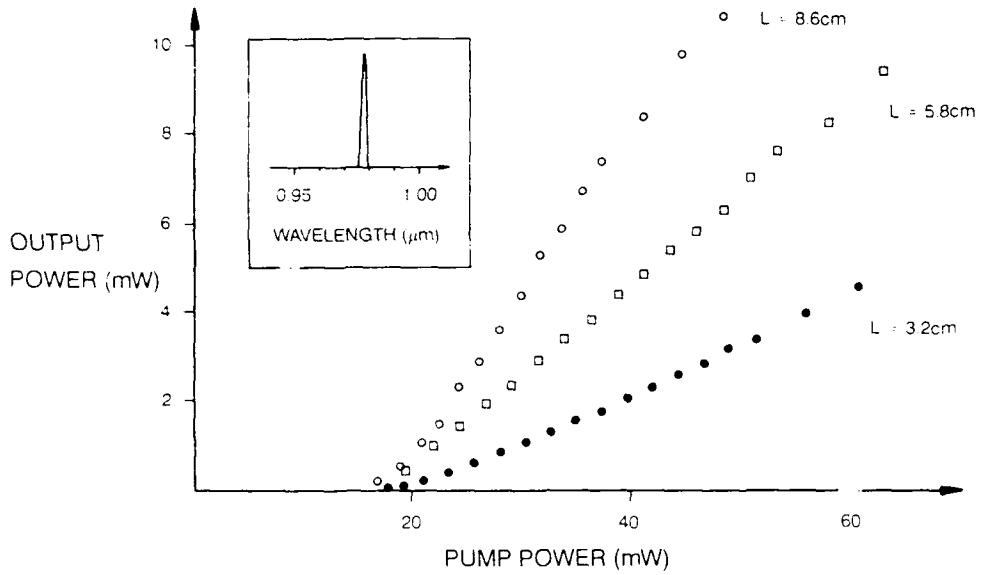

Figure 3 - Lasing characteristics at 980nm for three different lengths of Yb^{3+} doped fibre and lasing spectrum (inset)

characteristics for three different fibre lengths are shown in Figure 3. For the 8.6cm length of fibre, the slope efficiency against launched pump power is around 38%. Since equal powers are emitted from both ends of the cavity, and taking into account the fraction of launched pump power that is absorbed, all three lasers have close to 100% internal slope efficiency. Further increases in single-ended efficiency can be expected by using an asymmetric cavity consisting of a dichroic input mirror and a cleaved fibre end.

In conclusion, an Yb^{3+} fibre laser operating at 980nm has been demonstrated for the first time. Even though the doping density was as high as 2×10^{20} ions per cm^3 and a symmetric cavity was used, a single-ended slope efficiency of 38% was achieved. Work on Yb^{3+} fibres codoped with Nd^{3+} ions is in progress, in an attempt to produce a GaAlAs laser pumped 980nm source with which to pump an Er^{3+} doped fibre amplifier.

REFERENCES

1. R I Laming, L Reekie, D N Payne, P L Scrivener, F Fontana & A Righetti "Optimal Pumping of Erbium-doped fibre Optical Amplifiers" presented at ECOC'88, Brighton, U.K.

2. D C Hanna, R M Percival, I R Perry, R G Smart, P J Suni, J E Townsend & A C Tropper "Continuous-wave oscillation of a monomode ytterbium-doped fibre laser" Electronics Letters **24** 1111-1113 (1988)

3. E Snitzer "Laser emission at 1.06μm from Nd^{3+} -Yb^{3+} Glass" IEEE Journal of Quantum Electronics 2 562 (1966)

$^4I_{13/2} \leftrightarrow {}^4I_{15/2}$ EMISSION AND ABSORPTION CROSS SECTIONS FOR Er^{3+}-DOPED GLASSES

W.J. Miniscalco, L.J. Andrews, B.A. Thompson, T. Wei and B.T. Hall

GTE Laboratories Incorporated
40 Sylvan Road
Waltham, MA 02254

Widespread interest in Er^{3+}-doped glass lasers and amplifiers was stimulated by the first reports of single-mode fiber lasers [1] and amplifiers at 1.5 μm [2]. The excellent performance achieved by many research groups indicates a significant technological potential for Er^{3+}-doped fiber devices in sensor and telecommunications applications. With the exception of fluorozirconate fiber [3], however, the lasers and amplifiers reported have used Er^{3+}-doped silica codoped with aluminum or standard telecommunications fiber dopants such as germanium and phosphorus. The sensitivity of the gain and excited state absorption (ESA) spectrum to codopants and glass composition has not been extensively documented, and there have been few reports of cross sections for Er^{3+}-doped glasses. Since the gain and signal/noise ratio of three-level devices are quite sensitive to the cross sections, we have undertaken measurements of stimulated emission and absorption cross sections for the $^4I_{13/2} \leftrightarrow {}^4I_{15/2}$ transitions of Er^{3+} in a wide variety of glasses. In addition, Judd-Ofelt analysis has been used to calculate the glass composition dependence of the integrated strength of the ESA transitions that coincide with ground state absorption bands used for optical pumping.

The glasses investigated were representative silica, alumino-silicate, phosphate, fluorophosphate, and heavy metal fluoride compositions. For the silica compositions, the measurements were performed on fibers drawn from solution-doped [4] MCVD preforms. Samples of the other glasses were cut and polished from batch melts, and absorption cross sections were determined from absorption measurements and ion concentrations. The integrated $^4I_{13/2} \rightarrow {}^4I_{15/2}$ stimulated emission cross sections were determined by three independent procedures: Judd-Ofelt analysis, the measured absorption cross section, and the $^4I_{13/2}$ radiative lifetime.

Although the first two relationships are generally valid only for thermal energies (kT) greater than the transition bandwidth, they yield good results because each Stark level is a superposition of m_J states. This is confirmed by the insensitivity of lifetime to temperature [5]. Since accurate concentrations and doping profiles were not available for the fibers, the radiative lifetime was used to determine the integrated emission cross section from which was the integrated absorption cross section was calculated. Table 1 lists cross sections integrated with respect to frequency for representative glasses. The areas under experimental emission and absorption spectra were scaled to the integrated cross sections to generate peak cross sections and spectra such as are illustrated in Figure 1 for a fluorozirconate glass.

TABLE 1
$^4I_{13/2} \leftrightarrow {}^4I_{15/2}$ CROSS SECTIONS FOR Er^{3+}-DOPED GLASSES

	EMISSION		ABSORPTION	
SAMPLE	Integrated ($\times 10^{-8}$ cm^2/s)	Peak ($\times 10^{-21}$ cm^2)	Integrated ($\times 10^{-8}$ cm^2/s)	Peak ($\times 10^{-21}$ cm^2)
Silica P880324	2.7	8.9	2.4	7.4
Phosphate LG12	4.2	10.	3.7	7.8
Fluorophosphate LG11	4.0	8.9	3.5	6.7
Fluorophosphate LG14	5.3	10.	4.6	7.6
Fluorozirconate FG88	3.5	6.3	3.1	5.0

Table 1 reveals that phosphate and fluorophosphate glasses have the largest integrated cross sections while silicates have the lowest. The peak stimulated emission cross sections, however, are not in the same order because of large variations in bandwidth. The glasses are listed in Table 1 according to the observed trend in bandwidth, from silicates with the narrowest to fluorides with the broadest. The width and shape of the spectra are determined by the strengths of the individual Stark transitions which are resolved at low temperature. This, along with the displacement between the emission and absorption spectra and their temperature dependence, indicates that the bands are homogeneous at room temperature. Judd-Ofelt analysis of the ESA transitions indicates that they also follow the order in Table 1, being strongest for the silicates and weakest for the fluorides.

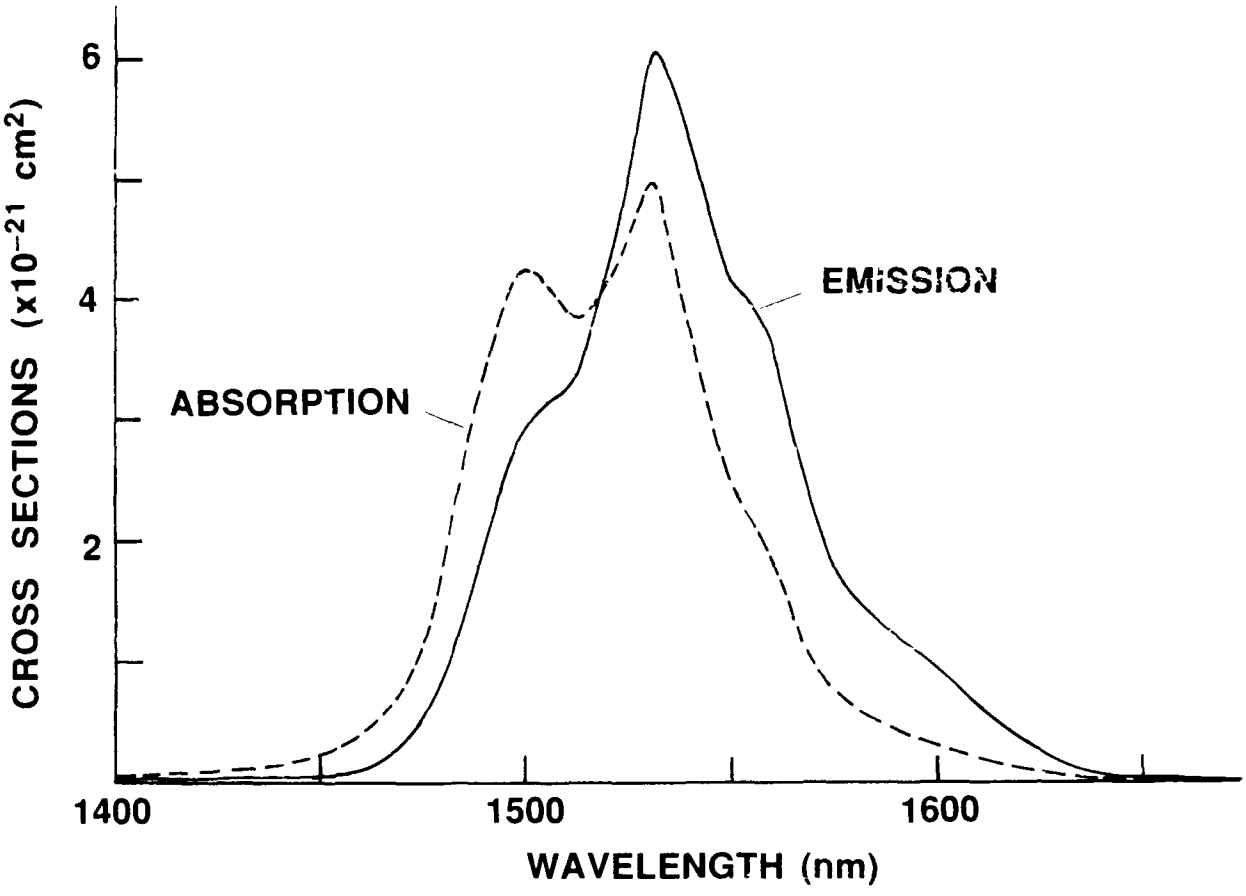

FIGURE 1: Emission and absorption cross sections for the $^4I_{13/2} \leftrightarrow {}^4I_{15/2}$ transition of Er^{3+}-doped Zr-Ba-La-Al-Na fluorozirconate glass.

[1] R.J. Mears, L. Reekie, S.B. Poole, and D.N. Payne, Electron. Lett. **22**, 169 (1986).

[2] R.J. Mears, L. Reekie, I.M. Jauncey, and D.N. Payne, OFC/IOOC'87, Tech. Digest Series 1987 **3**, 167 (1987).

[3] C.A. Millar, M.C. Brierley, and P.W. France, ECOC'88, IEE Conf. Publ. No. **292** - Part 1, 66 (1988).

[4] J.E. Townsend, S.B. Poole, and D.N. Payne, Electron. Lett. **23**, 329 (1987).

[5] T.J. Whitley, private communication.

NOTES

TUESDAY, MAY 2, 1989

NAUSET IV

8:00 AM–9:15 AM

TuA1–TuA5

ALEXANDRITE LASERS

Ivan A. Shcherbakov, USSR Academy of Sciences,
Presider

Amplification of 100 fsec, mJ Pulses in Alexandrite using Chirped Pulse Techniques

M. Pessot , J. Squier, G. Mourou
Laboratory for Laser Energetics
University of Rochester
250 East River Road
Rochester, New York 14623

Donald J. Harter
Allied Signal, Inc.
Corporate Technology
P.O. Box 1021R
Morristown, NJ 07960

The advent of chirped pulse amplification (CPA) [1] has led to a renewed interest in the development of solid-state amplifiers for ultrashort pulses. The broad bandwidths and high energy storage capabilities of solid-state materials such as alexandrite and Ti:sapphire point to the potential for these materials in the production of high energy femtosecond pulses. Recently, we reported on the generation of 300 fsec pulses at the millijoule level in an alexandrite regenerative amplifier [2]. In this paper we present new results extending the CPA technique to the generation of 106 fsec pulses with peak powers of 20 Gw.

For the generation of 100 fsec pulses, the amplifier was seeded with the self-phase modulated output from an optical fiber and grating expander. Streak camera measurements of the injected pulse revealed a strongly modulated temporal structure. We conjecture that this modulation arises from a linear analogue of optical wavebreaking [3] , in which frequency-shifted light in the leading (trailing) edge of the pulse overtakes unshifted light in the forward (rearward)tail.

The alexandrite regenerative amplifier (Fig. 1) uses a single Pockels cell to both Q-switch

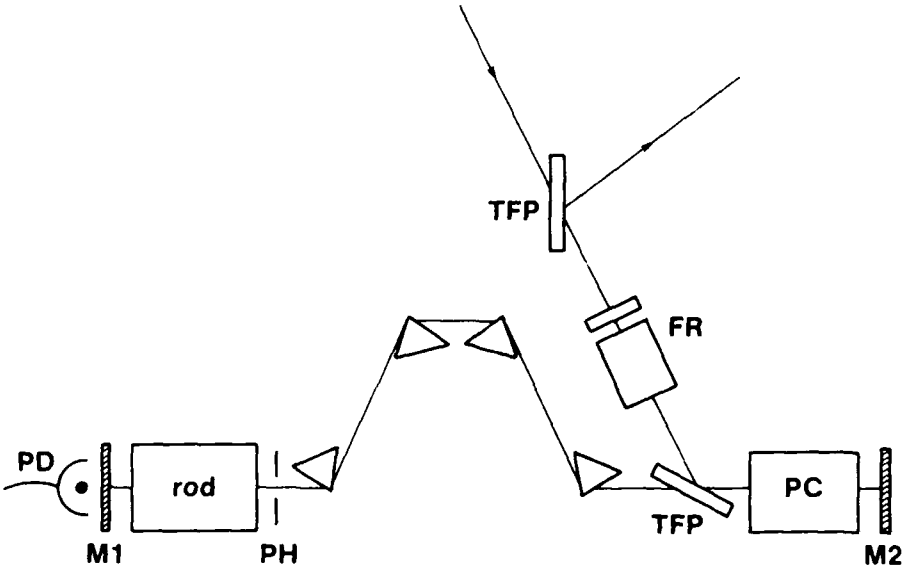

Z684

Alexandrite regenerative amplifier cavity. Four SF-10 prisms are used for higher order dispersion compensation.

and cavity dump the laser. A single pulse of 10 nj energy and 120 psec duration is switched in and trapped in the cavity. After about 40 roundtrips, the pulse is cavity dumped with an energy of 5 mJ.

The multipass regenerative amplifier configuration can present a substantial material path, particularly in a relatively low (single-pass) gain amplifier. The dispersion contributed by the material elements imposes limits on the achievable output pulse duration in a system which uses only gratings for compression. In Fig.2, we plot the output pulse correlation width as a function of the input pulse, under the assumption that the compression gratings have been adjusted to remove the linear chirp. The residual quadratic chirp limits our compressed pulsewidth to about 200 fsec. Compensation of both the linear and quadratic chirp can be achieved by using a combination of gratings and prisms [4] for the compression. Placing the prisms within the laser cavity allows one to take advantage of the large number of round trips so that relatively large amounts of quadratic dispersion can be compensated. With the insertion of four SF-10 prisms within the regenerative amplifier cavity (fig. 1), an overall compression factor of 1100x, to 106 fs was achieved, with peak powers in the 20 Gw range. A single shot autocorrelation of the compressed pulse is shown in Fig.3

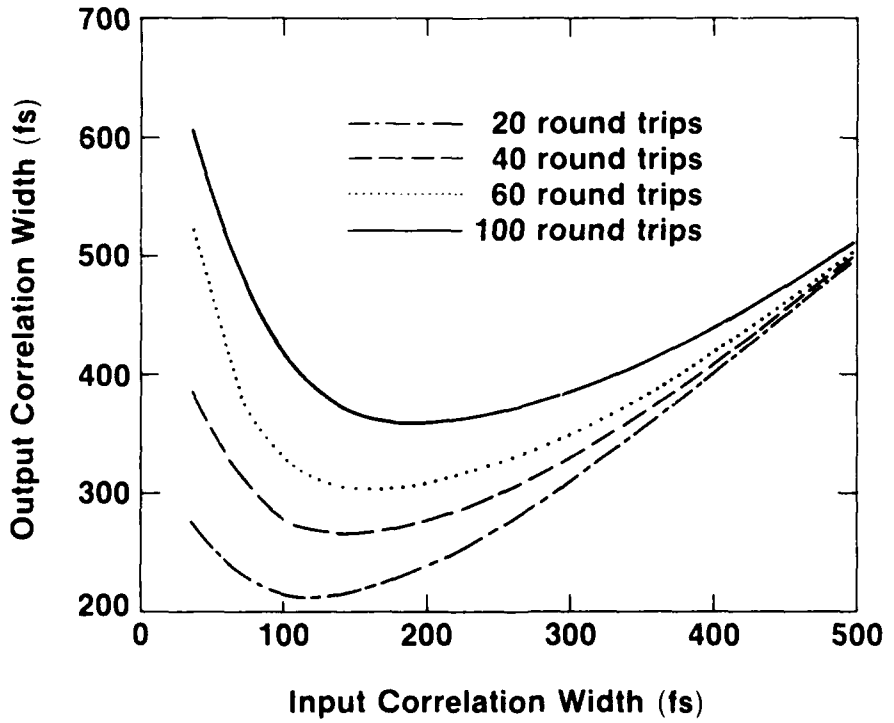

Z505

Pulsewidth limitations due to a residual quadratic chirp. Each curve is for a different number of roundtrips within the cavity.

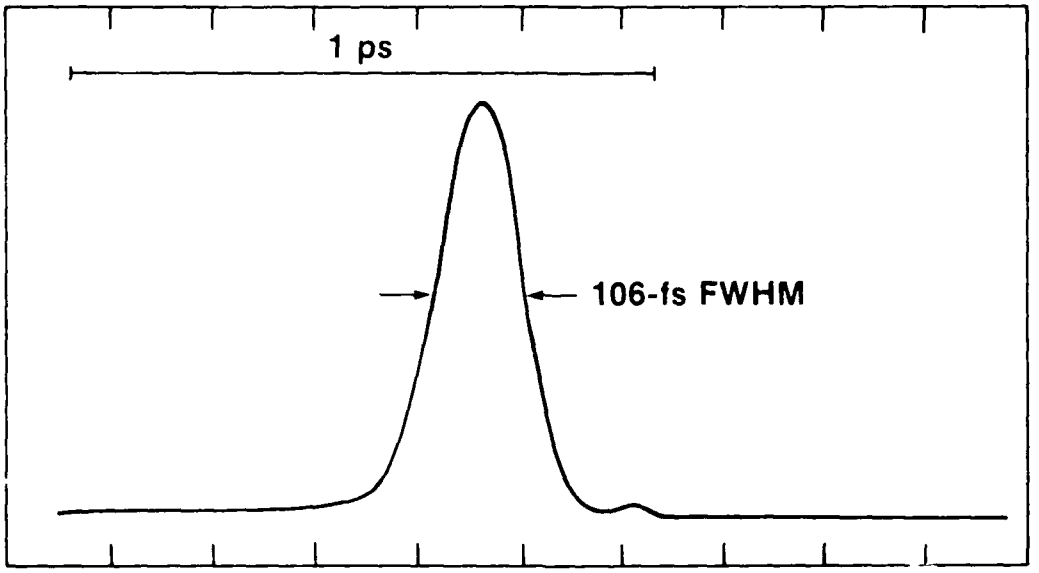

Z631

3. Background free, single-shot autocorrelation of the compressed pulse. Deconvolution is with a $sech^2$.

Precise wavelength matching of the source and amplifier was found to be critical for amplification of the broadband pulses. With an overall gain as large as 10^6, detunings as small as 3 nm from gain center were observed to severely modify the output spectrum. Evidence of gain narrowing and frequency pulling effects have been observed. Implications of these observations for the amplification of ultrashort pulses will be discussed.

In conclusion, we have extended the technique of chirped pulse amplification to the amplification and compression of pulses to the 100 fsec level in a broadband solid-state amplifying medium. A prism/grating compression system allowed for the compensation of quadratic dispersion which would otherwise severely limit the achievable pulse duration from such a source. Extensions of the work presented here point to the possibility of terawatt and higher powers with femtosecond pulses in the near future. This would have exciting applications in the areas of strong field physics and xuv/xray sources.

REFERENCES

1. P. Maine, D. Strickland, P. Bado, M. Pessot, G. Mourou, IEEE J. Quantum Electron. QE-24, 398 (1988).
2. M. Pessot, J. Squier, P. Bado, G. Mourou, D. Harter, to be published, IEEE J. Quantum Electron., January 1989.
3. W.J. Tomlinson, R.H. Stolen, A.M. Johnson, Opt. Lett. 10, 457 (1985).
4. R.L. Fork, C.H. Brito Cruz, P.C. Becker, C.V. Shank, Opt. Lett 12, 483 (1987).

Acknowledgements

This work was supported by the Laser Fusion Feasibility Project at the Laboratory for Laser Energetics which has the following sponsors: Empire State Electric Energy Research Corporation, New York State Energy Research and Development Authority, Ontario Hydro, and the University of Rochester. Additional support was provided by the United States Air Force Office of Scientific Research under contract F49620-87-C-0016 to the Ultrafast Optical Electronics Center at the Laboratory for Laser Energetics of the University of Rochester. Such support does not imply endorsement of the content by any of the above parties. The authors would like to thank Don Harter and Allied-Signal Inc. for a generous loan of equipment during the course of this work.

UNSTABLE ALEXANDRITE REGENERATIVE AMPLIFIERS FOR SHORT PULSE AMPLIFICATION

Jeff Squier
Laboratory for Laser Energetics
University of Rochester
Rochester, New York 14620

Gerard Mourou
Phillippe Bado
University of Michigan
EECS
1301 Beal Avenue
North Campus
Ann Arbor,MI.

Don Harter
Allied Signal, Inc.
Corporate Technology
P.O. Box 1021R
Morristown, New Jersey 07962

ABSTRACT

Unstable alexandrite regenerative amplifiers which can amplify nanosecond, picosecond, and femtosecond pulses to energies in excess of 200 mJ will be described.

We are interested in obtaining 100 fs range pulses at the joule level for possible new scientific studies in x-ray generation and nonlinear optics. Both excimer and solid-state lasers are presently being developed for these applications. Solid-state lasers have the advantages of being more compact and having substantially less ASE than excimer lasers. (ASE measurements will be presented.) For the amplification of 100 femtosecond pulses chirped pulse amplification (CPA) is necessary to prevent optical damage and whole beam self-focusing in the optical components. We have already applied CPA techniques to alexandrite to amplify 100 fs pulses to the millijoule range [1]. In chirped pulse amplification the 100 fs pulses are stretched at least 1000 times to 100 ps before being amplified. Currently, our stable alexandrite regenerative amplifier is limited by damage considerations to amplifying pulses in the 100-500 ps range to the 10 mJ level [2]. In an effort to extract more energy with the same type of pulse durations, a series of unstable alexandrite amplifiers have been investigated. In this paper we describe positive and negative branch unstable resonators which have allowed the pulse energy to be increased to 30-200 mJ.

In all the amplification systems presented here, a gain-switched laser diode capable of generating 100-500 ps pulses is used to seed the regenerative amplifier. The laser diode is a good alternative to a stretched 100 fs pulse in testing these amplifiers since it is compact and very reliable. The pulse duration and bandwidth are appropriate for testing damage thresholds and gauging any gain narrowing which occurs.

In the design of all of the unstable resonators a relatively low magnification (between the ranges of M=1.5 to 2) was used. This range was suitable for the round trip gain of 5-6 obtained from alexandrite.

Confocal negative branch unstable resonators were first considered. An aperture was placed at the internal focus and its diameter varied. A pockel cell (for switching the pulse in and out)

was to one side of the aperture while a thin film polarizer and the alexandrite rod occupied the other side. Normally it is desirable to switch the pulse out before the aperture after it has completed its last round trip through the rod. In these tests the pulse was allowed to travel through the aperture after its final pass through the rod. This was done to further clean the beam, and, since alexandrite lases in only one polarization, switching out in the other direction is difficult. With the aperture closed down so that the resonator was self-filtering [3], 10 mJ pulses were generated. Larger aperture sizes (which then removed the self-filtering condition) allowed the extraction of up to 30 mJ pulses before damage resulted. As the aperture diameter was increased the beam quality decreased. To further increase the amount of energy that can be safely extracted from alexandrite larger spot sizes on the damage prone elements of the resonator are needed. This requires increasing the resonator length in order to retain the same magnification. Unfortunately, for such low magnification these lengths become prohibitively long.

Positive branch unstable resonators have yielded substantially larger pulse energies while maintaining reasonable dimensions. The resonator configurations used were also confocal or near confocal. With these resonators up to 200 mJ in a 100 ps pulse have been obtained before optical damage resulted. The hard aperture used in these designs produces Fresnel ringing which must be cleaned up in order to obtain diffraction limited focusing. Thus far measurements of the output beam reveal that 55 to 70% throughput is obtained if the beam is spatially filtered. Resonators using other apertures to enhance beam quality will also be described.

Two unstable resonators used in tandem can be used to increase the pulse energy from 200 mJ to the joule level. The second amplifier is a positive branch unstable resonator in which the injected pulse makes two to three round trips. The spot size of the input pulse increases by a factor M (equal to the magnification of the resonator) for each round trip taken. The magnification of the

resonator is chosen such that the beam area will grow at the same rate as energy is accumulated,with the energy density remaining constant. The advantages of using the resonator in this manner, and initial results will also be presented.

REFERENCES

1. M.Pessot, J.Squier, G.Mourou, and D.Harter "Chirped Pulse Amplification of 100 fs Pulses", submitted to *Optics Letters.*

2. P.Bado, M.Pessot, J.Squier, G.Mourou, D.Harter "Regenerative Amplification in Alexandrite of Pulses from Specialized Oscillators", *IEEE J. Quantum Electron.*,vol.QE-24,pp.1167-1171,1988.

3. P.G. Gobbi, S.Morosi, G.C.Reali, and Amin S. Zarkasi,"Novel Unstable Resonator Configuration with a Self-Filtering Aperture: Experimental Characterization of the Nd:YAG loaded Cavity", *Appl. Opt.*, vol.24,pp.26-33,1985.

Birefringence of Solid-State Laser Media: Broadband Tuning Discontinuities and Application to Laser Line Narrowing

J.S. Krasinski, Y.B. Band*, T. Chin, D.F.Heller, R.C. Morris and P.A. Papanestor
Allied-Signal Inc., Corporate Technology Center, P.O.B. 1021R, Morristown, N.J. 07960
* Permanent Address, Ben-Gurion University, Beer-Sheva, Israel

Most lasers incorporate intracavity polarization sensitive elements, e.g. Brewster plates, birefringent tuners[1-3], windows, etc. Generally, a light beam propagating in a birefringent material splits into two orthogonally polarized components (ordinary and extraordinary) that propagate with different velocities and different ray paths. The intensities of the components depend on the mismatch angle between the polarization axis of the cavity and the crystal axis, and on the gain and loss for each component. For rays propagating parallel to the z axis, the velocities of the two rays are determined by n_x and n_y. When the electric vector lies off axis in the x-y plane, there is a relative phase shift Δ between ordinary and extraordinary ray components, $\Delta = 2\pi|n_x - n_y| l/\lambda$ (l is the total path length of the light in the birefringent material before entering the polarizer, and λ is the wavelength) and the exit beam is elliptically polarized. The electric field components can be written as

$$E_x = E_0\, g_x^{1/2} \cos\alpha \cos(\omega t+\Delta_x)\,, \qquad (1)$$

$$E_y = E_0\, g_y^{1/2} \sin\alpha \cos(\omega t+\Delta_y)\,, \qquad (2)$$

where $\omega=c/\lambda$ is the frequency of the wave, α is the angle between the x axis and the axis of the polarizer, g_x and g_y are the intensity amplification factors ("gain" from polarizer to polarizer) for polarization along the x and y axes, respectively, and the phase shifts are $\Delta_x= -2\pi n_x l/\lambda$, and $\Delta_y = -2\pi n_y l/\lambda$.

For a polarized beam with electric field E_0 incident on an optical system consisting of a birefringent gain medium and a polarizer (with axis parallel to E_0), the output electric field is given by:

$$E_{out} = E_0 [\, g_x^{1/2} \cos^2\alpha \cos(\omega t+\Delta_x) + g_y^{1/2} \sin^2\alpha \cos(\omega t+\Delta_y)]\,. \qquad (3)$$

The time averaged output intensity is

$$I_{out} = E_0^2/2\, \{[g_x^{1/2} \cos^2\alpha + g_y^{1/2} \sin^2\alpha \cos(\Delta_y-\Delta_x)]^2 + [g_y^{1/2}\sin^2\alpha \sin(\Delta_y-\Delta_x)]^2\}. \qquad (4)$$

The maximum modulation depth is obtained when $\alpha=\pi/4$. For $g_x = g_y = 1$, the solution for the intensity (Eq. 4) corresponds to the standard Lyot filter solution.[1-3] Clearly, from Eq. (4), the transmitted intensity, I_{out} is periodic in wavelength with the free spectral range is given by

$$\Delta\lambda = \lambda^2 / (|n_x - n_y|\, l)\,, \qquad (5)$$

where l is the total path length of the light in the birefringent material before entering the polarizer. In a standing wave cavity laser containing a birefringent gain medium of length L and a single polarizing element $l=2L$, since the light passes through the gain medium twice before entering the polarizer. For a ring laser, or for a standing wave cavity configuration in which the laser medium is sandwiched between two polarizers, the light beam passes only once through the gain medium before entering a polarizer. Thus, $l = L$, and the free spectral range is twice that of a standing wave cavity containing one polarizer. In all cases, the free spectral range decreases with increasing birefringence and with propagation length.

If continuous tunability without modulation of the intensity as a function of frequency is desired, very careful alignment of the gain medium at $\alpha=0$ in order to maintain the polarization of the incident beam is necessary. Alternatively, one can intentionally misalign the rod at $\alpha\approx\pi/4$ and

utilize the resulting selectivity to obtain narrow bandwidth from the laser. This will result in laser output in a narrow range of wavelengths near the maxima of the function given in Eq. (4). However, continuous tunability can be achieved by insertion of an adjustable intracavity birefringent compensator.

For a c-axis cut alexandrite laser rod [Cr^{3+}:$BeAl_2O_4$ with optical principal axes (x,y,z) coinciding with the crystallographic axes (c,a,b) respectively and propagation along the optical x axis], the free spectral range is given by Eq. (5) with n_x and n_y replaced by n_a and n_b respectively. Fig. 1 shows the gain as a function of wavelength for g_b=3, g_a=1.18 and the rod sandwiched between polarizers for α = 5, 15, 25 and 45^0. The modulation (and selectivity) increases with mismatch angle and reaches a maximum at 45^0 while the gain at transmission maximum decreases with angle and reaches a minimum of about 70% of g_b at 45^0. The decrease of the intensity at the transmission maximum with increasing mismatch angle α results from the fact that $g_a \neq g_b$. Note that an anisotropic gain medium does not act as a polarizer since it does not reject components polarized perpendicular to the high gain axis.

Fig. 2a shows the transmission spectrum of a typical five element birefringent tuner. Fig. 2b shows the transmission spectrum of an unpumped polarizer-alexandrite rod-polarizer system. The b axis of the alexandrite crystal in Fig. 2b was intentionally misaligned by $\alpha=\pi/4$ which corresponds to maximum contrast of the transmission curve. Fig. 2c shows the spectrum of a pulsed alexandrite laser containing the same rod sandwiched between two polarizers, but also containing a very low dispersion glass prism. The prism permitted lasing over a large bandwidth. In the lasing experiment, Fig. 2c, the rod was misaligned by only a few degrees. Clearly, there is a very good correspondence between the transmission peaks of the passive system and the lasing wavelengths. The transmission period is about 0.77 nm, in agreement with Eq. (5). The resolution in Figs. 2a-c is instrumentally limited to ~0.3 nm. The selectivity of the tuner (Fig. 2a) is much less than that of the alexandrite rod (Fig. 2b).

Without introduction of additional intracavity elements, the output is narrow-band and tunable only in discrete jumps of a few angstroms, corresponding to the free spectral range of the rod-tuner. This was demonstrated in our laboratory by tuning with a five element birefringent tuner and utilizing the birefringence of the rod at an angle of $\pi/4$ between the polarizer axis and the b-axis of the crystal. The output wavelength hopped by increments equal to that obtained in Eq. (5). The output power was periodically modulated as a function of wavelength with maxima (minima) at wavelengths corresponding to the maximum (minimum) of the product of the transmissions of the tuner and polarizer-rod-polarizer system. Inserting an adjustable birefringent compensator permits the laser to be tuned continuously (simultaneously adjusting the birefringent tuner for maximum power). The resolved spectrum of the laser output consisted of two adjacent cavity modes. At higher pumping levels, more modes were observed. The spectral narrowing is obtained without insertion of any additional intracavity elements. The only "price" for the spectral narrowing is some gain reduction when $g_a \neq g_b$.

For tunable birefringent solid-state lasers, we have shown that the birefringence of the active medium can be used for spectral narrowing of the laser output. The polarizing element together with the laser rod form a birefringent Lyot type filter[1-3] whose gain is polarization dependent. An inadvertent few degree misalignment is sufficient to cause significant modulation of laser output power with wavelength. For alexandrite rods, a free spectral range of a few angstroms for a typical length rod (~10 cm) can be obtained. We have exploited these effects to produce narrow-band tunable output from an alexandrite laser. This method of obtaining narrow-band output is easy to implement since it does not require insertion of additional intracavity elements. High selectivity is obtained since the rod behaves as a very thick birefringent filter and therefore a very narrow laser bandwidth is obtained without intracavity etalons. Continuously tunable narrow-band output is obtained with introduction of a birefringent compensator. This method is applicable not only for alexandrite lasers but also for lasers based on all other birefringent gain media, e.g. ruby, Ti-sapphire, Nd-BEL, Nd-YLF, etc.

References

1. B. Lyot, Compt. Rend. 197, 1593-1595 (1933).
2. A.L. Bloom, J. Opt. Soc. Amer. 64, 447-452 (1974).
3. G. Holtom and O. Teschke, IEEE J. Quant. Electron. QE-10, 577-579 (1974).
4. J.C. Walling, H. Jenssen, O. Peterson, and R.C. Morris, IEEE J. Quant. Electron. QE-16,1302 (1980).

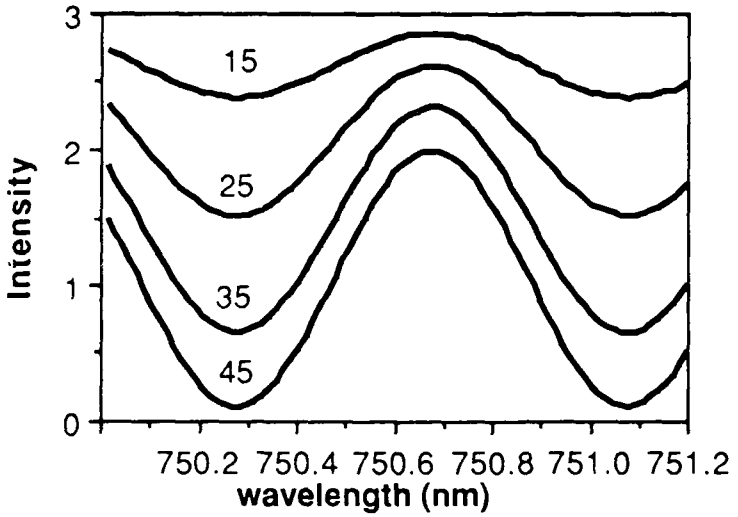

Fig. 1. Wavelength dependence of amplification for g_a= 1.18, g_b= 3 and various misalignment angles. α = 15, 25, 35, 45 ^{0}. Rod length L equals 128.8 mm.

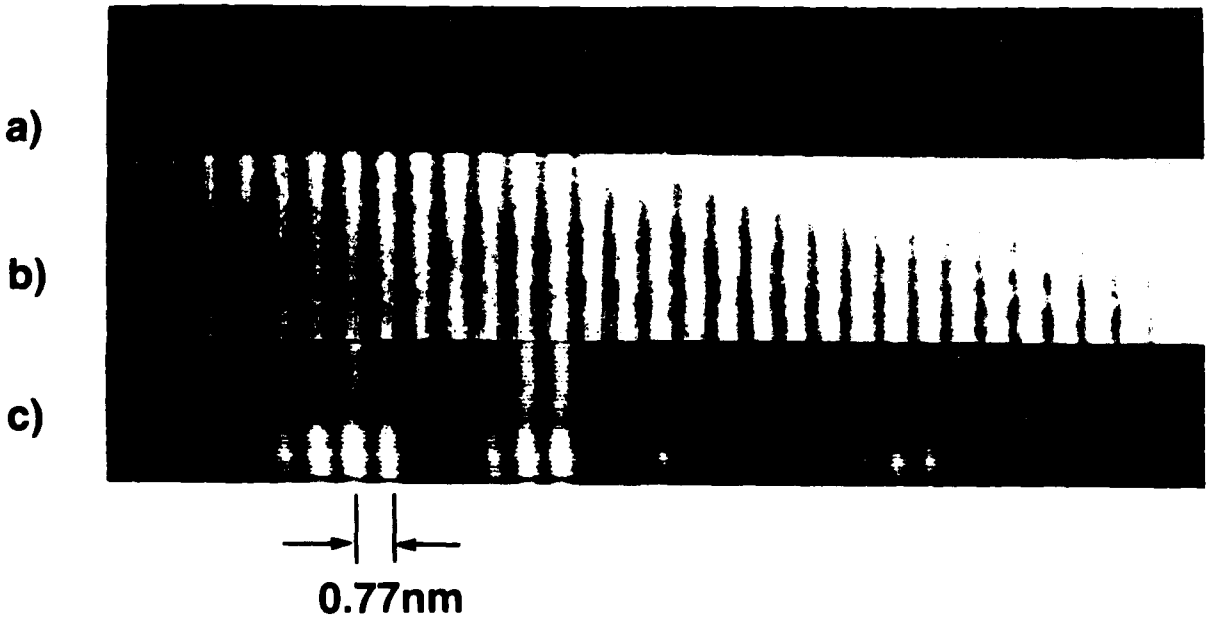

Fig. 2. (a) Transmission of a five element tuner (quartz plate thickness ratios 1:2:2:5:5 where 1 equals 0.513 mm). (b) Transmission spectrum of an unpumped polarizer- alexandrite rod-polarizer configuration. (c) Output spectrum of an alexandrite laser containing the rod sandwiched between two polarizers (same rod as in Fig. 1, $\alpha=\pi/4$).

FREQUENCY DOWN-CONVERSION OF A LOW PEAK POWER ALEXANDRITE LASER THROUGH MULTIPLE INTRACAVITY STIMULATED RAMAN SCATTERING

F. de Rougemont, J. Frey and R. Frey
Laboratoire d'Optique Quantique du Centre National de la Recherche Scientifique, Ecole Polytechnique, 91128 Palaiseau Cedex, France

Stimulated Raman scattering (SRS) has been demonstrated to be an efficient technique for extending the tuning range of available tunable lasers.[1] Nevertheless, as the Raman gain is proportional to the peak power of the pump laser, efficient frequency down-conversion can be obtained only for high peak power lasers. This is not the case for low energy (some tens of millijoules) alexandrite laser: due to the low gain of alexandrite material, the pulse duration is large (some hundreds of nanoseconds). When SRS is performed inside a high Q cavity, efficient down-conversion can be obtained also for low peak power lasers if there is no absorption at the Stokes frequency. This point is very crucial in the infrared: namely, most of the Raman materials (liquids and gases) exhibit overtones absorption bands. Among the possible Raman media, only hydrogen does not suffer from this disadvantage. On the other hand, as the vibrational Raman shift (4155 cm^{-1}) is larger than alexandrite tunability (about 1000 cm^{-1}), it is impossible to get a continuous tunability in the infrared by using the standard multiple stimulated Raman scattering technique.[1]

The paper presents a technique which can lead to the generation of continuously tunable infrared sources through multiple intracavity SRS. The principle is to perform inside the same cavity one or several rotational SRS (Raman shift

: 600 cm^{-1}) of the first Stokes frequency ω_v generated inside the cavity through vibrational SRS.

The experimental setup was simply constituted of an alexandrite Q-switched oscillator [2] and a Raman cavity. The alexandrite laser was operated at a 10 Hz pulse repetition rate and delivered 20 mJ energy pulses in a 300 ns duration; its wavelength was tunable between 0.72 μ m and 0.78 μm and the spectral bandwidth was less than 0.1 cm^{-1}. The laser beam was focused into the nearly concentric Raman cavity. Both mirrors were located inside the hydrogen cell, thus ensuring weaker losses than 1% at frequency ω_v.

As a demonstration of the process, figure 1 shows the output energy (continuous line) together with the reflectivity of the cavity mirrors (dashed line) versus wavelength for three SRS (one vibrational and two rotational). The decrease of intensity obtained around 1.26 μm was due to larger losses at this wavelength, thus reducing the efficiency of the energy extraction.

When the cavity was without losses at the second Stokes frequency (R > .98) a third rotational Stokes component appeared around 1.31 μm with substancial energy (0.3 mJ). Such an observation demonstrated the possibility of extending the tuning range down to the IR by multiple intracavity SRS process. The duration of the infrared pulses varied from nearly 200 ns to 30 ns depending on the Q factor of the cavity. Finally the quantum efficiency of the down-conversion process was about 10%. Larger values could be obtained with a monomode pumping laser ensuring a better spatial matching of cavity and pump laser transverse modes.

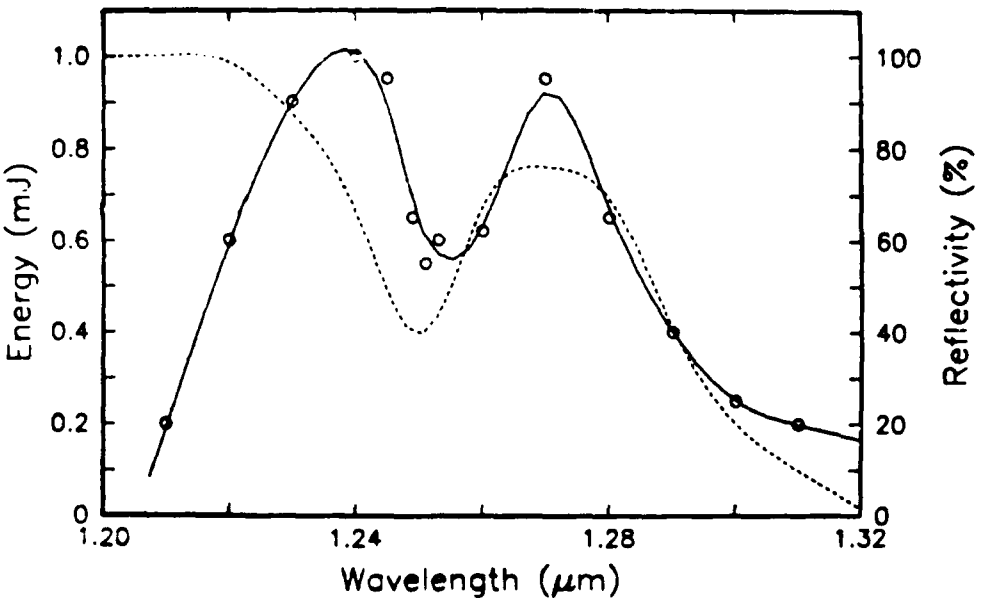

Figure 1. Output energy of the second rotational Stokes component (continuous line) and reflexion coefficient of the mirrors of the cavity (dashed line) versus wavelength.

Experiments are presently under way to extend the tuning range down to the infrared by using other coatings for the mirrors of the cavity.

References

1. A. de Martino, R. Frey and F. Pradere, IEEE J. of Quant. Electron., QE 16 1184 (1980)

2. F. de Rougemont, V. Michau and R. Frey, Tunable Solid State Lasers II , Eds A. B. Budgor, L. Esterowitz and L. G. DeShazer, Springer Verlag, Berlin (1986)

TuA5-1

Enhancement of CW Alexandrite Laser Performance

R. E. Bonanno
Lawrence Livermore National Laboratory
P. O. Box 808
Livermore, California 94550
415/422-9975

and

D. J. Harter and O. Montoya
Allied-Signal Corporation
P. O. Box 1021R
Morristown, New Jersey 07960
201/455-5117

Summary

CW alexandrite laser technology, as compared to pulsed alexandrite laser technology, is still in its infancy. The physical and laser properties of alexandrite have been extensively reported elsewhere.[1,2] The parameter most germane to cw operation is the stimulated emission cross section-upper state lifetime product (0.7×10^{-20} cm$^2 \times 262$ μsec), which is 50-100 times smaller than in Nd:YAG, and roughly the same as in Ti:Sapphire. The low emission cross section and concomitant low gain make lamp-pumped cw operation of alexandrite challenging. In this paper we report on three areas of research: pump reflector design, rod quality characterization, and optical resonator design, which have led to improved performance of cw alexandrite lasers.

Highly distorted thermal lensing is observed in cw alexandrite due to the focusing nature of the elliptical pump reflectors in combination with the small (~1 mm) arc diameter of the Hg lamps and the high pump powers required to achieve lasing. This can degrade the performance of the laser in terms of both output power and beam quality. In an effort to mitigate the effects of the thermal lens, a non-imaging, single-lamp pump reflector has been designed and fabricated. We have compared the performance of the non-imaging reflector, called an "invellipse", to a single-

lamp elliptical pump reflector. Although the laser performance for these two pump reflectors is the same, the thermal lensing observed with the non-imaging reflector is reduced by more than a factor of 2. This is a result of more uniform pumping, which reduces the thermal gradient in the rod.

Rod quality is critical to cw alexandrite performance. The output power from rods of the same diameter and dopant concentration can vary by as much as an order of magnitude. This is clearly indicated in Fig. 1 which shows the input versus output power curves for a selection of 3-mm rods. One of the goals of this research was to identify and quantify the cause of this wide variation in cw laser performance. We believed that optical quality was a possible determinant in laser performance. It is known that the optical quality of a rod can be improved by annealing it to relieve core-induced stresses.[3] Thus, we hoped that through annealing we could improve laser performance. We compared the performance of several rods before and after annealing and have found no significant improvement in laser performance due to the annealing process. We will report on a series of loss measurements that identify small-angle scattering as the dominant factor in laser rod performance. We believe that this technique can be useful in selecting low-loss boule sites from which rods can be cored for use in cw alexandrite laser systems.

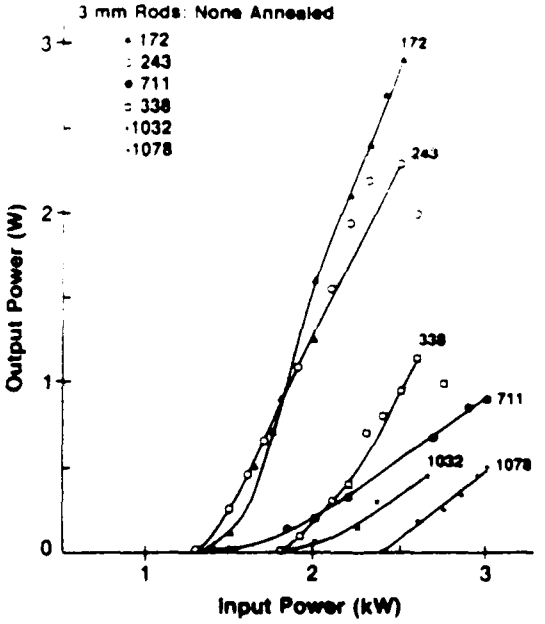

Fig. 1. Comparison of performance for 3-mm rods

Thermally insensitive resonators have been designed which provide high power in a large TEM_{00} mode from cw Nd:YAG lasers.[4] We have used similar design techniques to obtain enhanced multimode output in cw alexandrite lasers. We will compare the results obtained with the thermally insensitive resonator to those obtained in a more conventional resonator. We will discuss the effect of varying the TEM_{00} mode size on beam divergence and output power.

References

1. J. C. Walling, O. G. Peterson, H. P. Jenssen, R. C. Morris, and E. W. O'Dell, *IEEE J. Quantum Electron.*, **QE-16**, 1302 (1980).

2. H. Samelson, J. C. Walling, T. Wernikowski, and D. J. Harter, *IEEE J. Quantum Electron.*, **QE-24**, 1141 (1988).

3. D. J. Harter, unpublished results.

4. S. De Silvestri, P. Laporta, and V. Magni, *Opt. Lett.* **11**, 785 (1986).

TUESDAY, MAY 2, 1989

NAUSET III

9:15 AM–10:15 AM

TuB1–TuB6

Cr RELATED ISSUES / POSTER SESSION

Robert C. Morris, Allied-Signal, Inc., *Presider*

Laser Pump Chamber Optimization: Modeling and Experimental Verification of Absorption in Biaxial, Trichroic Media

Richard E. Boyd, Jerry W. Kuper, Donald J. Harter

Allied-Signal Inc.
P.O. Box 1021R
Morristown, NJ 07960
(201) 4555110

Summary

To predict and optimize solid state laser performance, the excitation and heat deposition profiles within the gain medium must be known. These profiles are determined by the distribution of pump radiation at the surface of the gain medium and the absorption of this radiation in the medium. The absorption is simply calculated using Beer's Law with the appropriate coefficient. Most media are isotropic, and the absorption coefficients depend only on wavelength. Alexandrite, however, is a trichroic, biaxial crystal, and requires a complex calculation to determine the absorption coefficient.

A model which handles energy propagation and absorption in a generalized transmitting medium has been formulated. Depending on the values of the physical constants used, the model can calculate energy deposition in crystals which may exhibit pleochroism and which are isotropic, uniaxial, or biaxial.

The model has been used to calculate the relative excitation efficiency of various materials. For example, results of

comparing pumping on the axis of Nd:YAG and alexandrite rods indicate that when both materials are pumped such that the excited state population is the same in each, the energy into heat in alexandrite is only 55% that of Nd:YAG. This is because alexandrite is nearly three times as efficient as Nd:YAG in converting lamp energy to useful excited states.

In order to experimentally verify the model, the spectral, angular, and spatial distribution of pump energy incident on the gain medium must be determined. Lamp spectra, experimentally measured at several angles and which include the effects of any optical coatings, were used as inputs for the model. This data was incorporated into a three dimensional raytrace program so that the radiation distribution from available pump chambers could be modeled. This program will be described in a later talk. By performing this more detailed calculation of the incident radiation, an experimentally observable excitation profile was obtained.

Spatially resolved gain measurements of several pump chambers with alexandrite rods were performed. A laser amplifier was probed with an oscillator and the video image of the output was stored in a computer. A pixel-by-pixel ratio and natural logarithm of an amplified shot and an unamplified shot produces a cross-sectional map of gain for the rod. Details of the technique and results will be discussed.

Laser Pump Chamber Optimization: Raytrace Modeling and Optimization Algorithm

David Benfey, Richard Boyd, David Brown, Donald Harter

Laser Technology Associates, Inc.
25 Ozalid Road
Johnson City, New York 13850
(607)798-9064

Allied-Signal Inc.
P.O. Box 1021R
Morristown, New Jersey 07960
(201)455-5112

Summary

A critical factor in laser system performance and efficiency is the pump chamber design. Non-uniform pumping of lasers results in degraded performance; higher divergence, incomplete mode fill, or hotspots which can cause damage to the laser medium or optics. When pumping rod geometries, an elliptical specular reflector is often used with the lamp and rod at the foci. This still results in non-uniform pumping because the lamp is an extended source. A more recent approach has been to use sections of an involute around the rod and lamp. Analyses of these geometries have been rather limited, employing closed form calculations to estimate performance. Experimental determination of an optimal combination of specular pump chamber parameters is yet more involved and often requires numerous prototyping steps. Diffuse reflectors have improved uniformity but with great loss of efficiency. This paper describes a comprehensive approach to the analysis and

optimization of specular laser pump chambers by using a three dimensional ray-tracing model in conjunction with a non-linear optimization algorithm to parametrically search for an optimum design.

We have developed a computer program to analyze and optimize generalized laser pump chamber geometries for maximum excitation uniformity and efficiency. The model combines three dimensional ray-tracing from the lamp to the laser medium with a detailed model of energy propagation and spectral absorption in the medium. The absorption model is essentially universal in that it handles biaxial and trichroic media, and has been successfully applied to alexandrite.

During a model run, thousands of rays are emitted from the flashlamp in three dimensions. Rays are traced to intersections with optical components in the chamber, and reflected and refracted at each surface. A ray entering the laser medium is transformed to an ordinary and extra-ordinary ray according to the anisotropy of the medium and their direction of propagation. Spectral absorptivity is also directionally dependent and is calculated for both rays. As each ray passes through the laser medium, it is spectrally attenuated. The absorbed energy is summed in volume elements to produce an absorption profile for the medium. Figures 1a and 1b show the profiles for two typical pump chamber configurations.

Since the output of flashlamps has never been adequately modeled, and since many optical coatings which modify the output of a lamp are in use, the model uses experimentally measured lamp spectra. The spectrum of each type of lamp used is measured at several emission angles to generate a detailed database of the lamp output. Of course, the model can use any source, such as laser diodes, in any pump configuration.

We present calculations showing the effects of pump chamber geometry on pumping alexandrite rods. We first examine some single and dual ellipse pump chambers. Using the optimization algorithm, we have achieved significant improvement in pump uniformity without loss of efficiency. The optimization of the elliptical pump chamber in figure 1b for ellipticity and rod and lamp position resulted in the absorption profile in figure 2. Comparisons with experimental data will be made.

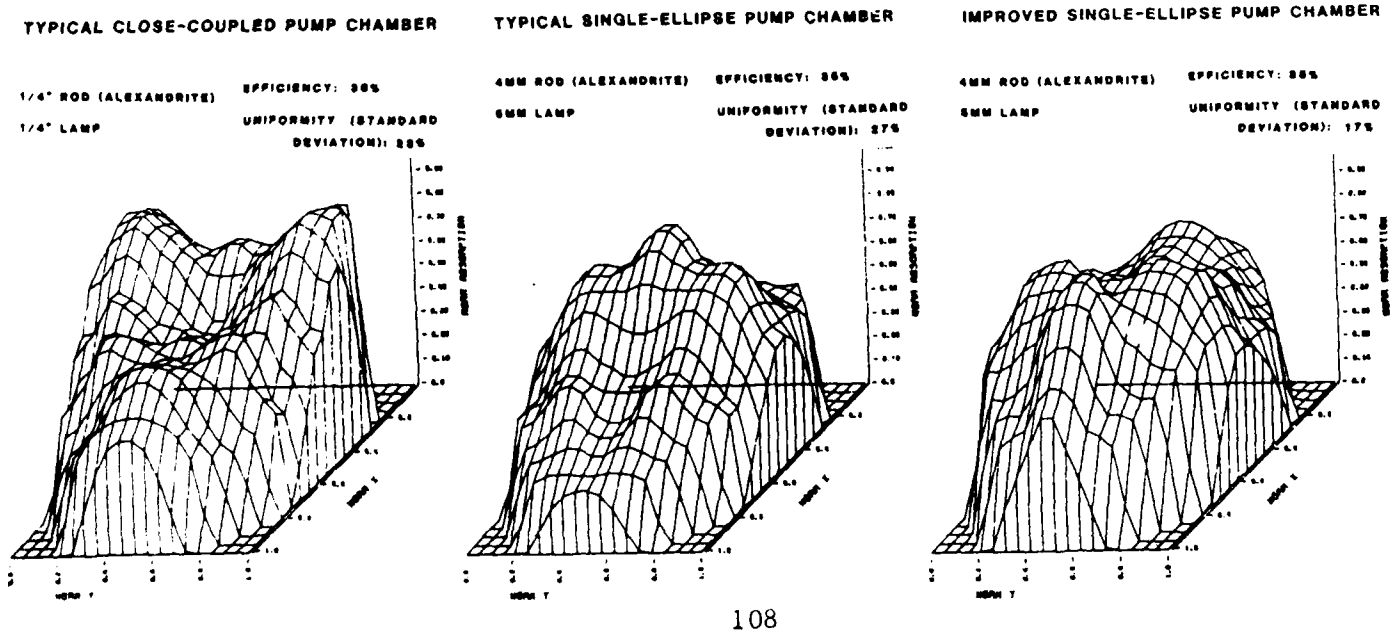

Passively Q-Switched Narrow Line Alexandrite Laser

S. G. Post
Air Force Weapons Laboratory
Kirtland Air Force Base, NM 87117

and

N. Mukherjee, J. McIver, Y. S. Kuo, and R. Pastel
Department of Physics and Astronomy
University of New Mexico
Albuquerque, New Mexico 87131

Line narrowing of electro-optic [1] and acousto-optic [2] Q-Switched Alexandrite lasers with resulting 0.005 Å bandwidths has been demonstrated. Here we report a passively Q-Switched Alexandrite laser using saturable dyes with a final linewidth less than 0.005 Å. The intensity saturation of the saturable dyes helps line narrowing and generates 150-250 nanosecond pulses of smooth temporal profile.

The basic resonator, consisting of a 100 percent (5 mcc) reflector and a 55 percent flat output coupler, contained an Alexandrite rod which was doped with a Cr^{3+} concentration of 5.6×10^{19} cm^{-3}. The operating temperature of the rod was 80°C and the flashlamp pump duration was 130 microseconds. The flashlamp was pumped at a 1 Hz pulse repetition frequency (PRF).

The free running laser spectrum was approximately 40 Å wide and consisted of strongly modulated 3 Å wide bands with a rough periodicity of 6 Å. The laser rod fluorescence was studied under the same excitation conditions and no periodic structure was evident.

Though the origin of this periodic spectrum is not understood, it certainly favored laser line narrowing. Insertion

of a five-plate birefringent filter provided tunability and simultaneously line-narrowed the laser to less than 1 Å. Further narrowing was achieved through the use of a 1 mm etalon with a 1.8 Å free spectral range (FSR) and a broadband 20 percent reflectivity and a 2 mm etalon with FSR = 0.9 Å and 20 percent reflectivity. A linewidth of less than 0.005 Å was reached by creating a resonant reflector (RR) output coupler using the existing 55 percent reflector and an additional 4 percent reflector. The complete laser resonator schematic is shown in Figure 1.

Six saturable absorber dyes (HITCI, HITCP, DTTCI, DTTCP, IR-144, AND HDITCP) which have significant absorption at the 755 nm lasing wavelength were chosen for Q-Switching the resonator. All six dyes were dissolved in DMSO. A flowing dye cell with AR coated windows spaced 0.030 mm apart was used.

The laser spectrum was analyzed by a Fabry-Perot interferometer with FSR = 0.02 Å and a Finesse of 30. Figure 2a shows an oscilloscope trace of a 8 mJ, Q-Switched pulse using a DTTCP dye concentration of $3x10^{-3}$ gm/l, and Figure 2b shows the corresponding Fabry-Perot fringes, suggesting a linewidth of less than 0.005 Å.

References

1. R. C. Sam, F. P. Roullard III, Narrow Band, Tunable Alexandrite Laser for Meteorological LIDAR, Electro Optical Systems Design, July 1982.

2. J. Pelon, G. Megie, C. Loth and P. Flamant, Narrow Bandwidth Q-Switch Alexandrite Laser for Atmospheric Applications, Opt. Comm., Vol. 59, 213 (1986).

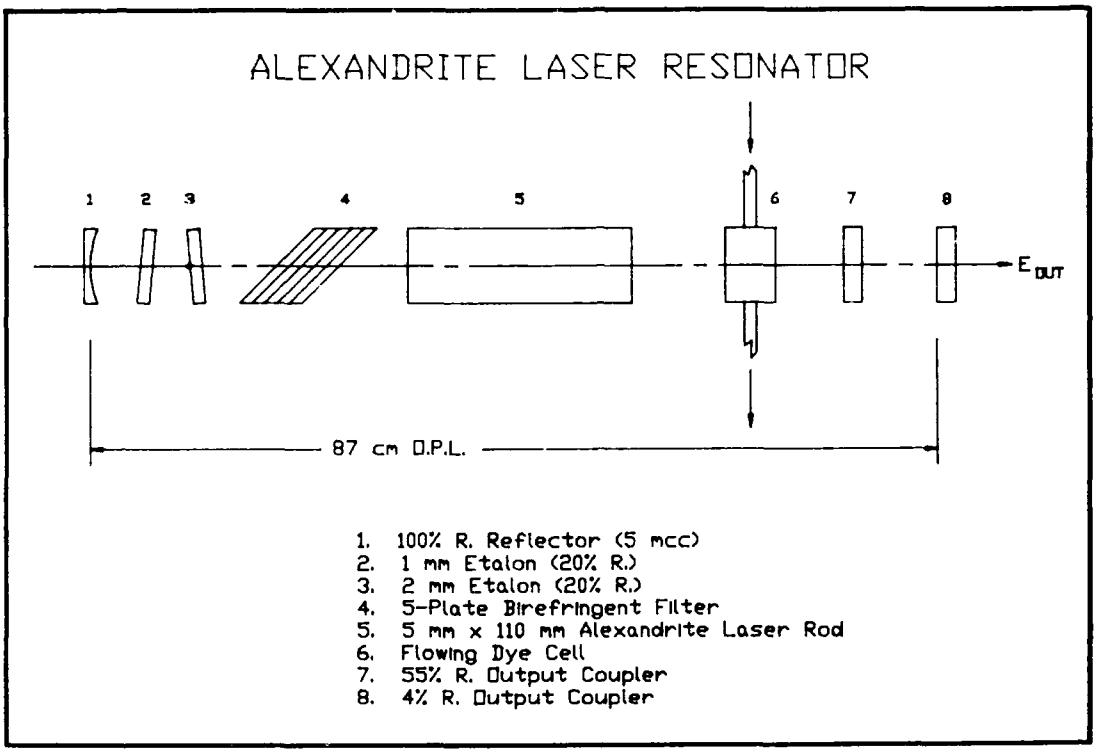

FIGURE 1
Alexandrite Laser Resonator Schematic

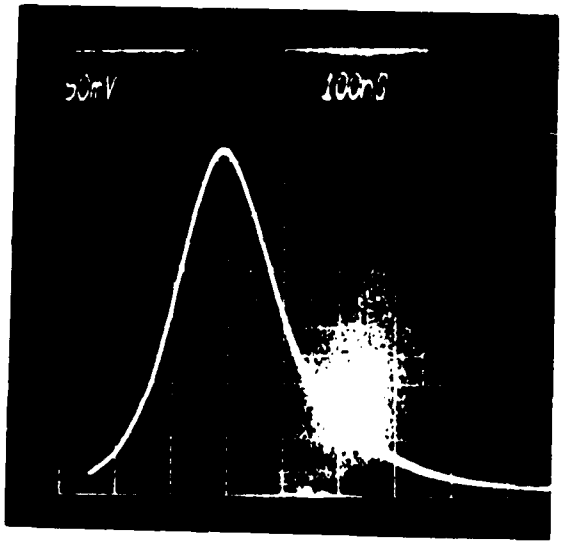

FIGURE 2a
Ocilloscope Trace of a 8 mJ, 210 ns FWHM, Passively Q-Switched Pulse (Using DTTCP Dye).

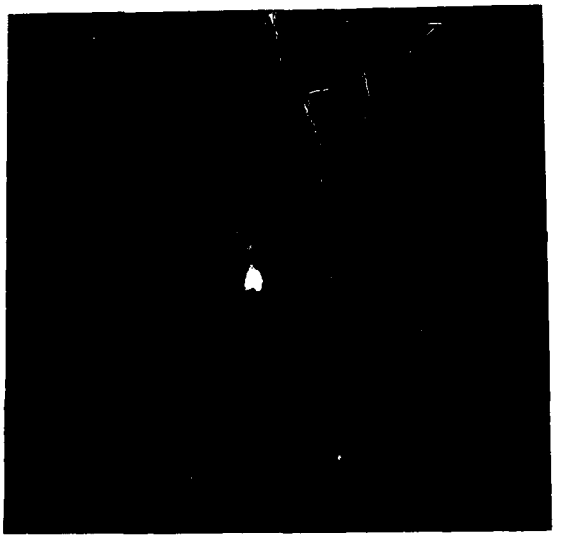

FIGURE 2b
Fabry-Perot Fringes of a Passively Q-Switched Pulse (Using DTTCP Dye).

Energy Levels of Cr^{3+} Ions in C_{3i} Sites of $Y_3Al_5O_{12}$

Clyde A. Morrison

US Army Laboratory Command

Harry Diamond Laboratories, Adelphi, MD 20783, USA

John B. Gruber

Department of Physics

San Jose State University, San Jose, CA 95192, USA

Marian E. Hills

Chemistry Division

Naval Weapons Center, China Lake, CA 93555, USA

Low-temperature (15 K) absorption spectra have been taken on two single crystals of Cr^{3+}-doped $Y_3Al_5O_{12}$ (YAG). The optical measurements were made on samples in the form of discs cut parallel to the (111) planes of the crystal. The absorption spectra were measured between 0.7 and 0.22 μm with a Cary Model 2390 spectrophotometer whose resolution was better than 1 A. The crystals contained 1.20 and 0.01 at. % chromiun based on aluminum.

The dilute crystal allowed us to resolve the structure of the most intense bands at approximately 15,200, 16,400, 21,100, and 34,000 cm^{-1} and a number of vibronics. No electronic electric dipole transitions were observed, which agrees with the assumption that the Cr^{+3} ions enter the C_{3i} site in YAG. All the levels used in the analysis are believed to be due to electronic magnetic dipole transitions. The more concentrated crystal was used to examine the weaker Cr^{3+} levels at 14,533, 30,600, 31,120, 32,562, and 32,590 cm^{-1}. The observed absorption bands of the two crystals are in reasonable agreement with earlier work [1].

In the analysis of the spectra we use the free-ion Hamiltonian,

$$H_{FI} = H_c + \alpha L(L+1) + \gamma G(R_5) + \zeta_d \sum_{i=1}^{3} \vec{s}_i \cdot \vec{\ell}_i \qquad (1)$$

for the $3d^3$ configuration of Cr^{3+}. In (1), H_c is the Coulomb interaction of the electrons with the Slater parameters $F^{(k)}$, α and γ are interconfiguration parameters, and ζ_d is the spin-orbit constant. The $G(R_5)$ is the Casimir operator for the R_5 rotation group. The crystal-field interaction for the $3d^3$ configuration of Cr^{3+} in C_{3i} symmetry was taken as

$$H_{CF} = B_{20} \sum_{i=1}^{3} C_{20}(i) + B_{40} \sum_{i=1}^{3} C_{40}(i) + B_{43} \sum_{i=1}^{3} [C_{43}(i) - C_{4-3}(i)] \qquad (2)$$

where

$$C_{kq}(i) = \sqrt{4\pi/(2k+1)}\, Y_{kq}(\theta_i, \phi_i)$$

and the crystal-field parameters, B_{kq}, are all real. The experimental energy levels were used in a least-squares fit to values computed by using (1) and (2) with the parameters varied. Initial values for the free-ion parameters were obtained by ignoring the fine structure produced by the spin-orbit interaction and assuming cubic symmetry ($B_{20} = 0$, $B_{43} = \sqrt{10/7}|B_{40}|$). Additional levels were gradually added to the fitting, starting with the most confident experimental levels, until we identified 31 levels; with all the parameters varied we obtained an rms of 21 cm^{-1}. The final parameters are $F^{(2)} = 53{,}119$, $F^{(4)} = 38{,}283$, $\alpha = 143$, $\gamma = -248$, $B_{20} = 1091$, $B_{40} = -21{,}529$, and $B_{43} = 27{,}184$ (all in cm^{-1}). These parameters correspond to B = 650, C = 3038, Dq = 1604, v = 853, and v′ = -84.1 (all in cm^{-1}).

A point-charge calculation was performed to obtain the crystal-field components, A_{kq}, for three sites, $Y(D_2)$, $Al_1(C_{3i})$, and $Al_2(S_4)$, and radial factors ρ_k where obtained by equating the crystal-field parameters, B_{kq}, for the C_{3i} site by $\rho_k A_{kq} = B_{kq}$ with the B_{kq} given above. This procedures gave the crystal-field parameters

$$B_{20} = 1{,}014, \quad B_{40} = -29{,}146, \quad B_{44} = 11{,}449 \ (cm^{-1}) \tag{3}$$

for the Al_2 site with S_4 symmetry and

$$B_{20} = -320, \quad B_{40} = -2904, \quad B_{44} = 8173 \ (cm^{-1}) \tag{4}$$

for the Y site with D_2 symmetry. Actually in D_2 symmetry there are also B_{22} and B_{42}, as well as the parameters given in (4), but we are unable at present to calculate the crystal-field splittings for such low symmetry; therefore the B_{kq} for D_2 symmetry were approximated to S_4 symmetry. The energy levels for Cr^{3+} were calculated for the S_4 site using (3) and for the D_2 symmetry site using (4). The free-ion parameters obtained from fitting Cr^{3+} in the C_{3i} site were used in this calculation, and comparision of the result with the experimental data is proceeding.

REFERENCES

[1] D. L. Wood, J. Ferguson, K. Knox, and J. F. Dillon, Jr., J. Chem. Phys. 39 (1963), 890. See also M. O. Henry, J. P. Larkin, and C.F. Imbusch, Proc. R.I.A. 75 (1975) 97; D. S. McClure, J. Chem. Phys. 36 (1962) 2757; B. K. Sevast'yanov, D. T. Sviridov, V. P. Orekhovo, L. P. Pasternak, R. K. Sviridova, and T. F. Vermeichick, Sov. J. Electron. 2 (1973) 339.

TuB5-1

Iron-group Lumophores: Broken Paradigms and Low-symmetry Thexi States

Christian K.Jørgensen

Section de Chimie(Sciences II),University,CH 1211 Geneva 4,Switzerland

The goal-oriented quest for tunable lasers is to a great extent guided by two highly distinct regions of theory(mainly developed since 1954),one of J-levels of a partly filled $4f^q$ shell(where the trivalent lanthanides present numerous narrow absorption bands for q=2 through 12,and one band for q=13) closely analogous to gaseous atoms and monatomic cations,and another,the "ligand field" description common to partly filled 3d,4d and 5d shells(q=1 through 9) strongly determined by the local symmetry of nearest neighbor atoms.The one-electron energy differences are typically 1 to 4 eV,to be compared with effects well below 0.1 eV separating the (2J+1) states of a given lanthanide J-level.The original description of d or f orbitals perturbed by the (tiny) non-spherical part of the (huge) Madelung potential broke down around 1960 [1-5] and it is now confirmed [6-8] that the common origin is the increased kinetic energy of anti-bonding electrons,almost as strong in the d groups as in typical main-group molecules,but a small second-order effect in the 4f group,as well as in M(III) and most M(IV) $5f^q$ compounds.

It has a great influence on our opinions that the excited states of $3d^q$ and $4f^q$ were charted in absorption spectra.The crowded J-levels between q=3 and 11 were almost completely identified [9-12] up to 4 eV before 1968, assisted by the Broer-Gorter-Hoogschagen theory refined (in 1962) independently by Judd and by Ofelt.Such a treatment is not applicable for d^q oscillator strengths [3,13,14] to the first approximation borrowing intensity from electron transfer bands [13,15] at higher wave-numbers.The excited states of such intense bands correspond to one or more reducing neighbor groups(ligands) collectively having lost one electron to the d shell now being d^{q+1}.Such electron transfer bands are also known [10-12,16] of europium(III),ytterbium(III),cerium(IV),uranium(VI) and other f^{q+1} cases.They have no analogy in atomic spectra (and hence tend to be neglected) contrary to the many intense transitions to $4f^{q-1}5d$ and $5f^{q-1}6d$ states.

It is a truism that excited states luminesce,if they do not exclusively develop thermal vibrations (or perform photochemistry).The luminescence of $4f^q$ J-levels can be described by the same Judd-Ofelt parameters (three for each combination of a higher and a lower J-level of a given lanthanide(III), and three material parameters for a given environment,usually not varying dramatically between adjacent lanthanides[11]).In particular,the branching ratio to various lower J-levels (including the groundstate) is not modified by non-radiative competition,all the transition rates (Weber,1967) increased by the same factor,perhaps rendering the optical emission very weak.Such a difficulty can be circumvented in the laboratory by careful photon counting very soon after the illuminating flash.If the radiative life-time is 10^{-a} s and the quantum yield (almost quenched by non-radiative de-excitation) 10^{-b}, the luminescence during the first 10^{-a-b-1} seconds still has the same order of magnitude as the long-lived (say 10^{-3} s) transitions.Again,there is no comparable description available of the quantum yield of $3d^q$ luminescence, and it is (to a large extent) found by trial and error,whether it is 0.9 or 0.1 or 0.01.

As far as (vitreous or crystalline) laser materials go,the conditione sine qua non is to obtain population inversion(higher concentration of the

emitting state E_2 than of the terminal state E_1).Though the first laser in the visible was the ruby $Cr_xAl_{2-x}O_3$ (Maiman,1960) acting as a three-level system,it is highly preferable that E_1 is several times kT above the ground state.Hence,the best $4f^q$ lasers involve E_1 being an excited J-level,because discrimination between the (2J+1) states of E_0 requires strong cooling to low T.It is also true that the quantum yield preferably should be high,but four-level action may still be induced by sufficient pumping.The requirement of tunable four-level lasers can be satisfied by organic colorants (such as rhodamines or oxazines) in solution,conceptually also in the higher vibrational levels of uranyl luminescence [16] and in many cases of $3d^3$ Cr(III) in crystals (e.g.alexandrite $Cr_xAl_{2-x}BeO_4$) or in limpid glass-ceramics [7] containing,for instance,micro-crystallites of spinel-type $MgCr_xAl_{2-x}O_4$.

The tunability of such $3d^q$ systems is usually described in a model of totally symmetric stretching,all six Cr-X distances multiplied by the same scaling factor(close to 1).This seems far too simplified;the gaseous $5d^3$ IrF_6 (accepting the Born-Oppenheimer approximation) has 15 mutually independent internuclear distances,and hence,the potential surface needs 16 dimensions.Actually,elpasolite-type crystals [17] containing $CrCl_6$ or $CrBr_6$ are known to have the minima of the excited $^4T_2$ surface at two shortened and four elongated Cr-X distances (though the six X nuclei remain on Cartesian axes).One can expect the worst from other systems related to this weakness of the "breathing" paradigm,in particular in Tanabe-Kamimura unstable states [7].Another intrusive problem is electron transfer bands.Already the yellow gas IrF_6 (mixed with colorless xenon) forms intensely purple liquids and solids by cooling [18] having $5d^4$ Ir(V) & $5p^5$ Xe(I) excited states.The $3d^1$ titanium(III) lasers are marred by parasitic absorption in the near infrared.It seems [19] that corundum-type $Ti_xAl_{2-x}O_3$ has Ti(III)→Ti(IV)electron transfer bands,comparable to the Fe(II)→Ti(IV) transitions (with Fe(III) & Ti(III) in the excited state)giving the blue color of sapphire $Fe_xTi_xAl_{2-2x}O_3$.The former crystal also shows violet emission from a Ti 4s like orbital.

It is appealing [7,11] to apply glasses or glass-ceramics as lasers,rather than crystals.Glasses are characterized by a much wider dispersion of internuclear (e.g.Cr-X) distances,frozen in at a rather high temperature,when the nuclei became immobile on the time-scale of subsequent cooling.No cryogenic spectroscopy can make absorption and emission bands of such glasses <u>much</u> sharper.It is felt [20] that the irregular distortion of CrX_6 is the main origin of low quantum yield of Cr(III) emission (much lower than in many glass-ceramics [7]).On the other hand,the absence of perfect crystallization may have beneficial effects on tunability.

A major problem for d group lasers is the difficult feeding of higher E_2, especially in the case of exceedingly weak manganese(II) absorption bands [21].On the other hand,Mn(II) in fluoride glasses [22-25] in the simultaneous presence of neodymium(III) and other lanthanides may store energy in the very long-lived,first $3d^5$ quartet state,enhancing the efficiency of laser glasses. The local symmetry is by no means close to regular octahedral,and the quartet may have manifolds of optimized Mn-X distances quite different from the sextet groundstate of each site.The low-symmetry equilibrium shapes of the lowest quartet corresponds to the concept <u>thexi state</u> (thermally equilibrated vibrations of excited electronic state) of Adamson [26] in photochemistry.

Like in atomic spectra,one should not confuse success of classifying the energy levels [3,12] with high-quality wave-functions being available for Z above 20;the squared amplitude of the Hartree-Fock result in the groundstate is some 0.5 ± 0.2,and the heats of atomization per atom [27-29] well below 10^{-4} times the total electron binding energy for Z above 30.We perform inductive studies;strictly deductive trans-calcium quantum chemistry is far beyond reach.

Acknowledgments.I am very grateful to Professor Renata Reisfeld,Jerusalem, for fruitful collaboration since 1974,and to Professor Claus E.Schäffer, Copenhagen,for angular overlap discussions since 1963.

[1] C.K.Jørgensen,R.Pappalardo and H.H.Schmidtke,J.Chem.Phys.39,1422(1963).
[2] C.E.Schäffer and C.K.Jørgensen,Mol.Phys.9,401(1965).
[3] C.K.Jørgensen,Oxidation Numbers and Oxidation States(Springer,Berlin & New York,1969).
[4] C.K.Jørgensen,Modern Aspects of Ligand Field Theory(North-Holland, Amsterdam,1971).
[5] J.Glerup,O.Mønsted and C.E.Schäffer,Inorg.Chem.15,1399(1976).
[6] C.K.Jørgensen,M.Faucher and D.Garcia,Chem.Phys.Lett.128,250(1986).
[7] R.Reisfeld and C.K.Jørgensen,Structure and Bonding 69,63(1988).
[8] C.K.Jørgensen,Chem.Phys.Lett.153,185(1988).
[9] W.T.Carnall,P.R.Fields and K.Rajnak,J.Chem.Phys.49,4412,4424,4443(1968).
[10] R.Reisfeld and C.K.Jørgensen,Lasers and Excited States of Rare Earths (Springer,Berlin and New York,1977).
[11] R.Reisfeld and C.K.Jørgensen,in: Handbook on the Physics and Chemistry of Rare Earths (eds.K.A.Gschneidner and L.Eyring),9,pp.1-90 (North-Holland,Amsterdam,1987).
[12] C.K.Jørgensen,ibid.,11,pp.197--292(North-Holland,Amsterdam,1988).
[13] C.K.Jørgensen,Advanc.Chem.Phys.5,33(1963).
[14] R.F.Fenske,J.Am.Chem.Soc.89,252(1967).
[15] C.K.Jørgensen,Prog.Inorg.Chem.12,101(1970).
[16] C.K.Jørgensen and R.Reisfeld,Structure and Bonding 50,121(1982).
[17] R.Knochenmuss,C.Reber,M.V.Rajasekharan and H.U.Güdel, J.Chem.Phys.85,4280(1986).
[18] J.D.Webb and E.R.Bernstein,J.Am.Chem.Soc.100,483(1978).
[19] R.Reisfeld,M.Eyal and C.K.Jørgensen,Chimia 41,117(1987).
[20] R.Reisfeld and A.Kisilev,Chem.Phys.Lett.115,457(1985).
[21] R.Reisfeld,A.Kisilev and C.K.Jørgensen,Chem.Phys.Lett.111,19(1984).
[22] R.Reisfeld,M.Eyal,C.K.Jørgensen,A.H.Guenther and B.Bendow, Chimia 40,403(1986).
[23] M.Eyal,R.Reisfeld,A.Schiller,C.Jacoboni and C.K.Jørgensen, Chem.Phys.Lett.140,595(1987).
[24] R.Reisfeld,M.Eyal,C.Jacoboni and C.K.Jørgensen,Chimia 42,145(1988).
[25] R.Reisfeld and C.K.Jørgensen,Structure and Bonding,in preparation.
[26] A.W.Adamson,J.Chem.Educ.60,797(1983).
[27] C.K.Jørgensen,Chimia 42,21(1988).
[28] C.K.Jørgensen,Quimica Nova(São Paulo) 11,10(1988).
[29] C.K.Jørgensen,Topics Current Chem.150,1(1988).

Transparent Glass Ceramics Doped by Cr(III) and Codoped by Cr(III) and Nd(III) as Potential Materials for Tunable Lasers

Renata Reisfeld

Department of Inorganic and Analytical Chemistry
The Hebrew University of Jerusalem, Jerusalem 91904 Israel

Transparent glass ceramics containing Cr(III) were suggested as materials for tunable lasers [1]. Glass ceramics are solids in which the microcrystallites of the mother material are imbedded in a matrix of glass [2]. Their preparation may be achieved by annealing the original glass with nucleating agents such as TiO_2 or ZrO_2. In these materials Cr(III) is concentrated in submicroscopic crystallites having dimensions smaller than the wavelength of visible radiation. Line narrowing experiments have been performed on Cr(III) in some of the glasses and glass-ceramics [3,4]. These enable the establishment of the local site symmetry of Cr(III) in the ceramics. Information of this type can be derived from the size of R_1 - R_2 separation, the ratio of the oscillator strengths and the polarization of the R lines.

In the present lecture we report on some additional spectroscopic findings, discuss the nucleation mechanism of the glass ceramics, deal with nonradiative relaxation in Cr(III) and finally calculate the laser cross-section for tunable lasers.

The absorption and luminescence of Cr(III) originates from transitions in the unfilled 3d electronic shell. Such transitions are Laporte-forbidden in sites having a centre of symmetry [5,6]. The designations of the transitions in Cr(III) in octahedral symmetry have been elaborated by Sugano et al. [7].

Steady state absorption allows determination of the ligand field strength acting on the Cr(III) ion. The absorption due to $^4A_2 \rightarrow {}^4T_2$ spin-allowed transition peaks around 650 to 560 nm [8]. As a result of stronger ligand field which is exerted on Cr(III) having shorter distances to its ligating oxygens in more rigid glass-ceramics than glasses the $^4A_2 \rightarrow {}^4T_2$ absorption peak is shifted to shorter wavelengths, i.e. higher energies. Ligand field parameters for the glass ceramics studied are given in Table I.

Table I. Ligand field parameter Δ (in the unit 1000 cm^{-1}) for $Cr(III)O_6$ in glass-ceramics (g.c.); Solids and complexes in solution.

Spinel-type g.c.	original glass	15.5
"	glassy micro-phase	15.95
"	micro-crystallites	17.25
Gahnite-type g.c.	original glass	15.6
"	glassy micro-phase	16.0
"	micro-crystallites	18.35
β-quartz g.c.	glassy micro-phase	16.0
"	micro-crystallites	16.8
Petalite-like g.c.	original glass	15.6
"	glassy micro-phase	16.0
"	micro-crystallites	17.5
Various silicate glasses		15.2-15.5
Various phosphate glasses		14.5-15.1
Lithium-lanthanum phosphate glass		15.45
Lithium aluminium borate glass		16.4

Alexandrite $Al_{2-x}Cr_xBeO_4$	17.35
Beryl-type emerald $Be_3Al_{2-x}Cr_xSi_6O_{18}$	16.5
Spinel $MgAl_{2-x}Cr_xO_4$	18.2
Spinel-type $MgAlCrO_4$	17.65
Spinel-type $MgCr_2O_4$	17.15
Ruby $Al_{2-x}Cr_xO_3 (x < 0.04)$	18.0
$Al_{1.9}Cr_{0.1}O_3$	17.8
Greyish-pink $Al_{1.6}Cr_{0.4}O_3$	17.55
Green $Ga_{1.93}Cr_{0.07}O_3$	16.6
Green Cr_2O_3	16.6
NaCl-type $Cr_{0.05}Li_{0.05}Mg_{0.9}O$	16.2
NaCl-superstructure $LiCrO_2$	17.3
Perovskite $YAl_{0.5}Cr_{0.5}O_3$	17.05
Perovskite $YCrO_3$	16.45
Perovskite $LaCrO_3$	16.35
$Cr(dmso)_6^{+3}$ [dimethylsulfoxide $(CH_3)_2SO$]	15.9
$Cr(urea)_6^{+3}$ [urea $(NH_2)_2CO$]	16.0
$Cr(dmf)_6^{+3}$ [dimethylformamide]	16.9
$Cr(OH_2)_6^{+3}$ (aqua ion)	17.45
$Cr(ox)_3^{-3}$ [oxalate $C_2O_4^{-2}$]	17.5
$Cr(mal)_3^{-3}$ [malonate $H_2C(CO_2^{-2})_2$	17.5

Comparison of the values in Table I shows that the ligand field of Cr(III) in the crystalline phase of the glass ceramics is higher than in the glassy phases or in the glasses and its value is comparable to that of Cr(III) in ruby (and alexandrite). The ^2E level is 1000-3000 cm^{-1} below the minimum of the $^4T_2$ level. Such a situation permits thermal equilibrium beween the two levels as has been found previously in many complexes and crystals.

The Cr(III) ion is a powerful nucleating agent in glasses for which little published information exists. This ion, which is paramagnetic and luminescent, makes it possible to follow the nucleation by several techniques. In particular spectroscopic techniques have been studied on Cr(III) doped silicate glasses: they are Small Angle Neutron Scattering (SANS) and Small Angle X-Ray Scattering (SAXS) to determine the size and the growth of the microcrystallites between either 40 and 100 A (SAXS) or 100 and 400 A (SANS). By Electron Microscopy and X-Ray Diffraction we were able to see the shape of the particles and to define their crystallographic nature whereas Electronic Paramagnetic Resonance (EPR) and Laser Spectroscopy techniques give the information about the local structure of the Cr(III) luminescent probe ion during its transformation from a component of the glass to that of a well developed crystalline phase.

In order to obtain a more detailed insight into the nature of the emitting Cr(III) sites a comparison of the optical spectra and decay dynamics between the transparent glass ceramics and microcrystallites is performed. Different crystals, glasses and glass ceramics have been grown and their steady state spectroscopy and time-resolved spectroscopy studied. These include Cr(III) in magnesium aluminate spinels, gahnite-type ceramics and mullite transparent glass ceramics. Time-resolved spectroscopy enables to follow the establishment of the equilibrium between the metastable long-lived ^2E state and the shorter-lived $^4T_2$ state.

The significant feature of Cr(III) in glass-ceramics is its high quantum efficiency of luminescence (0.91-1) at room temperature as opposed to only 0.07-0.19 in the parent glass [9].

The position of the $^4T_2$ state of Cr(III) in both media can be estimated from the absorption spectra [8]. There is a shift from 620 nm (16100 cm^{-1}) to

530-560 nm (18850-17850 cm^{-1}) in mullite glass-ceramics. The shift of the $^4T_2$ level to higher energies in glass-ceramics can be attributed to higher ligand fields in the latter. This fact can explain to some extent the lower relaxation rate of Cr(III) in mullite glass-ceramics since the crossing point between $^4T_2$ and the $^4A_2$ ground state will occur above the lowest vibrational levels of the $^4T_2$ state.

The decay curves for the glass-ceramics and glasses at ambient temperature and at 4.4 K deviated slightly from exponential behaviour over the wavelength range 680-720 nm in the vicinity of the ^2E level and deviated strongly in the 720-800 nm spectral range.

Energy transfer between Cr(III) and Nd(III) in mullite glass-ceramics was studied by the dynamic method using laser excitation [10]. Comparison of the data with those of glasses shows that the energy transfer rate is higher in glasses, but the overall transfer efficiency is higher in glass-ceramics due to lower nonradiative relaxation of Cr(III) in the latter. The values of transfer efficiencies will be presented.

Stimulated cross-section was calculated for mullite glass-ceramics using the model of McCumber [11] and experimental parameters of lifetime of the lasing level, quantum yield and corrected emission spectrum. At pumping wavelength of 550 nm the cross-section was calculated to be σ_e = **0.675 pm^2**. This cross-section can be compared to the cross-section obtained for Cr(III) in gallium scandium gadolinium garnet (GSGG) at 756 nm, which is 0.7 pm^2 [12], and for alexandrite at 750 nm, 0.76 pm^2 [13]. Laser threshold for a rod length of 1 cm and a doping concentration of 0.1 w.p. of Cr^2O^3 (1.8 x $10^{19}/cm^3$) was also calculated.

This work was performed under US Army Contract No. DAJA 45-85-C-0051

REFERENCES

1. R. Reisfeld and C.K. Jørgensen, Structure and Bonding **69** (1988) 63.
2. P.W. McMillan (ed.) **Glass Ceramics**, 2nd edition, Academic Press, New York, (1979).
3. F.J. Bergin, J.F. Donegan, T.J. Glynn and G.F. Imbusch, G.F., J. Luminescence **34** (1986) 307; **36** (1987) 231.
4. Y. Kalisky, V. Poncon, G. Boulon, R. Reisfeld, A. Buch and M. Ish-Shalom, Chem. Phys. Lett. **136** (1987) 368.
5. R. Reisfeld and C.K. Jørgensen, Cr(III) broad-band quartet-quartet luminescence in glass-ceramics with higher yield than in complexes. E.L. King, D.H. Busch and R.E. Sievers, (eds.). Abstracts of 23rd Intl. Conf. Coordination Chemistry, Boulder CO 1984, p.162.
6. C.K. Jørgensen, **Oxidation Numbers and Oxidation States**, Springer-Verlag, Berlin-Heidelberg-New York 1969.
7. S. Sugano, Y. Tanabe and H. Kamimura, **Multiplets of Transition Metal Ions in Crystals**, Academic Press, New York, 1970.
8. R. Reisfeld, A. Kisilev, A. Buch and M. Ish-Shalom, J. Non-Cryst. Solids **91** (1987) 333.
9. R. Reisfeld, A. Kisilev, A. Buch and M. Ish-Shalom, Chem. Phys. Lett. **129** (1986) 446.
10. R. Reisfeld, M. Eyal, A. Buch and M. Ish-Shalom, Chem. Phys. Lett. **147** (1988) 148.
11. D.E. McCumber, Phys.Rev., **134A** (1964) 299; **136A** (1964) 954.
12. B. Struve and G. Huber, J. Appl. Phys., **57** (1985) 45.
13. J.C. Walling, H.P. Jensen, R.C. Morris, E.W. O'Dell and O.G. Petersen, Opt. Lett., **4** (1979) 182.

TUESDAY, MAY 2, 1989

NAUSET IV

10:15 AM–12:15 PM

TuC1–TuC6

DIODE PUMPED LASERS

Rudolf G. Buser, U.S. Army Night Vision and Electro-Optics Laboratory, *Presider*

DIODE PUMPED SOLID STATE LASERS

I.I.Kuratev and Yu.V.Tsvetkov. Moscow Physical Technical Institute, USSR

SUMMARY

At present great success in development and industrial production of high-power laser diodes and GaAlAs-laser diode arrays makes possible to develop high-efficiency solid state lasers using semiconductor emitter as a pump source.

In this paper are shown the results of theoretical and experimental investigation of generation parameters of diode-pumped neodymium lasers operating in different generation modes.

In end-pumped lasers a wide range of Nd-doped host materials was used: Nd:YAG, Nd:$YAlO_3$, Cr, Nd:GSGG, Nd:$LaMgAl_{11}O_{19}$, $LiNdP_4O_{12}$.

10 mm wide one or two single-stripe GaAlAs laser diodes were used as pump sources.

The Nd:YAG emits 357 mW cw in TEM_{oo} mode at 1.06 mm (11% efficiency). The maximum cw output power was 670 mW at electrical input power 6.4 W. The total electrical to optical conversion efficiency was 10.4%. Output power was 285 mW at 1.32 mm and electrical input power 6.4W (4.4% total efficiency).

Detailed theoretical and experimental investigation of generation features of diode pumped passive Q-switch lasers have beam performed. Using the GSGG passive laser shutters and optimization of diode end-pumped solid state lasers we obtained maximum output in Nd-doped host materials.

Table 1. Performance of passive Q-switch diode pumped solid state lasers

Laser medium	Threshold (w)	Pulsed Energy (μJ)	Maximum output power (kW)	Pulse width (ns)
$Nd:Y_3Al_5O_{12}$	0.98	29	6.7	4.3
$Nd:YAlO_3$	1.07	18	4.9	3.7
$Nd:LiYF_4$	1.00	25	6.9	3.6
$Cr,Nd:Gd_3(SeGa)_5O_{12}$	0.86	22	8.1	2.7
$Nd:YVO_4$	0.89	5,8	4.4	1.3

We investigated the features of intracavity second harmonic generation in diode pumped solid state lasers. We obtanied output power 80 mW at 0.53 incw single mode Nd:YAG laser at electrical input power 3.2 W (2,5% total efficiency) by using SHG $LiIO_3$-crystal 20 mm long. The maximum output power was 130 mW at electrical input power 6.4W (2% efficiency). The output power was 19 mW at 0.67 mm and electrical input power in $Nd:YAlO_3$ laser.

Scaleable Laser Configuration for Laser Diode Pumped Nd:YAG

J. Frauchiger, P. Albers, H.P. Weber
Institute of Applied Physics, Uni. Berne, Sidlerstr. 5,
3012 Berne, Switzerland, Tel. 41-31-658949

Recent research in laser diode pumped solid state lasers can be divided into two main areas:

1) low power application up to a few Watts with longitudinally pumped systems,
2) high power application of more than ten Watts with transversally pumped systems.

Longitudinally pumped lasers have a superior geometrical overlap between pump- and laser-beam that enables high efficiency but are limited in power by the pump power of the available laser diodes. Transversally pumped systems can reach higher power levels by using several diodes but have lower efficiency at comparable beam parameters.

It was our goal to design a new type of resonator that combines high efficiency with high power in the fundamental mode. We chose the resonator given in Fig.1 where each single Nd:YAG disk is pumped longitudinally via reflection of the laser diode pump beam at the back surface of the foregoing disk. This arrangement allows us to scale the whole system not only by increasing the power of the laser diodes but also by adding many times a system part consisting of a laser diode, a coupling optic and a Nd:YAG disk.

Up to now we have shown that the system works in the TEM_{00} mode with up to three disks in a resonator about 1cm shorter than a 30cm concentric resonator. The resulting spot size is 100µm and the confocal parameter 6cm. Thus, all disks run practically under the same conditions. At a beam divergency of about 5mrad an optical to optical conversion efficiency of 22% and a slope efficiency of 27% (see Fig2) was measured with 5.5% output coupling.

Astigmatism and spherical abberation of the imaging make it necessary to work with laser diodes of very high spatial uniformity. We used Siemens laser diodes SFH 48 E1 with an

efficiency of about 25% which where driven up to twice the specified output power of 250mW. Using a 3mm path in the YAG-crystals 90% of the incident power is absorbed.

The measurements given in Fig2 where obtained with non optimized coupling optics; the imaging of the diode output into the lasing crystal did match the lasing volume by only about 40% to 50%. The wall plug efficiency that is given by the product of the diode-, optics- and resonator- efficiencies is presently 3.9% (0.25x0.7x0.22). By using new generation laser diodes with efficiencies of more than 40% and better optics we are confident to reach with our system a wall plug efficiency of about 10% with high beam quality. The total power level is given first by the power of the laser diodes available and second by the number of disks which can be incorporated in one system. With 5 disks each excited by 7 diodes of 5W output power we extrapolate to get about 20W TEM_{oo} output power with a wall plug efficiency of 10%. Investigations are in progress to find the limits of this system with respect to the number of disks and effects of astigmatism, spherical abberation and alignment requirements.

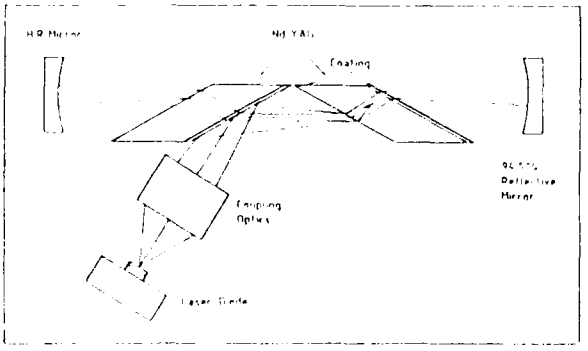

Fig.1: Multielement resonator not in scale; optics , diodes and disks can be added for high power

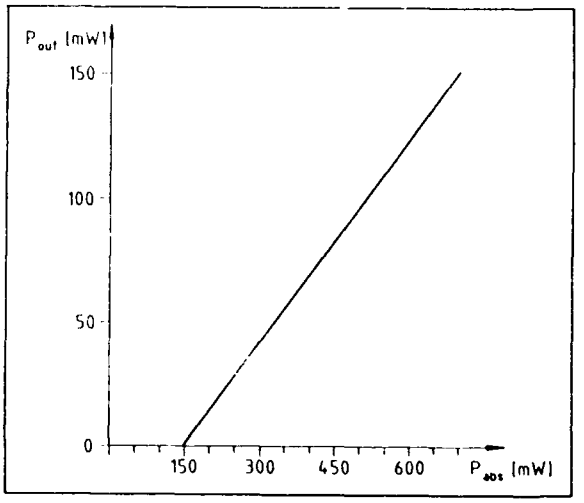

Fig.2: Absorbed laser diode pump power versus Nd:YAG output power

Spectroscopic and Laser Studies of Nd-Doped Materials for Diode-Pumped Lasers*

T. Y. Fan
Lincoln Laboratory, Massachusetts Institute of Technology
Lexington, Massachusetts 02173

M. R. Kokta
Union Carbide Corporation
Washougal, Washington 98671

D. S. Knowles and A. Cassanho
Massachusetts Institute of Technology
Crystal Physics Laboratory
Cambridge, Massachusetts 02139

Gain media with long upper-state lifetimes and large absorption bandwidths are desired for Q-switched, diode-laser-pumped solid-state lasers. Long upper-state lifetimes allow greater energy storage for a given value of pump power,[1] and large absorption bandwidths reduce the sensitivity of the Nd laser operation to wavelength differences from diode to diode and to thermally induced wavelength chirp of the diode lasers. Three Nd-doped materials that may offer advantages over Nd:YAG are Nd:LaF_3, Nd:$LaMgAl_{11}O_{19}$ (LMA), and Nd:BaY_2F_8. The low concentration upper-state lifetimes in these materials are 735 μs, 320 μs, and 660 μs all of which are longer than the 240 μs value for Nd:YAG. In addition, the first two materials have broad absorption features compared to Nd:YAG.

We have demonstrated laser operation in end-pumped, continuous wave Nd:LaF_3 and Nd:LMA lasers using a Ti:Al_2O_3 laser to simulate a diode laser as the pump source. With a 98% reflective output coupler, slope efficiencies of 47% in Nd:LaF_3 and 32% in Nd:LMA were achieved. The lower slope efficiency in Nd:LMA is consistent with previous end-pumped laser measurements.[2,3] We attribute the reduced slope efficiency in Nd:LMA to excited state absorption of the 1.05 μm output. One indication that excited state absorption may be occurring is that 77 K absorption spectra show that there are

* The Lincoln Laboratory portion of this work was sponsored by the Department of the Navy for the Strategic Defense Initiative Organization

energy levels in resonance for absorption of a 1.05 μm photon by an ion in the $^4F_{3/2}$ upper laser manifold.

Nd:LaF_3 and Nd:LMA have lower peak effective stimulated emission cross sections than Nd:YAG, which has a cross section of ~ 3 x 10^{-19} cm^2. Based on our spectroscopic and laser measurements the peak effective cross section in Nd:LaF_3 is ~ 2 x 10^{-20} cm^2 in the π polarization (E||c) at 1.064 μm. The stimulated emission cross section in Nd:LMA is 6 x 10^{-20} cm^2 in the σ polarization (E⊥c) at 1.053 μm in Nd:LMA based on our laser measurements. Previous reports of the emission cross section in Nd:LMA have varied from 3 x 10^{-19} to 6 x 10^{-20} cm^2 (Refs. 4 and 5); we believe the large discrepancy is due to the excited state absorption. The cross section in Nd:BaY_2F_8 has been reported to be ~ 2 x 10^{-19} cm^2 (Ref. 6) which would make it a high gain cross section, long lifetime material. This would be ideal for both cw and Q-switched lasers. We are currently performing spectroscopic and laser measurements on this material.

References:

1. T. Y. Fan, G. J. Dixon, and R. L. Byer, Opt. Lett. **11**, 204 (1986).

2. L. D. Schearer, M. Leduc, D. Vivien, A. M. Lejus, and J. Thery, IEEE J. Quantum Electron. **QE-22**, 713 (1986).

3. J. Hamel, A. Cassimi, J. Abu-Safia, M. Leduc, and L. D. Schearer, Opt. Commun. **63**, 114 (1987).

4. Kh. S. Bagdasarov, L. M. Dorozhkin, L. A. Ermakova, A. M. Kevorkov, Yu. I. Krasilov, N. T. Kuznetsov, I. I. Kuratev, A. V. Potemkin, L. N. Raiskaya, P. A. Tseitlin, and A. V. Shestakov, Sov. J. Quantum Electron. **13**, 1082 (1983).

5. V. M. Garmash, A. A. Kaminskii, M. I. Polyakov, S. E. Sarkisov, and A. A. Filimonov, Phys. Status Solidi A **75**, K111 (1983).

6. A. A. Kaminskii and B. N. Sobolev, Inorg. Mater. (USSR) **19**, 1718 (1983).

Continuously Tunable Single-Frequency Nd:YAG Microchip Lasers, J. J. Zayhowski and A. Mooradian, Lincoln Laboratory, Massachusetts Institute of Technology, Lexington, Massachusetts 02173

ABSTRACT: Single-frequency Nd:YAG microchip lasers have been constructed and characterized. They can be tuned continuously over several gigahertz, at rates from dc to tens of megahertz.

Single-frequency Nd:YAG microchip lasers were created by depositing dielectric cavity mirrors directly on a flat slab of Nd:YAG.[1] The thickness of the Nd:YAG (730 μm) was chosen so that the cavity mode spacing is comparable to, or greater than, the gain bandwidth of Nd:YAG, and only a single frequency will operate. After the mirrors were deposited, the Nd:YAG was cut into 1 × 2 mm pieces, which were tight-fitted into U-shaped beryllium-copper holders adjacent to a PZT piezoelectric transducer, as shown in Fig. 1. The transducer applies stress to the Nd:YAG, changing the cavity length. Because of the extremely short cavity length l_0, a small change in length, δl, results in a relatively large frequency shift $\delta\nu$ away from the initial operating frequency ν_0:

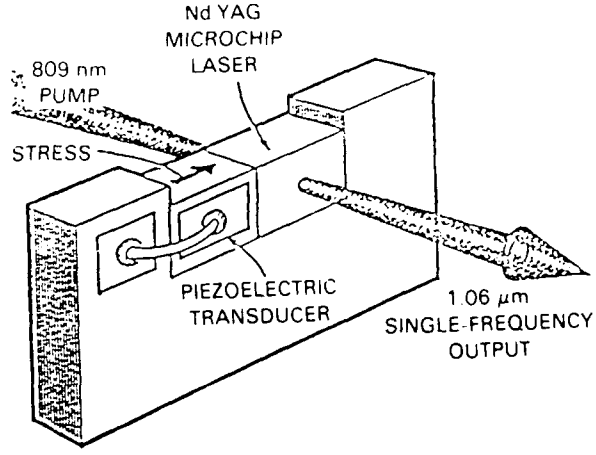

Figure 1. Illustration of a piezoelectrically tunable single-frequency Nd:YAG microchip laser package.

$$\delta\nu = \nu_0 \times \delta l / l_0.$$

A 1.06-μm Nd:YAG microchip laser with a 750-μm cavity tunes at a rate of 40 MHz per angstrom of cavity length change. The microchip lasers are longitudinally pumped at their absorption peak near 809 nm.

A Ti:Al_2O_3 laser was used as a pump source to characterize the microchip lasers. The room-temperature cw threshold is less than 1 mW absorbed power, with a slope quantum efficiency of 30%. The microchip lasers operate single-frequency at up to 40 times threshold (the maximum used in these experiments) and have a linearly polarized, circularly symmetric, diffraction-limited output beam. Heterodyne measurements give an instrument-limited linewidth of 5 kHz (Fig. 2). The Nd:YAG microchip lasers have also been pumped with the close-coupled, unfocused output of a 20 mW GaAlAs diode laser, with similar output characteristics.[1]

By applying a transverse stress to the microchip lasers, their length can be changed enough to tune them over the entire gain bandwidth of the Nd:YAG.[2] In contrast to the results of Ref. 2, the microchip lasers described above maintain single-frequency operation while being tuned continuously over the gain bandwidth either thermally or mechanically. To dynamically tune

the microchip laser, a voltage is applied to the transducer. The frequency offset of a tunable laser from a fixed-frequency laser was measured by heterodyning.

Figure 3 shows the heterodyne spectrum of a microchip laser driven by a ±20-V sine wave at approximately 3 kHz. The observed spectrum is in excellent agreement with calculations assuming that the output of the tunable laser varies linearly with applied voltage. Experimentally, the tuning response was measured to be 0.3 MHz/V for applied voltage between -1000 and +1000 V (the largest voltages used in these experiments), and was constant for modulation frequencies between dc to 80 kHz.

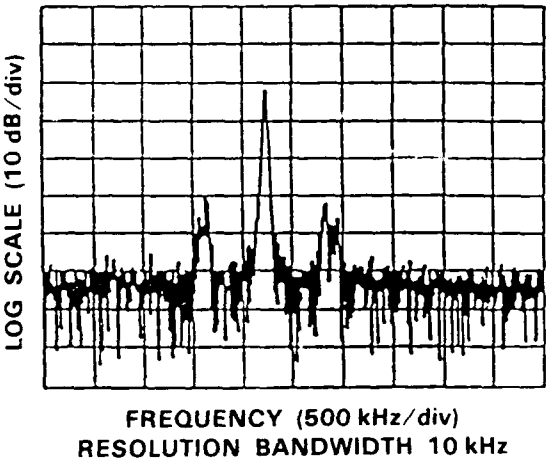

Figure 2. Instrument-limited heterodyne spectrum of two cw Nd:YAG microchip lasers on a logarithmic scale.

At modulation frequencies greater than 80 kHz, the tuning response of the microchip lasers is dominated by mechanical resonances of the microchip-transducer-holder system. These resonances enhance the tuning response, which shows no sign of a roll-off up to 25 MHz (the highest frequency used in the experiments). At resonant frequencies between 80 kHz and 1.0 MHz the tuning was typically enhanced by a factor of 5.

At a modulation frequency of approximately 1.1 MHz a very strong resonance was observed, which enhanced the tuning response by a factor of 44, to 13.2 MHz/V. This resonance was identiied as a fundamental acoustic resonance of the Nd:YAG crystal. Since the cross-sectional dimension of the active region of the microchip laser (30 μm in diameter) is small compared to the acoustic wavelength, it was possible to translate the active region along the Nd:YAG and map out the sinusoidal dependence of the tuning response on lateral position, experimentally confirming the above identification. The factor of 44 mentioned above corresponds to the maximum tuning response obtained. The acoustic resonances of the Nd:YAG crystal were observed at frequencies up to 25 MHz. The heterodyne spectrum of a microchip laser driven by a ±20-V sine wave at an acoustic resonance near 5 MHz is shown in Fig. 4. In this figure, each of the sidebands generated is resolved, and there is excellent agreement with the calculated FM spectrum using a peak frequency deviation of 20.75 times the modulation frequency.

With proper design of the piezoelectrically tunable, single-frequency microchip laser package it should be possible to improve both the maximum tuning rate before mechanical resonances are reached and the amount of piezoelectic tuning obtainable. The use of a stiffer material for the holder will help in both areas. Alternatively, the optical cavity length of the microchip lasers may be modulated using a different technique, such as

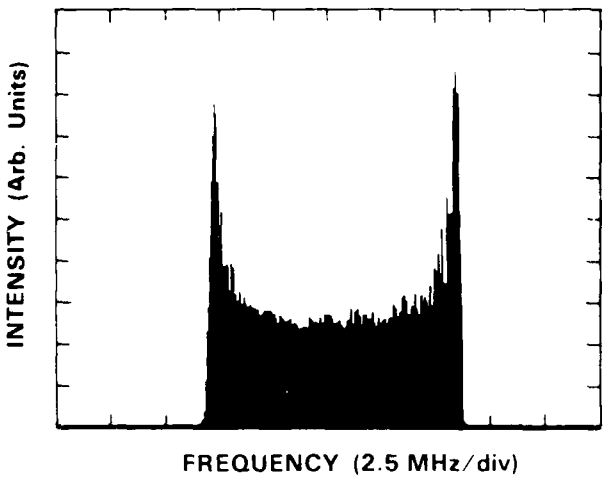

Figure 3. Heterodyne spectrum of a piezoelectrically tuned single-frequency Nd:YAG microchip laser driven by a ±20 V sine wave at approximately 3 kHz.

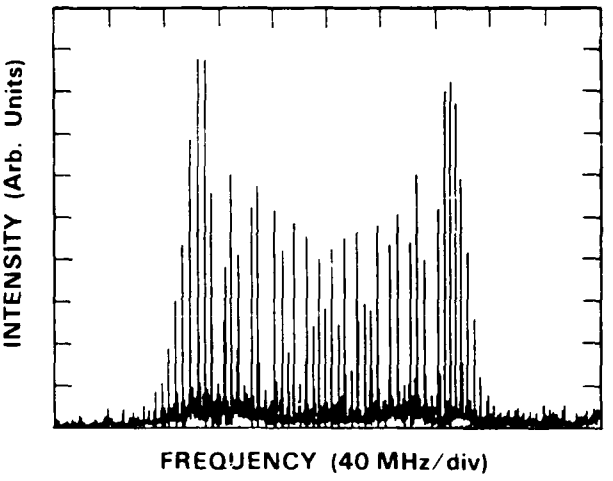

Figure 4. Heterodyne spectrum of a piezoelectrically tuned single-frequency Nd:YAG microchip laser driven by a ±20 V sine wave at an acoustic resonance near 5 MHz.

electro-optic tuning or movement of one of the cavity mirrors independent of the rest of the cavity.

The tuning capabilities of microchip lasers are unique. Larger lasers may be tuned in the same manner as the microchip lasers, but the longer cavity length greatly restricts both the tuning range and rate. The most common technique for tuning large lasers is to use an intracavity frequency-selective device and select individual cavity modes. Tuning is therefore discrete. An alternative technique is to modulate the cavity length at very nearly (but not exactly) a multiple of the longitudinal-mode frequency interval of the laser cavity.[3] Only the microchip laser allows continuous, single-frequency tuning across the gain bandwidth of the gain medium at an arbitrary rate.

With its tunability, low pump threshold, high efficiency, and single-frequency operation, the Nd:YAG microchip laser should find applications in many areas. Its simple construction and small size permit inexpensive mass production.

The technical assistance of R. C. Hancock, C. Dill, C. D. Hoyt and J. Keszenheimer is gratefully acknowledged. This work was sponsored by the Department of the Air Force, the Department of the Army and DARPA.

REFERENCES:

1. J. J. Zayhowski and A. Mooradian, Opt. Lett. **14** (1989).
2. A. Owyoung and P. Esherick, Opt. Lett. **12**, 999 (1987).
3. E. O. Amman, B. J. McMurtry, and M. K. Oshman, IEEE J. Quantum Electron. **QE-1**, 263 (1965).

Measurements of Heating and Energy Storage in Diode-Pumped Nd:YAG

T. S. Chen, V. L. Anderson, O. Kahan
Hughes Aircraft Company
P. O. Box 902
EC1/B129
El Segundo, California 90245

Thermal effects in flashlamp pumped Nd:YAG lasers arise from the fact that nearly ten percent of the flashlamp energy is converted to heat in the laser medium, while about three percent is stored in the inversion as useful gain at the time of lasing. This heating is due to the sizable quantum defect between the pump spectrum and the lasing wavelength, and quenching mechanisms. The normalized heating parameter χ is a measure of this effect. For flashlamp-pumped Nd:YAG, a value of χ around 3.3 has been reported in the literature [1].

Heating of the laser medium caused by thermalization of the waste energy is significantly reduced in diode-pumping due to the much smaller quantum defect. We have experimentally measured both the stored energy and the heat deposited. The stored energy was calculated from small-signal gain measurements. The heat deposition was calculated from interferometrical measurments of the thermally induced optical path length changes of the laser rod under test.

The Nd:YAG test rod was 15mm long and 2mm in diameter, 1.1% atomic Nd^{+3} doped, AR coating at one end and HR coating at the other end. The rod was pumped by 9mJ, 200μsec pulses from a 3-bar diode-array (model SDL 3220-J) with driver SDL-922, made by Spectra Diodes Lab.

A Q-switched Nd:YAG laser was employed as probe beam to measure the small-signal gain. Probe pulses were adjusted in time to coincide with the end of the pump pulse when the gain reached a maximum. The probe fluence was set to be less than one percent of the saturation fluence, guaranteeing operation in the small-signal regime. The round-trip gain G of the probe beam under diode-pumping was measured to be 1.2. The energy stored in the rod E_{st} is obtained by using the relation:

$$E_{st} = 1/2 \cdot E_{sat} \cdot A \cdot \ln \cdot G \qquad (1)$$

A is the rod area. E_{sat} is the Nd:YAG saturation parameter (~0.58 J/cm^2). The stored energy was calculated to be 1.5 mJ.

The heat deposited in the rod was obtained by measuring the interference fringe changes. The fringes were created by reflecting a He-Ne laser off the two polished rod end faces, Figure 1. The rod faces were parallel and no wedge developed during pumping. A TV camera and monitor were used to detect and

display the fringe pattern. A small pin-hole was inserted in front of the rod in such a way that only a small uniform spot in the center area of TV fringe pattern was shown. During the pumping period, the brightness of the spot changed periodically. The number of periods was determined by the optical length change of the rod. The periods were measured using a photodetector and a scope. Figure 2 shows the data obtained with 180 pumping pulses in 3 sec; the upper trace shows two full interference cycles during the heating period. The third peak identifies the beginning of the cooling period, which coincides with the end of the diode pumping, as shown by the lower trace.

The heating parameter, χ, of Nd:YAG was easily derived as a function of the optical path change in units of wavelength λ, the number of pumping pulses N_p, and the stored energy per pulse E_{st}, the relation is

$$\chi = 0.124 \cdot \frac{m}{N_p \quad E_{st}} \tag{2}$$

Here m is the number of wavelengths (λ). From Figure 2, the rod increased by 2.35λ in 3 sec with 180 pulses, so m = 2.35 and N_p = 180. The stored energy E_{st} was measured as 1.5 mJ. The χ parameter was calculated to be 1.1 by using the above equation, about one-third of the value of flashlamp pumped Nd:YAG.

The rod was thermally well isolated. The thermal time constant was measured to be about 27 seconds, Figure 3. This results in a 5.4% correction.

In Q-switching, the fraction of excited ions available for stimulated emission at the peak of the excited population pulse, is controlled by the pump excitation and the fluorescence losses during pumping. The fluorescence pumping efficiency, η_{pf}, is a function of the pumping pulse width τ_p and the rod fluorence time constant τ_f given by:

$$\eta_{pf} = \frac{1 - \exp\left[-(\tau_p/\tau_f)\right]}{(\tau_p/\tau_f)} \tag{3}$$

For Nd:YAG, τ_f = 200 μsec, and η_{pf} is 63% if the rod is diode-pumped for 200 μsec (τ_p). Without fluorescence losses the χ parameter derived from our measurement would be 1.1 x $\eta_{pf} \simeq 0.7$. Figure 4 shows the curve of χ as function of the normalized pulse width with respect to the decay time. The quantum efficiency (fraction not lost by quenching) at our level of doping (1.1%) is about 0.8 [2] and the quantum defect efficiency is 0.75, so the total quantum efficiency is about 0.6, which means for every unit of pump energy, only 60% would be stored energy and 40% would be heat. The ratio of the heat to the stored energy is about 2/3 or 0.67. Our measured value of χ = 0.7 without fluorescence decay is very close to the limit of .67.

References

[1] M. S. Mangir and D. A. Rockwell, "Measurements of heating and energy storage in flashlamp-pumped Nd:YAG and Nd-doped phosphate laser glasses," IEEE J. Quantum Electron., vol. QE-22, pp. 574-580, 1986.

[2] K. K. Deb, R. G. Buser, and J. Paul, "Decay kinetics of $^4F_{3/2}$ fluorescence of Nd^{+3} in YAG at room temperature," Appl. Opt. 20, pp. 1203-1206, 1981.

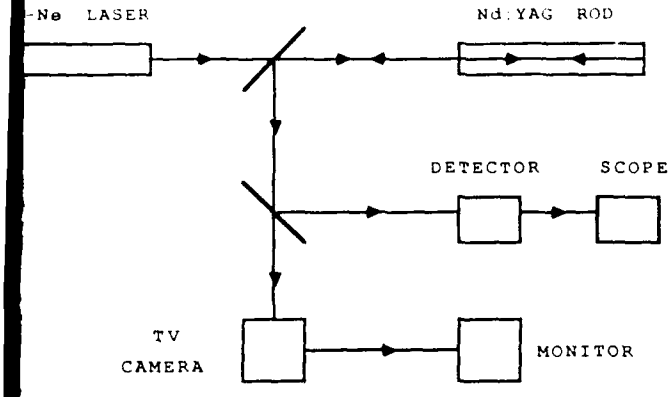

ig. 1 Schematic of the experimental apparatus used to measure the heat deposition in Nd:YAG rod .

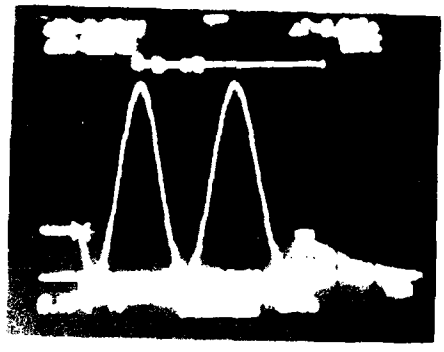

Figure 2. Brightness variation of the interference spot in 3 sec heating with diode-pumping; 0.5 sec/div .

Figure 3. Brightness variation of the interference spot in 1 sec heating with 90 pulses; 1 sec/dev .

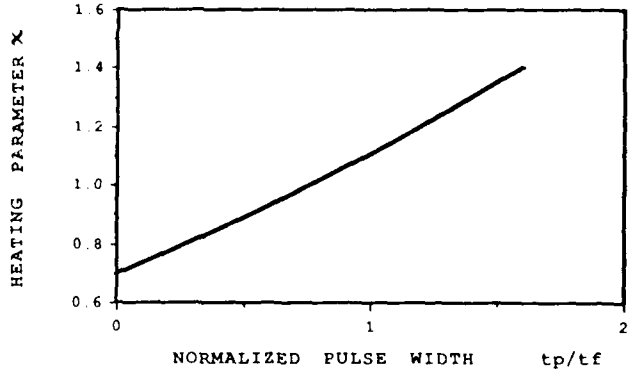

Fig. 4 Heating parameter versus normalized pulse width .

DIODE LASER END PUMPED NEODYMIUM LASERS: THE ROAD TO HIGHER POWERS

R. A. Fields, T. S. Rose, M. E. Innocenzi,
H. T. Yura and C. L. Fincher

Aerospace Corporation
P. O. Box 92957
Los Angeles, California 90035

The diode-laser end-pumped laser (DLEPL) has greatly expanded the applicability of solid state laser and non-linear materials. The DLEPL geometry optimizes the perfromance of diode pumped laser devices by (1) matching the pump volume to the lasing mode and (2) optimizing the length of the laser material with respect to crystal losses and pump light absorption (several mm's for most Nd^{3+} doped hosts). Consequently, the design parameter space for DLEPL's is considerably expanded over traditional solid state laser systems (which are lamp pumped from the side) and can now include materials with vastly differing emission cross sections and optical quality. This paper reports higher power DLEPL outputs, comparisons of efficiencies for different materials, and the impact of heating on DLEPL's.

Recently, a Nd:YAG laser side-pumped by a diode laser array demonstrated over 3 watts output at a total electrical efficiency of 2%.[1] DLEPLs will soon reach such levels, but at far higher efficiency. Single diode outputs, limited by catastrophic damage, of up to 6 and 8 watts for 100 and 200 micron apertures have been reported.[2] Pumping with such diodes, operated at derated levels and fiber coupled[3] to the laser, will result in a long-lived DLEPL in the 5 to 10 watt regime, at over 10% wall-plug efficiency.

We recently operated these new diodes individually in a standard hemispherical resonator.[4] Using a 10 stripe 100 μm wide SDL array, we demonstrated 19% electrical efficiency in a diode pumped Nd:YVO_4 laser of over 1.2 watts of cw TEM_{00} output. A less efficient 20 stripe device, coupled through an anamorphic prism, yielded 1.22 watts TEM_{00} output for an optical input of 2.0 watts, at a total optical efficiency of 61% (see Fig. 1). Portions of the DLEPL optical-input-to-optical-output (I/O)

curve exceeded 73% in slope efficiency. This is a surprising result, since the slope is related to the product of the quantum defect (76%), the effective absorbed power (measured at 89%), the spatial overlap of the pump and laser mode, and the quantum efficiency. Here and in our previous studies we have observed an increase in slope in the I/O curve (referred to as a kink) when the effective pump power (power absorbed after threshold) per mode volume in the crystal exceeds 2 kW/cm^3. Alternatively, one can refer to the normalized intracavity power S used by Risk[5] (and others referenced therein) where

$$S = 4 P_L \sigma \tau / \pi h \nu_L \omega_L^2$$

and P_L is the one-way intracavity power, σ is the peak emission cross section, τ is the radiative lifetime, ω_L is the laser mode radius and ν_L the laser frequency. We find that unless the laser reaches S = 80, a slope that corresponds to near unity quantum effciency is not observed. Also depicted in Fig. 1 are measured I/O curves for modes which are double (ω_L = 184 μm) and quadruple (ω_L = 260 μm) the volume of the mode associated with the highest output curve. They reach S = 80 at 1 and 2 watts pump power, respectively.

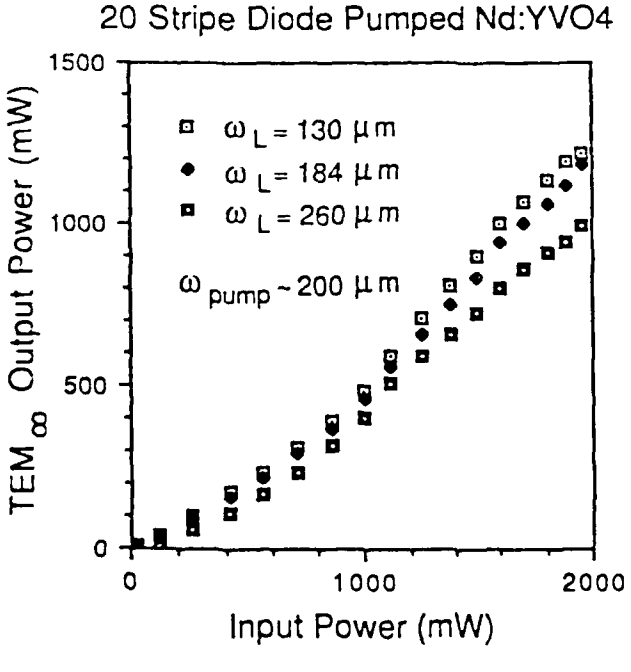

Figure 1

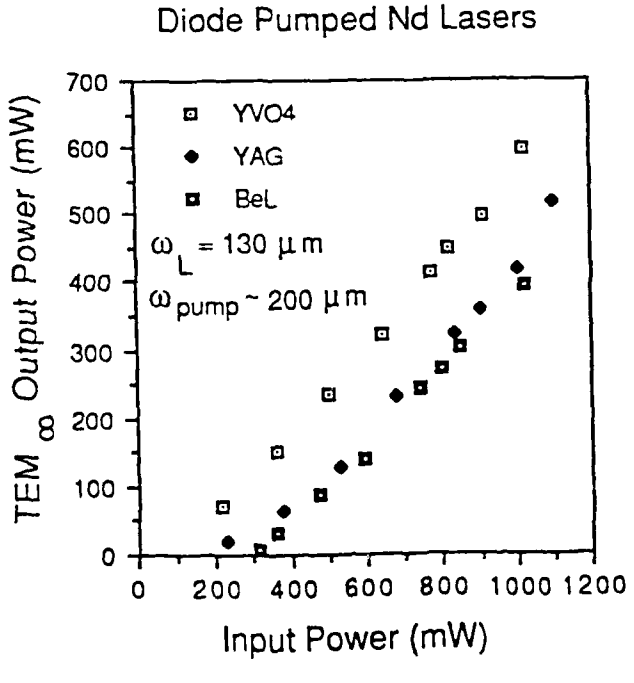

Figure 2

This value of S also appears consistent with our comparisons of materials. For identical resonators, S is directly proportional to the $\sigma\tau$ of each material. We have measured the performance of Nd^{3+} in YAG, YVO_4, and BEL where the $\sigma\tau$ ratios are approximately 1:1:6. As predicted, YAG and YVO_4 have the same high slope. BEL has a lower slope and is expected to reach its highest slope at 3 Watts of pump for this resonator. Experiments currently in progress at higher pump powers and/or with smaller modes, in conjunction with more detailed modelling, will help clarify various issues, i.e. the kink, the abnormally high slope, and the relative material performance.

Thermal effects can impact high power DLEPLs in two ways: (1) temperature changes can affect a material's absorption and gain and (2) temperature gradients can cause lensing effects. We have developed a simple model in order to estimate the magnitude of these effects. Since the thermal conductivity of our heat sink is much greater than that of the laser crystal, we assumed radial heat flow only. Based on this we obtained a temperature distribution within the crystal. To test consistency, we computed the axial gradient near the center of the crystal and found it to be less than 1% of the corresponding radial component. Recently Farrukh et al.[6] have obtained a solution to the time dependent heat equation for this geometry. Although the boundary conditions employed in Ref. 6 are somewhat different than those that apply here, we are attempting to see if the analysis of Ref. 6 can be used in the present case.

REFERENCES

1. R. Burnham and A. D. Hays, Opt. Lett., 14, 27 (1989).
2. D. F. Welch, CLEO Technical Digest, Anaheim, Calif. 1988, paper WH1.
3. J. Berger, D. F. Welch, W. Streifer, D. R. Scifres, N. J. Hoffman, J.J. Smith and D. Radecki, Opt. Lett., 13, 306 (1988).
4. R. A. Fields, M. Birnbaum, and C. L. Fincher, Postdeadline CLEO Technical Digest, Anaheim, Calif. 1988, paper PD3.
5. W. R. Risk, J. Opt. Soc. B, 5, 1412 (1988).
6. U. O. Farrukh, A. M. Buoncristiani, and C. E. Byvik, IEEE J. Quant. Elec., 24, 2253 (1988) Biography.

WEDNESDAY, MAY 3, 1989

NAUSET IV

8:00 AM–9:15 AM

WA1–WA4

NONLINEAR FREQUENCY CONVERSION

Klaus Petermann, University of Hamburg, *Presider*

Efficient, Broadly-Tunable, Beta-Barium Borate Optical Parametric Oscillator Pumped by a Xenon-Chloride Laser

Hiroshi Komine

Northrop Research and Technology Center
One Research Park, Palos Verdes Peninsula, CA 90274

Summary

Beta-barium borate optical parametric oscillators (OPO) pumped by ultraviolet lasers have been reported recently.[1-7] These OPO's are potentially tunable from the near ultraviolet to the near infrared regions, and they provide a new solid-state wavelength conversion technique for high-power ultraviolet lasers. This paper reports on progress made in a beta-barium borate OPO pumped by a xenon-chloride (XeCl) excimer laser with respect to wavelength tunability and conversion efficiency.

The OPO experiment used a type-I cut beta-barium borate crystal with the c-axis oriented at 36 degrees to the nominal beam propagation direction. The crystal length was 7 mm, and the end faces were polished and uncoated. The OPO cavity consisted of two identical cylindrical concave mirrors with a high reflectance coating over the 400 to 600 nm range. A small uncoated fused silica beam splitter was inserted in the optical cavity to couple out a small fraction of the resonant signal wave power. The idler wave power was transmitted through the cavity mirrors.

The XeCl pump laser source consisted of a linearly-polarized, narrowband oscillator and a power amplifier. The XeCl oscillator wavelength was 308.2 nm with a bandwidth of less than 30 GHz. The pulse length was typically 15 nsec, and the peak power was varied by adjusting the gain of the power amplifier. Using a beam reducing telescope and a cylindrical lens, the pump beam was focused onto the crystal through one of the OPO cavity mirrors. The polarization direction of the pump beam was parallel to the resulting line focus and to a plane containing the crystal c-axis and the propagation direction.

The OPO oscillation threshold was observed when the pump energy exceeded about 2 mJ. The signal and idler output beams were monitored by their respective photodiodes and pyroelectric joulemeters and by an optical multichannel analyzer. The signal output wavelength was tuned from about 420 nm to 616 nm by rotating the crystal orientation. The corresponding idler wavelength ranged from 1160 nm to 616 nm (i.e., degeneracy), respectively.

The output bandwidth was on the order of 0.1 to 0.2 nm when the OPO was operated far from degeneracy; however, the bandwidth increased as the crystal was tuned towards the degeneracy condition, as expected.

The pump energy conversion efficiency of the OPO was measured by monitoring the input and depleted pump pulses. These measurements were obtained at various signal and idler wavelengths. Figure 1 shows a representative plot of the fraction of the converted pump energy as a function of the incident energy for two sets of signal and idler wavelengths.

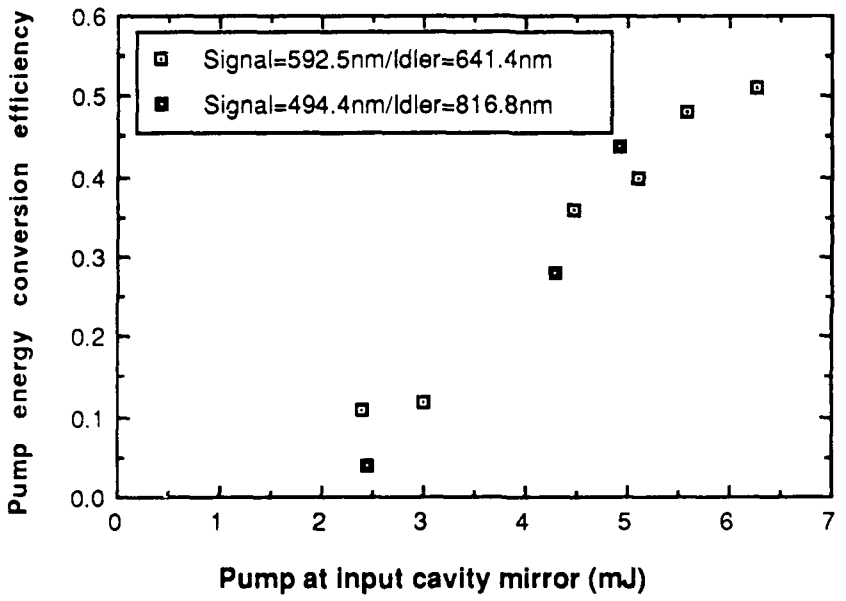

Figure 1 Pump conversion efficiency as a function of input pump energy.

The data indicate an energy conversion efficiency of up to 51% when the pump input is approximately three times that of the oscillation threshold pump energy. For this case, a comparison of the depleted pump pulse shape with the input pulse showed power conversion efficiencies of about 65% near the peak of the pulse.

As the signal wavelength was tuned from 440 nm to degeneracy, conversion efficiencies between 40% and 50% were obtained with pump input levels at about 1.9 to 2.3 times the oscillation threshold pump energy. Under these conditions, the energy of the idler output beam along the pump propagation direction, measured directly with a pyroelectric joulemeter, indicated pump-to-idler energy efficiencies ranging from 8% to 10%.

In summary, a beta-barium borate OPO pumped by a XeCl laser has demonstrated broad tuning in the visible and near infrared region from 420 nm to 1160 nm. Efficient pump energy conversion was achieved with up to 10% energy conversion into idler wave generation. Similar efficiencies for signal wave output may be expected with OPO resonators optimized for signal wave generation.

References

1. Y. X. Fan, R. C. Eckardt, R. L. Byer, C. Chen, and A. D. Jiang, *Conference on Lasers and Electro Optics* (9-13 June, San Francisco, CA), paper ThT4.

2. C. Chen, Y. X. Fan, R. C. Eckardt, and R. L. Byer, *SPIE Proceedings* Vol. 681, 12-19 (1986).

3. L. J. Bromley, A. Guy, and D. C. Hanna, *Conference on Lasers and Electro Optics* (25-29 April 1988, Anaheim, CA), paper MJ4; L. J. Bromley, A. Guy, and D. C. Hanna, Opt. Commun. **67**, 316 (1988).

4. Y. X. Fan, R. C. Eckardt, R. L. Byer, J. Nolting, and R. Wallenstein, *Conference on Lasers and Electro Optics* (25-29 April 1988, Anaheim, CA), paper PD31; Y. X. Fan, R. C. Eckardt, R. L. Byer, J. Nolting, and R. Wallenstein, Appl. Phys. Lett. **53**, 2014 (1988).

5. H. Komine, *Conference on Lasers and Electro Optics* (25-29 April 1988, Anaheim, CA), paper PD32.

6. L. K. Cheng, W. R. Bosenberg, D. C. Edelstein, and C. L. Tang, *Conference on Lasers and Electro Optics* (25-29 April 1988, Anaheim, CA), paper PD33; L. K. Cheng, W. R. Bosenberg, D. C. Edelstein, and C. L. Tang, Appl. Phys. Lett. **53**, 175 (1988).

7. H. Komine, Opt. Lett. **13**, 643 (1988).

HIGH GAIN OPTICAL NONLINEAR INTERACTIONS WITH A 1.73 μm PUMP

Norman P. Barnes
Keith E. Murray
NASA Langley Research Center
Hampton, Virginia 23665-5225

Summary

Two novel high gain optical nonlinear interactions have been demonstrated using an Er:YLF laser operating at 1.73 μm have been demonstrated. One of these interactions used the Er:YLF laser as a pump for an optical parametric amplifier. A $AgGaSe_2$ crystal provided the nonlinear media and a HeNe laser operating at 3.39 μm was the signal. Gains in excess of 13 were demonstrated and the experimental results agreed well with theoretical predictions. Another interaction, second harmonic generation in $LiNbO_3$, produced in excess of 1.5 mJ from a fundamental beam having only 13 mJ. However, results did not agree well with initial theoretical predictions. Differences in these results can be explained by examining the crystal quality.

For these experiments, the Er:YLF laser was well characterized so that accurate modelling of the interactions could be performed. Operation of the Er:YLF laser was confined to operation in the TEM_{00} mode through the use of a high quality, large diameter cavity which promoted nearly uniform pumping of the laser rod. Major diameter of the cavity was 55 mm while the minor diameter was 53 mm. By using a 5.0 mm diameter, Er:YLF laser rod, TEM_{00} mode operation was achieved with a 10 m radius of curvature highly reflecting mirror and a flat 0.8 reflecting output mirror. By using a pulse-forming network consisting of a 31.3 μF capacitor and a 14 μH inductor, threshold was 20 J while the slope efficiency was 0.003. Q-switched pulselength and energy

were measured for each pulse during the nonlinear optical experiments. Pulselengths were typically 180 nanoseconds in length at an energy output of 15 mJ.

A gain in excess of 13 was in agreement with a model which averaged gain of a 3.39 μm HeNe with a Gaussian beam profile over a Gaussian pump beam. For these experiments a 20 mm $AgGaSe_2$ crystal was used. Gain was measured as a function of the Er:YLF energy and pulselength. By curve-fitting the results to the theory, a value for the nonlinear coefficient, d_{36}, of 37.3 pm/V was obtained. These results are in good agreement with other measurements of this parameter. In addition, a tuning curve, that is gain as a function of crystal angle, was measured for this interaction. Clear secondary peaks were obtained corresponding to the expected $\sin^2(\Delta kl/2)/(\Delta kl/2)^2$ tuning curve. Measured acceptance angles agreed well with calculated acceptance angles indicating good crystal quality.

A conversion efficiency of 0.13 was measured for second harmonic generation in $LiNbO_3$ which is substantially less than expected. A 50 mm $LiNbO_3$ crystal was used in these experiments. When second harmonic energy is plotted versus the fundamental energy squared divided by the pulselength, the expected first power law is obtained, however the initial slope efficiency is an order of magnitude too low. Reasons for the lower than expected second-harmonic energy become apparent when examining the tuning curve. A curve of the second harmonic energy as a function of the crystal angle does not display the expected $\sin^2(\Delta kl/2)/(\Delta kl/2)^2$ curve. Instead, two pronounced peaks, believed to be associated with two distinct crystal domains, are observable. In the low conversion approximation, the peak second harmonic energy should be proportional to the crystal domain length squared while the width of the peak should be inversely proportional to the crystal domain length. Ratioing the peaks yields a ratio of crystal domain lengths of 1.70. Ratioing the widths

yields a ratio of crystal domain lengths of 1.59, in good agreement with the previous ratio. Comparing the calculated width with the observed width yields a crystal domain length of 15 mm. When this length is used as the effective nonlinear crystal length, the agreement between the calculated and observed conversion efficiencies is within a factor of 1.15.

In conclusion, a comparison of experimental tuning curves with the model can yield a significant amount of data concerning the quality of a nonlinear crystal. In the case of $AgGaSe_2$, good agreement between theoretical and experimental gain curves is expected because of the good agreement between the theoretical and experimental tuning curves. In the case of $LiNbO_3$, the tuning curve indicates that the crystal is multidomain. Using this data to estimate the effective length of the crystal yields good agreement between predicted and measured second harmonic generation.

Optical Parametric Oscillation in KTP for Tunable Mid-infrared Lasers

J. T. Lin and J. L. Montgomery
Center for Research in Electro-Optics & Lasers (CREOL)
University of Central Florida
12424 Research Pky, Orlando, FL 32826

Optical parametric oscillation (OPO) in nonlinear crystals provides a promising technique for the generation of widely-tunable coherent sources. The new crystal of beta-Barium-Borate (BBO) has been recently used in OPO devices for tunable visible lasers using UV lasers, excimer or tripled-YAG, as the pump.[1,2] The tuning curves of OPO in BBO and KTP pumped by doubled-YAG(532 nm), YAG(1064, 1320 nm) or Raman-shifted-YAG(1.54 or 1.9 microns) were reported based upon the available Sellmeier equations of refractive index.[3,4] Optical parametric amplification (OPA) of picosecond lasers in KTP was recently reported,[5] however, to our knowledge, there is no reported OPO in KTP for mid-IR sources for nanosecond lasers.

In this paper, we report the first demonstration of OPO in a KTP cyrstal pumped by a YAG laser(1064 nm). Within our available mid-IR coating, high efficiency, low threshold tunable OPO devices were demonstrated. The OPO curves were measured and compared with the calculated curves. The OPO gains were analyzed and compared for nonlinear crystals of BBO and KTP at various pumping wavelengths. Efficiency at various pumping powers and cavity lengths were measured. Finally, we propose the key factors for the improvement of OPO efficiencies.

A Quantel laser (model 580) was used as a pump source operating at 1064 nm, 15 ns pulse with TEM_{00} mode up to 60 mJ in energy. The pump beam was focused into the OPO cavity by f=1 focal lens yielding a ~ 1 mm spot size at the entrance plane of the KTP crystal. This crystals was 6.5 mm long (grown by flux method by Shandong University, China) and was cut for type II operation with an angle of 50° to c-axis in the ac-plane. The KTP cyrstal was polished but uncoated. The OPO cavity consisted of two plane dichroic mirrors. The front mirror has transmission (T) of 72.5% at the pump (1064 nm) and reflectance (R) of 75% at 2.07 um (idler) and 97% at 2.2 um (signal). The rear mirror has T=59% (at 1064 nm), 5% (at 2.07 um) and 13% (at 2.2 um).

Figure 1 shows the calculated OPO tuning curves based upon the Sellmeier equations of Ref.6. It is seen that our measured tuning curves are about three degrees smaller than that of the calculated curves. These differences, we believe are due to the accuracy of the measured refractive indexes particularly in the mid-IR regimes (1.4-2.5 um). Comparison with the calculated curves based upon a more accurate Sellmeier equation will be presented. Another cyrstal of KTP cut at 60° will also be used to extend the tuning curves.

As shown in Fig. 2, we had measured the total output energy of the signal (at 2.07 um) and idler (at 2.2. um) as a function of the pump energy (at 1064 nm) at various cavity lengths. As we expected a shorter cavity provides higher efficiency with lower threshold. We note that lower threshold may be achieved by using higher reflectance (at the signal/idler wavelengths) of the outcoupling mirror. On the other hand, larger slope efficiency (but also higher threshold) may be achieved by using higher tramsmittance (T) of the coupler. For comparison, we have shown the effici-

ency curves for T = (for signal, idler) (A) (5%, 13%) and (B) (70%, 70%) in Fig. 3.

We calculate the effective nonlinear coefficients (deff) for OPO, at the degenerate points, for BBO and KTP crystals at various pumping wavelengths as follows: for BBO, deff (in unit of pm/V) = 1.64 - 1.65 (for pumping wavelengths at 0.532 - 1.5 μm); for KTP, deff = 6.3 (for pump at 532 nm), 6.24 (at 1064 nm), 7.0 (at 1.32 μm), 6.45 (at 1.54 μm), 0.55 (at 1.8 μm) and 0.13 (at 2.1 μm). Note that KTP type II phase-matched up to about 1.75 μm(for the pump) and values of deff for type I (for pump wavelengths at 1.8 and 2.1 μm) are much lower than that of type II.

In this experiment the efficiencies achieved are limited by the damages of the AR-coated mirrors and the uncoated KTP crystal. Furthermore the tunablility and threshold power are limited by the available broadband, high-reflectance mirrors. Within our coating conditions, this experiment was operated at double-pass (for the pump), double-resonance oscillator. Stability of the output power may be improved by single-resonance oscillation coating. Work is continuing in our laboratory for the following: (1) BBO and $LiNbO_3$ will be used for comparison to KTP; (2) wider-band coating will be used for larger tunablility; (3) a telescope will be used to generate larger pump spot size for better wave-mixing in the cavity; (4) the tuning range will be extended to (2.8-3.5) μm and (3.8-4.5) μm regimes by using Raman-shifted-YAG at 1.54 and 1.9 um, respectively, as the pumping source.

References:

1. Technical Digest, CLEO'88, postdeadline papers: (a) M. Ebrahimzadeh et al, PD30; (b) Y. X. Fan et al, PD31; (c) H. Komine, PD32; (d) L. K. Cheng et al, PD33.
2. C. Chen et al, Proc. SPIE vol. 684, 12(1987).
3. J. T. Lin, Technical Digest, CLEO'87, TUH4.
4. J. Q. Yao, J. T. Lin, N. Due and Z. Liu, Technical Digest, CLEO'88, paper TUJ5.
5. H. Vanherzeele, Technical Digest, OSA 1988 Annual Meeting, paper TUN3.
6. T. Y. Fan et al, Appl. Opt. 26, 2390(1987).

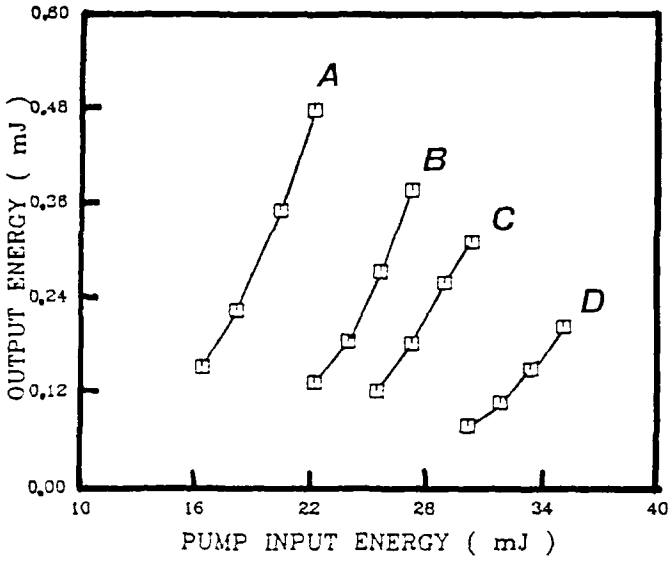

Fig. 1 Output energy as a function of pump energy at various cavity lengths (in cm.): (A) 3 ,(B) 4 (C) 4.5 and (D) 5 cm.

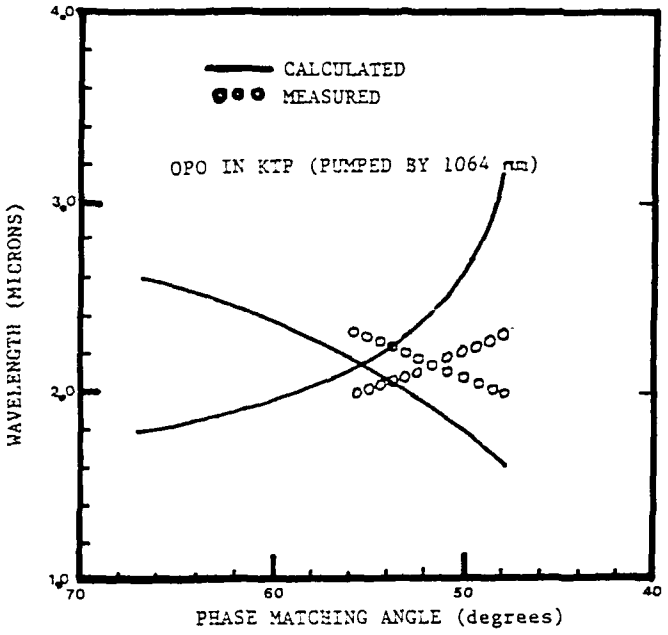

Fig. 2 Tuning curves of KTP crystal for OPO pumped by YAG laser (1064 nm).

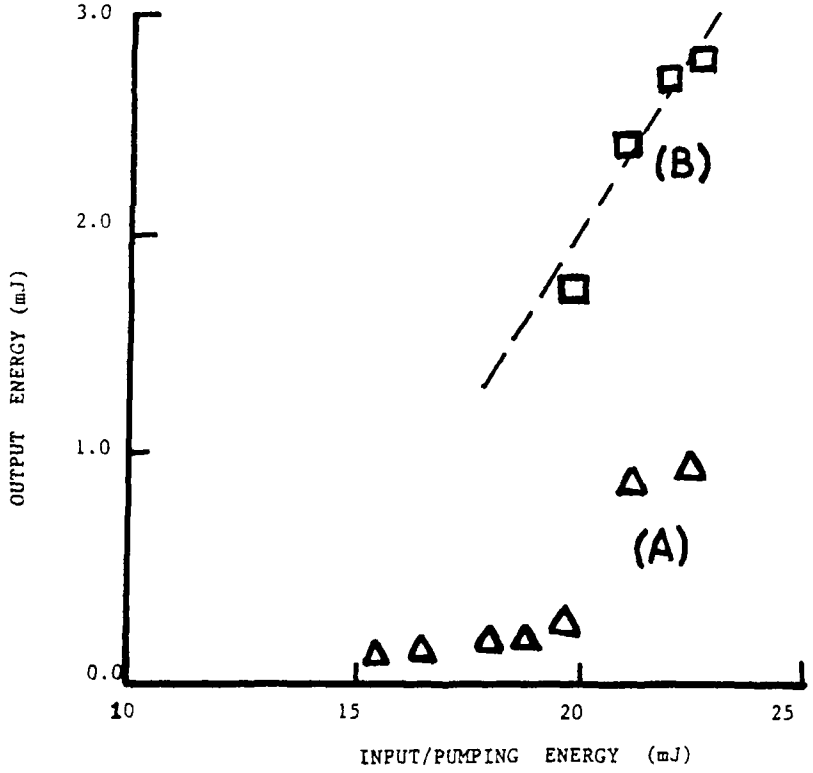

Fig. 3 OPO output at various outcoupling mirror transmittance : curve(A): T=(5%, 13%) for (signal, idler) and (B): T=(70%,70%).

WA4-1

Temporal Pulse Synchronization for Optical Mixing

H. H. Zenzie, P. E. Perkins

Sanders Associates, Inc.

M/S MER15-2250

P.O. Box 2035

Nashua, NH 03061-2035

(603) 885-3010

Sum frequency generation (SFG) is a method used to extend the wavelength range of efficient Near IR lasers to the visible. Except for third harmonic generation (a special case of SFG), this method has not been widely used due to the difficulty of overlapping pulses from separate lasers. Since SFG is a non-linear process, short, high peak power pulses (20 nsec wide) are used which must be temporally overlapped to within 3-5 nsec for efficient mixing to occur. A reliable synchronization method would permit the development of a tunable blue-green source by SFG of Ti:Al_2O_3 (700-950 nm) and Nd:YAG (1 or 1.3 microns).

We report for the first time a temporal pulse synchronization technique which can be used to mix the output of two separate lasers. We achieve temporal simultaneity from two oscillators by pumping both with a single Q-switched pulse. The build-up time and pulse shape of each cavity can be made equal by varying the pumped spot size, coupling reflectivity and resonator length. If the oscillators have been properly designed, variations in pump amplitude (+/-10%) will not affect the synchronization accuracy since the build-up time of the pulses will still be equivalent.

To demonstrate this concept, we mixed the output of a Ti:Al_2O_3 laser at 796 nm with the output of a Nd:YAG laser at 1064 nm to produce blue light at 455 nm (Figure 1). A 20 Hz doubled Nd:YAG pump laser emitting up to 150 mJ at 532 nm

was used to resonantly excite both oscillators. After the pump beam was split between the two cavities with the polarizer/half-waveplate, it was focused through a dichroic high reflector to form a 1.2 mm diameter spot which matched the TEMoo mode volume of both resonators. The 1064 nm resonator contained a 5mm x 100mm Nd:YAG rod, Ward polarizer and a 37%R coupler while the 796 nm resonator consisted of a 6.35mm x 40mm Brewster cut Ti:Al_2O_3 rod, three plate (1:2:4 mm) quartz birefringent tuner and a 60%R coupler. At an output level of 13.5 mJ (Ti) and 5.2 mJ (Nd), the pulses were well synchronized as shown in Figure 2. The orthogonally polarized beams were combined and mixed in a Type II KD*P crystal. Data demonstrating the insensitivity of this method to pump amplitude variations will be presented.

With the addition of a flash-pumped Nd:YAG amplifier and a green pumped Ti:Al_2O_3 amplifier, we were able to generate 12 mJ of 455 nm light at 15% mixing efficiency. This technique can be applied to other systems as long as both materials can be pumped at the same wavelength. Variations in material cross-section can be accommodated by proper choice of oscillator length, coupling reflectivity and pumped volume.

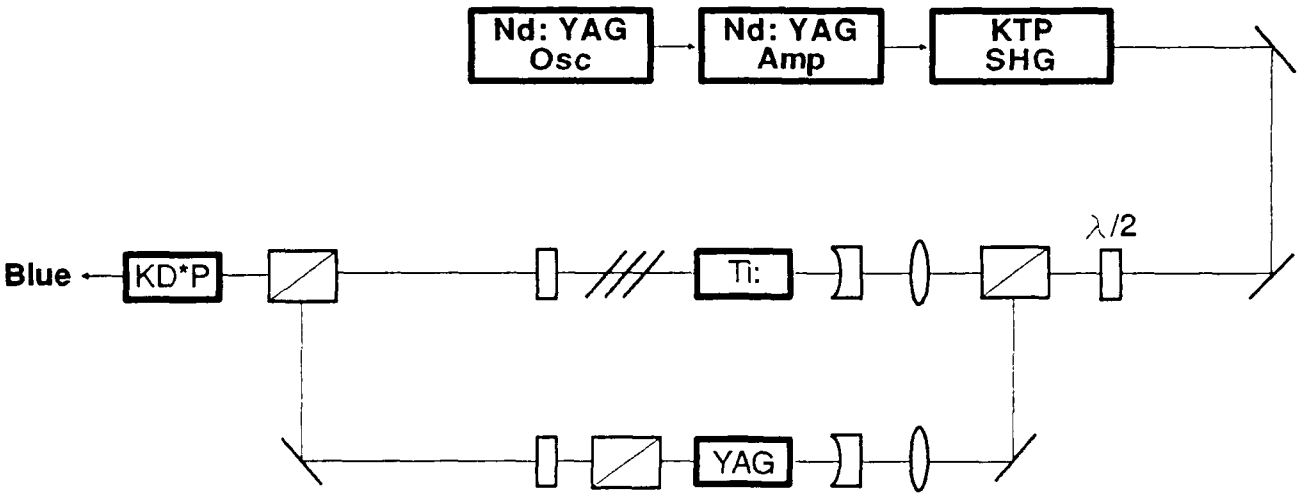

Figure 1 Mixing Experiment

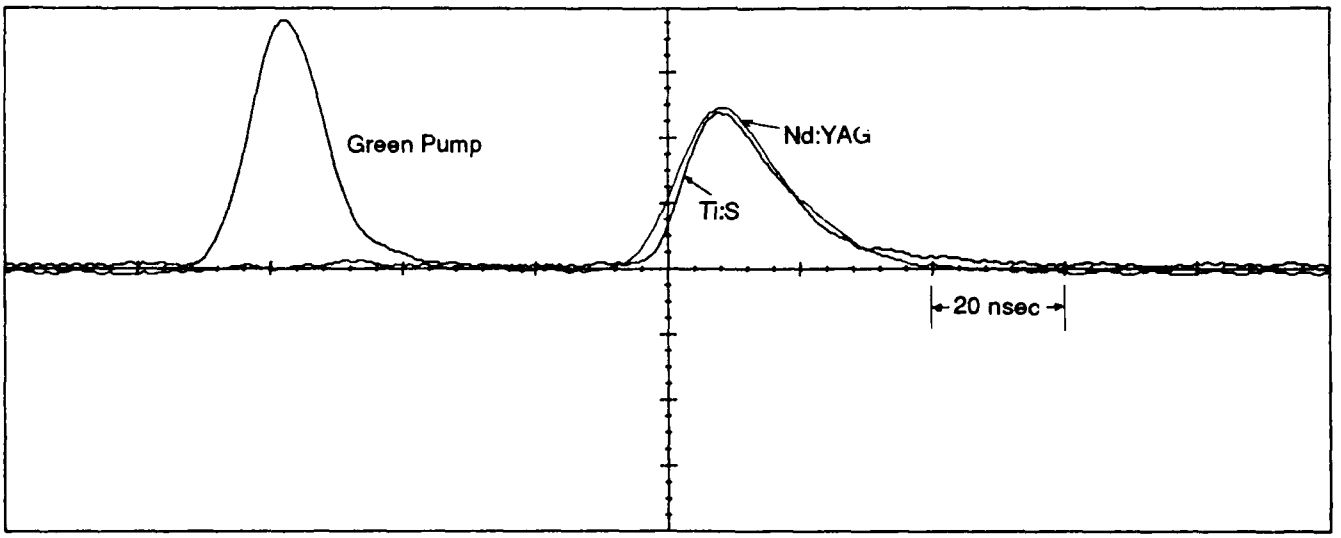

Figure 2 Temporal Pulse Overlap

NOTES

WEDNESDAY, MAY 3, 1989

NAUSET III

9:15 AM–10:30 AM

WB1–WB6

MOSTLY 1.3 MICRON Nd LASERS/ POSTER SESSION

Antonio Sanchez, MIT Lincoln Laboratory, *Presider*

Laser Techniques and Frequency Conversion for a Neodymium Based Blue Communication Transmitter

S.R. Bowman , B.J. Feldman, J.M. McMahon
Laser Physics Branch Code 6540
Naval Research Laboratory
Washington D.C. 20375

A.P. Bowman
Pacific Sierra Research Corp.
1401 Wilson Blvd.
Arlington, Va. 22209

Donald Scarl
Polytechnic University
Farmingdale, N.Y. 11735

The search for a reliable and efficient blue laser transmitter for submarine communication is well known. We have been pursuing a promising approach utilizing the $^4F_{3/2}$ to $^4I_{13/2}$ transition in Nd:$YAlO_3$. Tripling of this laser source and subsequent rotational Raman conversion in low pressure hydrogen or deuterium gas produces the desired wavelengths. A reasonable extrapolation of current technology suggest that a blue-green laser source based on diode pumped Nd:YALO would operate with an overall electrical efficiency of 2% or greater.

The choice of the 1.3 micron line in Nd:YALO was based on its frequency match to the desired wavelengths as well as its laser performance characteristics. The relatively high emission cross section for this transition compared to that for the $^4F_{3/2}$ to $^4I_{11/2}$ transition allows for workable 1.34 micron gain before 1.08 micron ASE becomes a problem. We have studied Nd:$YAlO_3$ laser extraction efficiencies at 1.34 micron for both flashlamp and laser diode pumping. For flashlamp pumping, slope efficiencies of 1.8% and overall efficiencies of 1.3% were measured for long pulsed operation. In preliminary

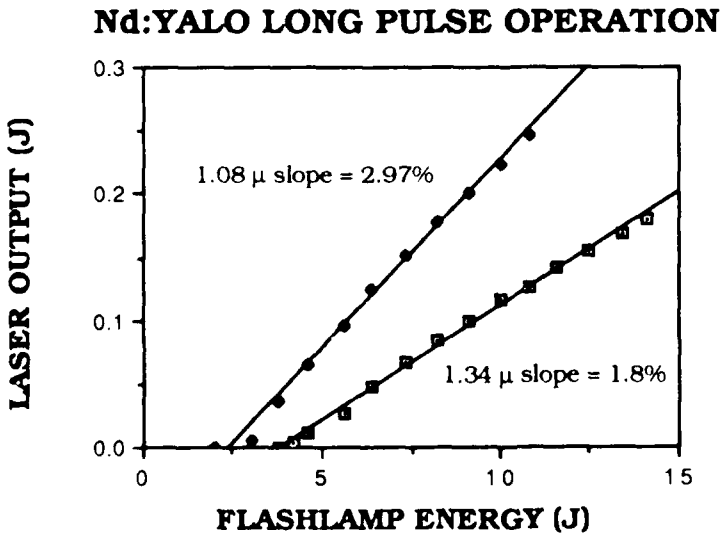

experiments with laser diode pumping, we have obtained 11.5% slope and 8.4% optical to optical efficiencies. In both cases threshold measurements indicate material losses of 0.007/cm and no indication of excited state absorption has been observed.

Exact frequency control for this system is aided by the fact that Nd:$YAlO_3$ has a broad 1.34 micron tunable linewidth (2.6nm)[1] and modest temperature tunability (+6.1pm/K.)[2]

In order to explore frequency conversion to the blue, we built a single transverse mode Q-switched Nd:YALO, 1.34 micron oscillator followed by three single pass amplifiers. The higher gain 1.08 micron transition was suppressed with high transmission coatings on all components. Single flash lamp laser heads and 1/4 by 3 inch "b" axis grown rods were used throughout. The beam was diverged to slightly overfill the last amplifier and was then collimated in a magnification 2.0 Galilean telescope. The system provides a very reliable source of 200 millijoule, 30 nanosecond, 1.3411 micron pulses at several Hertz firing rate.

Second harmonic generation of the Q-switched pulses was studied in several nonlinear materials. For many materials the absorption at this fundamental wavelength is a severe problem. Best samples of KD*P and CD*A had loss coefficients of 0.13/cm and 0.15/cm making them unacceptable for high power operation. Using an uncoated 8 millimeter long, type I barium borate crystal, internal second harmonic generation of 29% was obtained with 3.5 megawatts in a 75 nanosecond pulses. Similar results have shown 39% internal second harmonic of 1.34 microns using an uncoated, type II, 8 millimeter long KTP crystal.

While our results indicate that KTP is clearly the crystal of choice for second harmonic generation, for production of the third harmonic the answer is not so clear. Our attempts to use KTP for sum frequency generation resulted in laser induced color center formation. Also the depolarization of the fundamental frequency resulting from the type II phase matching, requires polarization correction optics or higher second harmonic conversion. [3] To date, our best results are 22% third harmonic conversion efficiency using a type I barium borate crystal and a type II KD*P mixer.

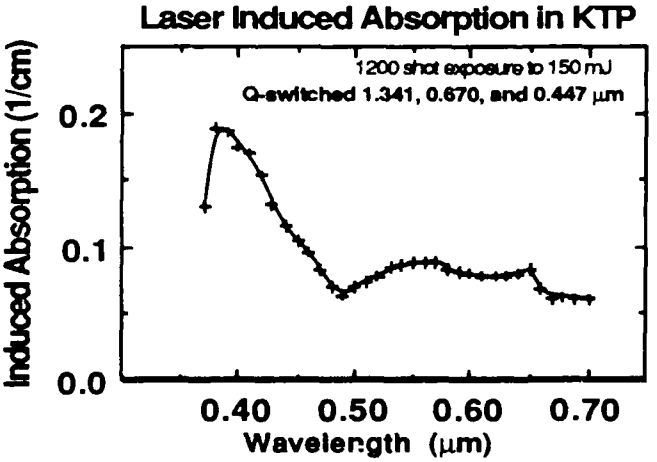

For the final frequency shift the third harmonic beam is converted to circular polarization and focused into a single pass Raman cell. With the gas pressure and polarization optimized, the threshold for first rotational Raman is 0.5 megawatts in deuterium gas and 0.2 megawatts in hydrogen gas. Good conversion efficiency is achieved

using a second, higher pressure Raman cell in series with the first. We have demonstrated 75% conversion from 447 to 459 nm in hydrogen gas and 34% conversion of the 447 nm pump beam to 455nm with deuterium gas. The Raman conversion in deuterium was lower because our pump power is very near the Raman threshold. Energy conversion to the lower vibrational Stokes modes is avoided through the use of circular polarization pump and low gas pressures.

The requirement that a Nd:$YAlO_3$ laser system deliver medium average power while maintaining efficiency creates some interesting materials problems. The material absorption at 1.34 microns makes most electro-optic switches too lossy for average power systems. We have encountered average power related laser damage to antireflection coating of laser rods at the 1.0 Watt/cm^2 level. Multipass amplifier schemes, desirable for high efficiency, are complicated by YALO's naturally birefringence. Gain at the correct wavelength exists only for the polarization parallel to the "c" axis. We have experimented with YIG Faraday rotators for passive double pass amplifiers. A YIG rotator also serves as an excellent isolation stage for the 1.08 microns gain. Unfortunately, YIG crystal uniformity and damage thresholds are still a problem.

Natural birefringence creates other problems in laser systems with high thermal loading. As shown below, the thermal focusing in Nd:$YAlO_3$ is highly astigmatic and several times stronger than Nd:YAG. To correct for this and other wavefront distortions, we are investigating SBS phase conjugate media at 1.34 microns. Here again, many of the SBS media used at 1.0 micron, exhibit too much absorption at 1.34 microns. To date our best results have been 93% SBS energy reflectivity with 100 nanosecond pulses in CS_2. While wavefront correction is required for a medium average power $NdYAlO_3$ system, we have observed that thermal induced depolarization is very small.

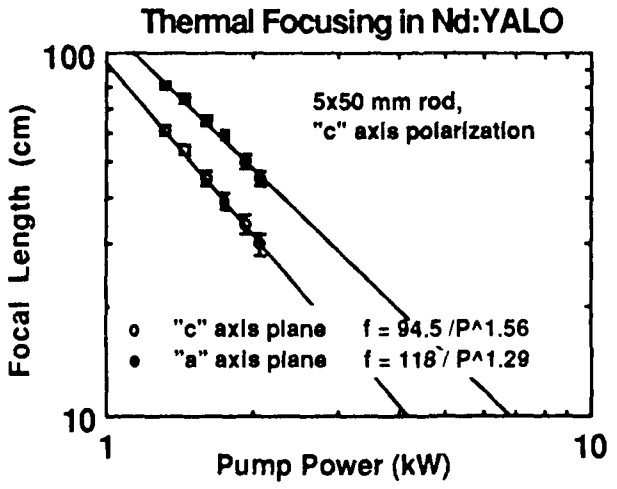

1. A.A. Kaminskii, et.al., Sov. J. Quantum Electron., 6, 1371 (1976).

2. N. Djeu (private communications).

3. R.S. Craxton, IEEE J. Quantum Electron., QE-17,1771 (1981).

Absolute Wavelength Standard for Tunable 1341 nm crystal laser

Donald Scarl
Polytechnic University, Farmingdale, NY 11735

Short cavity monolithic lasers (in which the mirrors are formed on the crystal ends) operate in a single longitudinal mode when their mode separation is comparable with or greater than the crystal emission linewidth. In the case of Nd^{3+}:$YAlO_3$ (YALO) at 1341 nm, a 1.2-mm cavity length leads to 0.48-nm mode spacing, comparable with the 1-nm gain width of the 1341-nm line.[1,2] A short cavity laser can be made to operate at almost any wavelength within the gain curve. The wavelength stability of a monolithic laser depends only on the change with temperature of the optical pathlength within the crystal. These monolithic temperature-tunable crystal lasers can be expected to be long-term-stable environmentally-insensitive narrow-line secondary-standard light sources.

YALO lasers can be tuned to two important He lines: the $2s\text{-}^3S_1\text{–}2p\text{-}^1P$ manifold centered at 1083.025 nm and the $3p\ ^1P_0\text{–}5s\ ^1S_0$ line at 1341.1686(3) nm (7454.1456(17)-cm^{-1}). A solid state laser locked to one of these lines could form a long-term stable wavelength standard. The 1083-nm line is also useful for manipulating He atoms in a beam or vapor.[3,4]

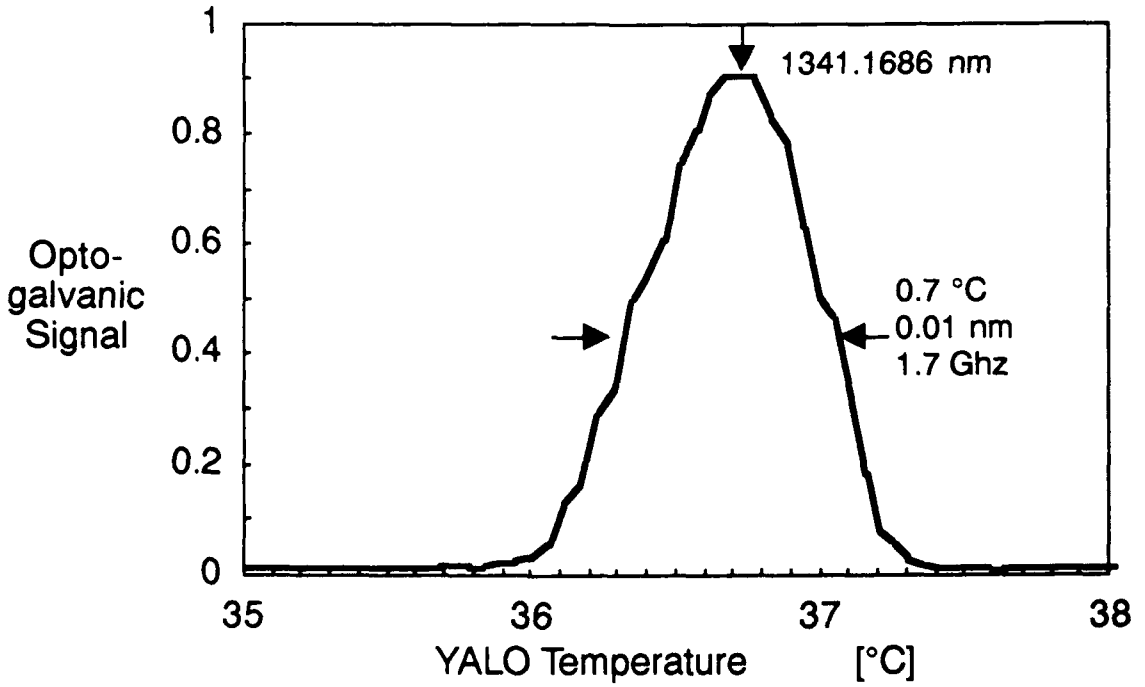

We have temperature scanned the wavelength of a monolithic diode pumped YALO laser from 1341.0 to 1341.6-nm and detected the optogalvanic signal from a He filled hollow cathode lamp.

The optogalvanic response is shown in Fig. 1. The Doppler-broadened He line has a full width at half maximum of 0.01-nm (1.7-Ghz or 0.054-cm^{-1}) which can be scanned with a laser temperature change of 0.7°C. The absolute wavelength of the laser can be determined relative to the He line with an accuracy of 1-pm (170-Mhz or 0.0054-cm^{-1})

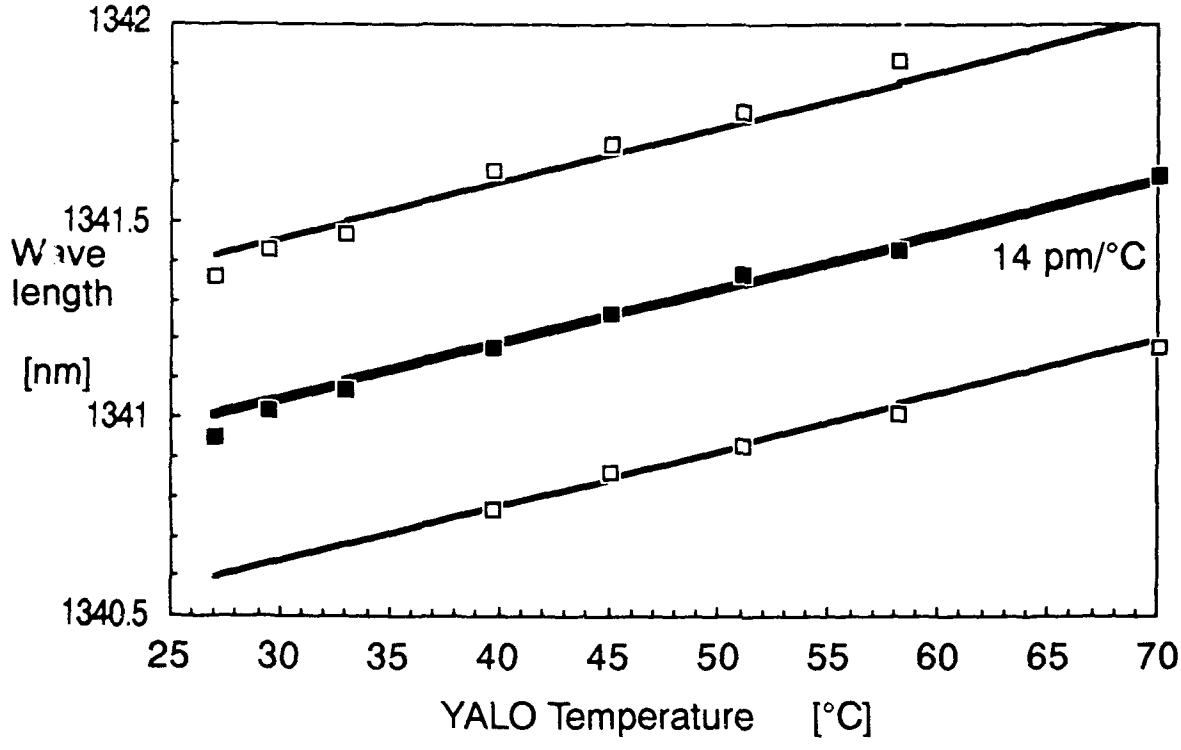

The laser can be tuned with high accuracy to any wavelength within its gain curve by offsetting its temperature a known amount from the temperature at which its wavelength matches the peak of the He line. The temperature tuning rate of the YALO laser is shown in Figure 2. The tuning function is a straight line with a slope of 14±.5-pm/°C over the entire tuning range . Using this slope, the laser can be set at any wavelength between 1341.0 and 1341.6-nm with an absolute accuracy of 0.015-nm

The YAlO rod, which was end pumped by a 40-stripe, 500-mW cw diode array (Spectra Diode SDL2450), was 1.19 mm long and 3 mm in diameter with its axis along the crystal *b* axis. Its input end, with a radius of curvature of 25 mm, was coated for maximum reflectivity at 1340 nm and antireflection coated at 807 nm. Its output end was flat with a reflectivity of 98%. The diameter of the almost cylindrical (in the crystal) TEM_{00} cavity mode was 68 μm. The YALO laser, with a threshold of 170 mW and a slope efficiency of .035, produced a maximum of 7 mW of TEM_{00} output power, 3-mW of which was in a single longitudinal mode..

The laser rod was centered in a 9-mm diameter 8-mm long electrically heated aluminum cylinder that was also drilled to accommodate a 10.0K Ω at 25.0°C precision interchangeable thermistor. The resistance of the thermistor was determined with an accuracy of ±1-Ω from the voltage generated by a 100μa current. At 37°C a ±1-Ω thermistor resistance uncertainty corresponded to a temperature change uncertainty of ±0.0042°C. At 70°C the uncertainty was ±0.017°C. This temperature accuracy is sufficient to maintain the wavelength accuracy mentioned above.

This diode-pumped monolithic crystal laser, temperature offset from an atomic line, can be an important secondary wavelength standard for frequency multiplexed and fm fiber optic and space communications . It can be used to calibrate wavemeters, monochromators, and Fourier-transform interferometers. Since its wavelength is determined only by the length of a crystal, it is compact and rugged, and is suitable for remote and space-based applications.

1. D. Scarl, B. Feldman, and R. Burnham, "Diode-Pumped 1.34nm Nd:$YAlO_3$ Laser," in *Technical Digest, Topical Meeting on Tunable Solid-State Lasers* (Optical Society of America, Washington, DC, 1987)
2. D. Scarl, R. Burnham, S. R. Bowman, and B. J. Feldman, "Diode-pumped 1.34-μm Nd^{3+}:$YAlO_3$ laser," Appl. Opt., to be published
3. L. Schearer and M. Leduc, IEEE Jl. Quantum Elect. **QE-22,** 756 (1986)
4. C. L. Bohler, L. D. Schearer, M. Leduc, P. J. Nacher, et al., J. Appl. Phys. **63,** 2497 (1988)

Tunable Single Frequency 1.3μ Nd:YALO Microlaser

L. S. Lingvay,* G. J. Dixon,* and N. Dieu
Department of Physics
University of South Florida
Tampa, FL 33620

We report the operation of a tunable single frequency Nd:YALO laser on the 1.34 μ transition. The laser consists of two elements, the Nd:YALO rod and an etalon output coupler. The etalon is coated with a metal film on the inside surface and a dielectric multi-layer on the outside surface. The etalon serves as a mode selector through the periodic modulation of its reflectivity.[1][2][3] By translating the etalon with respect to the laser rod, tunable single frequency output with varying power can be obtained over a limited range. By combining the translation with the heating of the etalon, one can obtain constant-power single frequency output over a much larger tuning range.

A schematic of the laser device is shown in Fig. 1. The Nd:YALO rod is 3 mm in length and is oriented along the b-axis. One end of the rod is curved with a radius of 30 cm, and is coated for maximum reflectance at 1.3 μ and high transmittance at 810 nm. The other end is flat and AR coated at 1.3 μ. The etalon is made from fused silica and has a thickness of 1 mm. It has a nichrome film on one side and a dielectric coating on the other. The latter transmitts 0.5% at 1.3 μ and more than 20% at 1.06 μ in order to suppress oscillation at that wavelength. The etalon is mounted on the PZT and is surrounded by a heating element for temperature control. The laser rod and the PZT are rigidly held inside a common housing. In operation, the gap between the laser rod and the etalon is typically on the order of 1 mm. With this arrangement the longitudinal mode spacing for the laser is approximately 20 GHz and the mode spacing for the etalon is 100 GHz. These numbers are to be compared with the linewidth of the 1.34 μ transition of approximately 500 GHz.

When pumped by a CW dye laser at 589 nm, the composite microlaser had a threshold of 70 mW. Single frequency output could be obtained for pump power as high as 400 mW. At that pumping level, the single frequency 1.34 μ output was in excess of 30 mW, yielding a power conversion efficiency of 8%. The maximum single frequency output was obtained by fine adjustments of the PZT voltage. Tuning of the single frequency output resulted directly from varying the PZT voltage. Fig. 2 shows superposed spectral scans of the laser output at these different PZT voltage settings as monitored by a spectrum analyzer with a free spectral range of 30 GHz. We see that the tuning range of the device as given by the half power points is approximately 6 GHz. Changing the PZT voltage beyond the half power points resulted in either mode hopping or multi-mode operation. We also successfully operated this laser with diode array pumping at 810 nm. In this case, the threshold power was 170 mW and maximum single frequency output was 14 mW for a pump power of 420 mW.

By heating the etalon in addition to PZT adjustment, the single frequency tuning range could be significantly increased. Fig. 3 shows typical results of this mode of operation. From the bottom the traces correspond to the etalon at 25.0, 27.1, 29.5, and 31.3°C respectively. As the etalon was heated, the PZT voltage was adjusted to continuously keep the output at maximum. We see that over a range of 15 GHz single frequency output at essentially constant power was obtained. Heating beyond the highest temperature caused mode hopping. The output power for these traces was approximately 10 mW with 400 mW dye laser pump. The reduced power is attributed to some noticeable degradation in the coatings of the elements due to handling. The single frequency tuning range of this type of device can probably be extended further with modifications such as the use of an appropriately chosen thinner etalon.

* Currently with AMOCO Laser Co., 1251 Frontenac Rd., Naperville, IL 60540

REFERENCES:

1. P. W. Smith, M. V. Schneider, and H. G. Danielmeyer, Bell Syst. Tech. J. 48, 1405 (1969).

2. W. Culshaw and J. Kannelaud, IEEE J. Quantum Electron. QE-7, 381 (1971).

3. J. Dixon, paper THG 5, CLEO '86, San Francisco, CA.

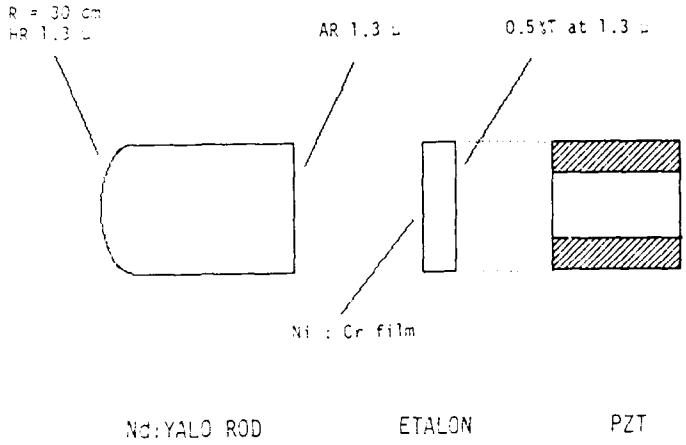

FIG. 1

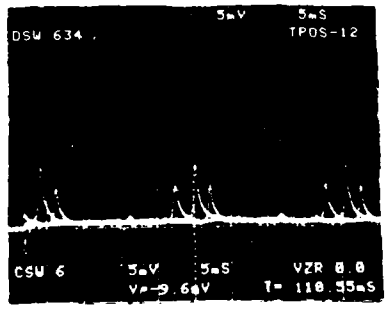

FIG. 2

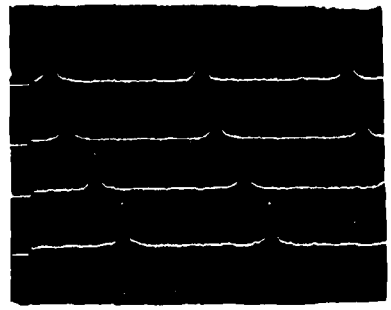

FIG. 3

Nd:BeL Laser at 1365 nm

J. Richards, K. Fueloep, R. Seymour, D. Cashmore, P. Picone, and M. Horsburgh

Surveillance Research Laboratory, PO Box 1650, Salisbury SA 5108, Australia

Summary

The fluorescence spectrum of neodymium in BeL (lanthanum beryllate) shows a reasonably strong line in the R-X manifold ($^4F_{3/2}$ - $^4I_{15/2}$) at 1365 nm, suggesting the possibility of lasing action at this wavelength. After frequency tripling the 455 nm blue light is near optimum for transmission through deep ocean water and is compatible with the cesium QLORD filter.

Detailed polarized fluorescent spectra were obtained from a small cube of Nd:BeL oriented along the principal axes of the refractive index ellipsoid and from these the stimulated emission cross-sections and their variation with optical polarization have been obtained for the various transitions of the Nd ion.

From these cross sections it is possible to determine crystal orientations for producing laser rods with maximum gain (for the R-X manifold) for the 1365 nm transition on an o-ray polarization. A laser cut along a crystallographic a* axis is a convenient choice.

To insure lasing at 1365 nm the laser cavity can be designed to discriminate against the other transitions using a combination of tailored mirror coatings (for the strong R-Y transitions) and walk off for e-rays (for the R- X transitions).

A significant water vapour absorption at 1365 nm introduces losses into laser if normal laboratory air is allowed to fill the optical path in the laser resonator. This can lead to unstable operation of the laser. In our laser experiments the optical path inside the resonator has been evacuated to overcome this problem. Using a highly efficient pump enclosure, output on the 1365 nm line has been obtained at an overall efficiency of 1% at significant energies (100 mj) from a simple oscillator. An overall efficiency of 5.5 % was obtained for the 1070 nm line with a similar arrangement.

Current experiments are examining Q-switching, amplification and frequency tripling.

GROWTH AND CHARACTERIZATION OF NI-DOPED GARNETS*

Horacio R. Verdún, L. M. Thomas, and Donna M. Andrauskas
Fibertek, Inc.
510-A Herndon Parkway, Herndon, VA 22070

1. Introduction

Several nickel-activated crystals have been lased in the past and have shown tunable output in the near infra-red (1.3-1.7 μm).[1] However, the performance of these lasers is rather poor, and exploratory work including the preparation and spectroscopic characterization of new systems containing this activator must continue since there is so far no adequate material for tunable solid state laser systems in the spectral re where oxide crystals doped with Ni^{2+} emit. Oxide garnets are general very good laser hosts, and most of them are, from the crystal-chemistry point of view, adequate candidates as crystalline hosts for Ni^{2+}. However, several of the best candidates such as $Y_3Al_5O_{12}$ (YAG), $Gd_3Ga_5O_{12}$ (GGG), and $Gd_3Sc_2Al_3O_{12}$ (GSAG), have octahedral sites occupied by trivalent ions, and when doping with Ni^{2+} a charge compensator is required to avoid creating undesirable color centers or for the purpose of achieving high doping levels. From ionic size and valence stability considerations, Zr^{4+} is the best choice for compensator. In our study of these systems we have concentrated in the development of growth conditions and the understanding of the spectroscopic characteristics of Ni,Zr:GGG and Ni,Zr:GSAG.

2. Experimental

Crystals of Ni,Zr:GGG and Ni,Zr:GSAG were grown by the laser-heated pedestal growth method.[2] The ceramic precursors used for the preparation of feed rods had up to 5at% nickel and zirconium. The actual composition of the crystals pulled from these feed rods is not accurately known since some evaporation was noted during the growth proces. The growth atmosphere varied from inert to oxidizing (100% O_2 at atmospheric pressure).

3. Results

Figure 1 shows the absorption and emission spectra of Ni,Zr:GGG and fig. 2 shows the absorption spectra for Ni,Zr,GSAG. The emission spectum of this system (not shown) is very similar to the emission spectrum of Ni,Zr:GGG. The fluorescence lifetime of Ni,Zr:GGG is 2 ms at 16 K and 0.8 ms at 300 K. The measurement of this lifetime for the other system is in progress. One interesting feature of both systems is the absorption peak at about 1.1 μm, which could allow pumping with a 1.064 μm Nd:YAG laser. Strong fluorescence excitation was observed in this band for Ni,Zr:GGG.

---

*Work supported by the U.S. Army Center for Night Vision and Electro-Optics, Fort Belvoir, VA.

The long tail of this band in Ni,Zr:GGG, which overlap and extensive portion of the emission band, may be an indication of significant inhomogeneous broadening in this host. This effect does not appear to be as significant in Ni,Zr:GSAG. Another feature that interferes with efficient emission is the absorption peak at about 2.2 μm. This absorption is due to Ni^{2+} in tetrahedral sites, a center that may not be possible to avoid in garnets with fairly large trivalent ions in the tetrahedral sites.

4. Conclusions

Nickel-zirconium-doped GGG and GSAG can be grown from the melt with high doping levels. The absorption spectrum of Ni,Zr:GGG shows evidence of significant inhomogeneous broadening. In contrast, this effect does not seem to be as strong in Ni,Zr:GSAG. The 1.1 μm excitation band is a very convenient feature for the development of efficient and compact laser systems using 1.064 um Nd:YAG lasers as a pump source. The presence of tetrahedral Ni^{2+} in the systems studied may represent a problem for achieving efficient laser operation.

5. References

1. P. F. Moulton, IEEE J. Quantum Electron. **QE-18**, 1185 (1982) and references therein.
2. R. S. Feigelson, in Tunable Solid State Lasers, Proceedings of the First International Conference, La Jolla, Calif., June 13-15, 1984, edited by P. Hammerling, A. B. Budgor and A. Pinto (Springer-Verlag, Berlin, Heidelberg, New York, 1985) p 129.

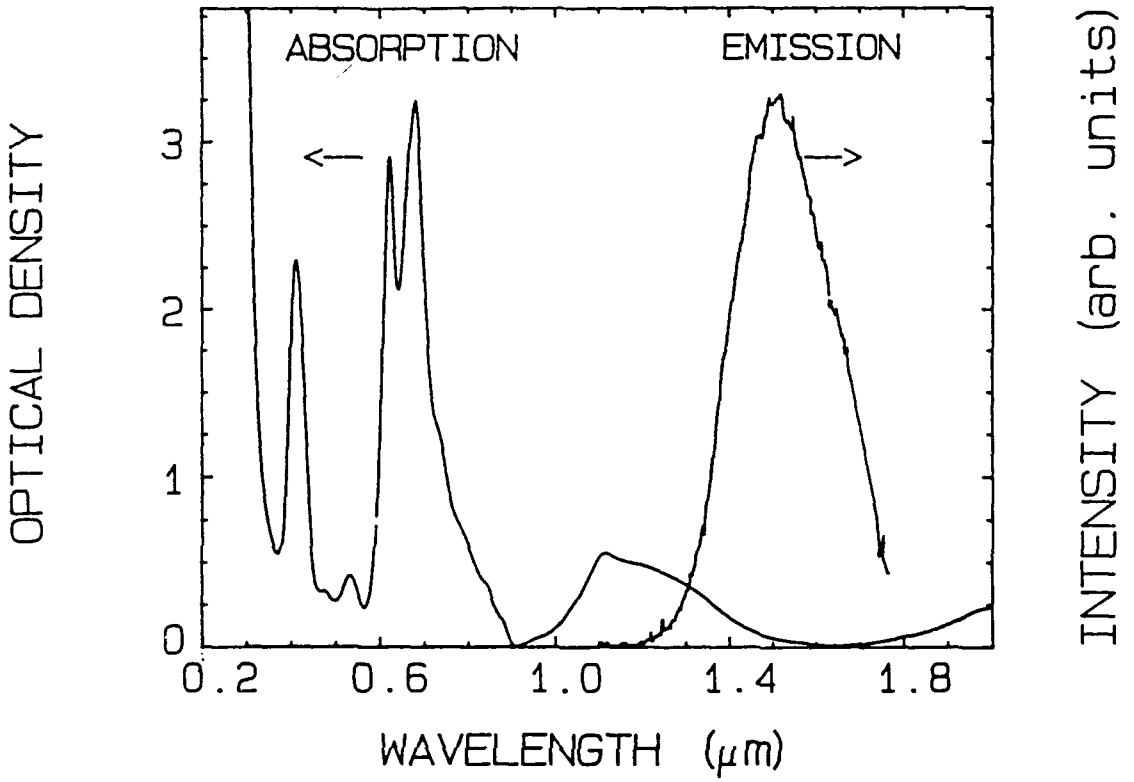

Figure 1. Room temperature absorption and emission spectra of a 5.07 mm thick Ni,Zr:$Gd_3Ga_5O_{12}$ crystal.

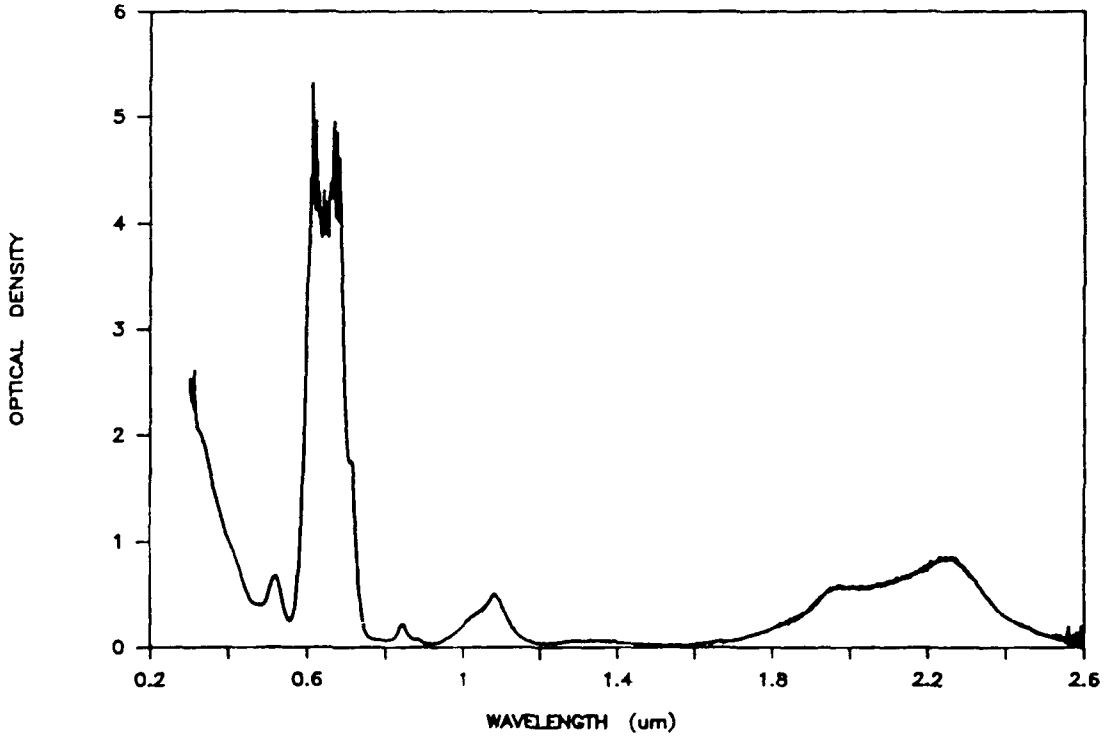

Figure 2. Room temperature absorption spectrum of a 7.24 mm thick Ni,Zr:$Gd_3Sc_2Al_3O_{12}$ crystal.

GROWTH AND CHARACTERIZATION OF Nd-DOPED ALUMINATES AND GALLATES WITH THE MELILITE STRUCTURE*

Horacio R. Verdún, Linda R. Black, German F. de la Fuente, and Donna M. Andrauskas
Fibertek, Inc.
510-A Herndon Parkway, Herndon, VA 22070

1. Introduction

Nd:YAG and Nd:YVO_4 are reportedly very efficient materials for diode-laser pumped lasers, with quantum efficiencies close to unity and with high absorption at the peak located at about 808 nm, a convenient wavelength for diode laser pumping. However, Nd-YAG suffers from having too narrow absorption bands in the diode emission region of the spectrum (full width at half maximum is about 1 nm for the Nd:YAG absorption peak at 808 nm) and Nd:YVO_4, having a fluorescence relaxation time of about 90 μs, is not a good material for pulsed mode operation because of its limited storage capability. Therefore, the search for new materials with broad absorption bands and high storage capability, and better than Nd-glass thermal performance is still required.

The availability of a high performance material with an absorption band at the diode laser output wavelength, and having a full width at high maximum of about 10 nm, will considerably relax the manufacturing tolerance requirements of diode laser arrays and make the diode array temperature control a system design parameter easier to manage. On the other hand, diode lasers are power limited devices; therefore for pulsed mode operation it is advantageous to have as long a fluorescence lifetime as possible. High gain is not necessarily an advantage when operating in this mode because of parasitic oscillations. However, low scattering losses are an important characteristic.

The above considerations may suggest that Nd-doped glasses would be the material of choice for pulsed mode operation of diode-laser pumped lasers, and indeed this family of materials shows good potential for this application. However, for high average powers the poor thermal performance of glasses will be a limitation. In view of this situation, it is of interest to appraise the laser performance potential of compounds that crystallize with disordered structures.[1,2] In these crystals the disordered occupation of regular lattice sites by cations with different electrical charges produces a random crystal field strength at the active ion site which translates into inhomogeneous broadening. Efficient energy transfer mechanisms interconnect all these sites and make them work cooperatively in the emission process. Crystals of the melilite family are typical examples of this crystal system.

The family of compounds ABC_3O_7, in which A = Ca, Sr, Ba; B = Y, La,..., Gd; and C = Al, Ga, form tetragonal crystals with the

*Work supported by the U.S. Army Center for Night Vision and Electro-Optics, Fort Belvoir, VA.

melilite structure [illegible] previous work on these compounds [illegible] polycrystalline samples obtained by sintering [illegible] mixtures of the components.[3] Single crystals [illegible] members of this family of [illegible] $SrLaGa_3O_7$ (SLGO), and $SrLaGa_3O_7$.[4] In terms of laser performance characterization, Nd:BIS is the melilite [illegible] most extensively

The results [illegible] growth and spectroscopic characterization of a number of Nd-doped melilites with emphasis on [illegible] for diode-laser pump lasers.

2. Experimental

Crystals [illegible] $Ca_{2-x}Nd_xGdGa_3O_8$, where x=0.01-0.06 [illegible] the laser-heated [illegible]

3. Results

Of the materials [illegible] crystals that did not produce a transparent single crystal was $Sr_2GdGa_3O_8$, which formed a tan, opaque monolith. The highest quality crystals grown were those of $SrGdGa_3O_7$ (SGGM). The absorption spectra of the materials prepared is shown in fig. 1a. Clearly, SGGM shows absorption features of the kind desirable for diode-laser pumped laser systems. The respective emission spectra for the spectral region around 1.05 μm are shown in fig. 1b . The fluorescence lifetime of the Nd:SGGM crystal used in this study was 180 μs.

4. Conclusions

As a result of this study a new host crystal, strontium-gadolinium-gallium melilite (SGGM), was discovered. Neodymium-doped SGGM shows spectral features highly desirable for diode-laser pumping. A high absorption feature in the region about 810 nm, with a maximum of 14 cm^{-1} and a full width at half maximum of 10 nm, together with a fairly high fluorescence lifetime of 180 μs, makes further study of this material for laser applications worth pursuing, and work is currently in progress at Fibertek to demonstrate laser operation.

5. References

1. A. A. Kaminskii, Laser Crystals (Springer, Berlin, Heidelberg, New York, 1981).
2. A. A. Kaminskii, phys. stat. sol. (a) **87**, 11 (1985).
3. A. A. Ismatov, Russian Journal of Inorganic Chemistry **15**, 1758 (1970).
4. A. A. Kaminskii, E. L. Belokoneva, M. V. Mill, S. E. Sarkisov, and K. Kurbanov, phys. stat. sol. (a) **97**, 279 (1986).
5. W. Piekarczyk, M. [illegible] and S. Zmija, J. Crystal Growth **71**, 295 (1985).
6. W. Ryba-Romanowski, M. [illegible] W. Piekarczyk, M. Berkowski, S. Mazura [illegible] J. Lumines. **36**, [illegible]

7. M. Kimura and Y. Tsuruta, Japan Kokai JP 52/139700, 21 Nov. 1977.
8. W. Ruba-Romanowski, B. Jeżowska-Trzebiatowska, W. Piekarczyk, and M. Berkowski, J. Phys. Chem. Solids **49**, 199 (1988).
9. R. S. Feigelson, in Tunable Solid State Lasers, Proceedings of the First International Conference, La Jolla, Calif., June 13-15, 1984, edited by P. Hammerling, A. B. Budgor, and A. Pinto (Springer-Verlag, Berlin, Heidelberg, New York, 1985) p 129.

Figure 1a: Nd–DOPED MELILITES

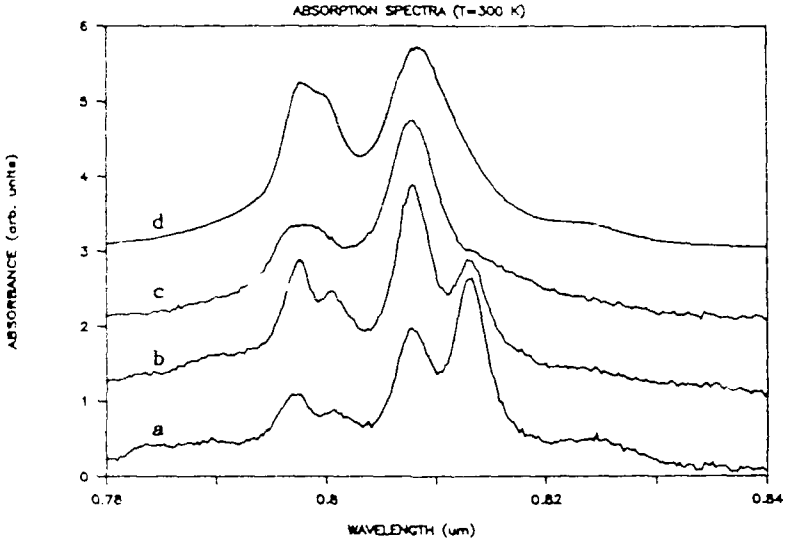

Figure 1b: Nd–DOPED MELILITES

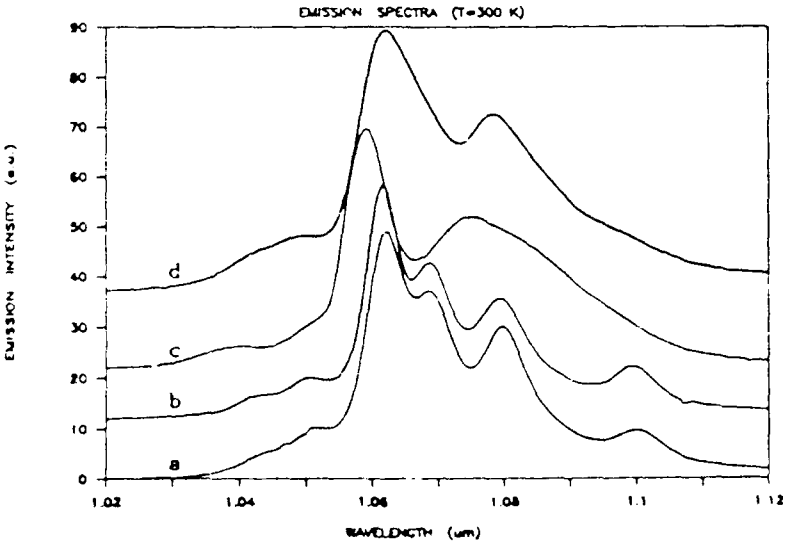

Figure 1 References: **a**: Nd:CYAM ($Nd:CaYAl_3O_7$); **b**: Nd:CGAM ($Nd:CaGdAl_3O_7$); **c**: Nd:BLGM ($Nd:BaLaGa_3O_7$); **d**: Nd:SCGM ($Nd:SrGdGa_3O_7$).

WEDNESDAY, MAY 3, 1989

NAUSET IV

10:30 AM–11:45 AM

WC1–WC4

INFRARED LASERS AND ENERGY TRANSFER

Larry G. DeShazer, Solidlite Corporation, *Presider*

NEW MATERIALS FOR INFRARED LASERS

A. A. Kaminski
A. V. Shubnikov Institute of Crystallography
Moscow, U.S.S.R.

Nonradiative Multiphonon Relaxation and Energy Transfer from the Strongly Quenched High -Lying Levels of Nd^{3+}- Ions in Laser Crystals.

dr.ph. T.T.Basiev,dr.A.Yu.Dergachev,dr.Yu.V.Orlovskii

General Physics Institute of the USSR Academy of Sciences

Moscow 117942, 38 Vavilov St., USSR, Tel.135-02-67

dr.S.Georgescu, dr.A.Lupei

Central Institute of Physics, Bucharest, Romania

The kinetics of luminescence decay from the high -lying strongly quenched levels of Nd^{3+} ions in LaF_3,SrF_2,CaF_2 and $YLiF_4$ laser crystals versus energy gap (ΔE), temperature (T) [1] (table 1) and concentration [2] were measured by direct nanosecond laser excitation and recording of the luminescence by a statistical single photon counting technique with a time resolution of up to 0.3ns. The dipole-dipole resonanse energy transfer mechanism (Nd-Nd) with no energy migration among Nd-ions was determined for $^4G_{7/2}$-level in LaF_3 crystal and extraordinarily high interaction microefficiency $C_{DA}(77K)=3.3\times10^{-37}cm^6/s$ has been obtained. It was found, that the resonance theory of Forster, which is based on the proportionality of the activator absorption spectrum (the transition $^4I_{9/2}\longrightarrow{}^4G_{5/2}+{}^2G_{7/2}$) and a sensitiser luminescence spectrum ($^4G_{7/2}\longrightarrow{}^4I_{11/2}$) gives a good qualitative agreement,but strong quantitave disagreement (more than 10^3) with the experimental results. The additional luminescence spectra measurements of the $^4G_{7/2}\longrightarrow{}^4I_{11/2}$ and $^4G_{5/2}+{}^2G_{7/2}\longrightarrow{}^4I_{9/2}$ transitions with the excitation of the $^4G_{7/2}$-level have confirmed the energy transfer from $^4G_{7/2}$ to $^4G_{5/2}+{}^2G_{7/2}$ multiplet.

The energy transfer microparameters C_{DA} were calculated from the Forster like kinetics of luminescence decay for each $^4F_{3/2}$,$^2P_{3/2}$, $^4D_{3/2}$,$^4G_{7/2}$,$^4G_{5/2}+{}^2G_{7/2}$-multiplets in LaF_3 crystal at 77K and 300K. The correlation between the probability of the multiphonon intracenter relaxation and radiationless energy transfer was found for above mentioned levels in LaF_3 (fig.1). This fact and the strong quantitave disagreement with Forster resonance theory of the $^4G_{7/2}$-level C_{DA} microparameter suggests multiphonon nonresonanse energy transfer mechanism for Nd^{3+} levels in LaF_3

crystal.

The similar measurements were made for SrF_2 crystal. The nonexponential decay curve was found even for 0.1% of Nd^{3+}-ion concentration for $^4D_{3/2}$, $^4G_{7/2}$, $^4G_{5/2}+^2G_{7/2}$ levels (the values of τ at the beginning and at the "tail" of the decay curve in table 1) having an increasing decay rate and nonexponentiality with increasing concentration for $^4G_{7/2}$ and $^4G_{5/2}+^2G_{7/2}$ multiplets.

[1] T.T.Basiev, A.Yu.Dergachev, E.O.Kirpichenkova Yu.V.Orlovskii, V.V.Osiko, Sov.J.Quantum Elecctron., 17(10), p.1289-1291 (1987)

[2] T.T.Basiev, A.Yu.Dergachev, Yu.V.Orlovskii, 3-d International Conference "Trends in Quantum Electron.", Bucharest-Romania, 29aug.-3sep., p.100-101 (abstracts), 1988

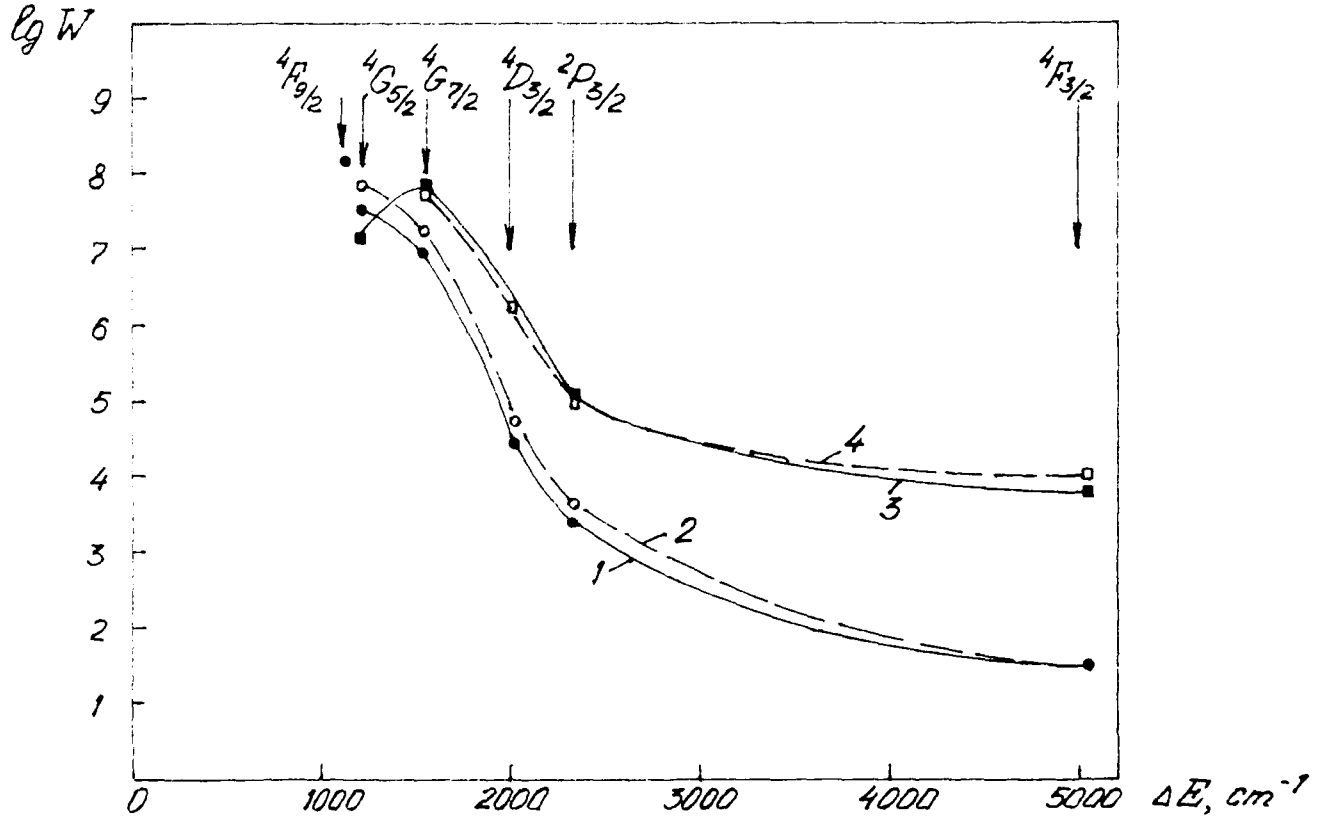

FIGURE 1

The probability of the intracenter multiphonon nonradiative relaxation: 1-77K, 2-300K, and the probability of the intercenter radiationless energy transfer ($W_{DA}=C_{DA}/R^6_{min}$): 3-77K, 4-300K, of the excited levels of Nd^{3+}-ion in LaF_3 crystal.

TABLE 1

The lifetime τ versus temperature (T) ,energy gap (ΔE) and limiting phonon energy ($\hbar\omega_{max}$) of the high -lying levels of Nd^{3+}-ion in laser crystals.

CRYSTAL	LaF_3	SrF_2	CaF_2	$YLiF_4$
$^2P_{3/2}$ 77 300K $\Delta E_{min}[cm^{-1}]$	405μks 225μks 2324			
$^4D_{3/2}$ 77 300K $\Delta E_{min}[cm^{-1}]$	35μks 13.5μks 2014	~32μks 5.8-8.1μks		
$^4G_{7/2}$ 77 300K $\Delta E_{min}[cm^{-1}]$	110.5ns 56.0ns 1546	27-69ns 1530	18-93ns 1450	14ns 1417
$^4G_{5/2}+^2G_{7/2}$ 77 300 $\Delta E_{min}[cm^{-1}]$	29.2 14.7ns 1201	12.5-26.6 8.7-16.8 1136		
$^4F_{9/2}$ 77K $\hbar\omega_{max}[cm^{-1}]$	6.5ns(ΔE_{min}=1121cm^{-1}) 400	450	525	570

Enhanced Energy Transfer Processes in Codoped Solid-State Laser Materials

F. X. Hartmann
Insitute for Defense Analyses
Science and Technology Division
1801 N. Beauregard St.
Alexandria, VA. 22311

and

S. R. Rotman
Ben-Gurion University of the Negev
Dept. of Electrical and Computer Engineering
P.O. Box 653
Beer-Sheva, ISRAEL

Codoped crystals have been the source of several of the most popular solid-state lasers, e.g. Nd, Cr:GSGG and Cr, Tm, Ho:YAG. The efficiency of transfer between the donors (which absorb the pump radiation) and the acceptors (which emit the laser radiation) is a crucial parameter in determining the feasibility of any particular laser candidate.

There is recent experimental data on europium and manganese doped alkali-halide crystals[1,2] which indicates that pairing can occur between donors and acceptors. The goal of our work is to modify the Foerster-Dexter-Inokuti[3] energy transfer model which explicitly assumes a random distribution of donors and acceptors in the crystal, exmamine whether present day laser materials may be exhibiting such an effect, and ultimately develop new, efficient solid-state lasers based on this principle.

The theoretical outlines for such an energy transfer model are as follows.[4] The standard model assumed that the radial probability of any acceptor being a distance r from a donor is constant, i.e. 1/V; the total probability is hence in spherical coordinates $\frac{4\pi r^2}{V}$. We replace such a radial probability distribution with a distribution as shown in Figure 1. Enhanced correlated placement is given by $A > 1$ while inhibited correlated placement is given by $A < 1$. The energy transfer rate can then be calculated; the solution in such a case assuming dipole-dipole interaction is given by

$$N_D(t) = N_D(0)\ \exp(-t/\tau_o \cdot A\sqrt{\pi}\, c/c_o\, (t/\tau_o)^{1/2} \qquad (1)$$

$$- (B - A)\,\Phi(z_1)/\exp(z_1) - (1 - B)\,\Phi(z_2/\exp(z_2))$$

where c is the acceptor doping concentration, Γ is the gamma function, c_o is the critical concentration of acceptors, and τ is the decay rate of the donor. The critical concentration c_o is that concentration for which the energy transfer rate and the natural donor decay rate are

equal for the average donor-acceptor distance r_0 (the critical distance); Φ (1, 1 - 3/s, z) is the degenerate hypergeometric function (written as $\Phi(z)$ for dipole-dipole interaction). z_i is defined as

$$z_i = \left(\frac{r_0}{r_i}\right)^6 \left(\frac{t}{\tau_0}\right) \qquad (2)$$

Figs. 2 and 3 give sample excited-state concentrations for the donors and acceptors, respectively, under enhanced, random, and inhibited distributions. A similar analysis has been performed for the multipole and exchange mechanisms. The mathematical results have been obtained and will be presented at the conference.

Several solid-state laser materials seem to exhibit such correlation. A small discrepancy in the Nd^{+3} emission is Nd,Cr:GSGG, first noted by E. V. Zharikov et al.[5], may be due to Nd-Cr enhanced correlation in GSGG. Both Nd,Ce:YAG and Nd:YAG (where Nd^{+3} is both the donor and the acceptor) gave data indicating excluded correlation.[7,8]. In these last two materials, the excluded correlation appears to be due to a "detrimental" mismatch between the donor/acceptor and its crystal site (e.g. both Nd^{+3} and Ce^{+3} are bigger than the ion for which they substitute); a "fortunate" mismatch in GSGG causes enhanced correlation (e.g. Nd^{+3} is bigger than Gd^{+3} and Cr^{+3} is smaller than Sc^{+3} in GSGG - thus the crystal strain is relaxed if pairing occurs).

In conclusion, a model is presented for Foerster-Dexter energy transfer in correlated solid-state materials. Initial analysis of present day lasers indicates that such correlation does occur, and could potentially lead to new solid-state lasers.

References

1. J. Rubio O. et al., Phys. Rev. B 31 (1), 59 (1985).
2. R. Capeletti et al., Phys. Rev. B 36 (10), 5124 (1987).
3. M. Inokuti and F. Hirayama, J. Chem. Phys. 43 (6), 1978 (1965).
4. S. R. Rotman and F. X. Hartmann, accepted for publication in Chem. Phys. Letts.
5. E. V. Zharikov et al., Kvant. Elek 11, 1565 (1984).
6. S. R. Rotman and F. X. Hartmann, Advances in Laser Science II, edited by M. Lapp et al., AIP Conf. Proc. 160 (1987) pp. 114-117.
7. S. R. Rotman, submitted to Appl. Phys. A.
8. S. R. Rotman, submitted to Appl. Phys. Letts.

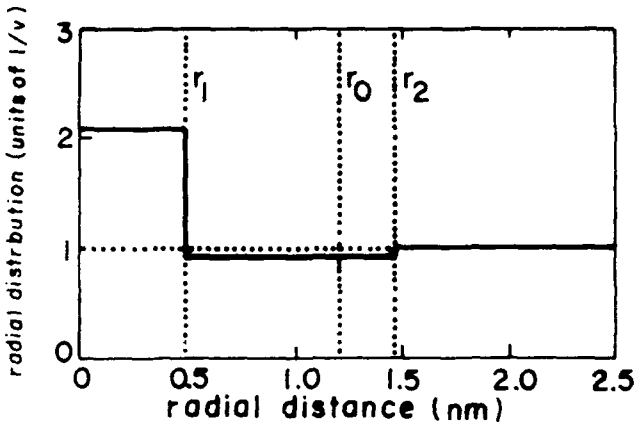

Fig. 1. Sample probability distribution for acceptor placement

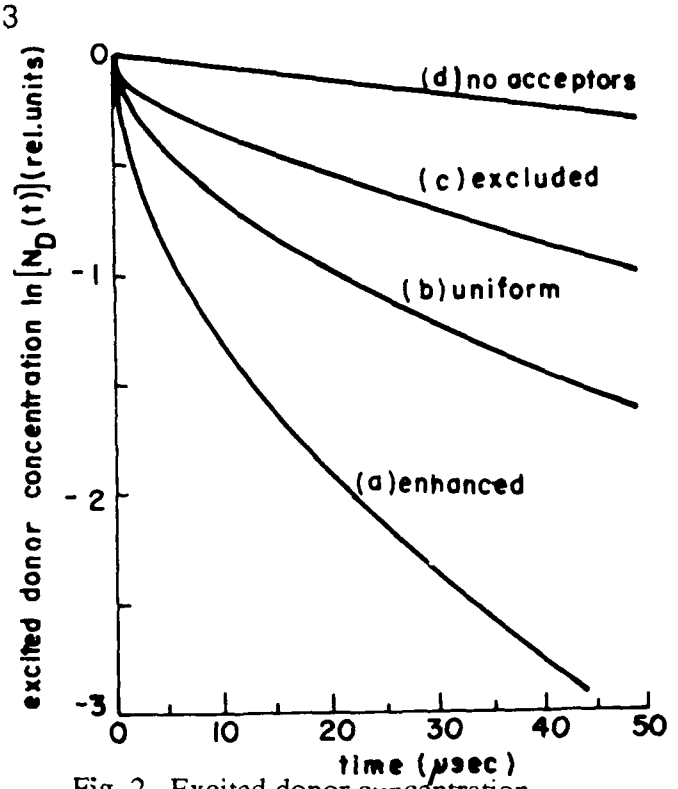

Fig. 2. Excited donor concentration for different acceptor distributions

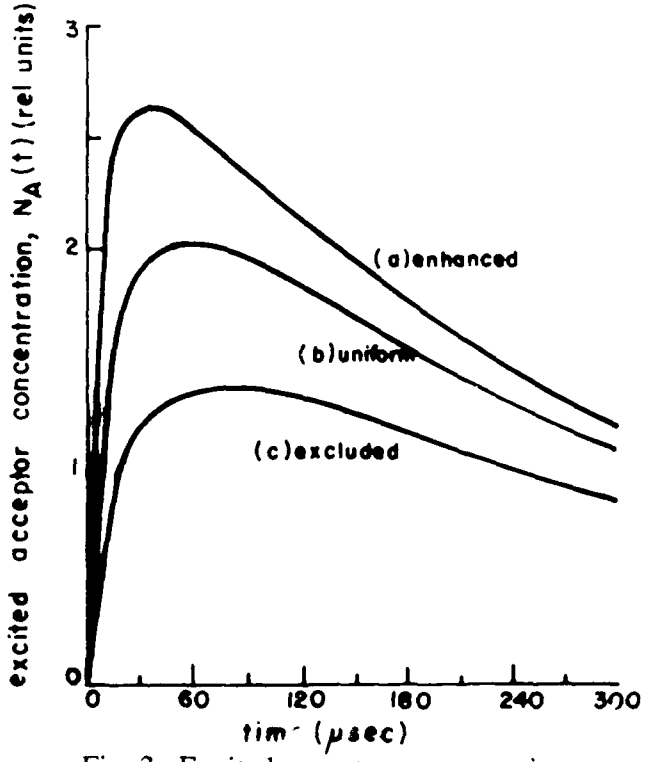

Fig. 3. Excited acceptor concentrations for different acceptor distributions

$Gd^{3+} \rightarrow Cr^{3+}$ energy transfer and Cr^{3+} decay dynamics in Cr^{3+} doped GSGG, GSAG and GGG.

D.S. Hamilton and Li-Ji Lyu
Department of Physics and Institute of Materials Science
University of Connecticut, Storrs, CT 06269
and
G.J. Pogatshnik
Department of Physics
Southern Illinois University, Edwardsville, IL 62026

There continues to be active interest in rare-earth and transition-metal doped GSGG [$Gd_3Sc_2(GaO_4)$] for high power and tunable laser applications.[1] In this paper we report on the observation of a rapid $Gd^{3+} \rightarrow Cr^{3+}$ energy transfer in Cr:GSGG and in the two related gadolinium garnets Cr:GSAG and Cr:GGG. The large energy of the Gd^{3+} exciton ($\approx$30,000 cm^{-1}) has implications for photoionization and color center formation in these materials. We have also observed nonexponential and wavelength dependent decay dynamics for the Cr^{3+} ion in GSAG and GGG. These results are interpreted in terms of an inhomogeneous site distribution for the Cr^{3+} ions.

The absorption spectra of Cr:GSGG is dominated by the broad $^4A_{2g} \rightarrow {}^4T_{2g}$ and $^4A_{2g} \rightarrow {}^4T_{1g}(a)$ transitions of the Cr^{3+} ion. In the gadolinium garnets there are also narrow absorption bands near 300 nm and 280 nm which result from transitions from the $^8S_{7/2}$ ground state of the Gd^{3+} ion to the ^6P and ^6I excited states. We have measured the excitation spectrum of these Cr^{3+} doped garnets by monitoring the Cr^{3+} $^4T_{2g} \rightarrow {}^4A_{2g}$ emission intensity as the wavelength of the exciting light was varied in the region of the Gd^{3+} absorption bands. The room temperature excitation spectrum of Cr:GSGG is displayed in Fig.1. The three peaks at 313 nm, 307 nm and 302 nm correspond to the $^8S_{7/2} \rightarrow {}^6P_{7/2}$, $^8S_{7/2} \rightarrow {}^6P_{5/2}$, and $^8S_{7/2} \rightarrow {}^6P_{3/2}$ transitions of the Gd^{3+} ion. The correlation between these peaks in the excitation spectra with those in the absorption spectra due to Gd^{3+} indicates significant $Gd^{3+} \rightarrow Cr^{3+}$ energy transfer.

We have also measured the time resolved decay dynamics of the Cr^{3+} ion following excitation into either the Cr^{3+} or Gd^{3+} absorption bands. A tunable dye laser with an optional frequency doubler was used as the excitation source. The dye laser had an 8 nsec duration pulse. Typical chromium fluorescence decay curves following $^4T_{2g}$

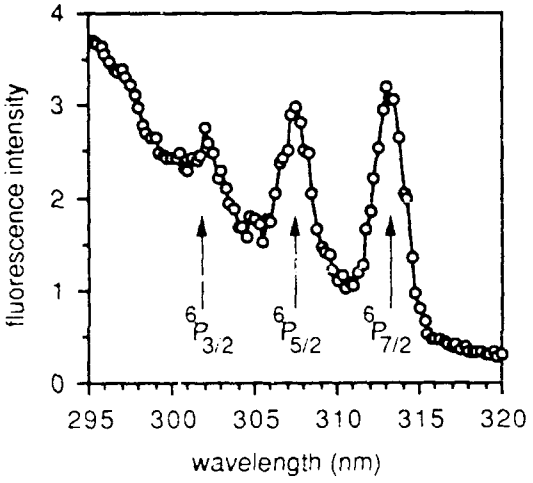

Fig.1. Cr:GSGG excitation spectrum at 300 K in the region of the Gd^{3+} absorption bands. The arrows indicate the upper Gd^{3+} level

pumping with the dye laser is shown in Fig.2(a). The decay for Cr:GSGG is exponential over two decades and the lifetime at 77 K was determined to be 187±2 μs. An identical decay lifetime is obtained for pumping the $^4T_{1g}$(a) or $^4T_{1g}$(b) Cr^{3+} absorptions. At a sample temperature of 300 K, the lifetime decreases to a value of 114±2 μs. This decrease in the lifetime at 300 K is interpreted[2] as an increase in the phonon assisted mixing of the ^2E_g and $^4T_{2g}$ states. The decay

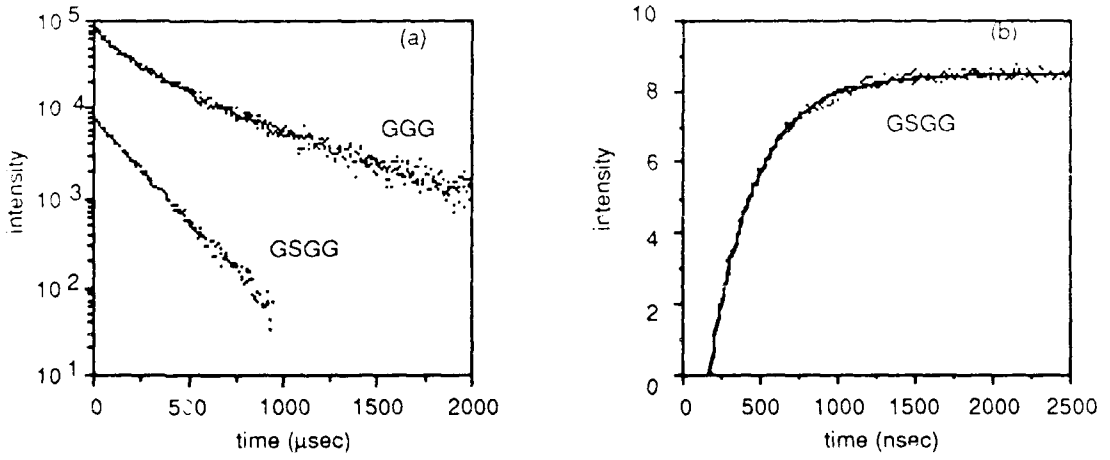

Fig.2. (a) Fluorescence decay curves for Cr:GSGG and Cr:GGG at 77K. (b) Initial rise of the Cr:GSGG emission at 300 K following pumping of the lowest Gd^{3+} absorption.

curve for Cr:GGG also shown in Fig.2(a) has a nonexponential time dependence. Moreover, the detailed shape of the decay curve changes with both excitation and emission wavelength. Thus the nonexponential nature of the decay is thought to arise from a superposition of Cr^{3+} ions with different local crystal fields. The decay dynamics for

Cr:GSAG are much less nonexponential than those of Cr:GGG, especially at room temperature. The Cr^{3+} lifetimes are summarized in table 1.

The short time dynamics of the Cr^{3+} emission at 300 K for 312 nm excitation into the lowest Gd^{3+} absorption band is displayed in Fig.2(b). The rise time is a measure of the $Gd^{3+}\rightarrow Cr^{3+}$ energy transfer rate. Assuming a single transfer time of T_t, the initial growth has been fit to the expression $I_\infty[1-\exp(-t/T_t)]$. The resulting values of T_t are shown in table 1. There is a significant host dependant variation in the transfer times and the temperature variation reflects the phonon mediated nature of the transfer process.

The observation of a photoconductivity signal following excitation of the Gd ions[2,3] and our measurement of $Gd^{3+}\rightarrow Cr^{3+}$ energy transfer suggests that the photoionization is not taking place on the Gd ion, but rather at other sites in the crystal. The Gd^{3+} exciton has sufficient energy to ionize many electron trapping sites (although presumably not Cr^{3+}) following an energy transfer process. Such multistep photoionization might be significant in describing color center formation and solarization processes in these garnet laser hosts.

TABLE I. Summary of the mean Cr^{3+} fluorescence decay times (T_d) and the $Gd^{3+}\rightarrow Cr^{3+}$ transfer times (T_t). A * indicates that the process is not characterized by a single parameter.

	T_d(300K)	T_d(77)	T_t(300K)	T_t(77K)
Cr:GSGG	114 μs	187 μs	200 ns	522 ns
Cr:GSAG	155 μs	260 μs*	150 ns	230 ns
Cr:GGG	185 μs*	1200 μs*	50 ns*	140 ns*

1. W.F. Krupke, M.D. Shinn, J.E. Marion, J.A. Caird, and S.E. Stokowski, J. Opt. Soc. Am A**3**, 102 (1986).
2. L.J. Andrews in "Tunable Solid State Lasers II", eds. A.B. Budgor, L. Esterowitz and L.G. DeShazer, Springer Verlag, Vol. 52, 44 (1986).
3. R. Moncorge, private communication.

ACKNOWLEDGEMENTS

We would like to thank Len Andrews and Steve Payne for providing us with the samples and Uwe Sliwczuck for help with the excitation spectra. This research was performed under the auspices of the Division of Material Sciences of the Office of Basic Energy Sciences, United States Department of Energy, under grant DE-FG02-84ER45056.

NOTES

WEDNESDAY, MAY 3, 1989

NAUSET IV

1:30 PM–3:00 PM

WD1–WD5

2 MICRON LASERS

Frank Allario, NASA Langley Research Center,
Presider

CROSS RELAXATION SOLID STATE LASERS

B.M. Antipenko
S.I. Vavilov State Optical Institute
199034 Goi Leningrad, USSR

Physical aspects of the new efficient 2 micron laser materials with cross relaxation pumping diagrams of laser transitions are reviewed.

Spectroscopic and laser properties of Tm-doped YAG at 2 microns

T. Becker, R. Clausen, G. Huber
Institut für Angewandte Physik, Universität Hamburg
Jungiusstr. 11, D-2000 Hamburg 36, F.R.G.

E. W. Duczynski, P. Mitzscherlich
Lasertec Hamburg GmbH
Stresemannstr. 364-368, D-2000 Hamburg 50, F.R.G.

Room-temperature cw operation of the $^3H_4$-$^3H_6$ transition of Tm^{3+} was observed for the first time in Cr,Tm:YSGG under cross pumping via Cr^{3+} [1]. Diode laser pumped Tm:YAG has shown high efficiency at 2.02 µm wavelength [2]. We have grown Cr,Tm:YAG and Tm:YAG with Tm-concentrations ranging from $7 \cdot 10^{18}$ cm^{-3} to $3 \cdot 10^{21}$ cm^{-3} in order to investigate the concentration dependence of laser performance, Cr-Tm transfer efficiency, and Tm-Tm cross relaxation efficiency. The cross relaxation $Tm^{3+}(^3F_4 \rightarrow {}^3H_4)$, $Tm^{3+}(^3H_6 \rightarrow {}^3H_4)$ is very important for this laser, because the thermal power dissipation can be drastically decreased by this process.

Table 1 summarizes the Cr-decay times (1/e-decay) and Cr-Tm transfer efficiencies at fixed Cr-concentration of $2 \cdot 10^{20}$ cm^{-3} and different Tm-concentrations. The transfer efficiencies have been obtained from the Cr-decay curves under the very reasonable assumption that the shortening of the Cr-decay is exclusively caused by the presence of the Tm-traps.

Table 1: Cr-Tm transfer in YAG. Cr concentration is $2 \cdot 10^{20}$ cm^{-3}

n_{Tm} [10^{20} cm^{-3}]	0	0.7	4	10	20	30
Cr-decay time [µs]	1890	900	120	5	≈3	≈2
Transfer efficiency	0%	40%	87%	98%	99%	≥99%

The nonexponential Cr decay could be fitted with a static dipole-dipole Cr-Tm interaction and a corresponding micropara-

meter $c_{DA}=1.5\cdot10^{-39}$ cm^6/s for the case $n_{Tm}=7\cdot10^{19}$ cm^{-3}. However, the fit has shown slightly smaller transfer rates in the first 30 µs of the decay. At higher Tm-concentrations $n_{Tm}\geq4\cdot10^{20}$ cm^{-3} the dipole-dipole fit became much worse. The reason for this is not clear yet.

The $Tm^{3+}(^3F_4\rightarrow{}^3H_4)$, $Tm^{3+}(^3H_6\rightarrow{}^3H_4)$ cross relaxation process can be measured directly via the $^3F_4$-$^3H_6$ fluorescence decay at 820 nm after resonant pulsed excitation of the $^3F_4$ level at 780 nm. The results are summarized in table 2.

Table 2: Tm-Tm cross relaxation at different Tm concentrations.

n_{Tm} [10^{20} cm^{-3}]	0.07	0.7	4	10	20	30
1/e-$^3F_4$-decay time [µs]	535	250	10	≈3	≈1	≤1
cross relaxation efficiency	0	38%	96%	≈99%	≈99%	≥99%

Tables 1 and 2 show that Tm-concentrations above $4\cdot10^{20}$ cm^{-3} yield an efficient Cr->Tm energy transfer and Tm-Tm cross relaxation.

The highest slope efficiencies for cross pumping via Cr with a krypton laser (λ_p = 647 nm) have been obtained with a crystal containing $1\cdot10^{21}$ cm^{-3} Tm and $2\cdot10^{20}$ cm^{-3} Cr. The power slope efficiency was 36 % when operated in a nearly concentric cavity (see Figure 1). The effective emission cross section at 2.02 µm is $1.6\cdot10^{-21}$ cm^2.

Figure 1 also shows the result for Tm-YAG under cw laser pumping at 780 nm with a Ti:Al_2O_3 laser, which simulates a diode laser pump. We observed a slope efficiency of 53 % which is similar to the value observed in refence [2].

Due to the cross relaxation the ideal pump quantum efficiency ε would be 2. With high reflecting mirrors we estimate in Cr,Tm:YAG the value $\varepsilon \approx 1.7$. However, this value

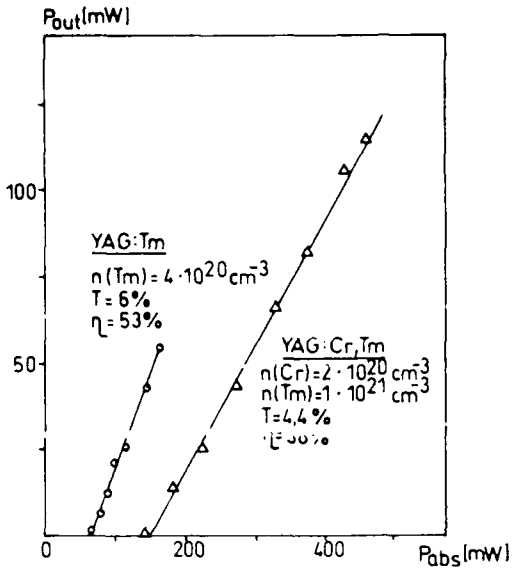

Fig. 1: Tm:YAG and Cr,Tm:YAG lasers at 2.02 µm pumped at 780 nm and 647 nm, respectively

decreases with increasing mirror transmittance down to $\varepsilon \approx 0.7$ for T = 10.5 %. Crystals grown without Cr show a similar, but less pronounced behaviour. The pump efficiency decreases only from $\varepsilon \approx 1.8$ (T = 0.4 %) to $\varepsilon \approx 1.3$ (T = 10.5 %). The strong decrease of ε in the Cr-doped crystals is probably due to a loss center for the 2 µm radiation, associated with Cr and the inversion density of Tm.

Tm:YAG is a very interesting laser material for generating 2 µm radiation. In comparison to the Tm,Ho:YAG laser the effective emission cross section for Tm σ_e(T... = $1.6 \cdot 10^{-21}$ cm^2 is lower than for Ho σ_e(Ho) = $8.1 \cdot 10^{-21}$. However, this can be compensated with higher concentrations of Tm^{3+}, because the effective absorption cross section at the laser wavelength is approximately 20 times lower for Tm^{3+} when compared to Ho^{3+}.

References

[1] E. W. Duczynski, G. Huber, P. Mitzscherlich, in Tunable Solid-State Lasers II, A. B. Budgor, L. Esterowitz, and L. G. DeShazer, eds. (Springer Verlag, Berlin, 1986), p. 282

[2] G. J. Kintz, R. Allen, L. Esterowitz, Conf. Lasers Electro-Opt., Opt. Soc. Amer., Anaheim, 1988, paper FB2

High Efficiency 2.09 μm Laser

Gregory J. Quarles, Charles L. Marquardt, Leon Esterowitz
Naval Research Laboratory
Code 6551
Washington, DC 20375-5000

and

Annette Rosenbaum
Sachs/Freeman Associates
Landover, MD 20785

We report our most recent progress in the development of a highly efficient flashlamp-pumped 2 μm laser operating at room temperature. Our current studies have concentrated on the 2.09 μm transition of Ho^{3+} in YAG, with sensitization by Cr^{3+} and Tm^{3+} codopants. In previous work on this sensitizer/activator combination[1,2] investigators have reported very efficient laser operation, without optimization of the host material or ion concentrations. Using the insights obtained through our recent measurements of Cr→Tm transfer efficiency in garnet crystals[3], we have achieved significant enhancement of slope efficiency and reduction of laser threshold by optimization of dopant concentrations and other system parameters.

The pumping scheme for a flashlamp-pumped Cr;Tm;Ho: YAG laser is illustrated in Fig. 1. Flashlamp light is efficiently absorbed by the broad bands of the Cr. After a nonradiative decay to the ^2E state, the excitation is transferred from the Cr to the Tm ion. One Tm ion in the $^3H_4$ state produces two Tm ions in the $^3F_4$ through an internal cross-relaxation process. Finally, the Tm ions transfer energy to two Ho ions in the $^5I_7$ upper laser level.

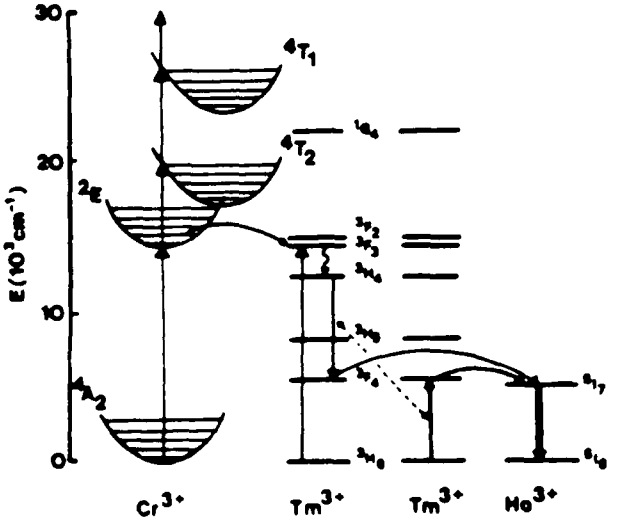

Figure 1 Pumping scheme for Cr;Tm;Ho:YAG laser.

In a study of aluminum and scandium garnets, we have shown the Cr→Tm transfer efficiencies are significantly higher in YAG than in YSAG or YSGG.[3] The transfer occurs via a dipole-dipole interaction and is enhanced by a resonance between the Cr and Tm energy levels. This resonance is demonstrated by the overlap of the ^2E emission of Cr and the $^3F_3$ absorption of Tm in YAG, as illustrated in Fig. 2. No analogous resonance was observed in the other garnets. Based on these observations YAG was selected as the preferred host material for the Cr;Tm;Ho laser.

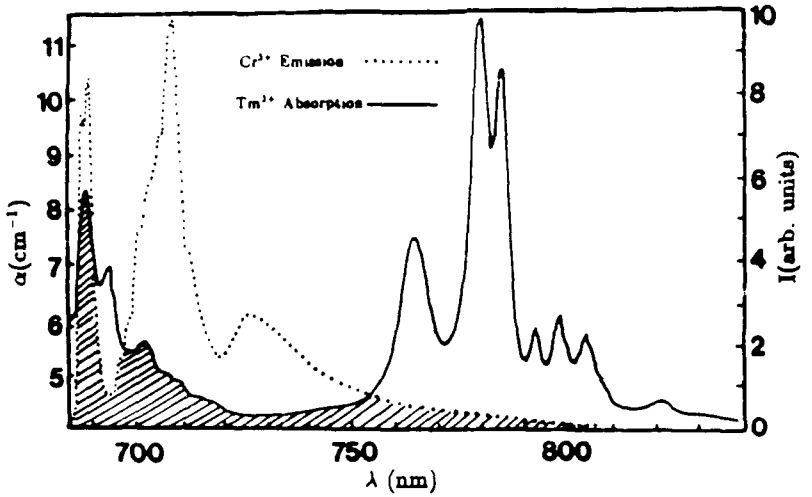

Figure 2. Spectral overlap of Cr^{3+} emission and Tm^{3+} absorption in YAG

Energy transfer measurements coupled with the laser efficiency measurements were used to optimize the Cr concentration for our free-running configuration. Energy transfer experiments on samples with 5.76% Tm and 0.36% Ho indicated that Cr→Tm transfer efficiency varied with Cr concentration from 94%,at 0.5% Cr, to 98% at 2.5% Cr.[3] In laser measurements on a similar group of samples the highest overall efficiency was obtained with 0.8% Cr. At Cr concentrations of 2.5% and greater we observed a clamping of laser output at high pump energies. This suggests that the decrease of efficiency at higher concentration is caused by thermal effects. Optimization of the Cr concentration is achieved by balancing these thermally induced losses against the gains produced by increasing the transfer efficiency.

The laser efficiency measurements were performed using a compact pump cavity with one Xe flashlamp of 63.5 mm arc length with a pulse width of 540μs FWHM. The resonator was 30 cm in length, the high reflector had a one meter radius of curvature, and the output coupler used was 20% transmissive. All rods studied were 5.0 mm x 72.6 mm, with their ends polished flat and parallel and AR coated at 2.1μm.

Figure 3 shows a typical electrical input energy versus laser output energy plot for the system described above with 0.8% Cr doping. Each data point in Fig. 3 is an average of ten consecutive shots taken at 1.0 Hz. The slope efficiency calculated from a linear fit to the data points, which are significantly above threshold, was 5.1%. This is the highest reported to date for a flash-pumped 2μm room temperature laser. We have measured thresholds as low as 28 J and absolute efficiencies of greater than 3.8%.

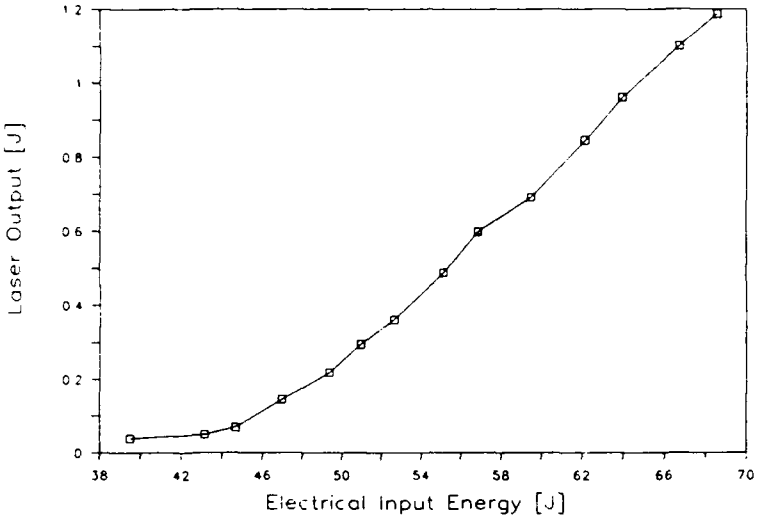

Figure 3. Performance of Cr;Tm;Ho:YAG laser.

REFERENCES

1. B.M.Antipenko, A.S.Glebov, T.I.Kiseleva, and V.A.Pis'mennyi, Sov. Tech. Phys. Lett. 11, 284 (1985); Opt. Spectrosc. 60, 95 (1986).

2. H.O. Teichmann, E.W. Duczynski, G. Huber, SPIE Proceedings, vol 1021, 1989 (To be published).

3. G.J.Quarles, A.Rosenbaum, G. Rosenblatt, and L.Esterowitz, in LEOS Annual Meeting, Conf. Proc., 1988 (IEEE Lasers and Electro-Optics Society, Piscataway, NJ 1988) pp 335-336.

4. A.M.Antipenko, J. Tech. Phys. 54, 385 (1984).

Ho:Tm:Cr:YAG AND Ho:Tm:Er:YAG LASER PERFORMANCE AT INTERMEDIATE TEMPERATURES

Donald J. Gettemy
Norman P. Barnes
Patrica L. Cross
Milan R. Kokta

NASA Langley Research Center
Hampton, Virginia 23665-5225

Summary

Ho:Tm:Cr:YAG and Ho:Tm:Er:YAG lasers are two attractive lasers for eyesafe applications. However, as the lower laser level is in the same manifold as the ground level, a large thermal population exists in the lower laser level. As such, operation resembles a three level laser with its attendant inefficiencies. Thermal population in the lower laser level can be mitigated by cooling the laser. Cooling of the laser requires power and detracts from the overall efficiency of the laser system. Optimum laser system efficiency can be obtained through judicious use of cooling. Optimum laser system efficiency is essentially a compromise between the power expended on pumping the laser and the power expended on cooling the laser.

Two Ho:Tm:Cr:YAG lasers with different Ho concentrations and a Ho:Tm:Er:YAG laser have been characterized and compared as a function of temperature. To effectively optimize the performance of the laser system, laser performance must be determined at intermediate temperatures. Laser performance of the three laser materials was measured as a function of the electrical energy, the operating temperature, and the output mirror reflectivity. Laser output energy as a function of electrical energy data can then be reduced to minimize the differences in the losses and the laser rod quality.

A flashlamp pumped laser system which allows the operating temperature of the laser rod to be independently varied was utilized to gather the data. A nearly critically damped pulse forming network allowed the laser to be pumped at a 60 J level with an ~200 μsec current pulselength. Temperature of the laser rod could be varied by regulating the flow of chilled dry nitrogen. A vacuum enclosure kept the heat transfer from the flashlamp to the laser rod minimized and prevented the formation of condensation on the optical surfaces.

Laser output energy versus electrical energy could be reduced to determine the parametric dependencies of the threshold and slope efficiency on temperature. At a given temperature, a set of laser output energy versus electrical energy curves for different output mirror reflectivities curves could be reduced to determine the losses in the laser rod. After factoring out the losses, the different laser rods could then be compared. At the lowest temperatures, the threshold of all three laser materials was approximately the same, ~25 J. However, as the temperature increased, the Ho:Tm:Er:YAG laser rod displayed the fastest increase in threshold. This can be correlated with the population density of the Ho $^5I_8$ manifold. As the Ho:Tm:Er:YAG laser rod has the highest Ho concentration, it also has the highest population sensitivity in the manifold. Slope efficiency was less sensitive to the temperature at lower temperatures. As the temperature increased above ~160°K, the slope efficiencies of all three laser materials decreased. More detailed information on the temperature dependencies of the slope efficiency and threshold will be presented.

Tunable 2.3 μm Tm^{3+}:$LiYF_4$ Laser

R. C. Stoneman and L. Esterowitz
Naval Research Laboratory, Code 6551, Washington, DC 20375

G. H. Rosenblatt
Sachs/Freeman Associates, Landover, MD 20785

Fluorozirconate fibers are expected to achieve losses which are significantly lower than those of silica fibers[1]. In order to exploit the projected superior performance of fluorozirconate fibers, lasers operating near the minimum loss in these fibers at 2.5 μm are required. The $^3H_4 \rightarrow {}^3H_5$ transition in Tm^{3+} at 2.3 μm is an example of a four level laser which operates cw near this minimum loss. This transition has been demonstrated in the hosts $LiYF_4$ (YLF)[2] and fluorozirconate fiber[3].

In order to tailor the performance of the Tm^{3+} $^3H_4 \rightarrow {}^3H_5$ laser to the ultra low loss fluorozirconate fiber it is desirable to tune the 2.3 μm output as closely as possible to the minimum loss at 2.5 μm. It is the purpose of this work to investigate this tunability. Tunable performance of this transition can also be used for spectroscopic studies and to increase the bandwidth of communication systems based on this laser transition.

Cw laser emission at 2.3 μm from the Tm^{3+} $^3H_4 \rightarrow {}^3H_5$ transition in a single mode fluorozirconate fiber pumped by a single mode laser diode has recently been achieved[3]. The emission spectrum for this transition indicates that this laser should be tunable over the range 2.2 μm to 2.5 μm. Cw laser emission of this transition has also been achieved with laser diode pumping in YLF[2]. For this host transitions between Stark levels of the $^3H_4$ and $^3H_5$ states correspond to wavelengths between 2.2 μm and 2.5 μm, while in YAG the corresponding wavelengths are between 2.1 μm and 2.6 μm. Tunability can therefore be achieved over these wavelength ranges on the transitions for which threshold is reached.

In this work we report room temperature cw laser emission tunable from 2.27 μm to 2.34 μm in Tm^{3+}:YLF pumped by a cw titanium:sapphire laser. Laser output is observed at eleven discrete wavelengths within this range. These lines correspond to transitions involving various combinations of the Stark levels of the $^3H_4$ upper laser level and the $^3H_5$ lower laser level. Within this tuning range ten lines are observed with more than 3% slope efficiency, and among these the strongest four lines have more than 6% slope efficiency. Specifically, the strongest lines produce 60 mW when pumped with 1 W from the titanium:sapphire laser.

An energy level diagram for Tm^{3+}:YLF is shown in Fig. 1. Only those levels relevant to the 2.3 μm $^3H_4 \rightarrow {}^3H_5$ laser transition are shown. The pump transition, from the $^3H_6$ ground state to the $^3H_4$ upper laser level, is shown at 0.78 μm.

The laser cavity is shown in Fig. 2. The laser crystal, consisting of YLF doped with 1.5% Tm^{3+}, has flat and parallel surfaces. The input surface has a dichroic coating, with high transmission at the pump wavelength 0.78 μm, and high reflection

at the laser wavelength 2.3 μm. The second surface of the crystal has an anti-reflection coating at 2.3 μm. The cavity is completed with a 10 cm radius of curvature output coupler, with 99.7% reflection at 2.3 μm. A quartz plate, inserted in the cavity at Brewster's angle, serves as a birefringent tuning element. The coatings have sufficient bandwidths, 0.2 μm, to allow tuning over the desired range. The YLF crystal is end pumped by a cw titanium:sapphire laser at 0.78 μm. The pump mode is focused into the cavity mode with a 10 cm focal length lens. The orientation of the birefringent filter is consistent with the linear polarization of the titanium:sapphire laser.

Future prospects for this work include extending the tuning range by using higher pump power and improving the laser cavity. For example, it should be possible to substantially improve the slope efficiencies quoted above, since the free-running (i.e. without tuning element) 2.3 μm $^3H_4 \rightarrow {}^3H_5$ laser produces 120 mW with 1 W of pump power. Tunability of the $^3H_4 \rightarrow {}^3H_5$ transition in Tm^{3+}:YAG will also be attempted. As noted above, this host potentially allows a wider tuning range than both YLF and fluorozirconate glass.

References:

1. D. C. Tran, G. H. Sigel Jr., and B. Bendow, J. Lightwave Tech. LT-2 (5), 566 (1984).

2. G. Kintz, L. Esterowitz, and R. Allen, Topical Meeting on Tunable Solid State Lasers Technical Digest Series, 1987 Volume 20, (Optical Society of America, Washington, DC 1987) p. 20.

3. R. Allen, L. Esterowitz, and I. Aggarwal, submitted to Conference on Lasers and Electro-Optics, 1989.

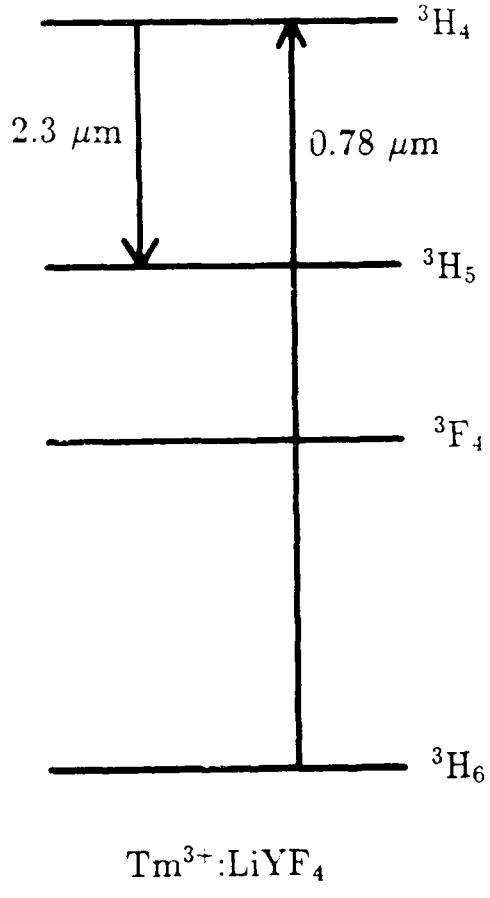

Figure 1. Pumping diagram for the 2.3 μm Tm^{3+}:$LiYF_4$ laser.

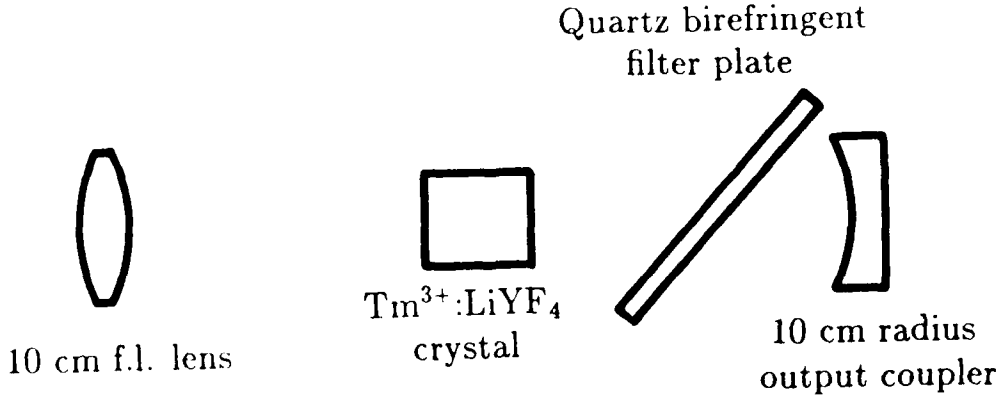

Figure 2. Laser cavity for the tunable 2.3 μm Tm^{3+}:$LiYF_4$ laser.

NOTES

WEDNESDAY, MAY 3, 1989

NAUSET III

3:00 PM–4:00 PM

WE1–WE6

RARE EARTH LASER MATERIALS / POSTER SESSION

Kenneth L. Schepler, U.S. Air Force Wright Aeronautical Laboratory, *Presider*

WE1-1

FLUORESCENCE DYNAMICS IN $LiYF_4$: Tm, Ho AFTER 800 nm LASER EXCITATION

A. BRENIER, R. MONCORGE and C. PEDRINI
Université Lyon 1, UA 442 du CNRS
69622 Villeurbanne Cédex - France

SUMMARY

The codoped system $LiYF_4$: Tm,Ho was recently proposed as a mid infrared diode-pumped solid state laser operating at 2 and 2.3 μm /1/ because recent progress make an attractive alternative to lamp-pumped operation and also because a very good spectral match exists between the GaAlAs diode emission and the Tm^{3+} absorption near 795 nm.

The diode laser excitation is simulated in the present work by using a pulsed dye laser followed by a Raman cell or by an home-made Ti^{3+} sapphire tunable solid state laser.

The excited-state dynamics of the Tm^{3+} ions in a singly doped crystal of $LiYF_4$ is first analyzed. It is proved that a very efficient cross-relaxation process occurs between adjacent Tm^{3+} ions of type $^3H_4$, $^3H_6 \longrightarrow {}^3F_4$, $^3F_4$ (Fig. 1, Table I). This mechanism populates the $^3F_4$ lowest excited state of Tm^{3+} ions so that for Tm_3 concentration high enough (>5 %), one excited Tm ion in the $^3H_4$ level gives effectively two excited Tm ions in the $^3F_4$ level.

The excited state dynamics of the Tm^{3+} and Ho^{3+} in the same host $LiYF_4$ is then studied in the codoped systems $LiYF_4$: 7% Tm^{3+} : x % Ho^{3+} (x = 0.5 ; 2 ; 5). The decay of the $^3H_4$ fluorescence and correlatively the rise of the $^3F_4$ fluorescence strongly vary with the Ho concentration (table II), indicating that, as sketched in figure 2, in addition to the cross-relaxation process occuring among the Tm^{3+} ions and previously mentionned, important energy transfer processes arise directly from the $^3H_4$ level of the Tm^{3+} ions to the Ho^{3+} ions. The quantum efficiencies of the three main mechanisms involved in the $^3H_4$ excited state dynamics, namely the Tm intra-center deexcitation, the $Tm^{3+} \longrightarrow Tm^{3+}$ cross-relaxation and the $Tm^{3+} \longrightarrow Ho^{3+}$ direct energy transfer can be deduced from experimental data and are gathered in table II. The first mechanism is very weak whatever the Ho^{3+} concentration x while the two other processes compete, the last one being predominant for x greater than 0.5 %. These results are in contradiction with the classical Tm $\longrightarrow$ Ho energy transfer

scheme for which only the lowest excited states of the ions are considered.

The $^3F_4 \rightleftharpoons {}^5I_7$ energy transfers are also analyzed. After a rapid rise behaviour characteristic of the above mentionned cross-relaxation process, the fluorescence decay of the $^3F_4 \longrightarrow {}^3H_6$ transition of the Tm^{3+} ions shows first a very strong and short component of a few tens of μs, characterizing the lifetime of $^3F_4$, and then a very long component with a time-constant of 15-19 ms. The time-dependence of the fluorescence of the Ho^{3+} ions associated with $^5I_7 \longrightarrow {}^5I_8$ transition near 2 μm presents a short built-up of a few tens of μs which is the feeding time of the $^5I_7$ level via the $^3F_4 \longrightarrow {}^5I_7$ energy transfer, followed by the same long decay as the one of the $^3F_4$ fluorescence, and characteristic of the lifetime of the $^5I_7$ state. The long component of the $^3F_4$ fluorescence decay is assigned to a $^5I_7 \longrightarrow {}^3F_4$ phonon-assisted back-transfer efficient enough at room temperature. The temperature dependence of this back-transfer confirms the existence of a Boltzmann population equilibrium between the $^3F_4$ and $^5I_7$ levels, with an activation energy of about $450 cm^{-1}$, in good agreement with the energy mismatch between the two excited states. The back-transfer is completely quenched for $T < 200$ K.

The increase of the apparent lifetime of the $^5I_7$ level with the Ho concentration, previously evidenced in $LiYF_4$: 50% Er^{3+} : x % Ho^{3+} /2/, is also observed in the present system and is explained again by the occurence of radiative energy transfers among the Ho^{3+} ions.

Measurements of fluorescence quantum efficiencies at 2 and 2.3 μm are also presented and discussed. The data are obtained by using either a CW or a pulsed Ti^{3+} sapphire solid state laser to simulate the diode laser excitation.

References

/1/ G. KINTZ, L. ESTEROWITZ and R. ALLEN
Tunable Solid State Lasers, Technical Digest Series 20, 20 (1987).

/2/ J. RUBIN, A. BRENIER, R. MONCORGE and C. PEDRINI
J. Phys. 48, 1761 (1987).

% Tm	0.1	1	7
(ms)	3.8	1.45	12.5×10^{-3}
1	100 %	38 %	0.3 %
2	0 %	62 %	99.7 %

Table I : Lifetimes of $^3H_4$ level and quantum efficiencies of the Tm^{3+} intra-center deexcitation (η_1) and the $Tm^{3+} \longrightarrow Tm^{3+}$ cross-relaxation (η_2) in $LiYF_4$: Tm^{3+} at room temperature after excitation of the $^3H_4$ level.

x (% Ho)	0	0.5	2	5
τ (μs)	12.5	6.5	3	1.2
η_1(%)	0.33	0.17	0.08	0.03
η_2(%)	99.67	51.83	23.92	9.57
η_3(%)	0	48.00	76.00	90.40

Table II : Lifetimes of $^3H_4$ level and quantum efficiencies of the Tm^{3+} intra-center deexcitation (η_1), the $Tm^{3+} \longrightarrow Tm^{3+}$ cross-relaxation (η_2) and the $Tm^{3+} \longrightarrow Ho^{3+}$ direct transfer (η_3) in $LiYF_4$: 7 % , Tm : x % Ho^{3+} at room temperature when the Tm^{3+} ions are excited in their $^3H_4$ excited state.

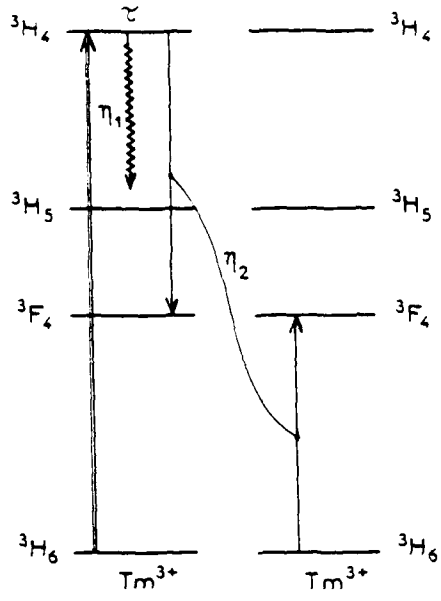

Figure 1 - The two channels of deexcitation of the Tm^{3+} ions at room temperature in $LiYF_4$:Tm after excitation of the $^3H_4$ level: the Tm^{3+} intra-center deexcitation (η_1) and the $Tm^{3+} \longrightarrow Tm^{3+}$ cross-relaxation process (η_2)

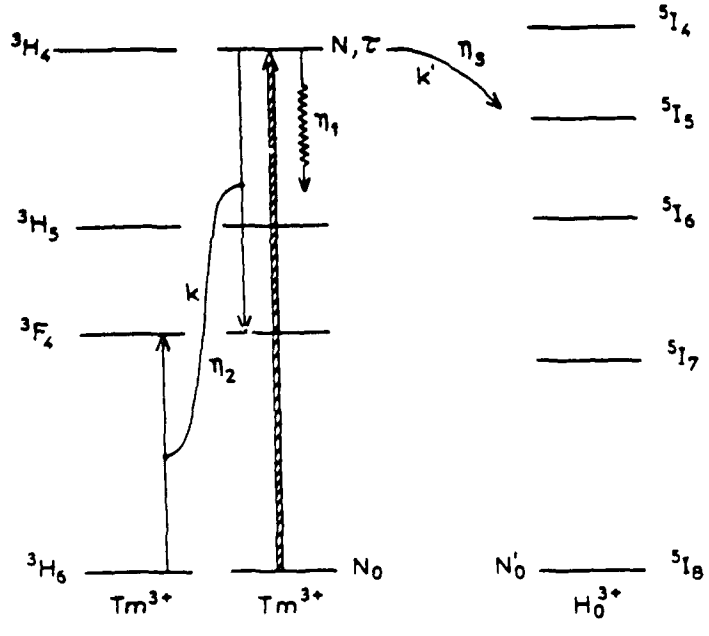

Figure 2 - The three channels of deexcitation of the Tm^{3+} ions at room temperature in $LiYF_4$:7 % Tm : x %Ho (x = 0.5, 2, 5) after excitation of the $^3H_4$ level : the Tm^{3+} intra-center deexcitation (η_1), the $Tm^{3+} \longrightarrow Tm^{3+}$ cross-relaxation process (η_2) and the direct $Tm^{3+} \longrightarrow Ho^{3+}$ transfer (η_3).

Laser Emission at 1.47 μm from Fluorozirconate Glass Doped with Tm^{3+} and Tb^{3+}

G. H. Rosenblatt and R. J. Ginther
Sachs/Freeman Associates
Landover, MD 20785

R. C. Stoneman and L. Esterowitz
Naval Research Laboratory
Washington, DC 20375

Laser emission at 1.47 μm is observed at room temperature from the $^3H_4 \rightarrow {}^3F_4$ transition in Tm^{3+} doped fluorozirconate glass pumped by a pulsed Alexandrite laser. This is the first observation to our knowledge of the Tm^{3+} $^3H_4 \rightarrow {}^3F_4$ laser transition in any host. The fluorozirconate glass host is codoped with Tb^{3+}, the presence of which provides a mechanism for the transfer of Tm^{3+} ions out of the $^3F_4$ lower laser level. The codoped Tm^{3+}, Tb^{3+} system therefore has the potential for four level cw laser operation, in contrast with singly doped Tm^{3+} which is self-terminating on the long-lived $^3F_4$ level. Four level cw operation of this transition near 1.5 μm would be applicable to optical communication using silica fibers, and would have advantages over three level lasers such as those based on the Er^{3+} $^4I_{13/2} \rightarrow {}^4I_{15/2}$ transition.

An energy level diagram for the Tm^{3+}, Tb^{3+} system is shown in Figure 1. The pump transition, from the $^3H_6$ ground state to the $^3H_4$ upper laser level, is shown at 0.79 μm. The laser transition is shown at 1.47 μm. The closely spaced Tb^{3+} ^7F levels are shown at the left. Several cross relaxation processes which are relevant to the laser are shown in Figure 2. At the bottom of the figure the cross relaxation which transfers ions from the lower laser level into the $^7F_0$ Tb^{3+} level is shown. This transfer is shown schematically by the curved line in Figure 1. The ions which are transferred to the ^7F levels rapidly decay to the ground state non-radiatively. There are at least two other cross relaxation processes which are possible in this system. These are shown at the top of Figure 2. Unfortunately these processes transfer ions out of the upper laser level. The process at the upper left transfers ions to the $^3F_4$ lower laser level, while the process at the upper right transfers ions to the $^3H_5$ level, which rapidly decays non-radiatively to the $^3F_4$ level. Since these processes are detrimental to the laser performance their influence needs to be kept to a minimum.

The laser cavity consists of a fluorozirconate glass laser rod and an output coupler. The 1.0 cm long rod has flat and parallel surfaces. The input surface has a dichroic coating, with high transmission at the pump wavelength 0.79 μm, and high reflection at the laser wavelength 1.5 μm. The second surface of the rod has an anti-reflection coating at 1.5 μm. The cavity is completed with a 10 cm radius of curvature output coupler, with 99.7% reflection at 1.5 μm. The laser rods are longitudinally pumped by a pulsed Alexandrite laser at 0.79 μm. The Alexandrite pulse width is 200 μs. The pump mode is focussed into the cavity

mode with a 5 cm focal length lens.

Laser performance was investigated for four samples having a variety of Tm^{3+} and Tb^{3+} concentrations. The observed pulsed threshold energies and slope efficiencies are shown in Table 1. The table also shows the measured lifetimes of the upper and lower laser levels for these samples. Also shown are the lifetimes for a sample containing 1% Tm^{3+} and no Tb^{3+}. The lower level lifetimes shown in the table indicate that a very small doping of Tb^{3+} is very efficient at quenching the lower laser level. This effect is due to the cross relaxation shown at the bottom in Figure 2. The upper level lifetimes also decrease as the Tb^{3+} concentration is increased. This effect is due to the cross relaxation shown at the upper right in Figure 2. The increase in the pulsed threshold energy as the Tb^{3+} concentration increases is due to this cross relaxation process. The optimum concentrations of Tm^{3+} and Tb^{3+} will be those which balance these cross relaxation processes against each other. The dependence of the upper and lower laser level lifetimes on the concentrations of both Tm^{3+} and Tb^{3+} will be investigated. Cw performance of the $^3H_4 \rightarrow {}^3F_4$ transition should be possible with optimized Tm^{3+} and Tb^{3+} concentrations.

Sample	Upper level lifetime	Lower level lifetime	Pulsed threshold	Slope efficiency
1% Tm	1.5 ms	12 ms	-	-
1% Tm, .1% Tb	510 μs	1700 μs	290 μJ	0.9%
1% Tm, .5% Tb	270 μs	400 μs	350 μJ	1.1%
1% Tm, 1% Tb	150 μs	190 μs	360 μJ	1.5%
.5% Tm, 1% Tb	300 μs	460 μs	395 μJ	1.2%

Table 1. Lifetimes and laser performance data.

Reference:

1. L. Esterowitz, R. Allen, G. Kintz, I. Aggarwal, and R. J. Ginther, in Conference on Lasers and Electro-Optics Technical Digest Series 1988, Vol. 7 (Optical Society of America, Washington, DC, 1988), paper THH1.

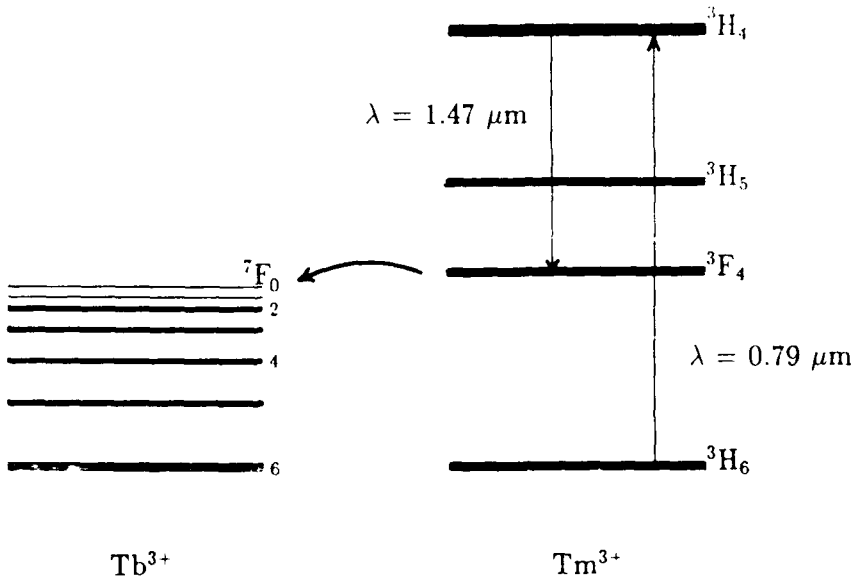

Figure 1. Pumping diagram for the 1.47 μm Tm^{3+}, Tb^{3+} fluorozirconate laser.

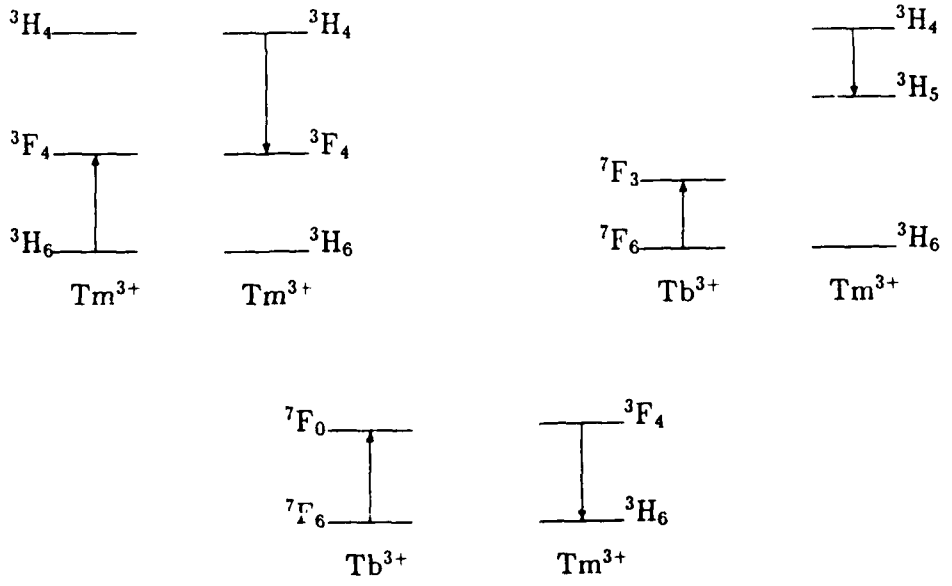

Figure 2. Energy transfer processes relevant to the 1.47 μm Tm^{3+}, Tb^{3+} fluorozirconate laser.

WE3-1

Continuous-wave oscillation of a monomode thulium-doped silica fibre laser.

D.C. Hanna R.M. Percival I.R. Perry R.G. Smart P.J. Suni A.C. Tropper.

Department of Physics
University of Southampton
Southampton S09 5NH
United Kingdom
(0703) 595000

SUMMARY

Tm^{3+} is an interesting activator ion for a glass fibre laser since it emits in a region of the spectrum where such lasers have not previously operated [1], and where fluorozirconate fibres provide low transmission loss. Furthermore the low threshold afforded by the waveguide geometry, and the location of a strong atsorption band at around 800nm (see fig.1) suggest that diode-laser pumping of thulium-doped fibre should be possible.

We have observed laser emission over the range 1.88-1.99μm from a germano-silicate fibre which has Tm^{3+} ions incorporated into the core at a concentration of - 830ppm. Figure 2 shows the fluorescence spectrum of the $^3H_4$-$^3H_6$ transition responsible for laser action. From this spectrum it appears that potentially laser operation might be achieved over the range 1700-2200nm. $^3H_6$ is the ground multiplet of the Tm^{3+} ion, and absorption losses due to population in the ground multiplet are responsible for the short wavelength limit of operation.

The laser cavity was formed by butting dielectric coated mirrors against the cleaved fibre ends. The fibre had a

cut-off wavelength of 1.7μm and was therefore monomode at the lasing wavelength. A Styryl 9 dye laser operating at 796 nm was used to excite the Tm^{3+} ions at the peak of the $^3H_6$-$^3F_4$ absorption band. Efficient operation depended on reducing ground multiplet absorption either by using a short fibre length or by immersing part of the fibre in liquid N_2 to depopulate the upper Stark levels. A 27cm length of fibre lased at room temperature with an incident pump threshold of 30mW (21mW absorbed) and a slope efficiency of 13% with respect to absorbed power for 3% output coupling. In this configuration the maximum laser output power achieved was 2.7mW at a wavelength of 1.91μm. Operation at 1.88μm could be obtained using a 1.3m length of fibre of which all except 10cm near each end was cooled in liquid N_2. The laser operated at progressively longer wavelengths with higher thresholds as the length of the cooled portion was reduced.

Further experiments are aimed at a more detailed characterisation of this laser's performance; results of this work will be reported.

REFERENCES

1. D.C. Hanna, I.M. Jauncey, R.M. Percival, I.R. Perry, R.G. Smart, P.J. Suni, J.E. Townsend, and A.C. Tropper, Electron. Lett. **24**, 1222-23, (1988).

Fig. 1

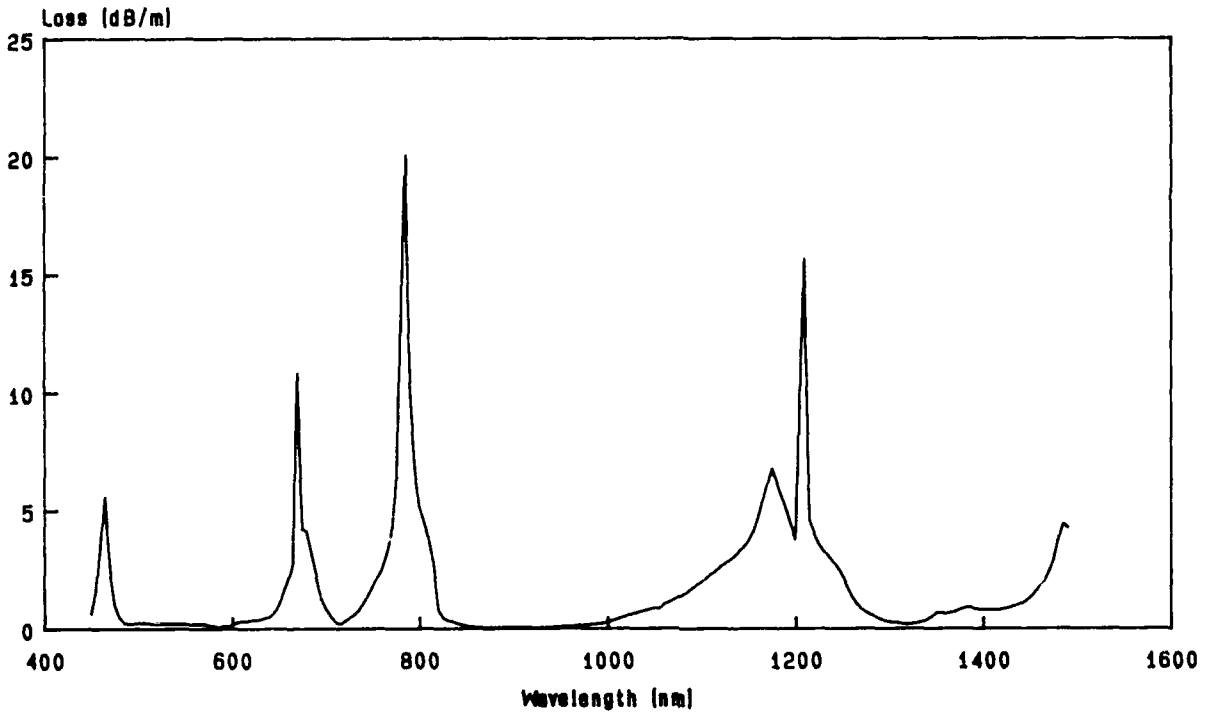
Tm Absorption
Loss (dB/m)
25
20
15
10
5
0
400
600
800
1000
1200
1400
1600
Wavelength (nm)

Fig. 2

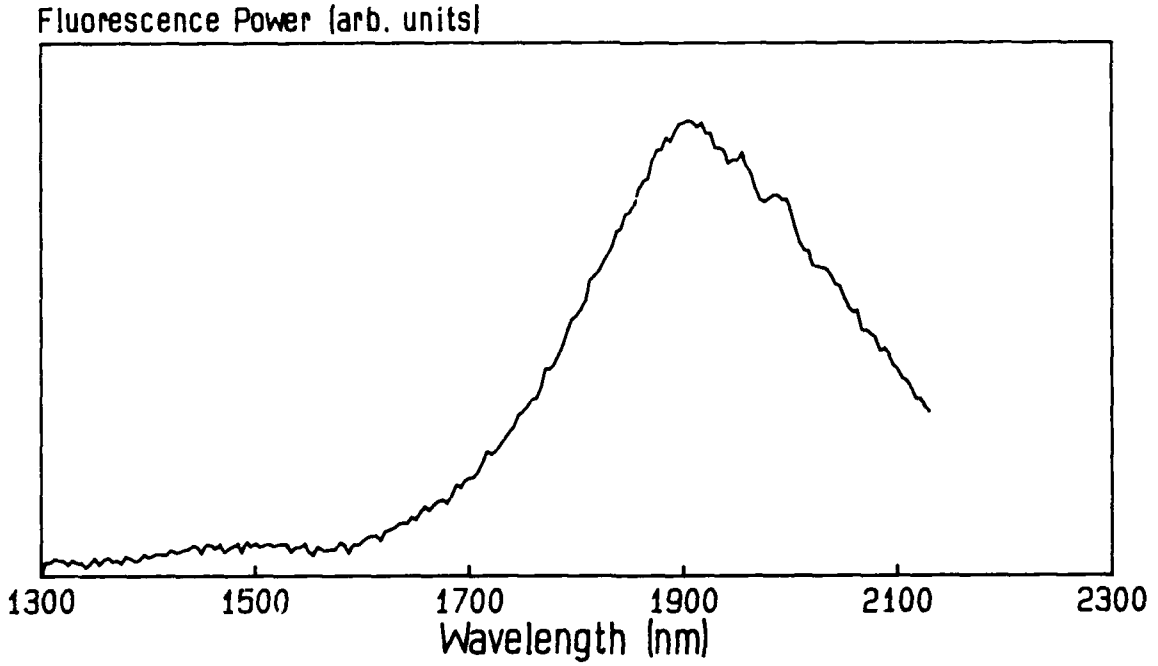
Fluorescence Power (arb. units)
1300
1500
1700
1900
2100
2300
Wavelength (nm)

ENERGY TRANSFER PROCESSES AMONG Cr, Tm AND Ho IONS IN YTTRIUM ALUMINUM GARNET CRYSTALS

G. ARMAGAN(*), A. M. BUONCRISTIANI (*), B. DI BARTOLO (**) and A. T. INGE (***)

The dynamics of solid state lasers utilizing multiply doped rare earth crystals depends critically on the inter-ionic interactions responsible for transferring excitation among them and so understanding these interactions is necessary for the optimal design of such lasers. For example, NASA is interested in the development of a 2 micron laser having short pulse duration (from 0.01 to 1 microsecond) for use in LIDAR remote sensing in the atmosphere. This application suggests a Q-switched laser and so one needs to know how the inter-ionic transfer process are related to the Q-switched operation. We have made a systematic study of YAG crystals doped in various ways with Cr, Tm and Ho by measuring the absorption, luminescence and excitation spectra and the integrated intensities and the lifetimes of Cr, Tm and Ho in these materials. These measurements were carried out on 13 samples with different Cr, Tm and Ho concentrations and in a range of temperature from either 8K or 78K to 350K.

The rate of energy transfer from a donor state to an acceptor state can be described in terms of a dipole- dipole microscopic interaction parameter which gives the probability of transfer when the donor and acceptor are separated by 1 cm. We have determined this parameter for YAG: Cr, Tm in two different ways and calculated the temperature and concentration dependence of the energy transfer rates and the microscopic interaction parameter for this system. We demostrated that the temperature dependence of the radiative decay probability of Cr is the cause of the temperature dependence of both the transfer rate from Cr to Tm and the interaction parameter for the Cr- Tm system. Furthermore, we were able to identify and quantify the energy migration among Cr ions and the cross relaxation rates of Tm ions. We have initiated a similar analysis for the determination of the energy transfer rates and the microscopic interaction parameters for Tm-Ho system and we will present the details of this study at the meeting.

In the following we describe some of the results of the Cr- Tm energy transfer dynamics that are important for laser design:

a) The integrated intensity of the Cr emission increases as the temperature increases from 78K to 350K while the lifetime decreases over the same temperature range. The temperature dependence of the radiative transition probability of Cr can be derived using the fact that the intensity is proportional to the measured lifetime and to the radiative transition probability.

(*) Christopher Newport College, Department of Physics, Newport News, VA 23606 U.S.A.
(**) Boston College, Department of Physics, Chestnut Hill, MA 02167 U.S.A.
(***) NASA Langley Research Center, MS468, Hampton, VA 23665 U.S.A.

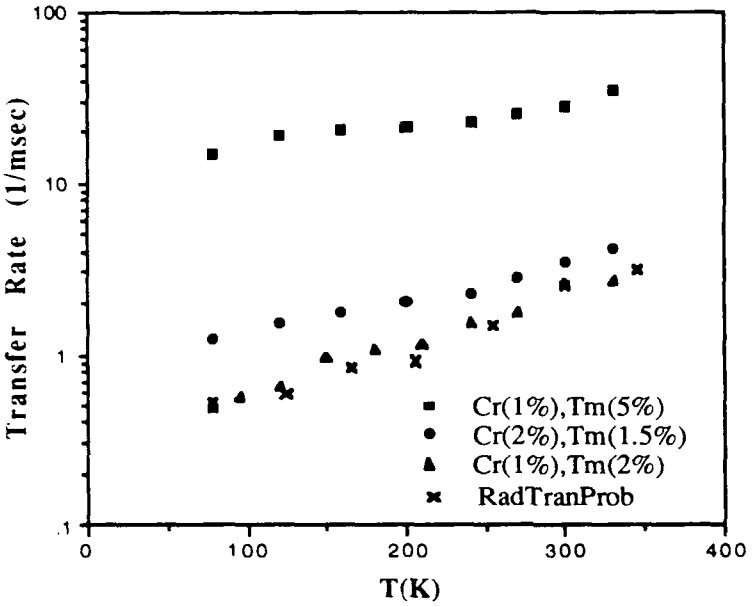

Fig.1. Temperature dependence of the Cr to Tm nonradiative energy transfer rates in various YAG samples. The radiative transition probability calculated for YAG: Cr(1% at.), Tm(2% at.) is arbitrarily matched.

b) The nonradiative energy transfer rate from Cr to Tm determined from the lifetime data of Cr in various Cr and Cr, Tm doped YAG samples is presented along with the radiative transition probability calculated up to a constant multiplier using the measured intensity and lifetime data on YAG: Cr(1% at.), Tm(2% at.) sample in Fig.1. The transfer rates were all found to have similar temperature dependences and increase with increasing temperature. While the match for the radiative transition probability is shown only for the YAG: Cr(1% at.), Tm(2% at.) sample, it can also adequately be shown for the other samples. We also note that the efficiency of the Cr- Tm energy transfer at a certain temperature was found to increase with increasing Tm concentration.

c) One method used in calculating the microscopic interaction parameter for the Cr- Tm coupling is the Dexter formula (Ref.1) which uses the measured spectral data to determine the oscillator strength (f- number) of Tm and the overlap between the normalized Cr emission and Tm absorption. The other method was using the measured decay curves of Cr ion in the presence of Tm ion to fit the Inokuti- Hirayama formula (Ref.2). The temperature dependence of the interaction parameter for Cr(1% at.), Tm(2% at.): YAG sample calculated both from the spectral data and the fitting of decay curves is presented in Fig. 2, along with the radiative transition probability calculated as explained in parts a and b). Using these results we can demonstrate that

the temperature dependence of the Cr lifetime is mainly due to the variation of its radiative transition probability and that this temperature dependence is reflected in the temperature dependence of the nonradiative Cr to Tm energy transfer rate as well as the microscopic interaction parameter of the Cr-Tm coupling as seen from the good match with both of these parameters in Fig.1 and Fig.2.

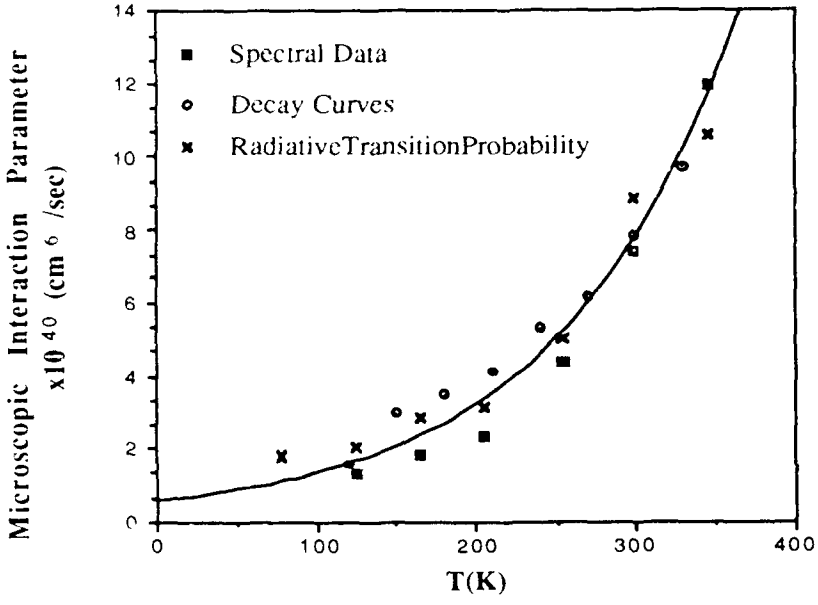

Fig.2. Temperature dependence of the microscopic interaction parameter obtained from both spectral data and decay curves for YAG: Cr(1% at.), Tm(2% at.). The radiative transition probability calculated for YAG: Cr(1% at.), Tm(2% at.) is arbitrarily matched. The curve is an exponential fit for the interaction parameter.

The results of our work show that in order to have a good transfer efficiency from Cr to the other rare- earth ions it is not always necessary to place the Cr ion in low- crystal field garnets. If the sharp R-line emission of Cr is in good coincidence with the absorption of the acceptor ions, the transfer may be a very efficient process as in the case of YAG: Cr, Tm system.

References

1) D. L. Dexter, J. Chem. Phys. vol. 21, no. 5, 836 (1953)

2) M. Inokuti and F. Hirayama, J. Chem. Phys. vol. 43, no. 6, 1978 (1963)

This work was partially supported by NASA grant NAG-1-796 and by the ASEE Summer Faculty Fellowship Program.

Er,Tm,Ho:YLF laser for spectroscopy applications

A. Di Lieto, P. Minguzzi, F. Pozzi, M. Tonelli
Dipartimento di Fisica dell' Università - PISA - ITALY

H. P. Jenssen
Crystal Physics Laboratory, Center for Material Science and Engineering, and Department of Electrical Engineering and Computer Science, Massachussets Institute of Technology
CAMBRIDGE , MASSACHUSSETS , U. S. A.

We have developed a cw laser employing a YLF crystal doped with Er,Tm, Ho which was mounted in a three-mirror astigmatically compensated resonator. The pump source is either the 514.1 nm line of Ar^+ laser or the 647.1 nm line of Kr^+ Laser. The strong lines excite the $^2H_{11/2}$ and $^4F_{9/2}$ levels of Er^{3+} respectively. By non-radiative energy-transfer processes from Er to Tm and finally to Ho, laser action is obtained on the $^5I_7 \rightarrow {}^5I_8$ transition[1].

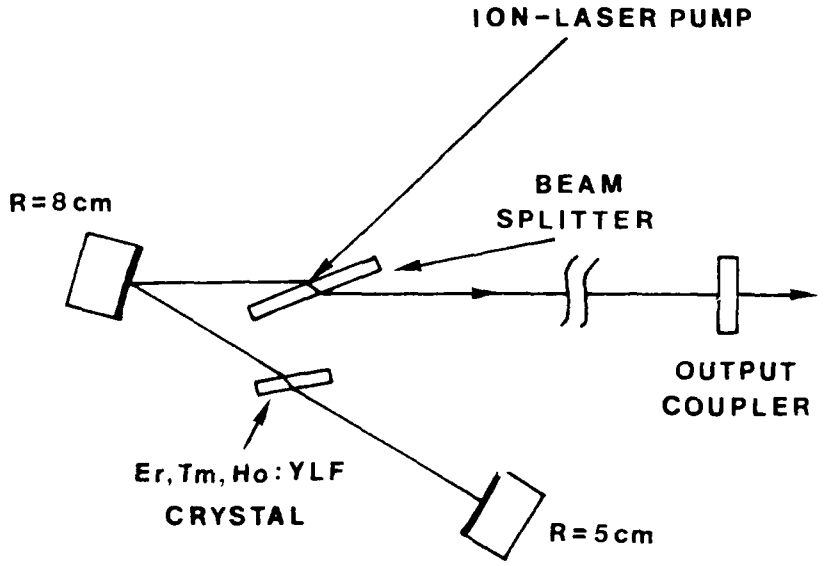

As shown in the figure the pump laser is injected into the resonator through a dichroic beam-splitter[2]; the active crystal is kept in a cryostat at liquid nitrogen temperature so that continuous-wave emission can be achieved, as required for high resolution spectroscopic studies.

The tunability ranges from 2.05 to 2.1 μm and work is in progress to improve the efficiency and the performances of the system.

Also the noise properties are studied with the aim to evaluate the feasibility of experiments in high resolution molecular spectroscopy.

[1] L.F. Johnson, L.G. Van Uitert, J.J. Rubin, R.A. Thomas: Phys. Rev. A 133, A494 (1964).

E.P. Chicklis, C.S. Naiman, R.C. Folweiler, D.R. Gabbe, H.P. Jenssen, A. Linz : Appl. Phys. Lett. 19, 119 (1971).

[2] M. Meucci, M. Tonelli, G. Baldacchini, U.M. Grassano, A. Scacco, F. Somma : Opt. Commun. 51, 33 (1984).

Optical Properties of Nd:$NaYF_4$ and Ho:$NaYF_4$

D. Knowles, A. Cassanho, and H.P. Jenssen

M.I.T. Crystal Physics Lab
Center for Materials Science and Engineering
Cambridge, Massachusetts 02139 Tel: (617) 253-6878

The recent development of mid-infrared lasers based on Er, Tm and Ho has prompted a search for materials that have a strong stimulated emission cross section to overcome the high non-radiative transition rate associated with these wavelengths. One possible way to increase the cross section of a given rare earth transition is to dope the ion into a non-inversion site, thereby increasing the forced electric dipole oscillator strength of the transition. Generally speaking, the farther away from octahedral symmetry, the more mixing of 4f wavefunctions and hence greater cross section. This is the rationale for investigating $NaYF_4$ as a possible laser host: the rare earth site has 9 nearest neighbors in a site without inversion symmetry. We have grown samples of (1%) Nd:$NaYF_4$ and (0.5%) Ho:$NaYF_4$, and early results indicate that the integrated cross section for Nd in this material is roughly a factor of two higher than in Nd:YAG. In addition, the broad absorption lines of Nd (see figure 1) suggest this material might be suitable for pumping with a diode array. The Ho sample, on the other hand, has a relatively long lifetime (17 msec.) similar to that of Ho:$LiYF_4$, indicating that the integrated cross section for Ho is similar to that of $LiYF_4$. The $^5I_7$-$^5I_8$ emission lines around 2000 nm are very broad (fig. 3) so that it may be possible to operate this material as a tunable laser in the mid-ir.

Little is known about the host $NaLnF_4$ (where Ln=Y, all lanthanide rare earths), especially with respect to the optical properties of RE doped $NaYF_4$ and RE:$NaLaF_4$. Research has shown the entire family to be hexagonal (P6) with 1.5 formula units per unit cell. <ref 1,2,3> The formula is often written as $Na(Ln_{1.5}Na_{.5})F_6$ to illustrate the similarity with the structure of the mineral gagarinite $Na(YCa)F_6$. The rare earth ion occupies two different sites: the smaller site has 9 nearest neighbors without inversion symmetry, while the larger site, which is randomly occupied by both the rare earth and Na ion, has been reported to be either octahedral <ref. 2>, or 9 fold coordinated similar to the first site <ref. 1>. Because of the relatively low refractive index (1.47) compared to oxides, an increase in the oscillator strength can still be accompanied by a relatively long lifetime. An intriguing aspect of this host is the possibility of selectively populating either of the rare earth sites. For example, in the crystal Nd:$NaYF_4$ the large Nd ion (compared to yttrium) should prefer the larger of the two Y sites, while in Nd:$NaLaF_4$ the Nd ion, being smaller than La, might preferentially populate the smaller site. It is not known at this time if such

a scheme if feasible, but the existence of both $NaYF_4$ and $NaLaF_4$ makes this an interesting area of research.

We are at present investigating both the optical properties and the crystal growth techniques for this material. The two samples described here (Nd:$NaYF_4$ and Ho:$NaYF_4$) were the first grown, and lack of seed material required growing the crystals on a wire leading to multinucleation and polycrystalline samples. While complete characterization will require single crystal samples, the measurements to date give strong indication that this host could become a useful laser material. Judd Ofelt analysis of Nd:$NaYF_4$ room temperature absorption data indicates that the intensity parameters (Ω_4, Ω_6) are a factor of 2 higher than in YAG, leading to proportionally higher integrated cross sections. (For this analysis, the segregation coefficient of Nd in $NaYF_4$ was assumed to be one; if less than one, the cross sections would be even stronger.) Figure 1 shows the absorption lines around 800 nm for both $NaYF_4$ and YAG, illustrating the pump bands for diode pumping. The emission at 1.06 μm is also broader than in YAG (see fig. 2), and it may be possible to tune the laser output around this region. The absorption and emission lines of each site have been identified at 10K, but the lifetimes of $^4F_{3/2}$ at this temp. are so similar (375 μs vs. 400 μs) as to be almost indistinguishable. (At 77K and above, the lifetime appears completely exponential). Because the two sites have similar oscillator strengths, the existence of two sites may not be detrimental to the operation of this material as a laser.

Initial measurements on the Ho sample $^5I_7$ lifetime at room temp indicate that this level shows exponential decay with τ=17 msec, similar to that of Ho:$LiYF_4$. The broad emission lines of $^5I_7$ - $^5I_8$ (see figure 3) combine to produce a band of emission from 1925 nm to 2075 nm, suggesting that this material might be operated in a tunable mode. Further results on both Nd and Ho doped $NaYF_4$ will be presented at the meeting.

This work was supported in part by NASA Langley Research Center Grant NAG 1-924.

References

1. J. H. Burns, "Crystal structure of hexagonal Sodium Neodymium Fluoride and related compounds", **Inorg. Chem. 4,** 881-886, (1965).

2. B. P. Sobolev, D. A. Mineev, and V. P. Pashutin, "Low temperature hexagonal modification of $NaYF_4$ having Gagarinite structure", **Dokl. Akad. Nauk. SSSR 150,** 791-794, (1963).

3. R. E. Thoma, H. Insley, and G. M. Hebert, "The Sodium Fluoride-Lanthanide Trifuloride system", **Inorg. Chem. 5,** 1222-1229, (1966).

Fig. 1

Nd ABSORPTION

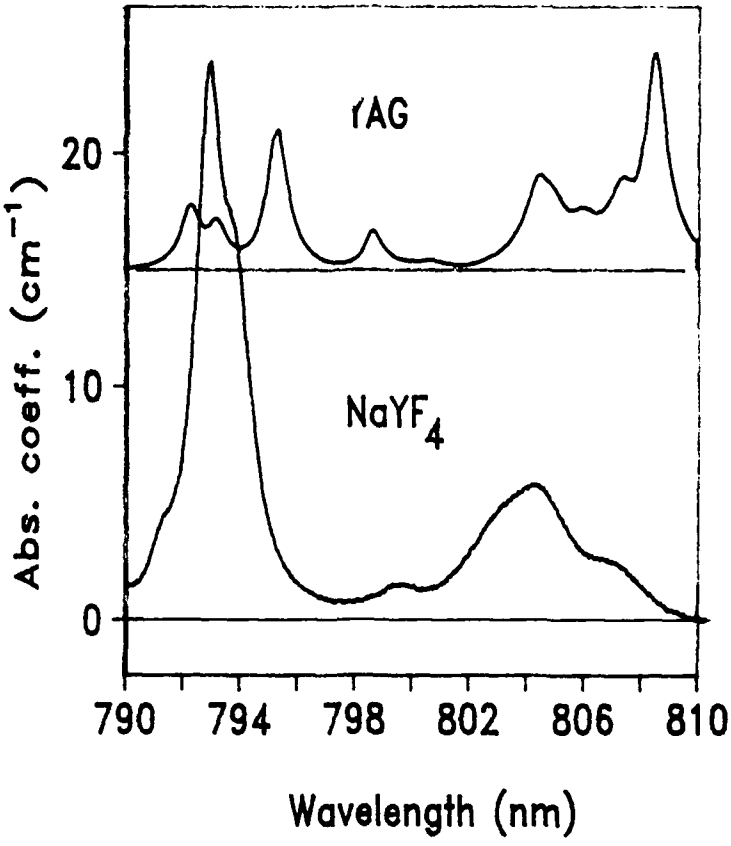

Fig. 2

Nd EMISSION

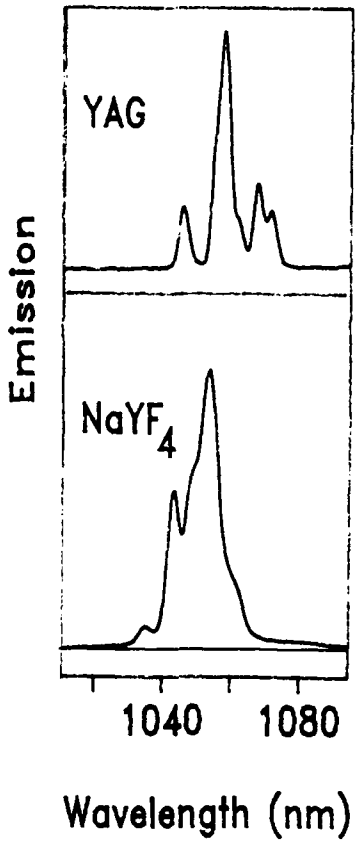

Fig 3: Ho EMISSION

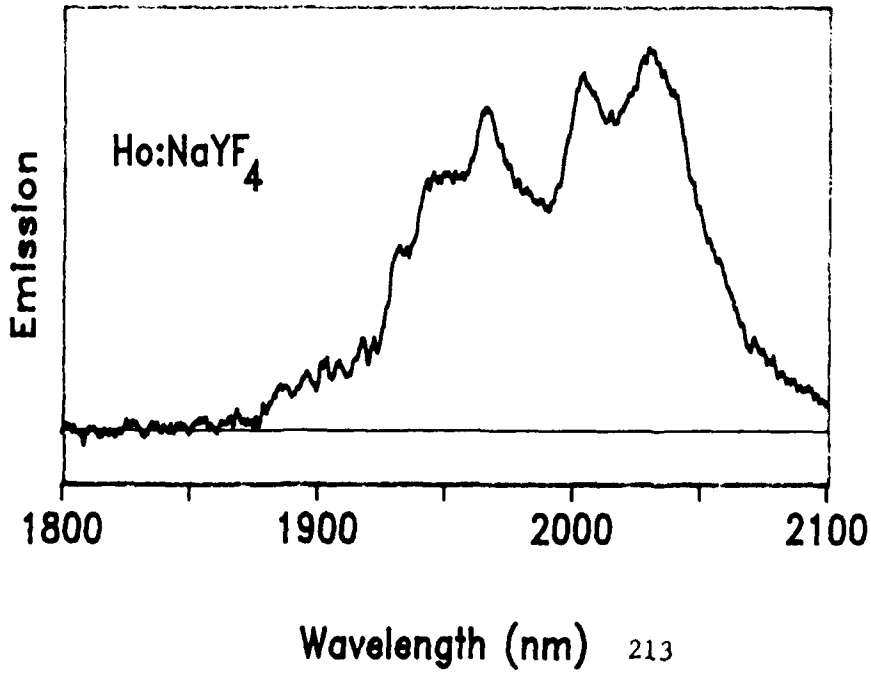

NOTES

WEDNESDAY, MAY 3, 1989

NAUSET IV

4:00 PM–5:30 PM

WF1–WF5

Er LASERS

Michael L. Shand, Allied-Signal Inc., *Presider*

NONLINEAR INTERACTIONS IN SCANDIUM GARNETS DOPED BY CHROMIUM AND ERBIUM IONS

Smirnov V.A., Shcherbakov I.A.

117942 Moscow, Vavilov Str. 38, General Physics Institute, Academy of Sciences of the USSR

In the doped crystals of scandium garnets the sensitizing of rare-earth ions (TR^{3+}) luminescence by chromium (Cr^{3+}) ions improves the efficiency of a number of lasers based on these crystals [1]. The analysis shows that the formation of inversed population as a rule is controlled by a number of mechanisms such as: direct optical pumping into TR^{3+} absorption bands, $Cr^{3+} \rightarrow TR^{3+}$ energy transfer and nonlinear interactions of excited TR^{3+} ions [2].

One of the main objects of our investigations was the yttrium-scandium-gallium garnet doped by Cr^{3+} and Er^{3+} ions ($YSGG:Cr^{3+}:Er^{3+}$) [1,3]. In this crystal the upconversion processes, which at high pumping densities in the real lasers can greatly influence the inversed population formation at $^4I_{11/2} \rightarrow {}^4I_{13/2}$ laser transition, have never been yet investigated. The upconversion process ($^4I_{13/2} \rightarrow {}^4I_{15/2}$, $^4I_{13/2} \rightarrow {}^4I_{9/2} \rightsquigarrow {}^4I_{11/2}$), which depopulate the terminal laser level $^4I_{13/2}$ and simultaneously populate the upper laser level $^4I_{11/2}$, at high pumping density eliminate the selftermination of the laser transition $^4I_{11/2} \rightarrow {}^4I_{13/2}$ (Fig.1) and provide the possibility to obtain CW laser operation [4]. At the same time the upconversion process ($^4I_{11/2} \rightarrow {}^4I_{15/2}$, $^4I_{11/2} \rightarrow {}^4S_{3/2}$) depopulate the upper laser level $^4I_{11/2}$ and simultaneously populate the pair of the excited states $^4S_{3/2}$, $^2H_{11/2}$ what yield two excitations ($^4I_{11/2}$, $^4I_{13/2}$ Er^{3+}) due to the crossrelaxation and, so, reduces the inverse population of the 3-mcm laser transition. In the experiments the samples from $YSGG:Cr^{3+}:Er^{3+}$ crystals were homogeneously excited by Ar-laser. Both CW and pulse excitation were applied. The number of excited Er^{3+} ions was less than 2% of nonexcited ones. The system of rate equations for Er^{3+} in the $YSGG:Cr^{3+}:Er^{3+}$ crystal has the form:

$$\begin{cases} \frac{dn_4}{dt} = -\beta n_1 n_4 + F_3(n_3, C_{Er}, t, C_{DA}, C_{DD})/2 + K_4 \\ \frac{dn_3}{dt} = \beta n_1 n_4 + K_3 - (W_{31} + W_{32}) n_3 - F_3(n_3, C_{Er}, t, C_{DA}, C_{DD}) + \\ \qquad + F_2(n_2, C_{Er}, t, C_{DA}, C_{DD})/2 \\ \frac{dn_2}{dt} = \beta n_1 n_4 + W_{32} n_3 - W_{21} n_2 - F_2(n_2, C_{Er}, t, C_{DA}, C_{DD}) \\ n_1 + n_2 + n_3 + n_4 = 1 \end{cases} \quad (1)$$

where 1,2,3,4 respectively indicate $^4I_{15/2}$, $^4I_{13/2}$, $^4I_{11/2}$, $^4S_{3/2}$ Er^{3+} states (Fig.1), W_{ij} - intercentral decay i→j, K_4 and K_3 - respectively, pumping of the $^4S_{3/2}$, $^4I_{11/2}$ states, β - crossrelaxation decay ($^4I_{15/2} \rightarrow {}^4I_{13/2}$, $^2H_{11/2} \rightarrow {}^4I_{9/2} \rightsquigarrow {}^4I_{11/2}$ and other processes *Fig 1.*) F_i (n_i, C_{Er}, t, C_{DD}, C_{DA}) - upconversion; C_{DA} and C_{DD} are the microparameters of the donor-acceptor and donor-donor interactions.

It is experimentally stated that at $C_{Er} \geq 10^{21} cm^{-3}$ steady-state dependences $(n_2^{St}(K_4))^2$, $(n_3^{St}(K_4))^2$ at high excitation densities become straightlined. Therefore :

$$F_i(n_i, C_{Er}, t, C_{DA}, C_{DD}) = \alpha_i n_i^2, \text{ where } \alpha_i = \text{const}(n_i), \ (i=2,3) \qquad (2)$$

Consequently, the average rate of the excitations approaching exceeds the rate of their upconversion interactions at the minimum distance, and the nonlinear processes can be described as $\alpha_i n_i^2$. With the help of decay-curve analysis of $^4S_{3/2}$, $^4I_{11/2}$ and $^4I_{13/2}$ excited states in the YSGG:Cr^{3+}:Er^{3+} crystal, parameters W_{ij} and were determined: (W_{21}= 310 s^{-1}, W_{31}= 110 s^{-1}, W_{32}= 800 s^{-1}, $\beta > 10^5 s^{-1}$ at $C_{Er} > 10^{21} cm^{-3}$)

Substituting (2) into (1) one derives α_i by analysing the functional time and pumping density dependences of $n_i(t, K_{3,4})$. The measurements show that the values $\frac{\alpha_i}{C_{Er}}$ determined by different techniques are in coincidence, independent of the C_{Er} and equal to: $\frac{\alpha_3}{C_{Er}} = 7.5 \cdot 10^{-16}$ cm^3/s, $\frac{\alpha_2}{C_{Er}} = 2.3 \cdot 10^{-16} cm^3/s$ ($C_{Er} = 1.5 \div 6\ 10^{21} cm^{-3}$).

Thus, the adequate model of the YSGG:Cr^{3+}:Er^{3+} active medium is elaborated (1),(2). The set of its parameters is measured. The independence of the upconversion parameters of erbium concentration ($C_{Er} = 1.5 \div 6 \cdot 10^{21} cm^{-3}$) indicates "superfast" excitation migration over metastable Er^{3+} states.

On the basis of the elaborated model of the active medium-YSGG:Cr^{3+}:Er^{3+} crystal the analysis of depopulation and relaxation processes of $^4I_{11/2}$, $^4I_{13/2}$ Er^{3+} laser levels was carried out. It was shown that in free running mode the interaction processes of Er^{3+} excited ions increase the behaviour of 3-mcm laser: at high pumping energies the lasing efficiency is practically independent of the excitation pulse duration (in the range <2 ms). This independence is due to the nonlinear upconversion processes. Meanwhile, in the Q-switching regime the upconversion strongly decreases the inversion population and, hence, deteriorates the laser parameters; in such regime a short pulse (~30 mcs) is fortunate for increasing the laser efficiency. Different channels of inversion

population formation on $^4I_{11/2}$, $^4I_{13/2}$ Er^{3+} transition are revealed. It is shown that the most effective of them is the sensitizing of Er^{3+} ions luminescence by Cr^{3+} ions, at which the upper $^4I_{11/2}$ laser level is populated only. It is found that impurity quenching of the lower $^4I_{13/2}$ Er^{3+} laser level increases the efficiency of lasers operating in various regimes. The obtained conclusions are confirmed in direct lasing experiments.

Interaction process of excited holmium ions ($^5I_7 \rightarrow {}^5I_8$, $^5I_7 \rightarrow {}^5I_6$ in the YSGG:Cr^{3+}, Ho^{3+} ($C_{Ho} = 8 \cdot 10^{20} cm^{-3}$) crystal was investigated, the constant of nonlinear interaction of Ho^{3+} ions ($5 \cdot 10^{-18} cm^3/s$) is measured, the recommendations on 3-mcm holmium laser ($^5I_6 \rightarrow {}^5I_7 Ho^{3+}$) optimization are given.

It is also stated that in the YSGG:Cr^{3+}:Tm^{3+}:Ho^{3+} crystal the upconversion process ($^3H_4 \rightarrow {}^3H_6 Tm^{3+}$, $^5I_7 \rightarrow {}^5I_5 Ho^{3+}$) at characteristic activators concentrations $C_{Tm} = 8 \cdot 10^{20} cm^{-3}$, $C_{Ho} = 5 \cdot 10^{19} cm^{-3}$ and pumping densities can substantially decrease output behaviour of 2-mcm holmium lasers. The main stokes and anti-stokes mechanisms of energy transformation in the givencrystal are found.

REFERENCES

1. V.A.Smirnov, I.A.Shcherbakov, IEEE Journal of Quantum electronics, vol. 24, N6, 1988, p.949
2. P.P.Feofilov, V.V.Ovsyankin, Appl. Opt., 6, 1828(1967)
3. E.V.Zharikov, et al., Kvantovaja elektronika, 13, 5(1986), p.973
4. G.Huber, et al., Tunable solid state lasers, Techn. Dig. Ser., 20, p.18, 1987, Williamsburg.

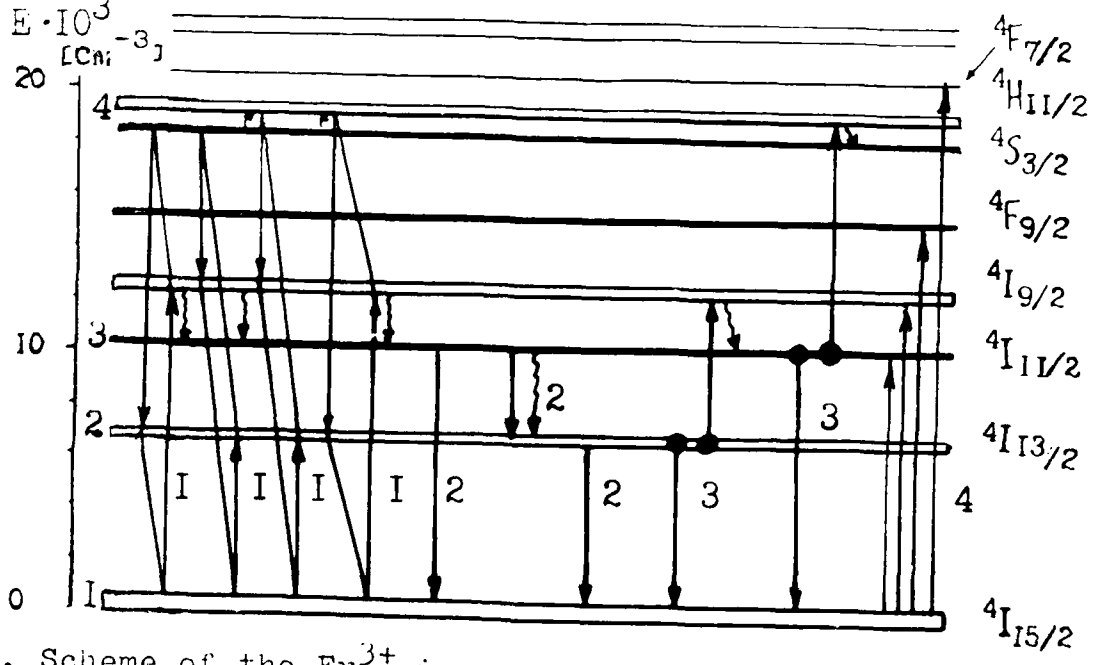

Fig.1. Scheme of the Er^{3+} ions energy states; 1)-crossrelaxation decay, 2)-intercentral decay, 3)-upconversion processes, 4)-pumping

Er:YLF LASER OPERATION AT 0.85 AND 1.73 um AND THE POSSIBILITY OF SELF CASCADE LASING

Norman P. Barnes
Keith E. Murray

NASA Langley Research Center
Hampton, Virginia 23665-5225

Summary

Er:YLF has the potential for self-cascade lasing, or simultaneous lasing at the same wavelength between two different sets of manifolds. To determine if self cascade lasing is occurring, both laser and spectroscopic data were investigated. Evidence for self cascade lasing can be obtained by comparing the laser performance of Er:YLF operating at 0.85 and 1.73 μm.

Since the 0.85 and 1.73 μm transitions originate from the same manifold, evidence for self cascade lasing can be obtained by comparing the slope efficiency of the two laser processes. Since the photon energy of the 0.85 μm transition is roughly twice the photon energy of the 1.73 μm transition and both transitions utilize the same upper laser manifold, the slope efficiency of the former may be expected to be twice the slope efficiency of the latter. However, experience has shown that the slope efficiencies are roughly equal.

A more detailed investigation on the slope efficiencies at the two wavelengths was performed to eliminate the effects of differing losses at the two wavelengths. Differences in the losses were factored out of the slope efficiency calculations by measuring the performance of the Er:YLF laser as a function of the output mirror reflectivity. Laser performance at the two wavelengths was measured as a function of the electrical energy and the output mirror reflectivity. Measured slope efficiencies, with the lowest output mirror reflectivity, were 0.023 and 0.0026 for the 0.85 and 1.73 μm

transitions, respectively. An analysis of this data indicated that the maximum slope efficiencies, after factoring out the effect of the losses, were still approximately equal.

Differences in the occupation factor of the lower laser levels are important in the operation of the Er:YLF laser as the laser is not a true four level laser. While the manifold which contains the lower laser level is not thermally populated to a significant degree, lifetimes of these levels are comparable to or longer than the flashlamp pulses. As such, the lower laser level can become populated during the lasing process and the Er:YLF laser operates as a terminated four level laser rather than a true four level laser. It can be shown that this effect limits the extractable energy, and thus the slope efficiency, to a factor of $Z_2/(Z_1 + Z_2)$ where Z_1 is the thermal occupation factor of the lower laser level and Z_2 is the thermal occupation factor of the upper laser level. For the 0.85 and 1.73 μm transitions at 300K, these factors are 0.78 and 0.84, respectively. The difference in these factors cannot account for the expected ratio of slope efficiencies.

Spectroscopic evidence for self cascade lasing was sought by observing the fluorescence from the various manifolds during the Q-switched laser. Fluorescence from the $^4I_{9/2}$ and and $^4I_{13/2}$ manifolds were monitored while Q-switching the $^4S_{3/2}$ to $^4I_{9/2}$ transition. Results of these spectroscopic investigations and the implications for self-cascade lasing will be presented.

Upconversion processes in Er-activated Solid State Laser Materials

Harry Chou and H.P. Jenssen
Center for Materials Science and Engineering
Massachesetts Institute of Technology
Cambridge, MA 02139

In the past few years, the phenomenon of stepwise upconconversion in Er-activated materials has been of considerable interest to researchers in the solid state laser community. The impetus of this interest is an efficient laser operating in the wavelength range of 3 μm. A number of researchers have examined the upconversion processes in Er in various materials <1-5>. The importance of upconversion has also been demonstrated in actual lasers in quasi-CW operations.<2,3,5>

In this paper, we have applied and extended an experimental technique pioneered by Zhekov et. al.<1> to cover a wide range of pump rates and doping concentrations. First the various feeding efficiencies of Er multiplets at low pump rates (where upconversion is negligible) are carefully measured. Then the upconversion processes are studied by observing the fluorescence dynamics of $^4I_{9/2}$ and $^4S_{3/2}$ when exciting Er at the argon laser wavelength (514.5nm) with a square pulse 30 ms in duration. Since the upconversion feeding is considerably slower than normal feeding, the upconverted population can be separated from the normally fed population. The experimental results are compared with the predictions of a rate equation model which has two adjustable parameters associated with the upconversion processes. The values of the upconversion parameters are deduced from fitting the model to experimental data. This was done up to a pump rate of 10^{21}ions/cm^3.s (=400 W/cm^3), over a concentration range of 10% to 100% in YLF as well as for 10%Er:BaY_2F_8 and 30%Er:$Na_{0.4}Y_{0.6}F_{2.2}$. The agreement between model and experiment is excellent.

Fig. 1 is a summary of the model. The parameter β is the feeding efficiency from $^4I_{9/2}$ into $^4I_{11/2}$, and is measured at low pump rates where upconversion is negligible. α_1 and α_2 are the upconversion rate constants and are the adjustable parameters obtained from fitting the model to experimental data. The values of these parameters are summarized in Table 1.

For a given inversion density, the model shows that of the five samples listed in Table 1, 10%Er:BaY_2F_8 gives the lowest pump rate, and 30%Er:$Na_{0.4}Y_{0.6}F_{2.2}$ the highest; and that between the 10% and 30%Er:YLF, the 10% sample will have a slightly lower pump rate. The 100%Er:YLF sample cannot lase in the CW mode.

If the material is pumped by a diode laser, then in addition to the processes of Fig. 1, excited state absorption of the pump light from both $^4I_{13/2}$ and $^4I_{11/2}$ may be important and should be taken into account. (The experimental determination of α_1 and α_2 is made at 514.5 nm, where excited state absorption of the pump light is not a problem.)

This work was supported in part by Lincoln Laboratory.

1. V.I. Zhekov, V.A. Lobachev, T.M. Murina and A.M. Prokhorov, Sov. J. Quant. Electron. 13 1235 (1983) and 14 128 (1984)
2. Kh. S. Bagadasarov, V.I. Zhekov, V.A. lobachev, T.M. Murina and A.M. Prokhorov, Sov. J. Quant. Electron. 13 262 (1983)
3. S.A. Pollack, D.B. Chang, and N.L. Moise, Appl. Phys. Lett. 49 1578 (1986)
4. S.A. Pollack, D.B. Chang, and N.L. Moise, J. Appl. Phys. 60 4077 (1986) and 64 2885 (1988)
5. G.L. Kintz, R. Allen and L. Esterowitz, Appl. Phys. Lett. 50 1553 (1987)

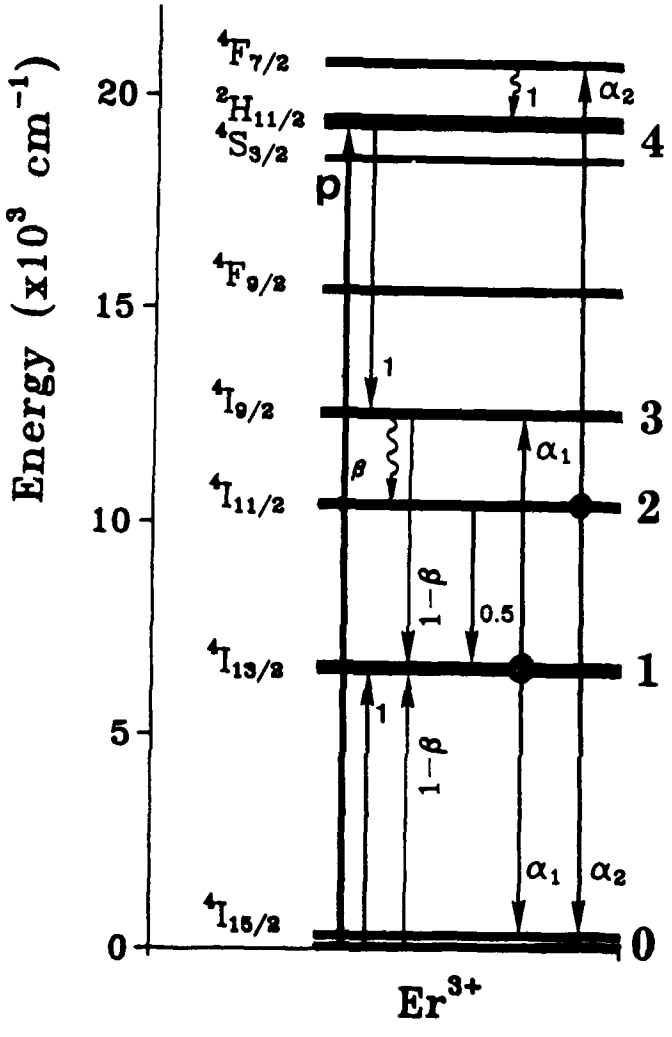

Table 1 Values of parameters in the model

Sample	β	α_1(x10^{-16} cm^3/s)	α_2(x10^{-16} cm^3/s)
10%Er:YLF	1	0.3	0.18
30%Er:YLF	0.75	0.8	0.3
100%Er:YLF	0.38	1.0	2.8
10%Er:BaY_2F_8	1	0.04	0.04
30%Er:$Na_{0.4}Y_{0.6}F_{2.2}$	0.75	0.52	0.4

Multiple-Wavelength Lasing of (Erbium, Holmium):Yttrium Aluminum Garnet

Russell Kurtz* , Laurie Fathe, Jason Machan, Michael Bass† , and Milton Birnbaum
Center for Laser Studies
University of Southern California
Los Angeles, CA 90089-1112

Introduction

Yttrium aluminum garnet (YAG), doped with 30% (at.) Er^{3+} and 1.5% (at.) Ho^{3+} ions, lased at 2.936 μm, 2.939 μm, and 2.796 μm within a single 300-μs pump pulse. Unlike previous multiple-wavelength lasers such as (Ho, Nd):YAG[1], which demonstrate a lasing redshift, (Er, Ho):YAG demonstrates a lasing blueshift, *i.e.*, the longer wavelength lasing occurs (temporally) before the shorter wavelength. (Note that redshift and blueshift, as used here, only refer to lasing transitions which occur between the same two energy manifolds, but different Stark levels.) This blueshift may be caused by excited-state absorption (ESA) in the holmium. The laser level lifetimes of both ions indicate moderate ion-ion interactions in this material.

Methods and Results

We performed the lasing tests in a laser cavity designed as an Er:YAG test bed. We measured lifetimes with a system based on a computer-controlled digital processing oscilloscope, which allowed averaging of up to 100 decay signals for signal-to-noise ratio improvement.

We observed lasing at 2.939 μm, 2.936 μm, and 2.796 μm, all of which correspond to previously-observed laser lines in Er:YAG. Although all three occurred within a single pump pulse, the 2.80-μm lasing occurred after the 2.94-μm lasing. The 2.939-μm and 2.936-μm pulses, however, were truly simultaneous.

A typical input-output graph appears in Fig. 1. The 2.80-μm lasing has a higher threshold and a higher slope efficiency than the 2.94-μm lasing. We checked this by measuring the relative losses and slope efficiencies at the two wavelengths (using the method of Birnbaum[2]), which suggests that the effective stimulated emission cross-section at 2.80 μm is approximately 5% larger than at 2.94 μm, while the total cavity losses (exclusive of the mirrors) are nearly 60% higher at 2.80 μm than at 2.94 μm.

Discussion

Expected lasing wavelengths[3] for Er:YAG include 2.9393 μm (A_2 to Y_7; A refers to the $^4I_{11/2}$ manifold and Y to the $^4I_{13/2}$) and 2.7960 μm (A_3 to Y_4). The 2.936 μm lasing we observed does not match any available transition in Er:YAG, although it has been observed[4] in Er:YAG without co-dopants. However, the known spectroscopy[3] is missing the Y_6 level in this material. If this level has an energy of 6873.4 cm^{-1}, the A_2-to-Y_6 transition is 2.9364 μm. It is possible that 6873 cm^{-1} is the approximate energy of this level, and the 2.936-μm transition is A_2 to Y_6.

The two simultaneously-lasing lines, 2.939 μm and 2.936 μm, are separable. Since they have different time signatures and different thresholds, they are separate transitions. We found that the 2.936-μm lasing had a repeatably lower threshold than the 2.939-μm lasing, even though this difference was typically only 3%.

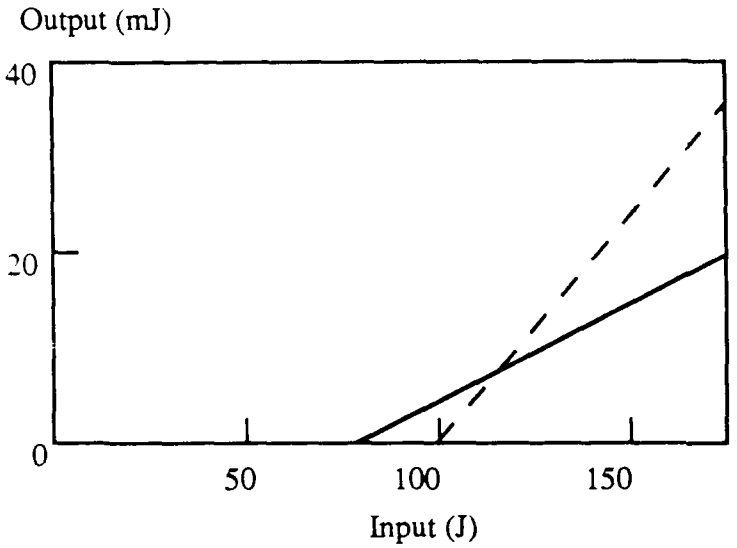

Fig. 1. Input energy *vs.* output energy. The solid line is 2.94 μm; the dashed is 2.80 μm.

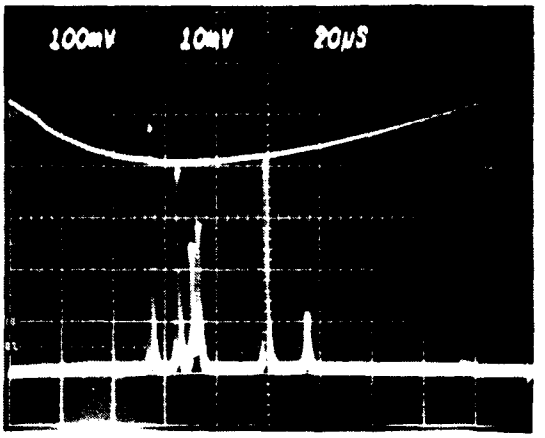

Fig. 2. Laser waveforms. The upper trace is the flashlamp; the lower trace is the laser. The group of five spikes is at 2.94 μm and he other two are at 2.80 μm.

We also discovered (Fig.2) that both the 2.936-μm and 2.939-μm lasing demonstrate self-termination, caused by a time-increasing loss in this wavelength region. This loss may be due to ESA in the holmium: there is a possible absorption from its Y_8 level ($^5I_7$ manifold) to the A_3 level ($^5I_6$), which corresponds to 2.938 μm and has a measured spectral width of about 0.005 μm. Since the lifetime data indicate that the $^4I_{13/2}$ manifold of erbium transfers energy into the $^5I_7$ manifold of holmium, as the erbium lases, the lower Stark levels of the $^5I_7$ manifold fill. Eventually, the Y_8 has sufficient population that its transition to the A_3 induces a loss at 2.94 μm which is large enough to prevent lasing. Since there is no such loss at 2.80 μm, this transition now has sufficient gain to lase.

This lasing blueshift is in contrast to the redshift seen in many other multiple-wavelength lasers. A redshift is usually caused by a time-increasing loss in the lasing ion itself. The most likely cause of the redshift is the filling of the lower Stark levels of the lower laser manifold, which were initially the lower levels for the lasing transition. As they fill, the inversion relative to these particular levels decreases until it is no longer greater than the loss, and lasing ceases. However, the inversion relative to higher Stark levels (at a lower energy difference from the upper laser level) is larger than the loss, so lasing switches to the next lower energy (longer wavelength) transition.

The 2.796-μm lasing demonstrated a higher lasing threshold than either of the 2.94-μm lines, and only began after the 2.939-μm and 2.936-μm terminated (Fig. 2). However, it showed a greater slope efficiency. This indicates that, while the 2.796-μm transition is slightly stronger than

the 2.936-μm or 2.939-μm, the cavity losses are larger at 2.796 μm. One possible explanation for this is atmospheric absorption. Many airborne contaminants, especially water vapor[5], have absorption features in this region. In fact, the atmospheric absorption is about seven orders of magnitude greater at 2.80 μm than at 2.94 μm. Thus, while the atmospheric losses are negligible at 2.94 μm, they may be significant at 2.80 μm, up to the 35% of total round-trip loss that we attribute to them here.

There are only slight changes in laser level lifetimes, indicating moderate ion-ion interactions between the erbium and the holmium. The Ho^{3+} $^5I_6$ lifetime in (Er, Ho):YAG is lengthened compared to Ho:YAG, and its similarity to the Er^{3+} $^4I_{11/2}$ lifetime indicates that there is significant energy transfer from the $^4I_{11/2}$ level to the $^5I_6$ level. The constancy of the Ho^{3+} $^5I_7$ lifetime in singly- and doubly-doped materials, on the other hand, suggests that any energy transfer between it and the Er^{3+} $^4I_{13/2}$ level is from erbium to holmium.

---

* On leave from: TRW, Redondo Beach, California 90278.

+ Currently at: University of Central Florida, Orlando, Florida 32816-0001.

[1]J. Machan, R. Kurtz, M. Bass, and M. Birnbaum, "Simultaneous, multiple wavelength lasing of (Ho, Nd):$Y_3Al_5O_{12}$", *Appl. Phys. Lett.* **51** (17), 26 October 1987, 1313 - 5.

[2]Milton Birnbaum, Armin W. Tucker, and Curtis L. Fincher, "Laser emission cross section of Nd:YAG at 1064 nm", *J. Appl. Phys.* **52** (3), March 1981, 1212 - 5.

[3]N. I. Agladze, A. A. Balashov, G. N. Zhizhin, and M. N. Popova, "High-resolution spectra in the $^4I_{15/2}$—$^4I_{13/2,11/2}$ transition region for an erbium-activated-YAG crystal", *Opt. Spectrosc.* **57** (3), September 1984, 228 - 9.

[4]M. Bass, W. Q. Shi, R. Kurtz, M. Kokta, and H. Deigl, "Operation of the high dopant density Er:YAG at 2.94 μm," in A. B. Budgor, L. Esterowitz, and L. G. DeShazer, eds., *Tunable Solid State Lasers II*, 1986: Springer-Verlag, Berlin, 300-5.

[5]William L. Wolfe and George J. Zissis, eds., *Infrared Handbook*, 1978: Office of Naval Research, Ch. 5.

VISIBLE AND INFRARED LASER OPERATION BY UPCONVERSION PUMPING OF ERBIUM DOPED FLUORIDES

R.A. McFarlane and M. Robinson
Hughes Research Laboratories, Malibu CA 90265

S.A. Pollack and D.B.Chang
Hughes Aircraft Company, Long Beach CA 90810

H.P. Jenssen
Massachussets Institute of Technology, Cambridge MA

Recently new interest has developed in upconversion laser pumping, whereby laser output is obtained on transitions of rare earth ions in a variety of hosts that initiate on an ionic energy level that is higher than can be accessed directly by a single pump photon. This result can come about through cooperative energy sharing by two or more excited ions or by a sequential absorption process having an intermediate excited state of adequately long lifetime. This second ionic level need not be the level immediately excited by ground state absorption of a pump photon. Levels thus excited can lead to laser emission at both shorter or longer wavelengths than that of the pump. Particularly interesting are visible and UV systems pumped at wavelengths that are available from semiconductor diode lasers and infrared emitting systems having high slope efficiencies made possible by very rapid upconversion transfer processes associated with the terminal laser level.

We have pumped $YLiF_4$:Er 5% continuously at 791 nm on the $^4I_{15/2}$ - $^4I_{9/2}$ transition and have obtained visible laser emission on two transitions:

$$^4S_{3/2} - {}^4I_{15/2} \quad 551 \text{ nm}$$

$$^4F_{9/2} - {}^4I_{15/2} \quad 671 \text{ nm}$$

The 671 nm transition operates strictly continuously when it alone is lasing. Operation at 551 nm results in a train of approximately 100 ns pulses at about a 100 kHz rate.[1] This is a self-Q-switched behavior arising from saturation of the $^4I_{13/2}$ - $^2H_{9/2}$ transition. When laser radiation at both wavelengths occurs simultaneously, a modulation is imparted to the 671 nm output which arises from the time dependence of the population of the $^4I_{13/2}$ level.

In the pulsed experiments, we have used as a pump the 1.53 μm output of a flashlamp-excited erbium:glass laser to excite the $^4I_{13/2}$ level of erbium in a BaY_2F_8 crystal host. Laser emission was observed on two transitions:

$$^4I_{11/2} - {}^4I_{13/2} \quad 2.769\ \mu m$$

$$^4S_{3/2} - {}^4I_{9/2} \quad 1.73\ \mu m$$

It is apparent that while a population inversion on the first transition can be accomplished with an energy pooling of two ions excited by the pump, the transition initiating on the $^4S_{3/2}$ level near 18500 cm^{-1} requires the simultaneous participation of three ions. Our study of the time delays for onset of laser emission and of the time dependence of the fluorescence from the several energy levels involved, reveals that the pumping process is

not a simple simultaneous multiphoton absorption but indeed requires a cooperative energy sharing by excited ions.

By solving a set of nonlinear kinetic rate equations, we have modeled the upconversion pumping process using a limited number of energy levels.[2] The model includes a cross-relaxation parameter which can be expressed as a function of laser delay time. From our measurements of the behavior of the 2.769 μm laser emission we obtain a value of this parameter of 1.5×10^{-15} cm^{-3} sec^{-1} for the $^4I_{13/2}$ level of erbium in BaY_2F_8. Independent measurements we have made of the relative importance of pair processes in the decay of fluorescence from this state, in crystals of $YLiF_4$, CaF_2 and BaY_2F_8 exited by 10 ns 1.5 μm pulses, show this large value to be consistent with data reported for the other materials. The significance of this result will be examined for IR laser performance.

References.

1. A.J. Silversmith and R.M. Macfarlane, Appl. Phys. Lett. **51**, 1977 (1987).
2. S.A. Pollack, D.B. Chang and N.L. Moise, J. Appl. Phys. **60**(12), 4077 (1986).

KEY TO AUTHORS, PAPERS AND PRESIDERS

TECHNICAL PROGRAM COMMITTEE

Michael L. Shand, *Cochair*
Allied-Signal, Inc.

Hans P. Jenssen, *Cochair*
Massachusetts Institute of Technology

Norman P. Barnes
NASA Langley Research Center

Rudolf G. Buser
U.S. Army Night Vision and Electro-Optics Laboratory

Larry G. DeShazer
Solidlite Corporation

Leon Esterowitz
U.S. Naval Research Laboratory

Gunter Huber
University of Hamburg, Federal Republic of Germany

William F. Krupke
Lawrence Livermore National Laboratory

Peter F. Moulton
Schwartz Electro-Optics, Inc.

Antonio Sanchez
MIT Lincoln Laboratory

Kenneth L. Schepler
U.S. Air Force Wright Aeronautical Laboratory

Ivan A. Shcherbakov
U.S.S.R. Academy of Sciences

William A. Sibley
National Science Foundation